ASSESSING THE EFFECTS OF LAND USE/LAND COVER CHANGES ON CARBON STORAGE OF NATURAL FOREST ECOSYSTEMS IN SOUTHERN AFRICA: A REMOTE SENSING APPROACH

Reuben Lungu Lembani

(729593)

A thesis submitted to the Faculty of Science, University of the Witwatersrand, Johannesburg, in fulfilment of the requirements for the degree of Doctor of Philosophy

School of Geography, Archaeology and Environmental Studies

Johannesburg, 2018

DECLARATION

I declare that this thesis is my own, unaided work. It is being submitted for the Degree of Doctor of Philosophy in the University of the Witwatersrand, Johannesburg. It has not been submitted before for any degree or any other examination in any other University.

Reuben Lungu Lembani

Student number: 729593

22nd day of October, 2018 in Johannesburg

DEDICATION

I dedicate this work to Professor Mary Scholes from the School of Animal, Plant and Environmental Sciences for giving me the platform to pursue and excel in my postgraduate studies at the University of the Witwatersrand.

ACKNOWLEDGEMENTS

I am very grateful to both my supervisors Professor Jasper Knight and Doctor Elhadi Adam for supervising this project and for their guidance and timely comments. I am greatly indebted to the National Research Fund (NRF) for the scarce skills PhD scholarship. I also want to thank the University of Witwatersrand for the continued financial and material support through the Postgraduate Merit Award.

I also greatly thank the School of Geography, Archaeology and Environmental Studies, particularly Professor Jasper Knight for permitting me to conduct my soil analysis in the Environmental Laboratory and his valuable advice during the analytical processing of samples. I acknowledge the Field Assistants from both Luanshya, Zambia and Thorndale Village in South Africa for being handy while ensuring my safety during field measurements. I am also grateful to the Zambia Meteorological Department and South African Weather Service and for availing to me climate data for the study areas. Lastly, but not the least, I would like to thank my family, Agness, Yamikani and Temwani for their unwavering moral support during the course of my study.

ABSTRACT

The extensiveness of Africa's natural forests with approximately 20% of the continent's land cover, makes them an important source of livelihood to over 100 million people. The exclusion of many natural forest types from the United Nations Reducing Emissions from Deforestation and forest Degradation Plus schemes suggest that very little is known about their contribution to global carbon sequestration storage. Furthermore, there is often significant underestimation of forest total carbon storage as most studies have focussed mainly on monitoring, reporting and evaluating carbon stocks in aboveground live biomass. This is partly because the belowground carbon pool is influenced by several spatially heterogeneous abiotic and biotic factors which are themselves not well studied. This thesis uses multi-temporal Landsat remotely sensed images to map land use/land cover changes and aboveground forest carbon stocks for the periods 1986-1998, 1998-2001, 2001-2004, 2004-2011 and 2011-2016 in Luanshya, Zambia, and the periods 1992-1998, 1998-2001, 2001-2006, 2006-2010 and 2010-2016 in Bushbuckridge, South Africa. Aboveground forest carbon stocks were estimated from the regression model relating *in situ* estimates in 30 x 30 m plots to spectral reflectance measurements for different time periods. The study also used PCA to assess 11 edaphic factors associated with the spatial and downward vertical distribution of SOM content in three forest subsoil layers.

The calculated rate of forest regeneration was almost twice lower than the rate of deforestation, and thus over 68% of natural forests are secondary growth forests. From the ecological survey on 126 analogous forest sample plots of different succession stages, it was apparent that forest disturbances result in the replacement of bigger individual trees by smaller trees, and subsequent increase in tree density and reduction in species diversity. These anthropogenic and natural phenomena explained the mean changes in aboveground forest carbon stocks which were 44.20 t ha^{-1} in 1986, 43.85 t ha^{-1} in 1998, 54.81 t ha^{-1} in 2001, 53.02 t ha^{-1} in 2004, 46.83 t ha^{-1} in 2011 and 36.67 t ha^{-1} in 2016 for Luanshya, and 4.67 t ha^{-1} in 1992, 9.52 t ha^{-1} in 1998, 40.84 t ha^{-1} in 2001, 34.15 t ha^{-1} in 2006, 41.92 t ha^{-1} in 2010 and 24.95 t ha^{-1} in 2016 for Bushbuckridge. Conversely, the effects of these changes were also observed in the complexity in the spatial and downward vertical distribution of soil organic matter content. Mean soil organic matter stock in the three soil depth of 0-10 cm, 10-20 cm and 20-30 cm were 7056 g m^{-3}, 5427 g m^{-3} and 6135 g m^{-3} in Luanshya, and 5065 g m^{-3}, 4784 g m^{-3} and 4733 g m^{-3} in Bushbuckridge, respectively. Principal components analysis revealed that the percentage of clay and silt correlated consistently with increased soil organic matter content, while bulk density and sand% impeded its accumulation. The baseline data and the empirical models can be used as counterfactual scenarios for monitoring the emerging forest carbon projects in southern Africa. The patterns and strength of relationships can be used as input or validation datasets for improving soil carbon models and for devising more efficient strategies for forest management.

TABLE OF CONTENTS

LIST OF FIGURES

LIST OF TABLES

LIST OF ABBREVIATIONS

Acronym	Description
AGLB	Aboveground live biomass
ANOVA	Analysis of variance
BD	Bulk density
CDM	Clean Development Mechanism
CO_2	Carbon dioxide
DBH	Diameter at breast height
DEA	Department of Environmental Affairs
DEM	Digital elevation models
DVI	Difference vegetation index
DN	Digital Number
EVI	Enhanced Vegetation Index
EC	Electrical conductivity
FAO	Food Agriculture Organisation
IPCC	Intergovernmental Panel on Climate Change
ISODATA	Iterative Self-Organizing Data Analysis Technique
LOI	Loss-on-ignition
LULC	Land use/land cover
ML	Maximum Likelihood
MRT	Mean residence time
MRV	Monitoring, reporting and verification
MC	Moisture content
NDVI	Normalised difference vegetation Index
NPP	Net Primary Productivity
NIR	Near Infrared
PDF	Partially disturbed forest sites
PES	Payment for environmental services
PCA	Principal component analysis
PSD	Particle size distribution
REDD+	Reducing Emissions from Deforestation and forest Degradation Plus
RF	Regeneration forest sites
ROI	Region/s of interest
SF	Secondary forest sites
UDF	Undisturbed forest sites
SAVI	Soil adjusted vegetation index
SR	Simple ratio
SOM/c/s	Soil organic matter/concentration/stock
UNFCCC	United Nations Framework Convention on Climate Change
VI/s	Vegetation index/indices

CHAPTER 1 - INTRODUCTION

1.1 Background

Over the period from 1880 to 2012, the Earth's average surface temperature rose by 0.86 ± 0.30°C (Ciais *et al.*, 2014; IPCC, 2014). However, climate change exhibits substantial interannual and decadal variability. For instance, the rate of warming between 1998 and 2012 was averaged at 0.05°C per decade, while the rate of 0.12°C per decade was recorded for the period 1951-2012 (IPCC, 2014). Granted the importance of atmospheric gases in maintaining the greenhouse effect, anthropogenic activities and the subsequent accumulation of CO_2 have continued to alter the radiative forcing and energy balance in the Earth's system (Trenberth, 2001; Hartmann *et al.*, 2013). Based on the recent atmospheric CO_2 concentration of about 400 parts per million (2017) and all emission scenarios (MacCracken, 2009), deforestation and forest degradation remain a significant source of annual CO_2 emissions into the atmosphere (MacCracken, 2009). This has spurred research interests in global carbon sequestration, especially the responses of natural forest ecosystems to climate change associated with land use/land cover (LULC) changes (Lal, 2008; Poorter *et al.*, 2016; Reddy *et al.*, 2016; Williams *et al.*, 2016).

The Clean Development Mechanism (CDM) strategies of the United Nations Framework Convention on Climate Change (UNFCCC) aims at ameliorating the adverse effects of climate change through the reduction of atmospheric CO_2 concentration (Ghazoul *et al.*, 2010). This involves establishing carbon sequestration initiatives that captures atmospheric CO_2 into other sinks with a longer mean residence time (MRT). The three common CDM strategies are those that capture CO_2 from the atmosphere or point sources of emissions through (1) the natural process of photosynthesis, (2) engineering techniques and (3) chemical transformation (Lal, 2008). Underpinned by the process of photosynthesis, trees use solar radiation to convert atmospheric CO_2 and water into glucose and organic compounds, with subsequent accumulation of biomass in long-lived trees or forests (Lal, 2008; Picard *et al.*, 2012). The extensiveness of Africa's natural forest ecosystems, with approximately 20% of the continent's land cover (600 million hectares) or 15% of the global forest cover (2015), makes it an important ecosystem for sequestering CO_2 and mitigating climate change (Chave *et al.*, 2005; Sebukeera *et al.*, 2006; FAO, 2015; Negasi *et al.*, 2017). For the non-Annex 1 countries with extensive forest cover (Chazdon, 2008), forest and soil carbon sequestration (e.g. afforestation and reforestation), is arguably the most viable option for mitigating global climate change (Parker *et al.*, 2013; DEA, 2014; Negasi *et al.*, 2017).

Given Earth's varying climatic and geographic conditions, there is no single agreed definition of "forest". Based on the Forest Resource Assessment for 2000 (FAO, 2001), this thesis uses the terms forests or woodlands interchangeably, to define ecosystems dominated by perennial woody plants taller than 5 m and vegetation cover of more than 10% covering a continuous areal extent of at least 0.5 hectares (FAO, 2001; Kindt *et al.*, 2011). Through extraction of saleable resources such as timber, non-timber forest products and using the cleared land for agricultural expansion, over 100 million peri-urban and rural settlers in the tropics depend on natural forests for their livelihood (Chidumayo, 1993; Chidumayo and Mbata, 2002; Pielke *et al.*, 2011). Due to the extensiveness of these ecosystems, it is envisaged that natural forests have the potential of providing essential services that are critical in mitigating land degradation and climate change (Ciais *et al.*, 2014). However, studies by FAO (2012) and Ciais *et al*. (2014) show that the rate of forest cover loss has increased from approximately 360,000 hectares per year (1980-1990) to 5.2 billion hectares per year (2000-2010). The loss in woody cover, increase in forest fragmentation (Ciais *et al.*, 2014), and soil degradation result in significant alterations to the functioning of terrestrial ecosystems and with impacts on global environmental change (Foley *et al*., 2005; Mahmood *et al.*, 2010; Pielke *et al.*, 2011; Hegazy and Kaloop, 2015). Thus, there has been a change in the capacity of natural forests to provide ecosystem services (Chazdon, 2008; Poorter *et al.*, 2016), yet uncertainty remains regarding their contribution to carbon emission and sequestration (Chave *et al.*, 2005; Syampungani *et al*., 2014; Negasi *et al.*, 2017).

In the context of Reducing Emissions from Deforestation and forest Degradation Plus (REDD+) (Blom *et al*., 2010; Bond *et al.*, 2010; Ghazoul *et al.*, 2010), there have been fewer forest restoration initiatives on natural forests, particularly the tropical dry woodlands of southern Africa, when compared to other forests worldwide (Syampungani *et al.*, 2014). The exclusion of tropical dry forests from the carbon based payment for environmental services (PES) is partly because of the low and much variable tree density and biomass per unit area (Syampungani *et al.*, 2014). It is assumed that if REDD+ schemes can be extended to these forests, the aggregate sequestration of carbon in sustainably managed woodlands can be crucial for retaining long term forest carbon stocks (Kanowski *et al*., 2011). Even though recent studies have advocated the extension of REDD+ schemes to tropical dry forests (Burgess *et al.*, 2010; Negasi *et al.*, 2017), there is a lack of robust baseline scenarios and empirical data for measuring trends related with the nascent reforestation projects in the region (Burgess *et al.*, 2010; Negasi *et al.*, 2017). Traditionally, quantification of carbon stored in trees requires the use of allometric models developed from destructive estimates of tree biomass at oven dry weight, and conversion of biomass to carbon and carbon dioxide equivalent (Kanowski *et al.*, 2011; Picard *et al*., 2012). This approach is labour intensive, time consuming and unsafe, especially in remote regions, where systematic field measurements of forest biomass are difficult to obtain (Burgess *et al.*, 2010; Negasi *et al.*, 2017). Thus, accurate methodological applications are still lacking due to factors such as absence of scientific data, incorrect accounting of spatial dynamics of forest tree formation, variation in sampling strategy and inappropriate models (Kanowski *et al*., 2011). The application of high resolution remotely sensed data has been a major scientific breakthrough for land cover classification and pattern analysis for delineating forest cover changes at very fine spatial scales (Adam *et al*., 2010; Gara *et al*., 2016). Nevertheless, datasets such as WorldView-2, RapidEye and airborne laser scanner are underutilised because they are expensive and are difficult to acquire and process (Adam *et al*., 2010; Gara *et al*., 2016), particularly for community based conservation initiatives in developing countries. There are few known studies specific to southern Africa that have developed regression models between aboveground forest biomass/carbon and optical reflectance from freely and readily available remotely sensed data (Dube *et al*., 2016; Gara *et al*., 2016; Shoko *et al.*, 2016).

Monitoring, reporting and verification (MRV) of forest inventories and carbon stocks (aboveground and belowground) have been identified as key components for forest management and governance of PES (United Nations, 2007; UNFCCC, 2009; Herold and Skutsch, 2011). The concept of PES involves voluntary transactions where technical support and financial incentives are offered to environmental service providers for ensuring long term viability of forests (Jindal *et al*., 2008; UNFCCC, 2009). This ensures a continuous delivery of key ecosystem services and benefits, such as soil watershed protection, pollination, carbon sequestration and biodiversity conservation etc. (Lund and Treue, 2008; Ghazoul *et al*., 2010 Parker *et al.*, 2013). However, there is often significant underestimation of forest total carbon storage due to the complexity of the soil systems and difficulties in incorporating the belowground carbon pool into empirical models (Peichl and Arain, 2006; Ravindranath and Ostwald, 2008). Estimating the soil organic carbon pool is problematic because it is governed by geological and biogeochemical processes which have turnover rates that may range from decadal to millennial time scales. In addition, the dynamics of belowground processes are influenced by several spatially heterogeneous abiotic and biotic factors which are themselves not well studied (Jobbagy and Jackson, 2000; Dungait *et al.*, 2012; Nussbaum *et al.*, 2014). From the remote sensing perspective, masking of belowground absorption features by forest cover poses further challenges for quantifying and reporting carbon stocks of natural forest ecosystems in its entirety (Bartholomeus *et al*., 2011). Thus, most studies have focussed mainly on estimating carbon stocks in aboveground forest biomass (Stromgaard, 1985; Chidumayo, 1990; 1991; Nickless *et al*., 2011; Picard *et al*., 2012). Some researchers have evaluated soil organic matter (SOM), but have been mostly concerned with crop yield associated with depletion of soil organic content attributed to LULC changes, especially the conversion of forests to agricultural fields (Lal, 2005; Aynekulu *et al.*, 2011; Betemariam *et al.*, 2011; Schneibel *et al*., 2017a). According to Barančíková *et al*. (2010), the ratio of decomposable plant material (DPM) to resistant plant material (RPM) in tropical woodland is 0.25, while that of agricultural crops and grassland is between 0.67 and 1.44. Amid climate change, especially increase in temperature and decrease in annual precipitation and soil moisture deficit, deforestation and LULC changes often result in long term increase in the DPM/RPM ratio of the incoming plant material, which reduces the long term storage of soil organic carbon (Barančíková *et al*., 2010). Within forested areas, there is very little information about SOM dynamics in chronosequence woodlands of different tree structures and forest cover. Such a study is needed for integrated large scale spatial modelling and holistic MRV of aboveground and belowground forest carbon storage in southern Africa.

Studies based on the relationship between *in situ* measurements and the readily available remotely sensed data are needed so as to provide reference scenarios for timely intervention while providing a foundation for sustainable natural forest management. By providing baseline data and up-to-date information on carbon stocks in aboveground live biomass (AGLB) and soil, this research study advances the need for economical robust forest resource assessment in southern Africa. In addition to mitigating climate change through decreased deforestation and forest degradation (Kajembe *et al*., 2003; Chazdon, 2008; Negasi *et al.*, 2017), forest communities of the developing countries can explore opportunities for claiming financial, technical and capacity support from the United Nations REDD+ schemes and other carbon based PES.

1.2 Aim and objectives of the study

The overall aim of this study is to provide spatial data and empirical models for evaluating changes in forest carbon storage, under different forest disturbances and management. The main objectives were to:

i. map and quantify LULC changes that have taken place from 1986-2016 in Luanshya, Zambia, and from 1992-2016 in Bushbuckridge, South Africa using multi-temporal Landsat Earth observation data and change detection techniques;
ii. assess the effects of LULC changes on forest structure, and map the spatial-temporal variations of aboveground forest carbon storage using *in situ* measurements, vegetation indices and machine learning algorithm.
iii. evaluate how fluctuations in temperature and precipitation affects a remotely sensed measure of the general quantity and vigor of forests;
iv. quantify and characterise the spatial and downward vertical distributions of SOM in forest cover of different structure and characteristics; and
v. analyse and model factors influencing forest SOM using principal component analysis (PCA).

1.3 Thesis outline

This thesis is structured and presented in form of a single coherent book. In Chapter two, an "inverted pyramid writing style" is used, where a review of the global carbon cycle is first presented followed by a review of the terrestrial carbon pools, factors that influence the dynamics of carbon sequestration and storage, and the aggregate importance of local or community forest management and monitoring. Chapter three describes the remotely sensed datasets used in mapping and quantifying LULC changes (objective i) and the experimental design and field data collection employed in assessing the effects of LULC changes (objective ii) and interannual variability of climate (objective iii) on the spatial-temporal variations of forest carbon stocks. In addition, the section also describes the sampling protocol, estimates and analysis of forest SOM, and the other associated edaphic factors (objectives iv, v).

The results are systematically presented in Chapter three as per the order of research objectives for each study site: (1) estimates of LULC changes, (2) effects of LULC changes on the composition and structure of forests and (3) effects of temperature and precipitation fluctuations on forests. This is followed by the presentation of (4) estimates and distribution of SOM by depth and (5) analysis of forest soils using PCA. Likewise, the results are discussed in chapter five in the order of research objectives. Chapter six provides a summary of the main findings, limitations and recommendations.

CHAPTER 2 - LITERATURE REVIEW

2.1 The global carbon cycle

The global carbon cycle can be perceived as a series of Earth's carbon pools that are interconnected by fluxes (Ciais *et al.*, 2014). Conceptually, the four distinct global carbon pools, namely oceanic, geological, soil and biotic pools, are linked by the atmospheric phase of CO_2 (Lal, 2004; Ciais *et al.*, 2014). Several studies have described the interactive importance of terrestrial carbon pool in the global carbon cycle (Lal, 2005; Dungait *et al.*, 2012; Kirsten *et al.*, 2016). However, there are considerable uncertainties about these pools because terrestrial systems are subject to disturbance and climate change (Lal, 2004; Don *et al.*, 2007). Soil to 1 m depth is the third largest pool with 1500-2400 Petagram of carbon (PgC) and comprise of both soil organic carbon (1550 PgC) and soil inorganic carbon (950 PgC) (Ciais *et al.*, 2013; Kirsten *et al.*, 2016). The two terrestrial carbon pools interact with atmospheric CO_2 through the process of photosynthesis and respiration, meaning that soil organic and inorganic pools can change in storage capacity over time, mainly in response to climate change and LULC changes associated with human activities.

Prior to the industrial revolution, global Gross Primary Productivity (GPP) was estimated at 123±8 PgC yr^{-1} (Ciais *et al.*, 2013). Of this, approximately 60 PgC yr^{-1} returned to the atmosphere through autorespiration, while 63 PgC yr^{-1} known as Net Primary Productivity (NPP) was used by plants, partitioning for growth, maintenance and subsequent allocation of carbon in shoots and roots biomass (Figure 2.1). The loss of about 55 PgC yr^{-1} through microbial respiration resulted in Net Ecosystem Productivity (NEP), with only about 4.3 PgC yr^{-1} constituting Net-Biome Productivity (NBP) (Jansson *et al.*, 2010). In the absence of forest disturbance (e.g. deforestation and fire) and LULC changes (Jansson *et al.*, 2010), NEP is the balance that regulates photosynthetic fixation of atmospheric CO_2 and biotic carbon sequestration (Jansson *et al.*, 2010). Increased anthropogenic activities such as burning of fossil fuel, increased fire frequency and LULC changes (Chazdon, 2008; Poorter *et al.*, 2016), have reduced terrestrial carbon storage (Ciais *et al.*, 2014). These activities significantly affect forest succession, the geographical distribution of forest and turnover of SOM (Chazdon, 2008; Poorter *et al.*, 2016). Based on lignin composition and the ease with which plant tissues decompose, Lal (2004) categorised the soil carbon pool as labile, intermediate and passive pools. Labile pools have a shorter MRT which ranges from days-years, while intermediate have a turnover of years-decades (Lal, 2004; Barančíková *et al.*, 2010). The passive SOC pools have a longer MRT of more than several decades. Given the longer MRT of SOM from forest biomass, several studies suggest that afforestation and reforestation have the capacity to enhance NEP and long term carbon storage (Jenkinson *et al.*, 1999; Lal, 2005; Dungait *et al.*, 2012).

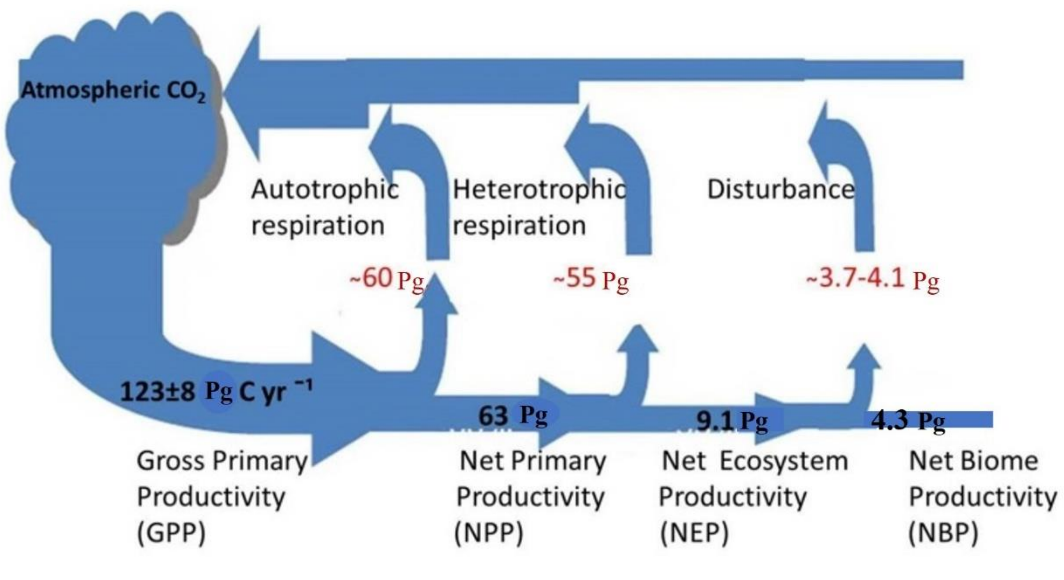

Figure 2.1: Simplified schematic diagram of global terrestrial carbon cycle prior to 1700. The black numbers and arrows represent the annual proportion of carbon fluxes in petagrams (Pg), while the red numbers and arrows shows fluxes from respiration and forest disturbance (deforestation and fire) (Lal, 2005; Ciais *et al.*, 2014).

2.1.1 Soil carbon pool

The soil carbon pool consist of two major components, mineral soil and organic matter (Ciais *et al.*, 2014; Maraseni and Pandey, 2014). Soil inorganic matter (SIM) is made up of mineral particles which vary in size, structure, and physical and chemical properties (Walczak *et al*., 2002; Sun *et al.*, 2009; Keller and Dexter, 2012; Weil and Brady, 2016). Based on the weathering properties of the parent material (Weil and Brady, 2016), SIM is further categorised into primary and secondary carbonates (Lal, 2004). The primary soil fractions are less distinct from the original parent material and are largely dominated by coarse fragments, such as calcite (Lal, 2004). On the other hand, secondary carbonates are very fine soil fractions which are formed from the weathering of less resistant parent material such as rocks containing SiO_4^{4-} or Fe_2O_3. Additional secondary mineral soil result from calcareous dust, irrigation water, manure and fertilizer, and their subsequent dissolution and interaction with CO_2 and cations (Lal, 2004). Conversely, SOM is characterised by a continuum of fresh to progressively decomposing and/or synthesised plant, microbial, animal debris and root exudates (Dungait *et al.*, 2012; Weil and Brady, 2016). These animal and plant tissues provide energy to soil microorganisms and vital elements needed by plants, such as nitrogen, phosphorus and sulphur (Dungait *et al.*, 2012).

2.1.2 Composition and classification of soil inorganic matter

Based on the principles of soil genesis, horizon formation, colour, texture, structure and, physical and chemical properties, soil is identified and described from the six hierarchical categories namely, Order, Suborder, Great Group, Subgroup, Family and Series (Figure 2.2) (USDA and NRCS, 1999; Bockheim *et al*., 2014). From generalised to specific nomenclature, the total number of soil types ranges from 12 to approximately 19,000.

Because of this extensiveness, the 12 soil orders form the basis for soil taxonomy and classification (USDA and NRCS, 1999):

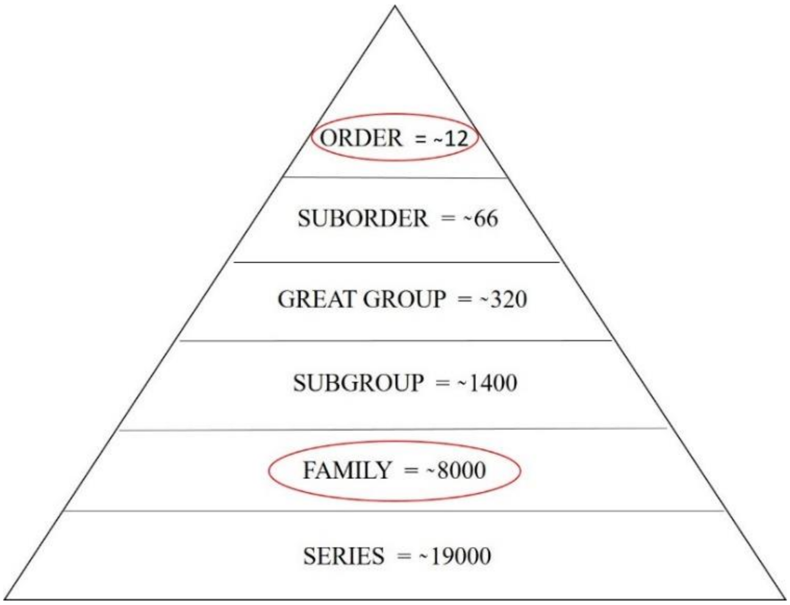

Figure 2.2: The hierarchical of soil classification system. The 12 soil order and soil texture by particle size distribution (Family) are the commonly used soil classification systems (circled; USDA and NRCS, 1999).

1. **Alfisols** - result from weathering processes that leach clay minerals and other nutrients. They are largely formed under forest or mixed vegetated cover.
2. **Andisols** - are formed from volcanic materials and are associated with unusually high water and nutrient retention capacity.
3. **Aridisols** - have low intensity in weathering processes and soil development. These dry soils are often found in areas with lack of moisture content (MC), such as deserts.
4. **Entisols** - occur in regions of recently deposited parent materials or in areas where deposition or erosion rates are higher than the rate of soil development. In these soil types, the pedologic horizons are not differentiated.

5. **Gelisols** – are common in areas of high elevations. They are notably identified by permafrost near the soil surface and cryoturbation in the subsoil.
6. **Histosols** - are identified by high content of organic matter and are found in areas rich in decomposed plant litter (e.g. wetlands and forests).
7. **Inceptisols -** have moderate degree of soil weathering and development, and are found in semiarid and humid environments.
8. **Mollisols** - form in climates that have a moderate or pronounced seasonal moisture deficit. They are identified by a dark colored surface horizon with relatively high organic matter content.
9. **Oxisols** - are found in stable land surfaces or areas that have been undisturbed for a long time. These highly weathered soils tend to have indistinct horizons that are dominated by low activity minerals such as iron oxides, quartz, and kaolinite.
10. **Spodosols** - are formed from weathering processes that strip a surface layer of reddish brown or black organic matter from the subsoil.
11. **Ultisols** – are formed from fairly intense weathering and leaching processes that result in clay enriched subsoil. Most of its nutrients are concentrated in the few uppermost centimeters of the pedologic horizons.
12. **Vertisols** - have a high content of clay minerals and a fairly high natural fertility. The conspicuous periodical cracks provide evidence of soil movement within the horizons.

In conformity to international classifications systems (e.g. USDA and NRCS), the South African classification system uses different diagnostic horizons or materials present in the soil profile as a guiding principle to construct a national taxonomic system (Weil and Brady, 2016). The 14 diagnostics horizon groups are, (1) Organic, (2) Humic, (3) Vertic and (4) Melanic for topsoil, (5) Silicic, (6) Calcic, (7) Duplex, (8) Podzolic, (9) Plinthic, (10) Oxidic,

(11) Gleyic for subsoil and (12) Cumulic, (13) Lithic and (14) Anthropic for young soils (Weil and Brady, 2016). Within the soil family, over 8000 soil types are differentiated by texture, mineralogy and temperature and are added to the horizon group name, or its abbreviation to form a two-name classification system (Weil and Brady, 2016). Under soil family category, particle size distribution (PSD) is another classification system that is commonly reported because of its importance in land management and plant productivity (Figure 2.2). In a given soil, PSD and texture assume added significance as they reflect the cumulative influence of individual particles on the overall soil properties (Weil and Brady, 2016). Even though different PSD soil classification systems are used to describe soil texture and its granulometric composition, all systems consistently describe four mineral particles sizes of gravel, sand, silt and clay (Figure 2.3).

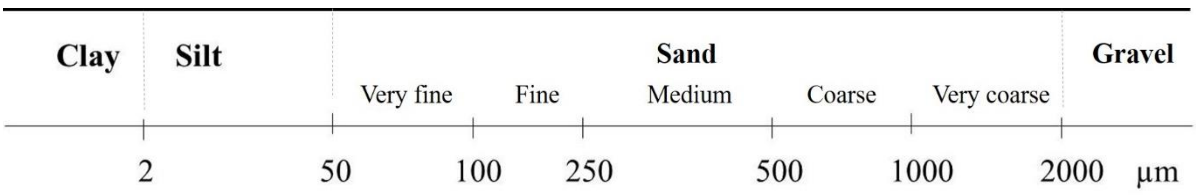

Figure 2.3: Classification of soil particles based on the United States Department of Agriculture System (USDA and NRCS).

1. **Sand-** These fractions are characterised by large pores between individual grains, a structure which results in a small surface areas per unit mass of soil. When wetted, sand grains are gritty with a loose structure and very little ability to stick or aggregate (Weil and Brady, 2016). As a result, soils with a higher percentage of sand have less supplemental storage of water and nutrients (Walczak *et al*., 2002; Esmaeilzadeh and Ahangar, 2014).

2. **Silt-** These are intermediate particles between sand and clay (2-50 µm) with transitional physical and chemical properties. Wet silt has a soapy texture with a relatively high aggregation tendency. Because of its structure and large surface areas, soil readily available water is mostly associated with silt (Walczak *et al*., 2002).

3. **Clay-** Compared to sand and silt, clay has the largest surface per unit mass of soil with microscopic pores between individual particles (Weil and Brady, 2016). Wetted clay particles are very sticky and can easily be moulded with less difficulty (Keller and Dexter, 2012). Since the adsorption of nutrients and soil aggregation are surface phenomena, clay grains hold water more tightly and retain the majority of nutrients held by mineral soil (Blanco-Canqui *et al.*, 2006; Seybold and Engel, 2008; Keller and Dexter, 2012; Esmaeilzadeh and Ahangar, 2014).

Since there can be an infinite combination of particle size percentage, a soil texture triangle has been formulated to conveniently group soil into 12 different textural classes (Figure 2.4).

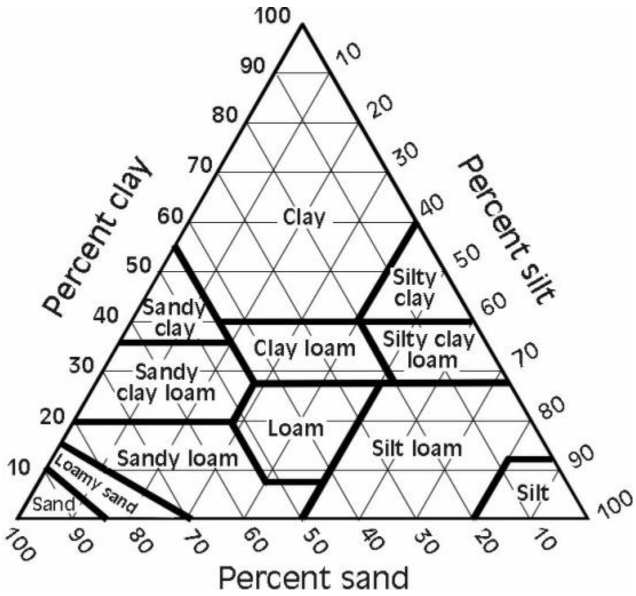

Figure 2.4: Soil texture triangle and classification based on the proportion of clay, silt and sand.

The three sides of a triangle represent increasing and decreasing percentages of clay, silt and sand. Soil texture is defined by locating the intersection point (soil textural name) from the percentage of clay (parallel horizontal line from left-right side), silt (downward slanting parallel line from right side-horizontal axis) and sand (upward slanting parallel line from horizontal axis-right side) (Weil and Brady, 2016).

2.1.3 Composition of SOM

Similar to plant tissues, SOM comprise of four major carbon-hydrogen organic compounds, carbohydrates, lignin, proteins and fats (Jobbagy and Jackson, 2000) (Figure 2.5). The proportion of organic compounds and the elemental composition contained in SOM vary depending on the source of plant litter and vegetation type (Kasozi *et al*., 2009; Martin and Thomas, 2011; Weil and Brady, 2016). Due to differences in the quality and decomposition rate of these organic compounds, the accumulation of SOM is a highly heterogeneous and complex phenomenon. For instance, woody material has high carbohydrate (cellulose and hemicellulose) and lignin content (Archibald and Bond, 2003; Weil and Brady, 2016), and soil rich in woody plant debris tends to be resistant to decomposition and often associated with long MRT. In addition to carbohydrates and lignin, organic compounds from non-woody plant tissue are generally rich in proteins and yield into easily decomposable nutrients such as nitrogen, sulfur, iron and phosphorus. Based on elemental analysis of dry weight tropical plant tissues, nearly all existing literature reports elemental composition of about 45-55% carbon, 40% oxygen and 8% hydrogen (IPCC, 2003; Gibbs *et al.*, 2007; Grossman, 2007; Martin and Thomas, 2011; Thomas and Martin, 2012; Weil and Brady, 2016).

When plant residues are added to the soil, microorganisms attack and derive energy from SOM, preferably from easily decomposable plant tissues to resistant woody plant materials. Through the process of heterotrophic respiration, CO_2 and water are also released as by-products. The easily decomposable proteins are broken down into amino acids and amides which are further reduced to readily available nutrients for plants (e.g. ammonia and nitrate; Weil and Brady, 2016).

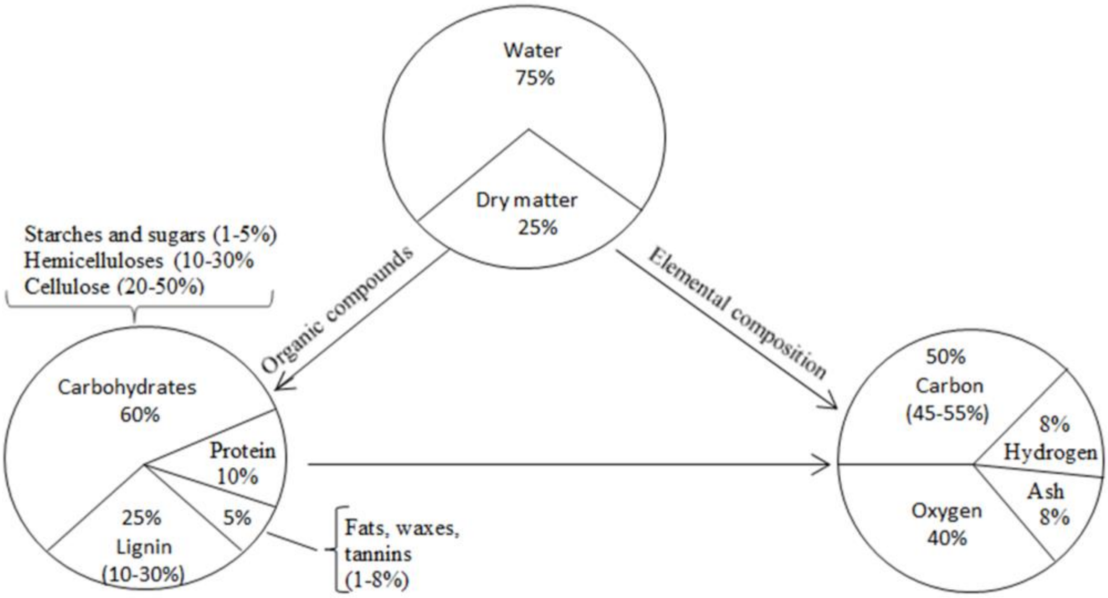

Figure 2.5: Representative organic and elemental composition of SOM. The proportion of organic compounds and elemental composition is based on the common ranges of soil plant residues (Weil and Brady, 2016).

2.2 Effects of SOM on physical and chemical soil properties

Soil organic matter comprises only approximately 5% of the total soil from 0-1 m depth, while SIM, water, and pore spaces represent the other arbitrary volume proportions of about 45%, 20-30% and 20-30%, respectively (Weil and Brady, 2016). Despite its relatively smaller proportion, SOM influences soil physical and chemical properties to a greater extent than the other components (Rawls *et al.*, 2003; Blanco-Canqui *et al.*, 2006; Dungait *et al.*, 2012; Yang *et al.*, 2014). Soil properties influenced by organic matter include: cation exchange capacity, water retention capacity, and soil structure e.g., soil plasticity and bulk density (BD). These properties are emphasised because they influence other properties (e.g. color, porosity and soil consistency) and the overall function, health and fertility of soils.

2.2.1 Cation exchange capacity

Soil organic matter and clay exist as colloidal fractions, where individual particles have a large surface area and are electrically charged. Unlike clay soil, SOM carries both negative and positive charges, an attribute that enables it to retain significant amounts of nutrients and water (Lal, 2005; Saiz *et al.*, 2012). Given that most essential plant nutrients exist as cations (ammonium: NH_4; calcium: Ca^{2+}; potassium: K^+; Magnesium: Mg^{2+}; Manganese: Mn^{2+}; iron: Fe^{2+} etc.), SOM and clay adsorb these ions by electrostatic forces. The ion trading of nutrients (cations) and H^+ from root respiration ensures a steady supply of nutrients and water to plants (Weil and Brady, 2016). The high cation exchange capacity (CEC) contributes to soil security by maintaining a stable granular structure which protects nutrients from leaching (Esmaeilzadeh and Ahangar, 2014; Weil and Brady, 2016).

2.2.2 Water retention capacity

Water retention capacity (WRC) is the total amount of moisture that soils can retain at field capacity. As a solvent which, together with soil cations, make up the soil solution, WRC regulates the amount of readily available water for transportation of nutrients and evapotranspiration (Weil and Brady, 2016). Because of variations in soil granulometric composition and volume composition of pore spaces, earlier findings on the effects of organic matter on soil WRC were contradictory (Hollis *et al.*, 1977; Lal, 1978; Kern, 1995). Recent studies have shown the importance of considering different proportions of clay, silt and sand when evaluating the effects of SOM on soil WRC (Rawls *et al.*, 2003; Yang *et al.*, 2014). From soils with the same percentage of clay and sand, Rawls *et al*. (2003) observed an increase in WRC with increased SOM content. However, there was a decrease in WRC with increased SOM for clay soils (>55% clay content). More recent findings have also reported similar strong correlations between SOM and WRC, but have highlighted its limitation in clay soil (Karhu *et al.*, 2011; Esmaeilzadeh and Ahangar 2014; Yang *et al.*, 2014).

2.2.3 Soil plasticity

Soil plasticity refers to the percentage of clay and a range of MC within which soil can be moulded (Dungait *et al.*, 2012; Keller and Dexter, 2012). Due to limited water lubrication, soil below the plastic consistency range is brittle and cannot be sheared without breaking. Above the wetting limit, the soil become a slurry as it tends to flow under gravity (Weil and Brady, 2016). According to the water film theory (Keller and Dexter, 2012), individual clay particles are surrounded by a water film which provides the needed lubrication and cohesive force to endure mechanic stress. Upon further wetting, water films coalesce, which results in less cohesive force (Lal 1978; Keller and Dexter, 2012). In practice, this mechanical behaviour provides synoptic information about soil texture and its ability to retain its original structure after disturbance. The influence of SOM on soil plasticity is often masked by the effects of soil texture (Keller and Dexter, 2012). For instance, Blanco-Canqui *et al*. (2006) and Seybold *et al*. (2008) found that SOM has no explicit or clear influence on the upper limit and plasticity index. A more robust methodological approach by Keller and Dexter (2012) on two soils of very similar texture demonstrated an isolated strong effect of SOM on plasticity. It further highlighted that SOM significantly reduce the cohesion force between individual clay particles, thereby decreasing the overall malleable property of the soil (Keller and Dexter, 2012; Weil and Brady, 2016).

2.3 Natural factors influencing SOM

In forest ecosystems without human disturbance (e.g. by deforestation and fire), biotic and abiotic factors responsible for the transformation, movement and partitioning of plant litter tend to be in dynamic equilibrium with each other (Caplow *et al.*, 2011; Kanowski *et al*., 2011; Robinson *et al.*, 2013). Parent material, topography, soil pH, vegetation type and climate are some of the natural factors operating within the soil hierarchical scale and naturally influencing the balance of SOM (Thomas and Pacham, 2007; Trouet *et al*., 2010; Kalaba *et al*., 2013).

2.3.1 Parent material and soil type

Typically, soils inherit physical, chemical and mineralogical properties of the underlying geology (USDA and NRCS, 1999; Bockheim *et al.*, 2014). As crystalline rocks become exposed over the Earth’s surface (Weil and Brady, 2016), they undergo mechanical and chemical weathering to form finely, medium or coarsely textured soils (Esmaeilzadeh and Ahangar, 2014; Weil and Brady, 2016). Since parent material determines the accumulation of carbonates (Weil and Brady, 2016), pH is one of the most important criteria of parent material specification which directly influence soil properties and fertility. Anderson (1988) provided a generalised rock stability ranking for weathering and soil formation from stable to less stable parent material: quartzite > chert > granite > basalt > sandstone > silt-stone > dolomite > limestone. Clayey soils (>55% clay) develop from less stable parent material, while soils with a high percentage of sand result from more stable rocks (Eckert and Sims, 1995; Kissel *et al.*, 2009). As earlier observed, these soil fractions are in different classification sizes because of the difference in structure and properties. For instance, finely textured soils from less stable rock retain large amounts of water and nutrients to support plant growth (e.g. seedlings) even in dry seasons (Eckert and Sims, 1995; Kissel *et al.*, 2009).

In contrast, the highly permeable coarse grained fractions allow water to infiltrate and leach cations, thereby reducing the soil pH (Eckert and Sims, 1995; Kissel *et al.*, 2009). As a result, soil genesis has a major influence on soil properties and the essential soil biological functions. Besides regulating soil texture, the degree of geological material (e.g. exposed rock) form a "funnelling-effect", which cause spatial and vertical heterogeneity in the distribution of SOM and water (Liu *et al.*, 2015).

2.3.2 Topography

Soil properties change across landscapes because of the modifying effects of topography and hydrology on soil forming and geomorphic processes (Liu *et al.*, 2015). Topography strongly influences the leaching of soil nutrients through translocation and redistribution of organic matter and fine soil particles across different landscape gradients. Soils tend to accumulate soluble ions (e.g. Ca, K, Mg and Na) from upslope and deposit at the footslope where leaching is less and soil enrichment is stronger (Johnson *et al.*, 2011; Dinka *et al.*, 2013). This directly affects composition of SOM, soil pH and microbial communities (Raghubanshi, 1992; Tsui *et al.*, 2004; Liu *et al.*, 2015). This is in agreement with Tsui *et al*. (2004) who reported marked variations in soil properties and a significant transitory increase in SOM and SOC across the catena.

2.3.3 Soil acidity

The two types of adsorbed cations, (1) hydronium (H_3O^+) and hydrogen (H^+), and (2) exchangeable bases have a contrasting effect on soil acidity and alkalinity. Soil pH is defined as the negative logarithm (base 10) of the hydrogen ion concentration (Eckert and Sims, 1995). This means that a unit increase in pH results in 10-times decrease in the concentration of H^+. The presence of carbonates, particularly sodium, calcium and magnesium is associated with the hydroxyl ions. Increase in the concentration of H^+ or decrease in soil pH imply a preponderance of hydrogen ions over hydroxyl ions (Weil and Brady, 2016). Acid soils are common in regions where precipitation is abundant, and in turn, leaches exchangeable bases. Decrease in soil pH leads to toxicity, where aluminium and manganese become soluble (Eckert and Sims, 1995; Kissel *et al.*, 2009; Weil and Brady, 2016). The uptake and assimilation of soluble aluminium and manganese results in restricted plant root growth, and decreased addition of belowground plant residues to the soil (Kissel *et al.*, 2009). Further, increased concentration of H^+ reduces microbial activities and the adsorption capacity of SOM (FAO, 2005).

2.3.4 Vegetation type

Through the addition and decay of plant debris, tree shoots are the main source of soil organic material (Trumbore and Czimczik, 2008; Maraseni and Pandey, 2014). Due to the different root networks and belowground biomass, the spatial and vertical partitioning of SOM differs by vegetation type (Holdo and Mack, 2014). Also, soil plant residues from plants or forests of different ages have organic compounds of diverse composition and quality which are associated with different decomposition rates (Trumbore and Czimczik, 2008; Ravindran and Yang, 2015; Weil and Brady, 2016). Previous work has shown that total SOM and SOC in the top 15 cm of the soil increase significantly with woody encroachment or conversion of agricultural areas and grasslands to forested areas (Murty *et al*., 2002; Maraseni and Pandey, 2014). Unlike herbaceous plants, forest ecosystems dominated by slow growing trees are associated with plant litter and SOM that act as long term carbon sinks (Archibald and Bond, 2003). A study by Coetsee *et al*. (2013) attributed SOM with long MRT to vegetation type and the development of fine root biomass. This has also been examined by Maraseni and Pandey (2014), and Hold and Mack (2014) who observed that forest soils of mixed species are richer in SOM than the less diverse root systems of single or few species.

2.3.5 Climate

Net primary productivity and accumulation of SOC in many terrestrial ecosystems are governed by precipitation and temperature regimes such as intensity and duration of wet and dry seasons (Wang *et al*., 2003; Edoga and Suzzy, 2008; Trumbore and Czimczik, 2008). Litter quality refers to the nutrient content such as carbon to nitrogen and lignin to nitrogen ratio. The amount of water available for NPP and the quantity of plant litter added to the soil vary primarily with rainfall intensity (Murty *et al*., 2002; Picard *et al*., 2012). A study by Trumbore and Czimczik (2008) showed that elevated temperature results in increased microbial activities and an exponential increase in the rate breakdown and decomposition of plant litter. Equilibrium between these natural factors creates an almost closed system of nutrient transfer between soil and vegetation. However, in human managed ecosystems, AGLB and the balance between accumulation and decomposition of organic matter are not only influenced by climate, but also by edaphic factors and human activities (Trumbore and Czimczik, 2008).

2.3.6 Changes in LULC composition and management practices

The LULC changes, especially urbanisation and conversion of forests to agriculture fields, have transformed a large proportion of the Earth's landscape (Foley *et al*., 2005; Pielke *et al.*, 2011; Schneibel *et al*., 2017a). Policymakers have failed to confront the paradox that although natural forests and forest based ecosystems services are essential, in many instances there are more pressing demands for the land that the forests occupy (Pielke *et al.*, 2011; FAO, 2012; IPCC, 2014). As human populations continue to rise, urban sprawl and the need for agriculture fields are inevitable changes (Shalaby and Tateishi, 2007; Dewan and Yamaguchi, 2009; Gibbs *et al.*, 2010; Hagazy and Kaloop, 2015). Since 1985, deforestation and conversion of forested areas to agriculture have enabled world crop productivity to double, with grain yield averaging over 2 billion tonnes yr^{-1} (Foley *et al.*, 2005). This is attributed to land practices such as soil tillage which speeds up decomposition and liberation of nutrients and higher CO_2 availability (FAO, 2005; Weil and Brady, 2016). As a result, croplands and pasture fields have become one of the largest terrestrial land cover (Foley *et al.*, 2005). Due to the unrelenting demand on forest land, the consequences of clearing forest include decrease in tree diversity and aboveground carbon storage (Foley *et al.*, 2005), disappearance of litter layer, reduction in soil microbial communities and a decline in per capita forest areas (Luoga *et al*., 2002; FAO, 2015). Nevertheless, forest assessments reports show that even though world's forest areas declined in the past 25 years (1990-2015) from 4.1 billion hectare to 4 billion hectare, there has been a reduced rate of forest loss in the last decade 2000-2010 (FAO, 2015).

Reduction in forest loss has been attributed to bush encroachment (Aide *et al.*, 2000; Hirota *et al.*, 2011; Poorter *et al.*, 2016), a phenomenon that results in natural succession of forests from unmanaged systems such as grasslands and agriculture fields (Scholes and Archer, 1997; Aide *et al.*, 2000; Ward, 2005; Wigley *et al*., 2009;). Bush encroachment is not ideal in areas of livestock farming as it reduces the carrying capacity of livestock (Ward, 2005; Brudvig and Asbjornsen, 2009). By convention, deforestation, grazing (Ward, 2005; Kotzé *et al.*, 2013; Holdo and Mack, 2014), changes in soil moisture, nutrients and differences in root distribution between grasses and trees are regarded as principal factors governing the covariation between grasslands and woody plants (Chidumayo, 1991, 2013; Stahle *et al.*, 1999; Chidumayo and Kwibisa, 2003). Based on the rooting niche separation (Ward, 2005;

Kotzé *et al.*, 2013; Holdo and Mack, 2014), field experiments have shown that mature trees outcompete grasses for nutrients and water, while grasses displace saplings and smaller trees (Hoffman *et al.*, 1990; Scholes and Archer, 1997; Ward, 2005). On the other hand, grazing effectively weakens the suppressive influence of herbaceous growth on saplings and forest regeneration (Ward, 2005; Kotzé *et al.*, 2013; Holdo and Mack, 2014). Even though bush encroachment has resulted in more than 50% of the global tropical forests being regenerating or secondary forests (FAO, 2010; Poorter *et al.*, 2016), these changes do not necessary reflect increasing forest biomass and carbon stocks (Chazdon, 2008). Understanding the dynamics of ecosystem succession is important for forest sustainability and in evaluating the ability of forest ecosystems to sequestrate and store carbon (Chidumayo, 1997; Flamenco-Sandoval *et al*., 2007; Blom *et al*., 2010; FAO, 2015).

2.4 Reducing deforestation and forest degradation

Tropical deforestation and forest degradation represent the second largest source of global greenhouse gas emissions, accounting for about 18-25% of annual emissions (Blom *et al*., 2010; Ghazoul *et al.*, 2010; Parker *et al.*, 2013). Under the UNFCCC, the REDD+ programme was developed to slow down the increasing trend of deforestation (UNFCCC, 2009; Ghazoul *et al*., 2010; Parker *et al*., 2013). This mechanism is designed to incentivise non-Annex 1 countries that demonstrate initiatives that reduce deforestation and forest degradation through (1) conservation, (2) sustainable management of forests, and (3) enhancement of forest carbon stocks (Ghazoul *et al.*, 2010). These initiatives are measured against counterfactual scenario (e.g. control sites) that represent the estimated rate of deforestation and degradation that would have occurred without REDD+ intervention (Lund and Treue, 2008). The livelihood dependency, local knowledge and physical proximity of forest-dwelling communities to natural forests suggest that the local communities are likely to be better custodians of forests and REDD+ initiatives (Lund and Treue, 2008). For this reason, community based forest management (CBFM), a form of participatory forest management (PFM) has been adopted as a model for implementing REDD+ activities (Lund and Treue, 2008; Blom *et al*., 2010). Thus, the co-benefits of REDD+ are extended beyond enhancement of forest carbon stocks, but also incorporates opportunities for sustainable economic development to communities that have the rights to forest carbon (Lund and Treue, 2008; Parker *et al*., 2013).

Given that the concept of carbon based PESs is nascent to the southern African countries, there is limited literature specific to Zambia and Southern Africa (Syampungani *et al*., 2014; Halperin *et al*., 2016; Tamene *et al*., 2016). Previous studies have manly focussed on the ecology and management of woodlands for sustainable livelihoods (Chidumayo, 1993; Chirwa *et al*., 2008; Pelletier *et al*., 2017). A review of REDD+ pilot projects from other countries within the region reflects a growing recognition of the significance of natural forests to the global carbon cycle, and their potential to provide economic benefits in the form of cash income and non-forest timber products (e.g. fruits) (Lund and Treue, 2008; Blom *et al*., 2010). Projects involving tree planting, and assisted and unassisted forest regeneration are gaining momentum in southern Africa. Evidence from the Nhambita Community Carbon Project in Mozambique shows the economic benefits of sustainable forest management, where rural communities received cash payments of USD 242.60 ha^{-1} for sequestrating over 0.5 $MtCO_2$-equivalent over a seven-year period (Jindal *et al*., 2008). For one hectare of forest cover, the payments averaged about USD 34.70 per household per annum. In Tanzania, an operational tree planting contract between local farmers and an NGO, International Small Group Tree Planting Program, has seen the forest dwelling communities earn USD 0.02 per tree per year since 1999. These and many other pilot projects provide a synopsis of the win–

win opportunities for increasing forest carbon storage and incentivising the participating local people.

2.4.1 Forest monitoring and assessment

In supporting climate change mitigation actions (UNFCCC, 2009), the Food and Agriculture Organisation (FAO) has implemented the Global Forest Survey (GFS) (FAO, 2015). The purpose of GFS is to establish an international and national network of monitoring strategies that deliver comparable and repeatable estimates of forest cover and forest carbon stocks (FAO, 2015). In accordance with this project, allometric models have been developed for the purpose of assessing forest volume and biomass with ease (Kanowski *et al*., 2011; Robinson *et al.*, 2013). The models are developed from destructive method which involves measuring tree characteristics, harvesting the whole tree and weighing the different tree components at fresh and oven dry weight (Stromgaard, 1985; Chidumayo, 1991; Chave *et al.*, 2005; Nickless *et al*., 2011; Picard *et al*., 2012).

According to Gould (1966), measurable characteristics of individual trees are statistically related. This biological rule is based on the ontogenic development of trees which extends to all species (Picard *et al*., 2012). If the tree cross-sectional area below a fork is not the same as the combined cross-sectional area of the branches above the fork, it would not be aligned with the tracheids transporting water and nutrients from the roots to the shoot (Gould, 1966). Therefore, regardless of size and species, the proportions between tree diameter at breast height (DBH) and the overall tree height, DBH and crown cover, and DBH and biomass, are always guided by this rule (Archibald and Bond, 2003). This principle has been widely adopted to develop allometric models from the most easily measurable tree characteristics (Archibald and Bond, 2003). Constructing allometric equations involves graphical exploration of the tree measured variables and selecting the model best fitting the datasets. The best model is defined by the least residual error, the sum of square error and root mean square error and the highest correlation coefficient. The models applicability are checked and validated by predicting observations independent of those used for fitting it (Nickless *et al*., 2011; Picard *et al*., 2012). Instead of using destructive sampling each time there is need to quantify tree or forest biomass, different allometric equations indicative of different tree species have been validated to accurately monitor, assess and verify changes in forest inventories with ease (Chave *et al*., 2005; Picard *et al*., 2012).

Given the vastness and diversity of forest ecosystems, field measurements and monitoring of forests is important, but cannot practicably be conducted at spatial scales that are commensurate with the LULC changes (Kanowski *et al*., 2011; Robinson *et al.*, 2013). Remote sensing, on the other hand, offers a practical and less labour intensive approach for estimating forest properties over large geographic areas (Gara *et al*., 2016). The approach is premised on the interaction between electromagnetic energy and the unique spectral signature of different regions of interest (Sims and Gamon, 2002; Gitelson *et al*., 2003; Poulain *et al.*, 2010; Shirima *et al*., 2015a). The spectral characteristics of different Earth's land cover types vary with wavelength (Figure 2.6). Leaf pigments (chlorophyll, carotenoids and anthocyanins), water, carbon and nitrogen are the main leaf constituents that affects the spectral reflectance measurements of vegetation (Sims and Gamon, 2002; Aggarwal, 2004). Due to variations in leaf pigments (Mayes *et al*., 2015), health vegetation have a low reflectance in the blue spectral band (0.45-0.50 μm), peaks in the green (0.50-0.57 μm) and decreases to a minimum in the red (0.62-0.70 μm) (Figure 2.6). Different vegetation types (e.g. tree and grass) are not clearly distinguishable in the visible region (0.40-0.70 μm) of the electromagnetic spectrum, but are distinctively defined in the near infrared band. The spectral properties of bare soil shows no marked variations with wavelength (Shahid *et al.*, 2010; Li *et al.*, 2013). Marginal differences in soil reflectance measurements are often associated with variations in MC, organic matter content, iron oxide content, and soil structure and texture (Aggarwal, 2004). On the other hand, the spectral signature of water is uniquely identified by high reflectance properties in the blue and/or green bands (0.48-0.57 μm) (Shahid *et al.*, 2010; Li *et al.*, 2013). Variations in turbidity due to the depth of water and suspended materials are factors that affect the reflectivity of water bodies (Aggarwal, 2004; Shahid *et al.*, 2010).

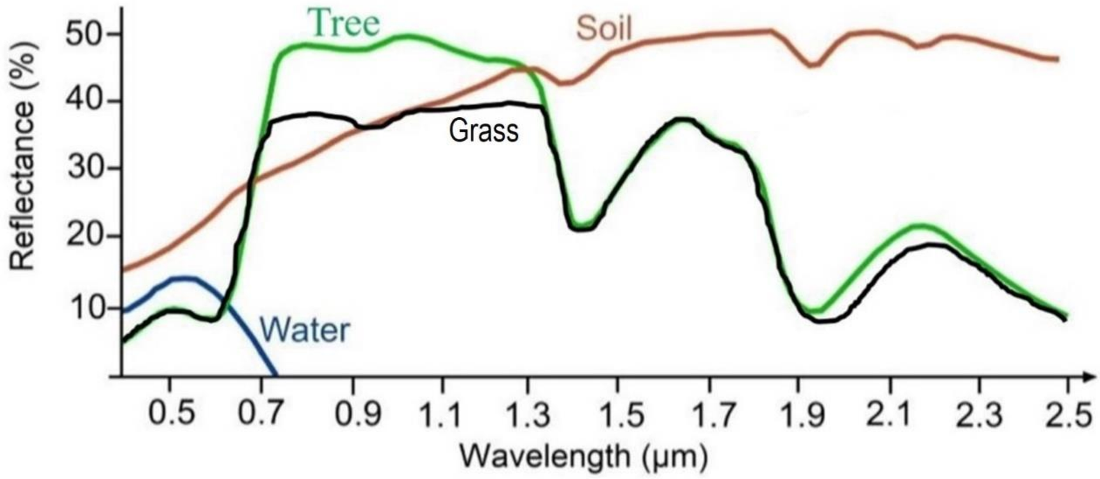

Figure 2.6: Spectral signatures representative of the major Earth's land cover types. The graph shows that different regions of interest have a unique interaction with electromagnetic radiation which makes them distinguishable within the fine wavelength intervals of the electromagnetic wavelength (Aggarwal, 2004).

Both forest ground measurements and remote sensing methods have limitations (Mayes *et al*., 2015), but each approach can inform the other to generate accurate estimates of forest resources (Goetz and Dubayah, 2011). The accuracy of remote sensing is achieved by linking and integrating field measurements with remote sensing data (Im and Jensen, 2008; Powell *et* *al*., 2010; Adam *et al.*, 2014; Schneibel *et al*., 2017b). This ensures that the costs and labour intensiveness associated with *in situ* measurements are replaced by fewer field measurements which can be extrapolated using repeated satellite optical reflectance and statistical spatial models (Im and Jensen, 2008; Powell *et al.*, 2010; Adam *et al.*, 2014). As a result, remote sensing has become a well-established, accurate, cost effective, rapid and reproducible technology for delivering measurable, reportable and verifiable forest inventory for REDD+ (Goetz and Dubayah, 2011; Croft *et al*., 2012; Gara *et al*., 2016; Schneibel *et al*., 2017b).

It is evident from the literature review that aboveground carbon storage and forest soil carbon stocks have been frequently studied, but are often reported separately (Dungait *et al*., 2012; Kalaba *et al*., 2014; Saiz *et al*., 2012; Kirsten *et al*., 2016). Further, the few published remotely sensed empirical models are site specific (Dube *et al*., 2016; Ene *et al*., 2016; Gandhi *et al*., 2015; Gara *et al*., 2016; Mayes *et al*., 2015; Shoko *et al*., 2016), which means that they are not applicable in forest ecosystems of different geographical area and climatic zone. This current study is different from the reviewed studies in that the model relating field estimates of carbon storage (0.50 x AGLB) and remotely sensed vegetation indices was developed from natural forest of different landscape and climatic zone, with different historic harvesting intensity. This will be useful and important in understanding the dynamics of forest change and factors that govern the functioning of natural forest ecosystems of southern Africa. The spatial-temporal data will also promote robustness and consistency in MRV forest changes, and will aid land managers in managing and evaluating the guided reconstruction of forests (e.g. assisted forest restoration projects) that are directed or prescribed by humans.

CHAPTER 3-MATERIALS AND METHODS

3.1 Study areas

The study was conducted in Luanshya on the Copperbelt Province, Zambia (13°08’26”S, 28°24’54”E) and the rural areas of Bushbuckridge in Mpumalanga Province, South Africa (24°38’48”S, 31°27’05”E) (Figure 3.1). The average altitude (1225 m above sea level) and spatial extent (54,232 hectares) of Luanshya formed part of the Zambian plateau or the high-flat to gently undulating landscape. Mean annual rainfall varies between 1200 mm and 1239 mm, while temperature ranges from 14.7°C to 28.3°C (www.world-clim.org). The Lowveld areas of Bushbuckridge were bordered by Kruger National Park and Manyeleti, Timbavati and Sabi Game Reserves. For safety concerns, only a total area (6194 hectares) covering Thorndale, Cortenburg and Seville was investigated. The undulating terrain of the three adjacent villages were characterised by an average altitude of approximately 600 m above sea level. It is a low rainfall area (mean of 550-600 mm yr^{-1}) with annual minimum temperature of 13°C and maximum temperature of 28°C (www.weathersa.co.za; www.world-clim.org). The underlying geology in both Luanshya and Bushbuckridge is largely Precambrian which includes Archean metavolcanics, metasediments of basement complex and intrusive granite gneisses and granite of different ages (MENR, 1994; CGS, 1997). Acrisols and some Ferrasols (equivalent to Alfisols and Ultisols in the USDA classification system) dominate the soil type in Luanshya (MENR, 1994; Frost, 1996), while Lithosols (equivalent to Entisols and Mollisols in the USDA classification system) is the dominant soil types in the Lowveld of Bushbuckridge (Rodger and Twine, 2002).

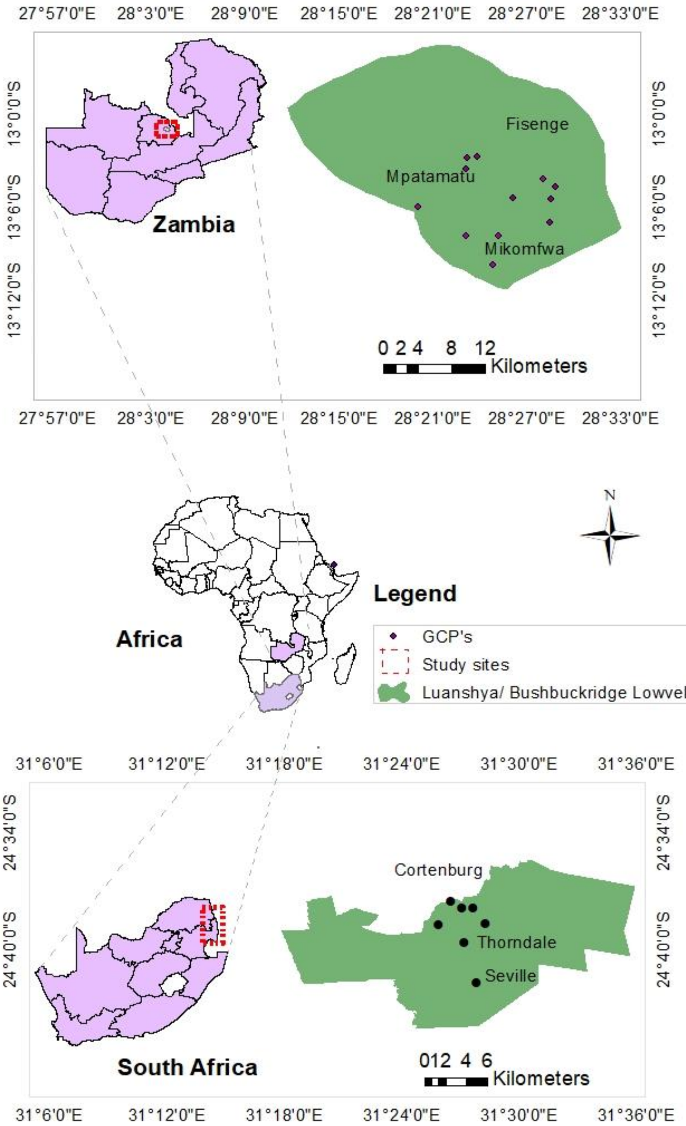

Figure 3.1: Study areas in Luanshya, Zambia and Bushbuckridge, South Africa. The map shows the map of southern Africa and the relative location of the study areas and some major ground control points (GCP) (source of GIS data: www.diva-gis.org).

Envisioned as a "garden town", Luanshya inherited a legacy of green space planning, development and conservation. Miombo woodland is the main vegetation type and form part of the most extensive natural forest type in Africa (approximately 2.7 million km^2 or 9% of continents land cover) which is found in regions receiving >700 mm of mean annual rainfall. The forested sites are uniquely identified by tree species in the family Fabaceae, subfamily Caesalpinioideae, especially in the genera *Brachystegia*, *Julbernardia* and *Isoberlinia*

(Chidumayo and Frost, 1996; Abbot *et al*., 1997). The introduction of mining activities in 1927 resulted in the clearing and conversions of forested areas to industrial and other non-vegetated areas. Towards the end of the 20th century (between 1990 and 1999), mining became increasingly uneconomic, causing significant economic recession in the area (Craig, 2001). With the majority of land under communal tenure where communities have rights to own land, the livelihoods of many households depended on Miombo woodlands as clearable and readily available land for agriculture, timber harvesting, and charcoal production (Chidumayo and Mbata, 2002; Lungu, 2008; Syampungani *et al.*, 2009; Mususa, 2010). To cope with the increasing population, small scale farming has developed into an important environmental, social and economic activity in the area. Maize (*Zea mays*), soya beans (*Glycine max*), wheat (*Triticum aestivum*) and groundnuts (*Arachis hypogaea*) are the commonly grown crops.

The savanna woodland of Bushbuckridge Lowveld (mean annual rainfall of <700 mm) is characterised by widely spaced trees and some patchy herbaceous layer of saplings and grasses. Described as a farming community, many households engage in some of form of subsistence agriculture and livestock farming, while the forested areas provide timber and non-timber forest products. The primary crops grown are maize (*Zea mays*), groundnuts (*Arachis hypogaea*), watermelon (*Citrullus vulgaris*) and beans (*Phaseolus vulgaris*) (Dovie *et al*., 2007). Extension of homes into cattle, goat and donkey ranches characterise most human settlements. Given the difference in climate between Zambia and South Africa, it is envisaged that the two study areas would provide a synoptic understanding of how the natural forests of southern Africa respond to different levels of forest disturbance and management. These study areas were chosen because they have the same LULC history, where the adjoining forests are both shaped by man through a long history of cutting. Furthermore, the nascent afforestation and reforestation initiatives makes the two areas ideal research sites for understanding the dynamics of carbon storage in forest ecosystems with different intensity of disturbance.

3.2 Landsat data acquisition

Landsat data from Multispectral Scanner (MSS), Thematic Mapper (TM) and Operational Land Imager (OLI) sensors were acquired from the Landsat archive of the United States Geological Survey (http://earthexplorer.usg.gov). These datasets were preferred because they are freely available with four-seven bands at 30-60 m spatial resolution and a repeated coverage of 16 days (Table 3.1). Because of differences in weather conditions, especially humidity, the percentage of cloud cover on the images was a decisive factor considered during the selection of Landsat images. Hence, the images and the assessed periods of LULC changes are not unified for the two study sites. Two datasets of six 185 km x 185 km cloudless scenes for Luanshya (1986, 1998, 2001, 2004, 2011 and 2016) and the Lowveld of Bushbuckridge (1992, 1998, 2001, 2006, 2010 and 2016) were downloaded using the world reference system (WRS) path 168 and 179, and row 077 and 069, respectively. Owing to the influence of different seasons and time of the day on the sun azimuth and angle of illumination, all datasets were acquired around 08:00 AM in winter months, between 29th April and 27th June for all years selected (Table 3.1).

Table 3.1: Characteristics of the acquired Landsat data

Sensor	Landsat MSS	Landsat TM	Landsat OLI	Date acquired
Scene ID: Luanshya	LM5172069**1986**129AAA03	LT5172069**1998**178JSA00	LC8172069**2016**132LGN00	09/05/1986 27/06/1998 11/05/2016
		LT5172069**2001**154JSA00		03/06/2001
		LT5172069**2004**147JSA00		26/05/2004
		LT5172069**2011**150JSA00		30/05/2011
Scene ID: Bushbuckridge	LM4168077**1992**142AAA04	LT51680771998134JSA00	LC8168077**2016**152LGN00	21/05/1992 14/05/1998 31/05/2016
		LT5168077**2001**126JSA0		06/05/2001
		LT5168077**2006**124JSA00		04/05/2006
		LT5168077**2010**119JSA00		29/04/2010
Spatial resolutions	60 m	30 m	30 m	
Temporal resolutions	16 days	16 days	16 days	
Spectral resolutions	4	6	7	
	Band 1: 0.55	Band 1: 0.49	Band 1: 0.44S	
Wave- -length (μm)	Band 2 : 0.55-0.65 Band 3: 0.65-0.76 Band 4: 0.76-0.92	Band 2: 0.49-0.57 Band 3: 0.57-0.66 Band 4: 0.66-0.84 Band 5: 0.84-1.68 Band 7: 1.68-2.22	Band 2: 0.44-0.48 Band 3: 0.48-0.56 Band 4: 0.56-0.65 Band 5: 0.65-0.86 Band 6: 0.86-1.61 Band 7: 1.61-2.20	

3.2.1 Image pre-processing

During scene capture, prevailing conditions such as variations in illumination, viewing geometry, weather conditions and sensor noise tend to cause distortions to reflectance measurements. These factors make raw or unrectified images of the same scene not readily comparable. Thus, the metadata files of all the imagery scenes were pre-processed or rectified for geometric, radiometric and atmospheric distortions using ENvironment for Visualising Images software (ENVI version 5.3).

3.2.1.1 Geometric correction

Motion of the sensor platform, rotation of the Earth and differences in altitude and terrain make remote sensing imagery inherently susceptible to geometric distortion. To compensate for these distortions, image auto-registration workflow in ENVI was used to geometrically align all the images to the same coordinate system so that corresponding pixels depict the same object on the ground. The auto-registration technique uses available spatial information from the two input images to geometrically correct the remotely sensed datasets to a common ground coordinate space. For each study area, the most recent image (2016) was used as the base image file, while historical images were individually selected as warp image files. Corresponding feature points or tie points were generated on the base image and located and matched on the warp images. The accuracy matching of individual tie points was defined by lower root mean square error (RMSE). The points with RMSE of greater than 0.30 were deleted and replaced. This was crucial in ensuring minimal error or deviation in the alignment of pixels. The accepted tie points were used to generate spatial parameters for geometric transformation of warp images which resulted in geometrically corrected images.

3.2.1.2 Radiometric calibration

To facilitate comparisons between images of the same scene collected by different sensors at different dates and times while maintaining a uniform illumination, all geometrically corrected images were calibrated to radiance and reflectance. Systematic radiometric calibrations were discretely performed on the two pairs of images. The procedure involved opening the metadata files in ENVI, selecting radiometric calibration and changing the calibration type to radiance before applying the operation. The pixel radiance values for all images were automatically computed using equation 3.1. Further, the procedure was repeated with the calibration type changed to reflectance. The pixel reflectance values were computed using equation 3.2. All calibrated images were investigated and verified by studying the spectral signatures of the different known features such as bare land, vegetation and water bodies.

$$L\lambda = \text{Gain} * \text{Pixel value} + \text{Offset} \qquad \text{Equation 3.1}$$

where $L\lambda$ is radiance, Gains and Offsets are default data values for each pixel and band in the images, all values in units of W/ (m^2 * sr * µm), and:

$$P\lambda = \pi\, L\lambda d^2/ESUN\lambda\ SIN\theta \qquad \text{Equation 3.2}$$

where $P\lambda$ is reflectance, $L\lambda$ is radiance and $ESUN\lambda$ is solar irradiance with both units in W/(m^2 * sr * µm), π is Pi=3.14, d is Earth's sun distance and θ is sun elevation in degrees.

3.2.1.3 Atmospheric correction

Before reflectance measurements are recorded by the sensor, solar radiation passes through the atmospheric layers twice. Thus, unrectified imagery includes spectral measurements or information of both the atmosphere and the Earth's surface. Removing atmospheric noise is an important step in image pre-processing. Fast Line-of-sight Atmospheric Analysis of the Spectral Hypercube (FLAASH) model was preferred and applied because of its ability to correct images of non-uniform landscapes obtained at vertical (nadir) and slanting viewing geometries (Kaufman *et al.*, 1997). The procedure involved applying FLAASH settings to each of the geometrically and radiometrically corrected files. The application of a single scale factor of 0.1 converted the imagery scenes to a floating-point format known as band interleaved line by pixel (BIL). From the BIL images, appropriate compensation parameters (e.g. sensor type, sensor altitude, ground elevation, pixel size, flight date, and time and scene options) were input into the model. The model iterated Equations 3.3 and 3.4 to rectify images for atmospheric noise. The first condition in Equation 3.3 corresponds to radiance that is reflected from the Earth's surface and recorded directly by the sensor, while the second condition relates to radiance scattered by the atmosphere (e.g. clouds and aerosols). Thereafter, the model applied Equation 2.4 to compute a spatially average radiance per pixel

(L_e) (Kaufman *et al.*, 1997). After atmospheric correction, spatial subsetting was applied to all pre-processed images to extract images covering 542.32 km^2 (54,232 ha) for Luanshya and 61.94 km^2 (6194 ha) for Bushbuckridge. In order to have images with comparable characteristics, the four-band multispectral images from Landsat MSS (for 1986 and 1992) with 60 m spatial resolution were resampled to 30 m resolution and seven bands by using the 2016 Landsat OLI data as base images.

$$L = \left(\frac{A\rho}{1-\rho_e S}\right) + \left(\frac{B\rho_e}{1-\rho_e S}\right) + L_a$$

(Equation 3.3)

$$L_e \approx \left(\frac{(A+B)\rho_e}{1-\rho_e S}\right) + L_a$$

(Equation 3.4)

where ρ is pixel surface reflectance, ρ_e is an average surface reflectance of each pixel and the surrounding pixels, S is the spherical albedo of the atmosphere, L_a is the radiance scattered by the atmosphere and A and B are coefficients or compensation parameters that depend on the atmospheric and geometric conditions.

Overall, the output of radiometric calibration (equations 3.1, 3.2) and atmospheric correction (equations 3.3, 3.4) was the conversion of raw digital numbers to top-of-atmosphere (TOA) reflectance, while the Fast Line-of-sight Atmospheric Analysis of Hypercube (FLAASH) model was applied to remove atmospheric noise or convert TOA reflectance to bottom-of-atmosphere (BOA) reflectance measurements (Kaufman *et al*. 1997).

3.2.2 Image classification: Deriving LULC maps

A classification method known as spectral pattern recognition was used to derive LULC maps. Hybrid classification approach involving unsupervised and supervised classification employed the spectral information represented by digital numbers (DN) to classify the raster layers into different LULC types. The initial classifications were based on 20 spectral classes generated using the unsupervised clustering technique, the Iterative Self-Organizing Data Analysis Technique (ISODATA). Owing to difficulties in validating past LULC types (e.g. Gandhi et al. 2015), the use of two different classifiers (using ENVI 5.3) was necessary to derive the required multi-temporal spectral classes (unsupervised classification) for past LULC types, while the use of supervised classification ensured high classification accuracy of both extant and past LULC classes. Unlike the ISODATA clustering technique which is often associated with some misclassifications, the kernel functions of the Support Vector Machine (SVM) technique was subsequently used to generate LUCL classification images from complex and noisy data (Karatzoglou et al. 2006; Kavzoglu and Colkesen 2009).

The SVM classifier is trained to find an optimal classification hyperplane through minimizing the upper bound of the classification error (Cortes and Vapnik, 1995). In a binary classification experiment, SVM maximizes the distance from the data points of each class to the optimal separating linear hyperplane axes created from each variable (Petropoulos *et al.*, 2011). Ideally, there are two supporting hyperplanes on the boundaries of the spectral data distribution and the data points on the edge of these hyperplanes are the support vectors of the algorithm. Since not all classes are linearly separable, SVM is optimised to search for a non-linear hyperplane using a non-linear kernel function such as polynomial and radial basis (Huang *et al.*, 2002; Oommen *et al.*, 2008). As a result, the classifier does not encounter any over-fitting problem (Burges 1998; Brown *et al.*, 1999; Cortes and Vapnik, 1995). Because the accuracy (overall accuracy and kappa coefficients) of LULC classification often vary depending on the classifier used, the reliability of the results was assessed by comparing the accuracy of the LULC maps generated from SVM with the maps produced from a traditional classifier, Maximum Likelihood (ML). With the aid of the 2010 land cover scheme II for Zambia and South African LULC scheme (RCMRD Geoportal, 2010; GeoterraImage, 2015), the 20 spectral classes were then regrouped into eight and six LULC classes in Luanshya and Bushbuckridge, respectively (Table 3.2).

More than 130 stratified random points per LULC class were generated on the Landsat scenes for 2016. In both study areas, field surveys were conducted between 26.11.2016 and 02.04.2017 to investigate the points by traversing the study areas and identifying and georeferencing the 20 extant (2016) spectral classes (of at least 30 m x 30 m spatial extent of homogenous LULC types) to an average positional error of ± 3 m using a hand-held Garmin Global Positioning System (GPS) device. In addition to the spectral pattern recognition and historical aerial images from Google Earth, the normalized difference vegetation index (NDVI) method was also used to identify and delineate the different spectral classes, and LULC types of historical datasets or past years (equation 3.5). Because the combination of reflectance measurements in the red and near infrared (NIR) is sensitive to the concentration of foliage chlorophyll, and structure and extent of vegetation cover, NDVI is well correlated with temporal changes in greenness (Gandhi *et al*. 2015). Negative NDVI values were associated with water bodies, while values of 0.0–0.1 corresponded to bare land, values of 0.2–0.39 to agriculture areas and grasslands, values of 0.40–0.59 to less dense woodlands, and values of >0.6 indicated dense woodlands (Craig, 2001). The 20 spectral classes were regrouped into eight LULC classes, and the reference data points for each image were divided into training (70%) and validation (30%) datasets.

$$\text{NDVI} = \frac{\text{NIR} - \text{Red}}{\text{NIR} + \text{Red}} \qquad \text{(Equation 3.5)}$$

where NIR and Red are reflectance measurements in the near infrared and red bands, respectively.

Table 3.2: Training and validation data set for the LULC classes

			AA	BL	BA	DW	GL	PA	RV	WB
Luanshya	1986	Training dataset		261	49	273	436	345	310	250
		Validation dataset	-	112	21	117	187	148	133	107
		Total	-	373	70	390	623	493	443	357
	1998	Training dataset	107	425	229	289	278	273	259	257
		Validation data set	46	182	98	124	119	117	111	110
		Total	153	607	327	413	397	390	370	367
	2001	Training data set	161	366	135	278	233	226	252	257
		Validation dataset	69	157	58	119	100	97	108	110
		Total	230	523	193	397	333	323	360	367
	2004	Training data set	268	371	229	294	245	376	189	257
		Validation dataset	115	159	98	126	105	161	81	110
		Total	383	530	327	420	350	537	270	367
	2011	Training data set	266	264	161	264	254	322	296	257
		Validation dataset	114	113	69	113	109	138	127	110
		Total	380	377	230	377	363	460	423	367
	2016	Training data set	266	266	296	280	254	322	296	257
		Validation dataset	114	114	127	120	109	138	127	110
		Total	380	380	423	400	363	460	423	367
Bushbuckridge	1992	Training data set	-	191	-	266	425	210	-	224
		Validation data set	-	82	-	114	182	90	-	96
		Total		273	-	380	607	300	-	320
	1998	Training data set	77	154	-	126	240	247	-	191
		Validation data set	33	66	-	54	103	106	-	82
		Total	110	220	-	180	343	353	-	273
	2001	Training data set	250	72	-	264	310	238	-	336
		Validation data set	107	31	-	113	133	102	-	144
		Total	357	103	-	377	443	340	-	480
	2006	Training data set	266	266	-	245	268	250	-	408
		Validation data set	114	114	-	105	115	107	-	175
		Total	380	380	-	350	383	357	-	583
	2010	Training data set	247	250	-	240	257	233	-	252
		Validation data set	106	107	-	103	110	100	-	108
		Total	353	357	-	343	367	333	-	360
	2016	Training data set	306	89	-	91	345	252	-	205
		Validation data set	131	38	-	39	148	108	-	88
		Total	437	127	-	130	493	360	-	293

Where AA=agricultural areas, BL=bare land, BA= built-up areas, DW=dense woodlands, GL=grassland, RV=riparian vegetation and WB=water bodies.

3.2.3 Post classification

In Luanshya, eight LULC classes were discerned: agricultural areas, bare land, built-up areas, dense woodlands, grasslands, paved areas, riparian vegetation, and water bodies (Table 3.3). The pixels of the six remotely sensed images for Bushbuckridge were clustered into six LULC classes: agricultural areas, bare land, dense woodlands, grasslands, paved areas, and water bodies (Table 3.3). A total of between 818-1009 reference points were used to derive confusion matrices which reported producer accuracies (PA), user accuracies (UA), overall accuracies and Kappa coefficients of the LULC maps generated from SVM and ML methods Confusion matrices were subsequently constructed for each Landsat scene to compute the UA, PA, overall accuracy and kappa statistic. Overall accuracy, which is expressed as a percentage, represents the probability that a randomly selected point is classified correctly on the map. The kappa coefficient provides a measure of the difference between the actual agreement between reference data and the classifier used to perform the classification versus the likelihood of agreement between the reference data and a random classifier. The PA indicates the probability that the classifier has labelled an image pixel into a correct LULC class, or vice versa for UA.

Table 3.3: Description of LULC classes

Classes	Description	LY	BB
1. Agricultural areas	: Rectilinear landscapes defined by distinct boundaries of regular straight boarders covered by ploughed fields, crop fields, bare land and pasture	✓	✓
2. Bare land	: Areas varying from very low vegetation to completely non-vegetated areas. It includes exposed soils due to active excavations (e.g. mine dumps and other mining activities)	✓	✓
3. Built-up areas	: Real estate developed areas with commercial or residential structures	✓	X
3. Dense woodlands	: Woody forested areas with NDVI >0.40	✓	✓
4. Grasslands	: Herbaceous plants with no persistent above-ground biomass characterised by the co-existence of shrubs and grasslands, and sparse trees	✓	✓
6. Paved areas	: Hard surfaced areas such as gravelled areas and concrete paving	✓	✓

Table 3.3 (*continued*)

7. Riparian vegetation	: Biomes (woody and grassy ecosystem) growing along permanent and seasonal low lying areas such as streams, dams or river margins banks. Unlike the dense woodlands, the vegetation was largely dominated by *Phragmites australis* species.	✓	X
8. Water bodies	: Permanent and perennial open water reservoirs (e.g. dams, and lakes)	✓	✓

Where LY is Luanshya and BB is Bushbuckridge and the ticks denotes the LULC types present (✓) or absent (X) in each study area.

3.2.4 LULC change detection method

Change detection metrics were used to identify, quantify and describe multi-temporal differences in the generated LULC maps from SVM method. With two images representing an “initial” and “final” state, the analysis identified and quantified LULC classes and the number of pixels that changed from the former to the latter state. From the LULC maps, five change metrics were generated for each study area, 1986-1998, 1998-2001, 2001-2004, 2004-2011 and 2011-2016 for Luanshya, and 1992-1998, 1998-2001, 2001-2006, 2006-2010 and 2010-2016 for Bushbuckridge (Figure 3.2). Information from LULC maps and change matrices was used to evaluate differences in the images. From the changed and unchanged areas of each LULC type, trajectories of LULC changes and different forest succession stages were developed for each observed period. This provided interactions (intensities of change) and linkages (transitional pathways) between the different LULC types. The rates of forest cover change due to deforestation and reforestation were estimated using a standardised equation 3.6 devised by Puyravaud (2003):

$$r = \left[\frac{1}{t_2 - t_1} \ln\frac{A_2}{A_1}\right] \times 100 \qquad \text{(Equation 3.6)}$$

where r is the rate of forest change (units in percentage per year), ln is the natural logarithm function of A_1 and A_2 or the areal extent of forests at time t_1 and t_2, respectively. Deforestation rates were calculated from the total forest areas in the initial state (A_1) and unchanged areas (A_2), while reforestation rates were calculated from unchanged areas (A_1) and the total area in the final state (A_2).

Further, two digital elevation models (DEM: each covering the study area in Luanshya and Bushbuckridge) with spatial resolution of 30 m were derived from the US interagency Elevation Inventory (http://opentop.sdsc.ed) to provide the topographic features of the study sites. Image registration technique in ArcGIS 10.4.1 was used to geometrically align the DEM to the coordinate system of Landsat images.

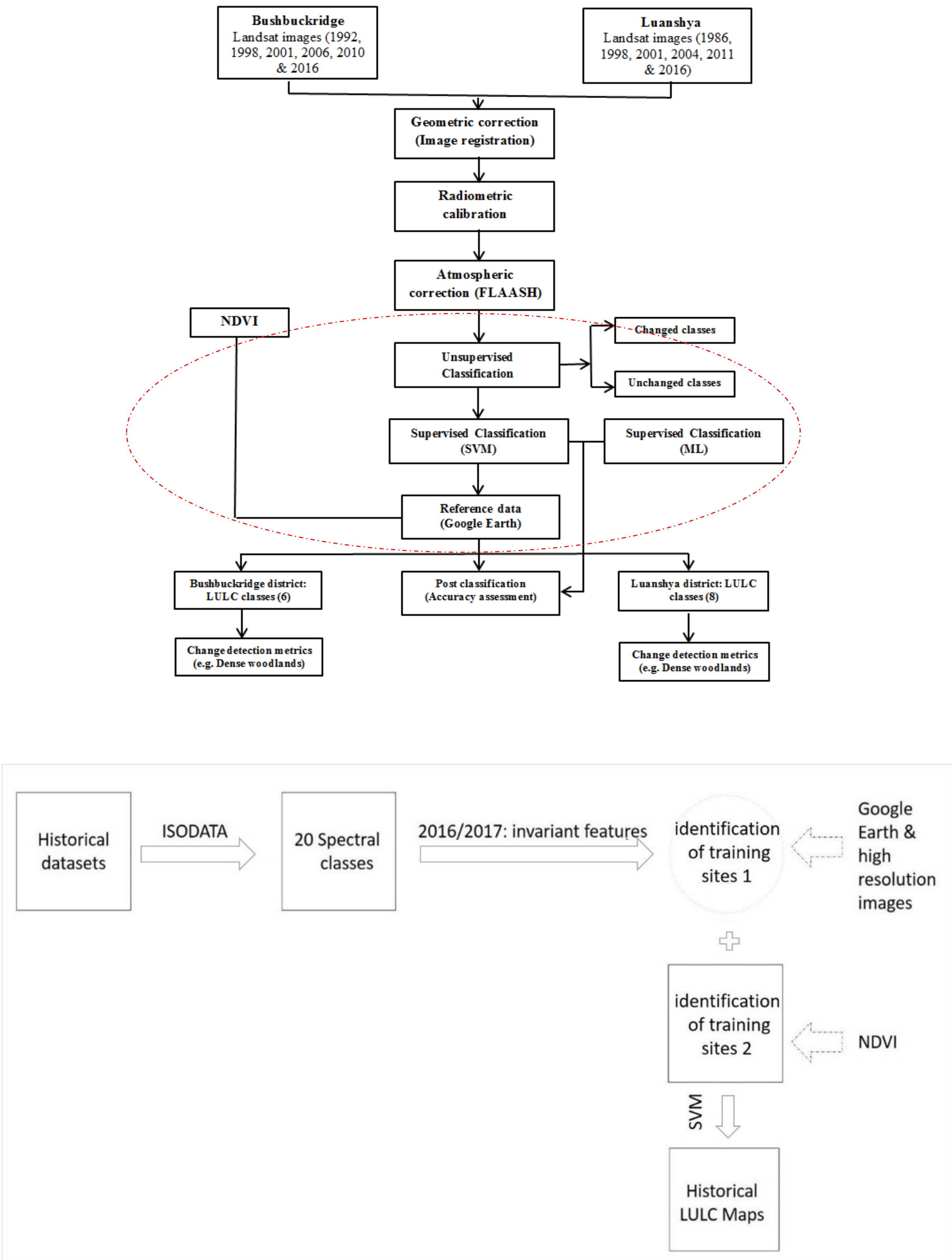

Figure 3.2: Flowchart of methodology used in quantifying LULC changes. The enlarged portion of the flowchart highlights the methodology used to generate training sites and LULC maps for historical datasets.

3.3 Field data collection

A stratified sampling approach was implored, where field measurements and samplings were done in seven 90 m x 90 m forest sites in both study areas. In order to extrapolate and map multi-temporal carbon stocks from the highly variable AGLB, sites with diverse forest cover were discreetly selected from a total of 126 generated stratified points (Luanshya: 63; Bushbuckridge: 63). The selected sites had a wide range of mean NDVI values (0.41-0.87) and temporal standard deviations (0.04-0.12). The centre coordinates of the identified forest sites were extracted from the LULC maps and located in the field by means of GPS navigation. Once positioned, a hand held Garmin GPS was again used to find and mark the central points to an average horizontal positional error of ± 3 m (Figure 3.3). With the use of materials such as a magnetic compass, measuring tape, ranging poles and a 500 m rope and help from two research assistants, north-south transects were set and marked 45 m to the north and south of the navigated points. The resulting north-south transects (90 m) were used as reference for marking and nesting the sampling sites with nine 30 x 30 m plots where quantifiable tree characteristics and soil were measured, sampled and recorded (Figure 3.3).

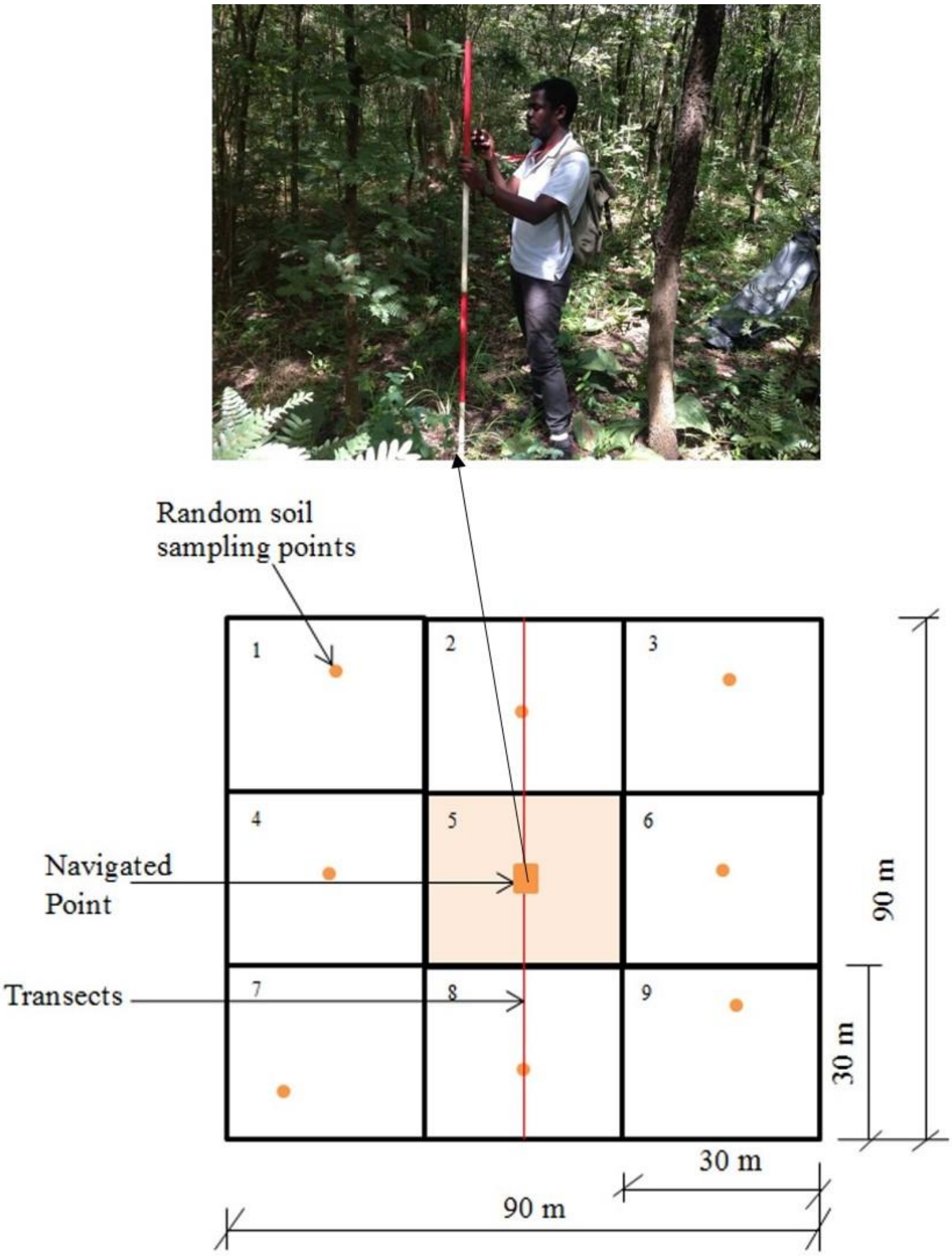

Figure 3.3: Sampling design for forest field measurements. North-south transects measuring 90 m were set from the navigated centre points. From the seven forest sites, sampling quadrats measuring 90 x 90 m were nested with nine-30 x 30 m sample plots which corresponded to the Landsat 30 m spatial resolution.

3.3.1 Species diversity and measurements of forest tree characteristics

All the tree species in the middle plot (plot-5) of each forest site were identified and recorded (Figure 3.3). Plant field guide books and a traditional botanist were used and engaged in identifying tree species. Trees that were difficult to identify were quoted by their local names of which their botanic name were looked-up from different research engines and the herbarium in Life Sciences Museum at University of the Witwatersrand. Under each forest site, the diameter of all individual trees per plots (30 x 30 m) were measured at breast height (1.3 m) using a diameter tape, whereas tree heights were calculated using a clinometer. Multi-stemmed trees with lower branching (<1.3 m) were counted and measured as separate trees. The measured forest tree characteristics were analysed using descriptive statistics and analysis of variance (ANOVA). Furthermore, the extent of variability in DBH and tree height within each site were assessed using relative standard deviation or coefficient of variation (CV), which is expressed as the ratio of standard deviation to the mean (Holdo and Mack, 2014). Forest species composition, which include species richness, diversity and evenness were calculated using the Simpson diversity index (Williams *et al.*, 2008; Kalaba *et al.*, 2013) (Equations 3.7 and 3.8):

$$D = 1 - \frac{\Sigma n_1(n_1 - 1)}{N(N-1)} \qquad \text{Equation 3.7}$$

$$E = \frac{n_i}{N} \qquad \text{Equation 3.8}$$

where D is the Simpson diversity index, E is evenness or dominance of a specific tree species, n_i is the tree count of each specific species and N is the total number of individual trees (population) per plot.

3.3.2 Estimating AGLB

For each plot, total AGLB was estimated by applying general allometric equations to the measured variables (DBH and/ or tree height) of all the individual trees per plot. The consistence of the results were assessed by comparing estimates from three different allometric equations developed by Stromgaard (1985), Chidumayo (1991) and Nickless *et al*. (2011) (equations 3.9-3.11). The three models were selected from the globallometree web platform (www.globalallometree.org) and were preferred because they were developed from the tropical dry forests of southern Africa with landscape and climatic conditions similar to that of Luanshya (for Stromgaard, 1985; Chidumayo, 1991) and Bushbuckridge (for Nickless *et al*., 2011). Further, the measured variables from Luanshya and Bushbuckridge were within the modelled range of the fitted and validated forest tree parameters (e.g. DBH and height size range). This means that the average biomass estimates from the three allometric equations were calculated and correlated to vegetation indices (VIs). The nine sample plots per site were split into six plots (plots 1-6) of training datasets (67%) and three plots (plots 7-9) of testing dataset (33%). Simply put, regression models were developed by relating AGLB from a total of 90 forest sample plots (from both Luanshya and Bushbuckridge) and vegetation indices (VI's). Conversely, biomass estimates from a total 36 sample plots were used for assessing the predictive power of the regression models using the allometric equations:

$$M = [(DBH^{1.382}) * (H^{0.640})] / 2.76 \qquad \text{(Stromgaard, 1985) (Equation 3.9)}$$

$$M = 23.34 *(DBH) -218.34 \qquad \text{(Chidumayo, 1991) (Equation 3.10)}$$

$$Ln (M) = a + b \ln (DBH) \qquad \text{(Nickless et al., 2011) (Equation 3.11)}$$

where M is biomass of an individual tree (kg), H is tree height (m), ln is the natural logarithm and constants: a = -3.47 and b = 2.83.

3.3.3 Developing regression model between forest biomass and vegetation indices

From the 2016 Landsat images, five VIs were calculated from the spectral reflectance measurements of the forests region of interest (ROI; Table 3.4). The five vegetation indices used were: (1) simple ratio (SR), (2) difference vegetation index (DVI), (3) NDVI, (4) enhanced vegetation Index (EVI), and (5) soil adjusted vegetation index (SAVI). The VIs were calculated from the reflectance measurements in near infrared, red and blue spectral bands (Table 3.4). The VIs were used as permutable independent variables, while the quantified totals of AGLB per plot were used as dependent variables. The best fit simple linear regression model was characterised by the highest coefficient of determination (r^2) and the smallest value of root mean square error (RMSE). The regression equation of the best fitting model was used to extrapolate and map the 2016 forest carbon stocks as well as 1986, 1998, 2001, 2004 and 2011 for Luanshya, and 1992, 1998, 2006 and 2010 for Bushbuckridge.

Table 3.4: Vegetation indices used in developing regression models

	Vegetation Index	Expression	Reference
1.	SR	$\mathrm{NIR}/\mathrm{Red}$	(Birth and McVey, 1968)
2.	DVI	$\mathrm{NIR} - \mathrm{Red}$	(Tucker, 1979)
3.	NDVI	$(\mathrm{NIR} - \mathrm{Red})/(\mathrm{NIR} + \mathrm{Red})$	(Rouse *et al.*, 1974)
4.	EVI	$2.5 * (\mathrm{NIR} - \mathrm{Red})/(\mathrm{NIR} + 6 * \mathrm{Red} - 7.5 * \mathrm{Blue} + 1)$	(Huete *et al.*, 2002)
5.	SAVI	$1.5 * (\mathrm{NIR} - \mathrm{Red})/(\mathrm{NIR} + \mathrm{Red} + 0.5)$	(Huete, 1988)

3.4 Mapping and assessing changes in forest carbon stocks

Mapping forest carbon stocks involved systematic conversions of individual pre-processed images, where three mathematical expressions were applied in ENVI band math tool. Firstly, the reflectance measurements were converted to VI single band images. This was achieved by applying the expression of the best fitting VI to the raster layers. Non-forested LULC areas were masked-out, where binary values of 1 were assigned to forest cover, while non-forested areas were given the value of 0. Since any number multiplied by zero equals zero, the VI of single band images were multiplied by the masked images so as to generate raster layers that excluded non-woody areas.

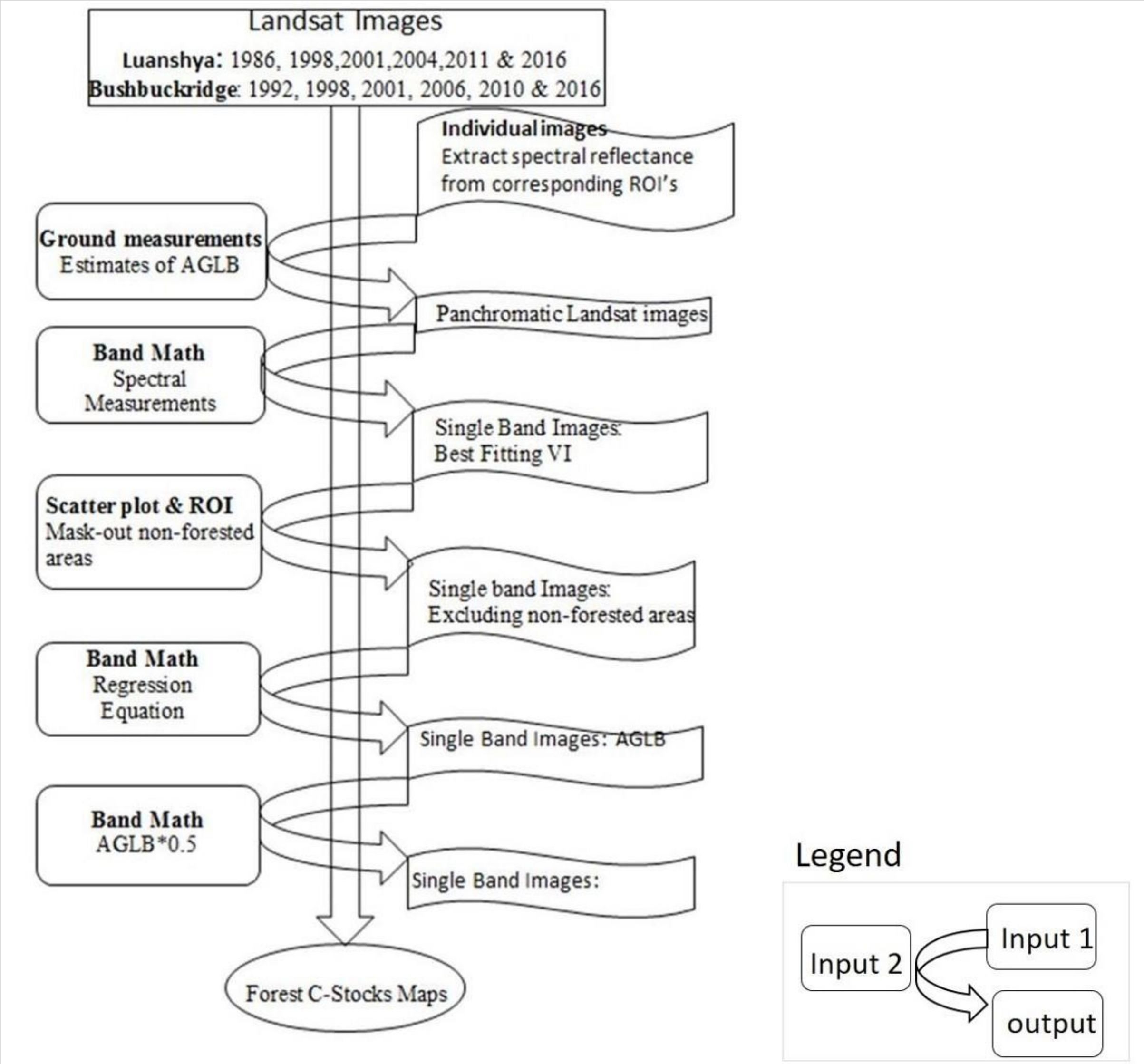

Figure 3.4: Flow chart for generating forest carbon stock maps for 1986, 1998, 2001, 2004, 2011 and 2016 for Luanshya, and 1992, 1998, 2006, 2010 and 2016 for Bushbuckridge.

Secondly, based on the highest regression coefficient, and the lowest mean absolute error (MAE) and root mean square error (RMSE), the equation of the best fitting regression model (relating AGLB per plot and vegetation index) was used to convert the VI single band images to imageries of AGLB using the methodology presented in Figure 2.4. Owing to the variability of carbon content (45% and 55%) in tropical forests (Grossman, 2007; Martin and Thomas, 2011; Thomas and Martin, 2012), the study assumed that 50% of the assessed AGLB was carbon. Thus, the single band images of AGLB were converted to carbon stocks by multiplying them by a conversion factor of 0.50. Afterwards, the images were used to generate time series forest carbon stock maps (Figure 2.4). The digital values of all the pixels were extracted from the forest carbon stock maps and analysed in R-statistical package. Changes in forest carbon stocks and sequestration capacity were evaluated by comparing spatial-temporal carbon stock values at the 10^{th}, 25^{th}, 50^{th}, 75^{th} and 90^{th} percentile level.

Observed climate records from the weather stations and high resolution data from the Climate Forecast System Reanalysis (CFSR) were acquired and related to spatial-temporal changes in forest VI. The datasets were obtained from the respective weather service (www.weathersa.co.za; www.zmd.gov.zm) and the National Centers for Environmental Prediction (NCEP) (http://globalweather.tamu.edu). Observed data (weather stations) had many gaps or missing records that were complemented by datasets from NCEP. Climate datasets were acquired from the closest weather stations situated in Ndola and Mpongwe which are located approximately 36.4 km and 60.9 km to the north-east and south-west of Luanshya, and the stations in Hoedspruit and Skukuza which are about 81.5 km and 90.6 km to the north-west and south-east of Thorndale village, respectively. The datasets were for the periods 1981-2016 in Luanshya and 1987-2016 in Bushbuckridge, and the mean daily rainfall, and maximum and minimum temperature from two weather stations per study area were related to changes in vegetation index (best explaining variations in aboveground forest carbon stocks).

3.5 Soil sampling

Two types of soil samples namely, undisturbed soil core samples (14) and disturbed composite (378) samples were collected from the two-63 forest plots by core and auger sampling methods, respectively (Figure 2.5). From the middle plot of each sampling site, soil pits measuring 30 cm x 30 cm x 30 cm were dug. The walls of the pits were evened-out, described and metadata such as site location, rooting depth and soil profiles recorded. A 311.15 g stainless steel cylinder measuring 19.70 cm long by 3.70 cm diameter (ø) wide was completely and carefully driven or hammered horizontally into the walls of the pits (until the ring of the cylinder were flush with the walls of the pits) at three different levels of soil depth (0-10 cm, 10-20 cm, 20-30 cm). From each depth, the core sampler was carefully excavated while retaining undisturbed soil. After levelling the protruding soil at both ends, field or wet mass estimates of the cylinder (filled with soil) were determined for all undisturbed soil samples using an electronic balance (Figure 2.5a-c). This sampling technique provided undisturbed samples from which soil BD the mass of soil per unit volume was calculated. Five additional samples of up to 30 cm depth were also randomly sampled within each plot using a soil auger (Figure 2.5d-f). After sampling soil from 0-10 cm depth, a soil auger was lowered into the same bored holes to extract soil from 10-20 cm, and then 20-30 cm depth. Taking into account the variability of soil properties, soil of the same depth and plot were pooled as composite samples, where <500 g of disturbed samples were collected in total. Both undisturbed soil core samples and disturbed composite samples from the sampling units of different soil depth, plots and sites were secured in zipper bags which were labelled (location, plot number, soil depth, sample type and wet mass). A total of 392 soil samples (from Luanshya and Bushbuckridge) were taken to the Environment laboratory in the School of Geography, Archaeology and Environmental Studies, University of the Witwatersrand.

Figure 3.5: Forest soil sampling in Luanshya and Bushbuckridge. The figure shows (a, b) core sampling method and (c) determination of field or wet mass of undisturbed soil, and (d) auger sampling method, (e) compositing soil of the same depth and plot and (f) weighing of wet soil using a field electronic balance.

3.5.1 Calculations: Laboratory soil processing

Soil samples were processed according to the standard operating procedure by the International Centre for Research in Agroforestry (ICRAF). This involved (1) air drying the soil samples by spreading them on a paper plate, (2) breaking up clods to aid drying and leaving them to air-dry in the laboratory for one/two weeks, (3) describing soil colours using Munsell soil color chart, (4) determining air dry mass, and (5) sieving the samples through a

2 mm mesh size sieve. Fragments (e.g. gravel and plant or woody materials) retained on the 2 mm sieve (coarse fractions) were weighed, recorded and disposed of. The proportion of coarse fragments were calculated per soil sample as a function of total air dry mass (coarse + fine fractions) using equation 3.12. Subsamples of fine fractions (<2 mm) were oven dried to a constant weight by putting the samples on metal plates and setting the oven to 105°C for 48 hours. For each sample, the percentage estimates of MC were determined using equation 3.13, while soil bulk densities for each site was calculated from oven-dry material collected using a core sampler of known volume (ø 3.70 x 19.70 cm or 211.71 cm^3). The use of a core sampler ensured that bulk density for 0-1- cm, 10-20 cm and 20-3 cm was estimated from undisturbed soil samples or soil in its natural undisturbed state (equation 3.14).

$$\text{Gravel (\%)} = \left[\frac{\text{Mass}_{\text{coarse}}}{\text{Mass}_{\text{Total air dried}}} \right] \times 100 \qquad \text{Equation 3.12}$$

$$\text{MC (\%)} = \left[\frac{\text{Mass}_{\text{wet}} - \text{Mass}_{\text{oven}}}{\text{Mass}_{\text{oven}}} \right] \times 100 \qquad \text{Equation 3.13}$$

$$\text{BD (g cm}^{-3}\text{)} = \frac{\text{Mass}_{\text{oven + coarse}}}{\text{Volume}_{\text{cylinder}}} \qquad \text{Equation 3.14}$$

where Mass $_{\text{coarse}}$ are soil fragments >2 mm, Mass $_{\text{Total air dried}}$ is the total weight of air dried coarse plus fine fractions, Mass $_{\text{wet soil}}$ is the weight of soil determined in the field, Mass $_{\text{oven dry soil}}$ is the constant weight of soil samples after oven drying (105 °C), Mass $_{\text{oven + coarse}}$ is the weight of oven dry mass plus weight of coarse fractions, volume $_{\text{cylinder}}$ is the known volume of 211.71 cm^3.

The particle size distribution (PSD) in soils was analysed from air dried fine fractions of less than 2 mm using a Mastersizer 3000 laser granulometer (Figure 3.6). The instrument uses laser diffraction to measure PSD from 10 nm to 3.5 mm. As dispersed particles repeatedly pass the beam processing unit, the parallel laser beams are scattered in different angles according to the geometric size of the individual particles. The recorded volume data are premised on the principle that small particles scatter light at relatively larger angles than big particles. Because the measurement sequence consisted of the background measurement and five consecutive analyses per cycle, the instrument provides rapid and reliable particle size measurements. The results of each analysis were descriptive statistics of PSD, histograms of relative volume (%) plotted against particle size (µm) and soil texture classification. Before the start of each consecutive analysis, a cleaning procedure was followed to flush previous particulates.

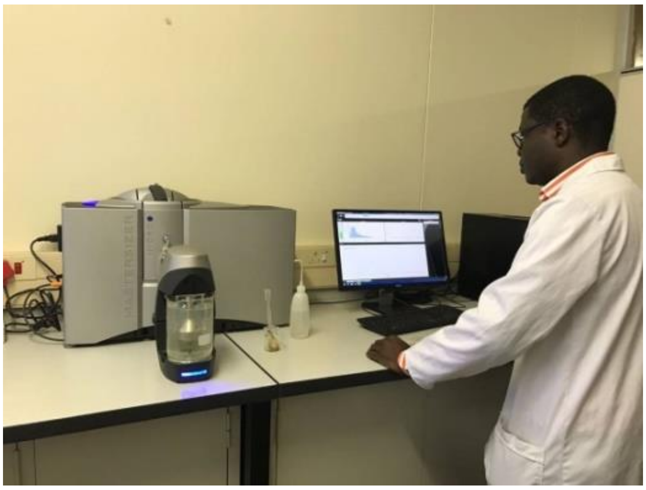

Figure 3.6: Determination of soil particle size distribution using laser diffraction, Mastersizer 3000.

Soil pH and electrical conductivity (EC) were measured from soil-water suspensions using a Yellow Spring Instrument (YSI Professional Plus). A procedure described by Eckert and Sims (1995), and Kissel *et al*. (2009) was followed where test tubes were filled with deionised water and subsamples of air dried fine fractions to the ratio of 1:1. Measuring 40 mL (deionised water) and 40 g (fine fractions), the test tubes were vigorously stirred at 50 revolutions per minute for one-hour using a mechanical shaker. Prior to undertaking readings, the YSI meter was calibrated for pH using two buffer solutions, K_2PO_3 with pH of 7.0 and NaCl with pH of 4.0. In addition, a 1413 µS cm^{-1} conductivity solution was used to calibrate equipment for EC measurements. The YSI electrodes were completely immersed in the supernatants to simultaneously record soil pH and EC measurements from the display monitor. In between measurements of different soil samples, the electrodes were cleaned with deionised water.

3.5.2 Loss-on-ignition (LOI): Estimating SOM concentration

For each sample, about 20 g of oven dried fine soil fractions (<2 mm) were placed in preheated porcelain crucibles and transferred into a Carbolite furnace for determination of SOM concentrations. In batches of 12 samples, the furnace was set at a temperature of 450°C for duration of up to 12 hours. Before and after combustion, the samples were weighed on an analytical balance to 0.0001 g precision (Figure 3.7). In order to identify, trace back and relate the soil samples to the forest sites and plots, the crucibles were systematically loaded from left to right with three rows and four columns. The positions of the crucibles were correspondingly noted on the record sheets (Figure 3.7a). For each sample, loss in weight (LIW) was calculated using Equation 2.14. Owing to inaccuracies that may arise due to the removal of H_2O-groups held by clay soils (Hoogsteen *et al.*, 2015), estimates of LIW were multiplied by the structural water loss correction factor to calculate SOM concentrations (SOMc; equations 3.15, 3.16) and SOM stock (SOMs; equation 3.17).

$$LIW\ (\%) = \left[\frac{(M_{crucible\ +\ soil} - M_{crucible})_{before} - (M_{crucible+soil} - M_{crucible})_{after}}{(M_{crucible\ +\ soil} - M_{crucible})_{before}}\right] * 100 \qquad \text{Equation 3.15}$$

$$SOMc\ (\%) = LIW\ (\%) * (1 - CF_{SWL}) \qquad \text{(Hoogsteen } et\ al.\text{, 2015) Equation 3.16}$$

or

$$SOM_C\ (g\ kg^{-1}) = \frac{SOC\ (\%)}{100} * Mass_{fine\text{-}soil\ sample}$$

$$SOM_{stock}\ (g\ m^{-3}) = SOM * BD * D \qquad \text{(Kirtsen } et\ al.\text{, 2016) Equation 3.17}$$

where $M_{crucible\ +\ soil}$ is the weighed mass of crucible plus fine fractions of <2 mm and $M_{crucible}$ is the weighed mass of pre-heated empty crucible determined before ignition, SOC (%, g kg^{-1}) is the soil organic carbon concentration, CF_{SWL} is the correction factor for structural water loss (0.04) associated with clay and LOI at 450°C, $Mass_{fine\text{-}soil\ sample}$ is the mass of soil samples or mass of crucible plus soil less the mass of crucible. D is the soil depth (0.1 m) and gravel is proportion of coarse fragments (>2 mm).

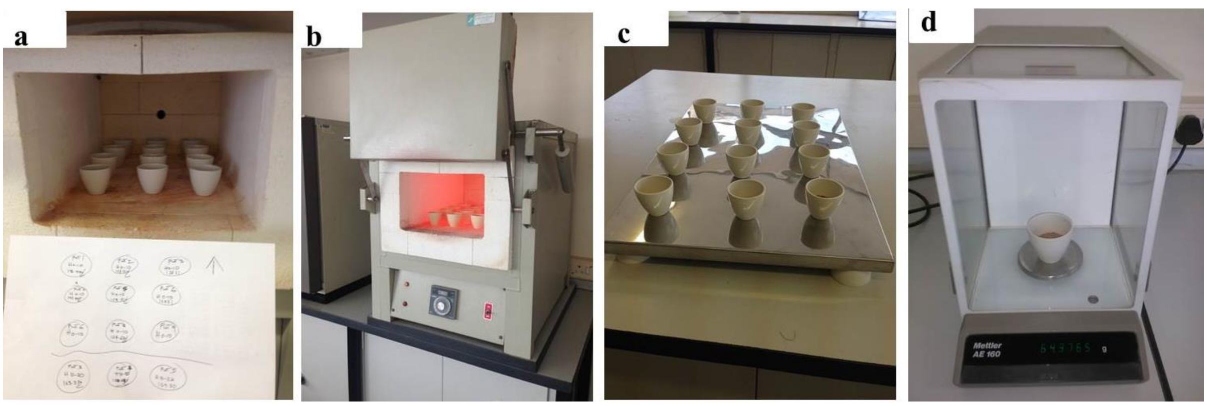

Figure 3.7: Determination of SOM concentration by loss-on-ignition method. The method involved (a) systematic loading of 12 samples per batch, (b) combusting soil samples at 450°C for 12 hours, (c) cooling the samples and (d) reweighing using an analytical balance with a precision of 0.0001 g.

3.5.3 Application of PCA for assessing the dynamics of SOM

Principal component analysis in R-statistical package was applied to reduce the dimensionality of the measured soil variables and to extract a small number of independent variables that largely explained the variability in the datasets (0-10 cm, 10-20 cm and 20-30 cm depth). For each soil depth, the two datasets from Luanshya and Bushbuckridge were arranged in a matrices of each soil depth, where each row of the matrix represented single observations, while the columns denoted soil properties namely, altitude, AGLB, BD, SOMc, EC, pH, and the percentage of clay, silt and sand, MC% and gravel (%). The factorability of the datasets were tested using Kaiser Meyer Olkin (KMO) test of sampling adequacy and Bartlett's test of sphericity. Based on the decomposition of eigenvalues, varimax rotation was applied to facilitate easy interpretation in the ordination of measured variables with respect to the principal components. The relationships between the 11 soil properties were assessed using PCA regression and leave-one-out cross validation method.

CHAPTER 4 - RESULTS

4.1 Introduction

Based on the analysis of multi-temporal remotely sensed images and field measurements, the results are separately presented in four different sections. The first segment presents the LULC maps, and the associated graphs and matrices describing change dynamics, especially that of natural forests (dense woodlands) and its concomitant LULC changes. The second section presents maps of aboveground forest carbon stocks and their spatial-temporal changes. The third segment outlines the consequences of anthropogenic disturbances and environmental factors on the distribution of SOM content in forest stands of different successional stages. Based on PCA, the fourth section describes the relationships between SOM content and the other 11 measured variables.

4.1.1 Spatial-temporal dynamics of LULC changes for Luanshya

From the LULC maps (Figure 4.1), changes in the areal extent of the eight LULC types are indicated by the spatial-temporal variation in the spectral reflectance measurements, spectral pattern recognition and subsequent classification of pixels into different clusters. Based on the LULC maps (Figure 4.1), the total area that underwent change for the period 1986-1998, 1998-2001, 2001-2004, 2004-2011 and 2011-2016 was 36,845 hectares (ha), 34,755 ha, 30,451 ha, 27,942 ha and 23,914 ha, respectively (Table 4.2). These changes denoted an average change of 67.94%, 64.09%, 56.15%, 51.52% and 44.10% of the total land cover (54,232 ha).

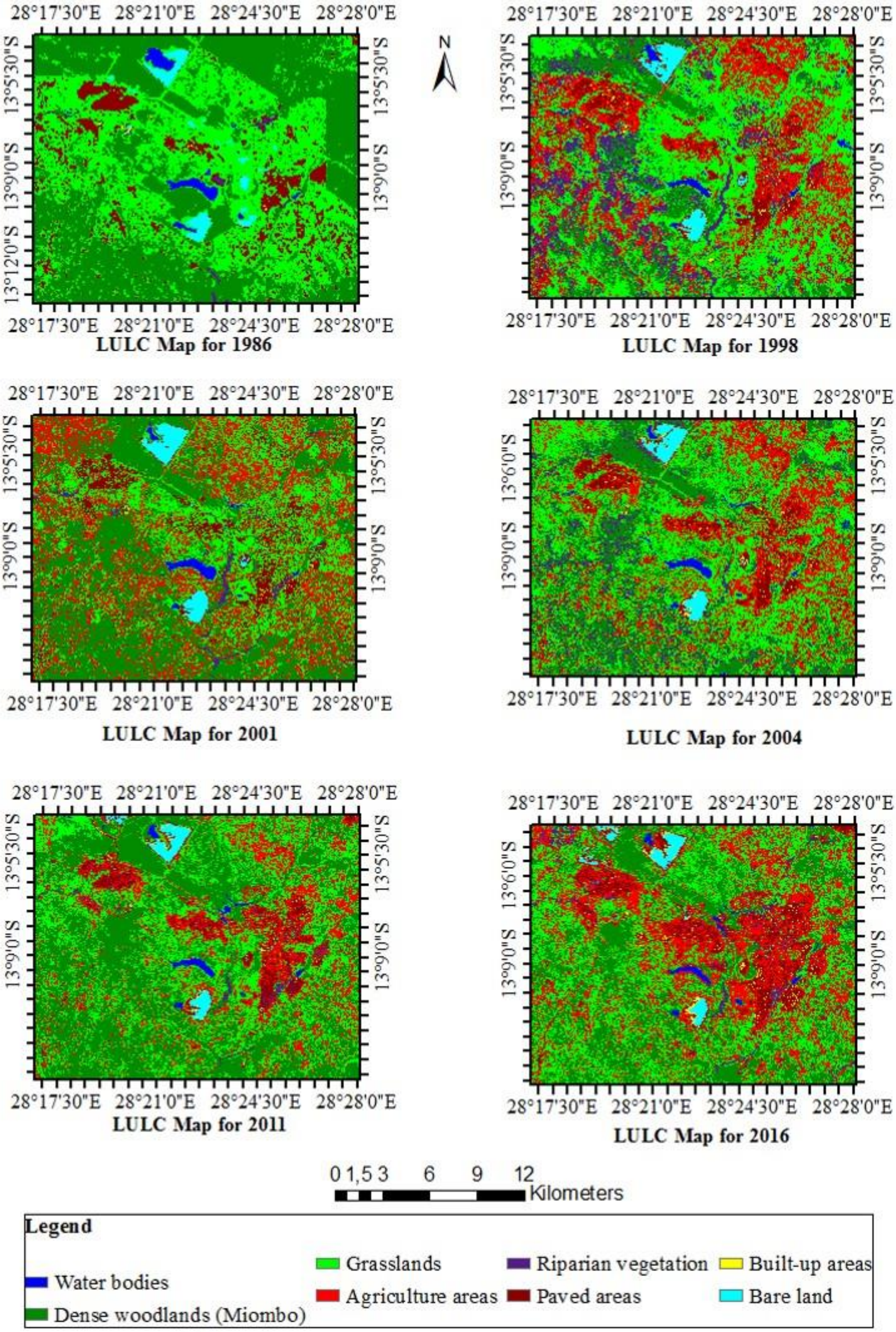

Figure 4.1: LULC maps for 1986, 1998, 2001, 2004, 2011 and 2016 in Luanshya.

Confusion matrices were generated to assess the accuracy of classifications by comparing variant and invariant features in LULC maps to ground truth information. The SVM classifier generated maps with an overall accuracy of 82-99%. Kappa coefficients of between 0.88 and 0.99 indicated the measure of the difference between actual and chance agreement between reference data and the classified images. Similarly, ML classifier reported high overall accuracies and Kappa coefficients of 91-99% and 0.91-0.99, respectively (Appendix A1). A two-way ANOVA with replication indicated that there was no significant difference (ρ = 0.00) between classified images or LULC maps generated from SVM and ML algorithm. Given this consistency, the reported quantitative analysis of LULC changes were calculated using the SVM method (Table 4.1).

Table 4.1 - Support Vector Machine: Classification error matrices for Luanshya

		Ground Truth ROI Pixels									
		Agricultural areas	Bare land	Built-up areas	Dense woodlands	Grasslands	Paved areas	Riparian vegetation	Water bodies	Total	UA (%)
LULC for 1986	Agricultural areas	-	-	-	-	-	-	-	-	-	-
	Bare land	-	0	3	0	0	0	0	0	115	97
	Built-up areas	-	0	18	0	0	0	0	0	18	100
	Dense woodlands	-	0	0	117	0	0	0	0	117	100
	Grasslands	-	0	0	0	187	0	0	0	187	100
	Paved areas	-	0	0	0	0	148	0	0	148	100
	Riparian vegetation	-	0	0	0	0	0	133	0	133	100
	Water bodies	-	0	0	0	0	0	0	107	107	100
	Total	-	112	21	117	187	148	133	107	825	
	PA (%)	-	100	86	100	100	100	100	100		
	Overall accuracy (%)		99%								
	Kappa coefficient		0.99								
LULC for 1998	Agricultural areas	45	0	0	0	1	1	0	0	47	96
	Bare land	0	181	2	0	0	0	0	0	183	99
	Built-up areas	0	0	96	0	0	0	0	0	96	100
	Dense woodlands	0	0	0	123	0	0	1	0	124	99
	Grasslands	1	0	0	0	118	0	3	0	123	96
	Paved areas	0	1	0	0	0	116	0	0	117	99
	Riparian vegetation	0	0	0	1	0	0	107	0	108	99
	Water bodies	0	0	0	0	0	0	0	110	110	100
	Total	46	182	98	124	119	117	111	110	1009	
	PA (%)	98	100	98	99	99	99	96	100		
	Overall accuracy (%)		99								
	Kappa coefficient		0.99								
LULC for 2001	Agricultural areas	69	0	0	0	3	0	1	0	73	84
	Bare land	0	156	14	0	0	0	0	0	170	92
	Built-up areas	0	0	44	0	0	0	0	0	44	100
	Dense woodlands	0	0	0	119	0	0	0	0	119	99
	Grasslands	0	0	0	0	97	0	0	0	97	100
	Paved areas	0	1	0	0	0	97	0	0	98	98
	Riparian vegetation	0	0	0	0	0	0	107	0	107	98
	Water bodies	0	0	0	0	0	0	0	110	110	100
	Total	69	157	58	119	100	97	108	110	818	
	PA (%)	84	99	76	98	97	96	77	100		
	Overall accuracy (%)		92								
	Kappa coefficient		0.92								
LULC for 2004	Agricultural areas	112	0	0	0	0	6	0	0	118	91
	Bare land	0	159	1	0	0	0	0	0	160	99
	Built-up areas	0	0	97	0	0	0	0	0	97	100
	Dense woodlands	0	0	0	120	0	0	6	0	126	93

Table 4.1 (*continued*)

	Grasslands	0	0	0	0	105	0	1	0	**106**	**94**
	Paved areas	3	0	0	0	0	155	0	0	**158**	**98**
	Riparian vegetation	0	0	0	6	0	0	74	0	**80**	**85**
	Water bodies	0	0	0	0	0	0	0	110	**110**	**100**
	Total	**115**	**159**	**98**	**126**	**105**	**161**	**81**	**110**	**955**	
	PA (%)	**93**	**100**	**99**	**94**	**96**	**96**	**78**	**100**		
	Overall accuracy (%)		**93**								
	Kappa coefficient		**0.93**								
LULC for 2011	**Agricultural areas**	113	0	0	0	2	0	0	0	**115**	**98**
	Bare land	0	113	5	0	0	0	0	0	**118**	**96**
	Built-up areas	0	0	64	0	0	4	0	0	**68**	**60**
	Dense woodlands	0	0	0	113	0	0	0	0	**113**	**94**
	Grasslands	1	0	0	0	107	0	0	0	**108**	**99**
	Paved areas	0	0	0	0	0	134	0	0	**134**	**97**
	Riparian vegetation	0	0	0	0	0	0	127	0	**127**	**100**
	Water bodies	0	0	0	0	0	0	0	110	**110**	**100**
	Total	**114**	**113**	**69**	**113**	**109**	**138**	**127**	**110**	**893**	
	PA (%)	**99**	**99**	**50**	**94**	**98**	**97**	**100**	**100**		
	Overall accuracy (%)		**90**								
	Kappa coefficient		**0.88**								
LULC for 2016	**Agricultural areas**	109	8	4	0	20	1	0	0	**142**	**77**
	Bare land	0	53	21	0	0	0	0	0	**74**	**72**
	Built-up areas	0	17	57	0	0	4	0	0	**78**	**73**
	Dense woodlands	0	0	0	112	1	0	1	0	**114**	**98**
	Grasslands	4	1	0	8	87	0	0	0	**100**	**87**
	Paved areas	1	35	44	0	0	133	0	0	**213**	**62**
	Riparian vegetation	0	0	1	0	1	0	126	0	**128**	**98**
	Water bodies	0	0	0	0	0	0	0	110	**110**	**100**
	Total	**114**	**114**	**127**	**120**	**109**	**138**	**127**	**110**	**959**	
	PA (%)	**96**	**47**	**45**	**93**	**80**	**96**	**99**	**100**		
	Overall accuracy (%)		**82**								
	Kappa coefficient		**0.8**								

Where PA is Producer accuracy, UA is user accuracy in percentage

Table 4.2 - Change matrix in Luanshya for the periods from 1986-1998, 1998-2001, 2001-2004, 2004-2011 and 2011-2016 (units in hectares). Bold values indicate unchanged LULC type.

	Area (hectares)				**LULC 1986**					
		Agriculture areas	**Bare land**	**Built-up**	**Dense woodlands**	**Grasslands**	**Paved areas**	**Riparian vegetation**	**Water bodies**	**Total**
LULC 1998	**Agriculture areas**	-	31	6	4843	4234	1248	57	11	**10,431**
	Bare land	-	**405**	1	18	100	6	0	72	**602**
	Built-up areas	-	6	**2**	13	36	41	2	4	**105**
	Dense woodlands	-	3	0	**8035**	1115	121	37	3	**9315**
	Grasslands	-	16	4	14,206	**7784**	1057	192	91	**23,349**
	Paved areas	-	163	11	957	1503	**905**	37	44	**3620**
	Riparian vegetation	-	2	1	3773	2046	354	**78**	4	**6258**
	Water bodies	-	0	0	272	75	3	27	**177**	**553**
	Total	**-**	**626**	**25**	**32,117**	**16,893**	**3734**	**431**	**405**	**54,232**
	Changes	**-**	**221**	**23**	**24,082**	**9108**	**2829**	**353**	**229**	**36,845**
					LULC 1998					
LULC 2001	**Agriculture areas**	**3772**	0	2	1292	6911	523	1040	22	**13,562**
	Bare land	1	**569**	11	0	3	50	0	1	**636**
	Built-up	1	2	**24**	0	1	12	0	0	**40**
	Dense woodlands	831	0	0	**7373**	10,179	59	4155	202	**22,800**
	Grasslands	4663	0	8	562	**5361**	1195	510	53	**12,352**
	Paved areas	1045	27	57	33	414	**1740**	84	11	**3412**

Table 4.2 (*continued*)

Riparian vegetation	109	0	2	55	414	25	**468**	93	**1166**
Water bodies	9	3	1	0	66	16	1	**171**	**266**
Total	**10,431**	**602**	**105**	**9315**	**23,349**	**3620**	**6258**	**553**	**54,232**
Changes	**6658**	**32**	**81**	**1942**	**17,988**	**1881**	**5791**	**382**	**34,755**

				LULC 2001						
LULC 2004	**Agriculture areas**	**3356**	0	1	803	4722	1087	67	4	**10,041**
	Bare land	0	**534**	1	0	0	4	0	0	**539**
	Built-up	1	44	**22**	1	2	45	1	0	**116**
	Dense woodlands	1652	0	0	**11,999**	763	34	287	11	**14,745**
	Grasslands	7924	0	1	6277	**5705**	447	519	45	**20,918**
	Paved areas	417	58	15	140	1054	**1789**	60	0	**3533**
	Riparian vegetation	198	0	0	3475	77	4	**171**	1	**3925**
	Water bodies	14	0	0	106	28	1	61	**205**	**415**
	Total	**13,562**	**636**	**40**	**22,800**	**12,352**	**3412**	**1166**	**266**	**54,232**
	Changes	**10,206**	**102**	**18**	**10,802**	**6647**	**1622**	**995**	**60**	**30,451**

				LULC 2004						
LULC 2011	**Agriculture areas**	**3712**	12	12	566	3040	1303	108	15	**8768**
	Bare land	26	**414**	7	65	95	24	10	0	**641**
	Built-up	13	38	**10**	5	28	14	0	0	**109**
	Dense woodlands	1250	1	2	**12,205**	8549	194	3411	123	**25,735**
	Grasslands	4435	6	5	1721	**8537**	684	301	55	**15,744**
	Paved areas	514	66	76	120	394	**1155**	20	1	**2346**
	Riparian vegetation	81	0	3	56	224	159	**74**	39	**636**
	Water bodies	9	0	0	6	53	0	1	**183**	**252**
	Total	**10,041**	**539**	**116**	**14,745**	**20,918**	**3533**	**3925**	**415**	**54,232**
	Changes	**6329**	**124**	**106**	**2540**	**12,381**	**2378**	**3851**	**233**	**27,942**

				LULC 2011						
LULC 2016	**Agriculture areas**	**5090**	17	7	1712	5543	570	104	25	**13,069**
	Bare land	40	**429**	17	104	51	67	0	0	**708**
	Built-up	41	75	**35**	28	40	99	2	1	**319**
	Dense woodlands	238	0	0	**15,156**	1247	19	18	22	**16,699**
	Grasslands	1702	1	1	7725	**7646**	82	36	17	**17,210**
	Paved areas	1142	107	39	233	597	**1390**	82	8	**3598**
	Riparian vegetation	488	0	0	760	601	59	**394**	1	**2305**
	Water bodies	26	12	11	16	20	61	0	**178**	**324**
	Total	**8768**	**641**	**109**	**25,735**	**15,744**	**2346**	**636**	**252**	**54,232**
	Changes	**3677**	**212**	**75**	**10,579**	**8099**	**956**	**242**	**74**	**23,914**

4.1.1.1 Changes for the period 1986-1998

With reference to Figure 4.1, it is apparent that dense woodlands (32,117 ha which represent 59.22% of the total area) and grassland (16,893 ha or 31.15% of the total areas) were the most dominant land cover types. Agricultural areas were not delineated in the LULC map for 1986 which suggested that farming activities could have only been practised at relatively smaller scale or later than 1986. However, the change matrix (Table 4.2) indicates that dense woodlands decreased from 32,117 ha in 1986 to 9315 ha (17.18% of the total land cover) in 1998. Assuming that change was linear (which is just an assumption for illustrative purposes), the difference between forest cover for 1986 and that for 1998 divided by 12 years represented an average annual rate change (decline) of 10.31%. As a result, the total area of dense forested areas or Miombo woodland decreased from the initial state to the final state, whereas grassland, agricultural areas, riparian vegetation increased noticeably (Figure 4.2a). Only about 25% of dense woodland cover remained unchanged. This is because approximately 24,082 ha of forested areas were converted to grassland (14,206 ha) and agricultural areas (4843 ha), while 5033 ha changed to riparian vegetation or non-vegetated areas. A total of 1280 ha of forest cover was gained through forest regrowth, mainly from grassland (1115 ha).

4.1.1.2 Changes for the period 1998-2001

Table 4.2 reveals that pixels initially (1998) classified as agricultural areas (9233 pixels or 831 ha), grassland (51811 pixels or 4663 ha), paved areas (11611 pixels or 1045 ha), riparian vegetation (1211 pixels or 109 ha) and water bodies (1000 pixels or 9 ha) were categorised as dense woodlands in the final state of 2001. Even though some forest cover was lost to grassland (6%) and riparian vegetation (1%), the previous trend of deforestation (1986-1998:

10.31% yr^{-1}) was reversed, with the total area of forest cover increasing from 9315 ha in 1998 to 22,800 ha in 2001 (Figure 4.2b). Increase in forest cover was also attributed to the fact that 79% of the 1998 wooded areas remained undisturbed while some non-forested areas became forested sites. In contrast, a different shift in the spatial extent of grassland was observed, where non-woody vegetation decreased from 23,349 ha to 12,352 ha. This means that 1942 ha of dense woodlands were lost, while 15,427 ha were replenished through secondary forest (SF) succession.

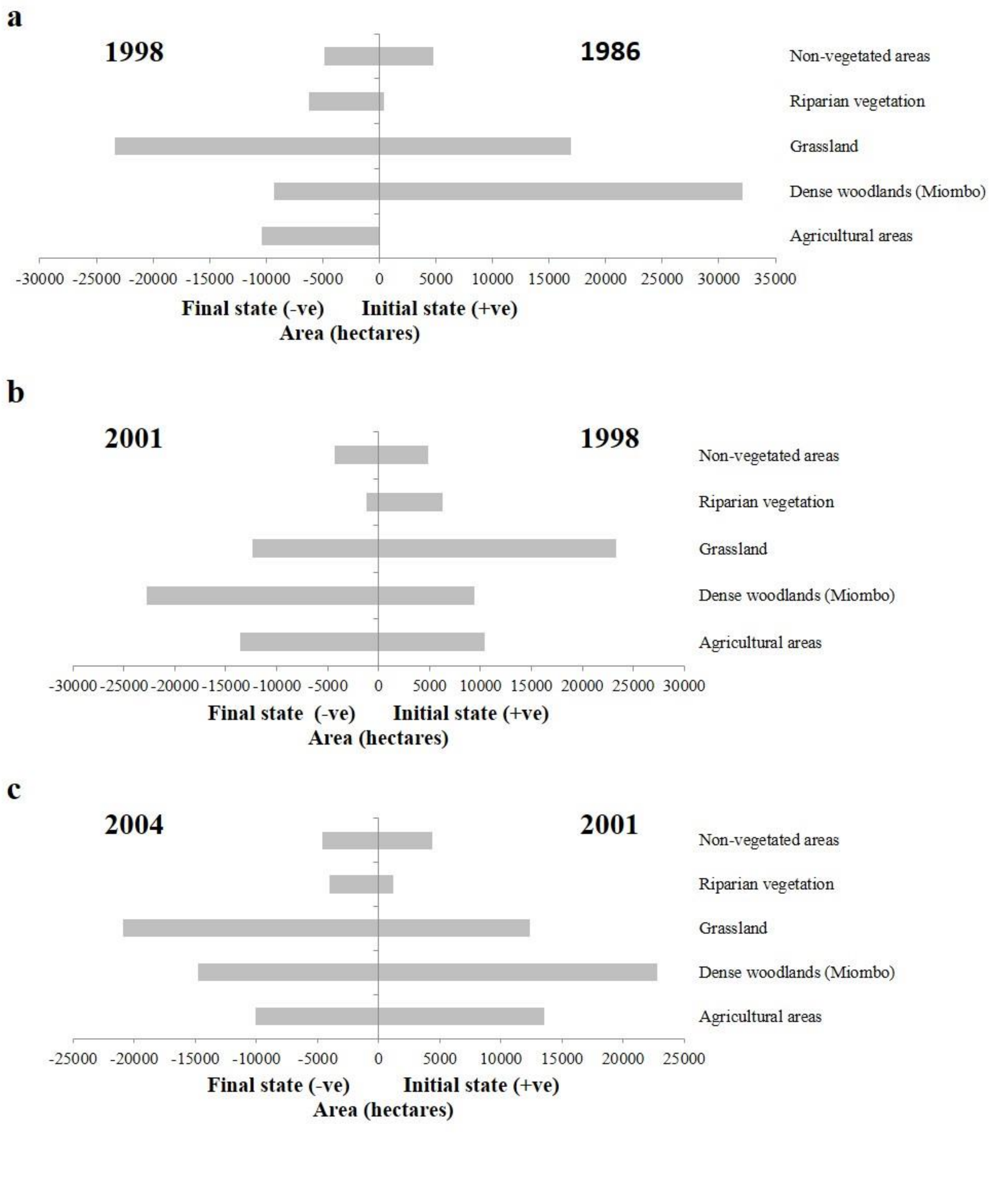

Figure 4.2: Dynamics of LULC changes for the period 1986-1998, 1998-2001 and 2001-2004. The graph shows the total areal changes for (a) 1986-1998, (b) 1998-2001, and (c) 2001-2004. The absolute values in the positive segment depict the different LULC types and the observed areal extent in the initial state, while the negative segments illustrate the final state.

The total areas in Figure 4.2a for 1986-1998 and Figure 4.2b for 1998-2001 indicated a natural phenomenon of natural forest succession and a covariation between the areal extent of dense woodlands and grassland. The difference between the total area of dense woodlands (22,800 ha) in the final state and forest cover that remained unchanged (7373 ha) from 1998 to 2001 suggested that 68% of Miombo woodland cover for 2001 were second growth forest stands. Largely through the conversions of dense woodlands, grassland and riparian vegetation, the results also showed a sustained expansion in agricultural areas by 3131 ha (1998-2001), while smaller changes were associated with non-vegetated areas (Figure 4.2b). Table 4.2 also indicates that bare land, largely from mining activities, maintained a marginal positive increase from 602 ha to 636 ha. Further, riparian vegetation decreased noticeably from 6258 ha to 1166 ha with the majority (66%) changing into dense woodlands.

4.1.1.3 Changes for the period 2001-2004

The three LULC classes that underwent major charges during the period 2001-2004 were dense woodlands, agricultural areas and grassland. The conversions from agricultural areas, dense woodlands and grassland constituted about 34%, 36% and 22% of the total change, respectively (Table 4.2). The areal extent of dense woodlands decreased from 22,800 ha in 2001 to 14,745 ha in 2004, at an average rate of 2685 ha or 11.8% per annum (Figure 4.2c). Conversion of woodlands to grassland (6277 ha), riparian vegetation (3475 ha) and agricultural areas (803 ha) were the prominent changes that resulted in the observed decline in wooded areas. Despite losing to agricultural areas and grassland, dense woodlands also gained a total of 2746 ha, mostly from agricultural areas, grassland and riparian vegetation (Table 4.2). This means that from 2001 to 2004, about 19% of dense woodlands were SF stands. It was apparent that non-vegetated areas (bare land, built-up areas, paved areas and water bodies) only had marginal changes (Figure 4.2c), while a notable increase in riparian vegetation may reflect increased annual rainfall in 2004.

4.1.1.4 Changes for the period 2004-2011

A reduced total change was observed from 2004 to 2011, a pattern which suggested a shift where LULC composition became more stable. This is evident by a total change of 27,942 ha or 52% of the total landscape undergoing an average change of 3992 ha yr^{-1}, which was significantly less than the total mean changes of 11,585 ha yr^{-1} for the period 1998-2001 and 10,150 ha yr^{-1} for 2001-2004 (Table 4.2). During this period (2004 to 2011), the cumulative changes from agricultural areas (6329 ha), dense woodlands (2540 ha) and grassland (12,381 ha) represented 76% of the total changes observed. The area gained by dense woodlands, primarily from riparian vegetation (87%), grasslands (41%) and agricultural areas (12%), was relatively less than the area that changed from woodlands into grassland (12%), agricultural areas (10%) and paved areas (<1%). Thus, an increase in dense woodlands from 14,745 ha in 2004 to 25,735 ha in 2011 was observed (Figure 4.3a), which constituted about 53% of forest secondary growth. Change (increase) in the spatial extent of dense woodlands occurred at an average rate of 8.00% yr^{-1}. As depicted by the change from the initial state to the final state (Figure 4.3a), covariation in the total areal extent of dense woodlands and grassland was again fundamental to LULC change dynamics.

4.1.1.5 Changes for the period 2011-2016

Table 4.2 shows a marginal upward trend in the total area that underwent change from 27,942 ha (3992 ha yr^{-1}) for the period 2004-2011 to 23,914 ha (4783 ha yr^{-1}) for 2011-2016. More recent changes show that grassland and agricultural areas have continued to increase at the expense of Miombo woodland. Conversion of dense woodlands to grassland and agricultural areas represented 73% and 16% of the total changes, respectively. A total of approximately 10,579 ha or 41% of dense woodlands was converted to other LULC types at an average rate of 2116 ha yr^{-1} or 9% yr^{-1}. As shown in Figure 4.3b, dense woodlands decreased from 25,735 ha in the initial state (2011) to 16,699 ha in the final state (2016).

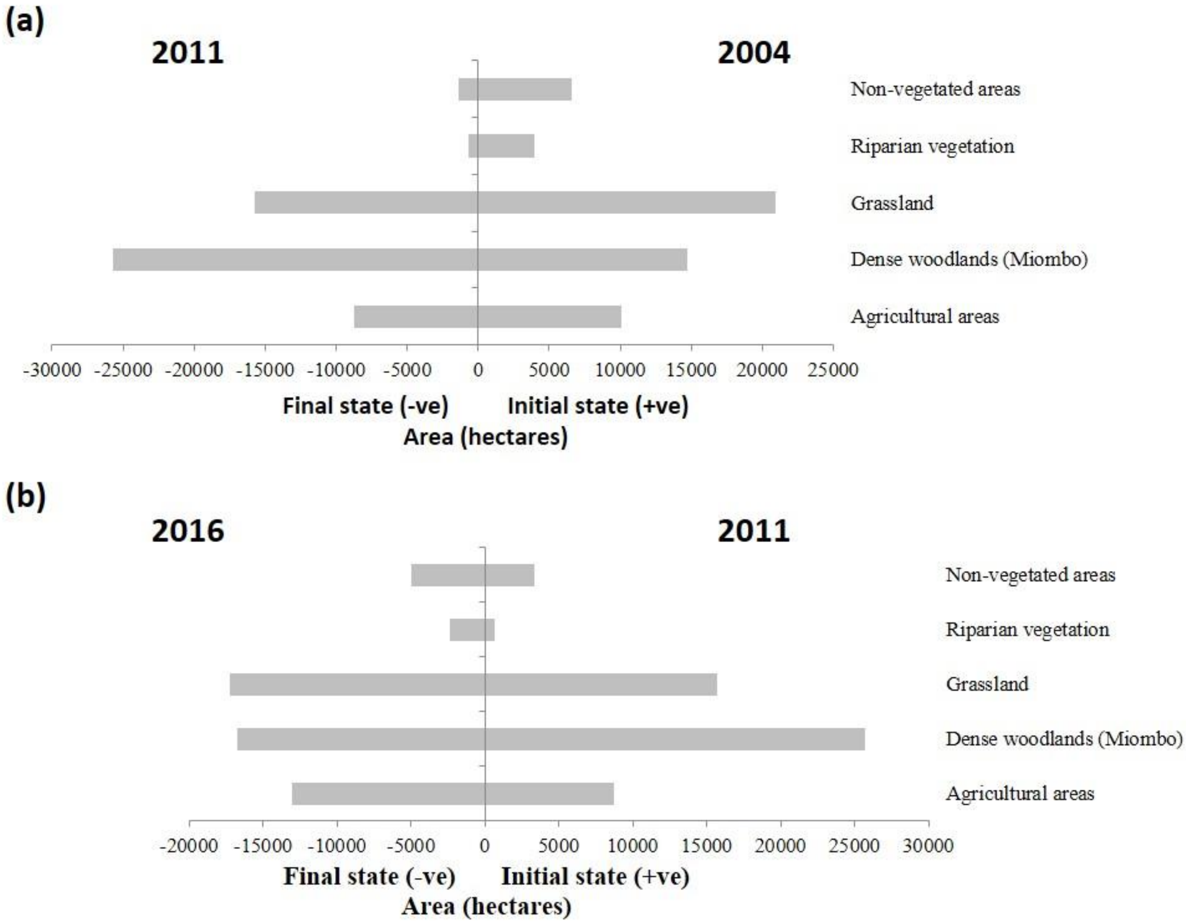

Figure 4.3: Dynamics of LULC changes for the period 2004-2011 and 2011-2016. The graph shows the total areal changes for (b) 2004-2011 and (b) 2011-2016. The absolute values in the positive segment depict the different LULC types and the observed areal extent in the initial state, while the negative segments illustrate the final state.

Relative to the other periods, SF succession between 2011 and 2016 (1.94% yr^{-1}) was greater than the average recruitment observed between 1986 and 1998 (1.23% yr^{-1}), but significantly lower than the estimates for 1998-2001 (37.63% yr^{-1}), 2001-2004 (6.87% yr^{-1}) and 2004-2011 (10.66% yr^{-1}). After undergoing a decline between 2004 and 2011, the total area of agricultural fields expanded from 8768 ha in 2011 to 13,069 ha in 2016. As depicted in Table 4.2, agricultural areas were converted largely from grassland (5543 ha) and dense woodlands (1712 ha). During the same period, non-vegetated areas (bare land, built-up areas and paved areas) and riparian vegetation also experienced moderate gains from dense woodlands and grassland.

4.1.1.6 Transitional pathways for 1986-1998 and 1998-2001

Based on the proportion of pixels within each land cover type, Figure 4.4 illustrates the different scenarios of transitional pathways for the period 1986-1998 and 1998-2001. The non-appearance of agricultural areas in the LULC map for 1986 (Figure 4.1) is indicated by absence of retained pixels (unchanged) and pathways departing from agricultural areas to other LULC classes (Figure 4.4a). "Unchanged" (curved arrows) means that the same LULC class was found at the same point on the ground in both initial and final states. From 1986 to 1998, about 44% of the total pixels classified as forested areas changed to grassland, while 15% changed to agricultural areas. During this period, 45% of the pixels classified as riparian vegetation changed to grassland. Some agricultural areas were established on land previously covered by riparian vegetation (16%) and non-vegetated areas (27%), while the majority of cultivated fields were converted from grassland (25%). These trajectories (1986-1998) mean that forested areas lost 75% of the 1986 land cover, and was the most converted land cover type, while agricultural areas (0 in 1986 to 10,431 ha in 1998) and grassland (16,893 ha in 1986 to 23,349 ha in 1998) were the main recipients of land cover loss from woodlands. The conversion of riparian vegetation to grassland in 1986-1998 (45%) (Figure 4.4a) and later to forested areas in 1998-2001 (66%) (Figure 4.4b), reveals that areas close to water sources are some of the preferred sites for natural vegetation growth (riparian vegetation, grassland and forested areas). This implies that spatial-temporal changes of these land cover types may indicate fluctuations in readily available water for vegetation growth. From 1998-2001 (Figure 4.4b), two-way transitional changes took place along pathways of agricultural areas→riparian vegetation, agricultural areas→non-vegetated areas, riparian vegetation→non-vegetated areas, and grassland→riparian vegetation, and vice versa. However, all of these pathways were significantly asymmetrical and of smaller magnitude (<20%). Changes with intensity of >20% occurred along one-way trajectories of riparian vegetation→forested areas (66%), and grassland→forested areas (44%), and a two-way transitional pathway between agricultural areas and grassland. The transitions associated with agricultural areas suggested two important changeovers: Firstly, clearing of naturally vegetated areas (forested areas: 14%; grassland: 30%; riparian vegetation: 16%) for both agricultural intensification and establishment of new fields, and (2) encroachment of previously cultivated fields, largely by grassland (45%).

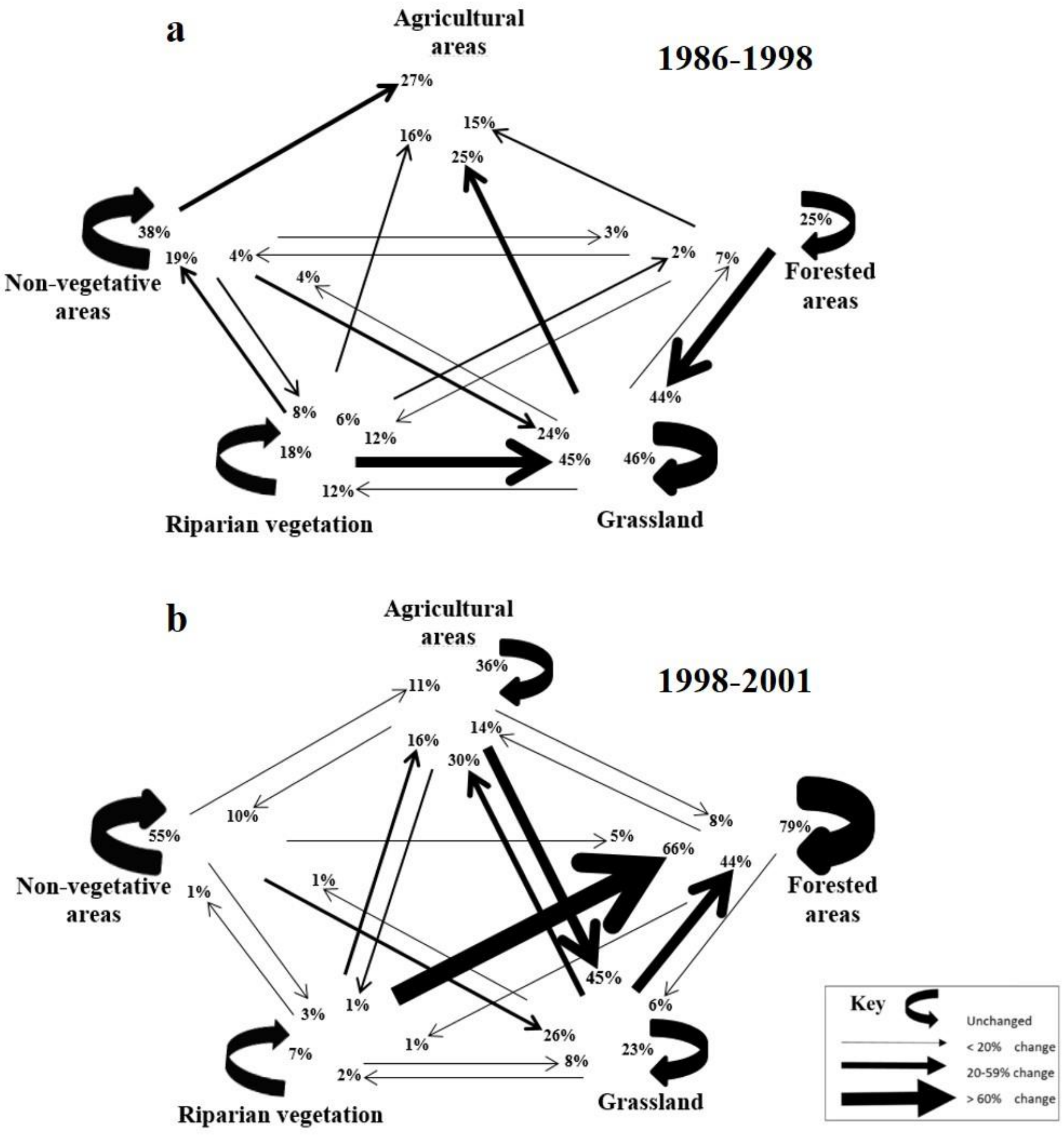

Figure 4.4: Transitional pathways associated with LULC changes for the periods 1986-1998 and 1998-2001 in Luanshya. The thickness of lines and arrows indicate the intensity or proportion of change and the class into which pixels changed into the final state, respectively. The curved arrows show the proportion of pixels that persisted or remained unchanged from the initial state (1986 for Figure 4.4a and 1998 for Figure 4.4b) to the final state (1998 for Figure 4.4a and 2001 for Figure 4.4b).

4.1.1.7 Transitional pathways for 2001-2004, 2004-2011 and 2011-2016

During the period from 2001-2004, all the LULC types did not show persistence within the same class (Figure 4.5a). As expected, non-vegetated areas which included bare land, built-up areas, paved areas and water bodies exhibited great persistence (62%), and was followed by forested areas (53%) and grassland (46%). On the contrary, the classes with the least persistence or highest vulnerability to change were riparian vegetation (15%) and agricultural areas (25%). Most of the transformed riparian vegetation and agricultural areas converted to grassland (45-58%). Through a two-way transitional pathway with intensities of >20%, about 38% of grassland was also converted to agricultural areas. From 2004 to 2011 (Figure 4.5b), LULC dynamics were intensified along pathways from riparian vegetation (41%) and grassland (87%) to forested areas. The majority (44%) of the cultivated areas observed in the LULC map for 2004 also changed to grassland in 2011 (Figure 4.1), which means that only 40% persisted from the initial state to the final state. The percentage of unchanged area averaged from the five transitional pathways (Figures 4.4, 4.5 and 4.6) entails that the unchanged area was more significant from 2011 to 2016 (61%) than the previous periods of 1986-1998 (32%), 1998-2001 (40%), 2001-2004 (40%) and 2004-2011 (42%). Therefore, only minimal trajectories (<35%) occurred between different classes (2011-2016) (Figure 4.6). Insight from the five periods (1986-1998, 1998-2001, 2001-2004, 2004-2011, and 2011-2016) revealed that LULC changes can be viewed as multiple and reversible transitional dynamics, where direction and size of change are likely influenced by human activities and climate variability.

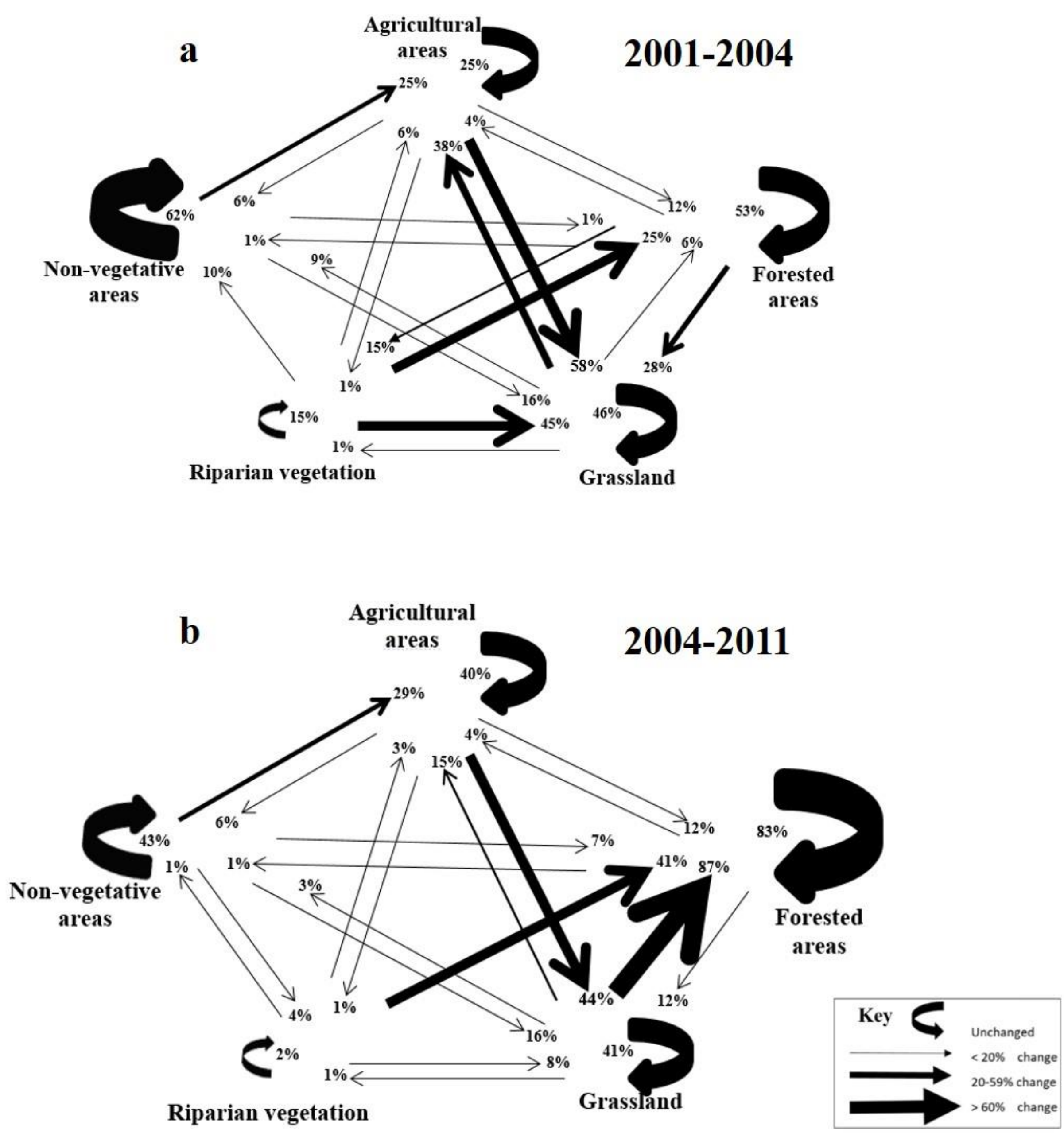

Figure 4.5: Transitional pathways associated with LULC changes for the periods 2001-2004 and 2004-2011 in Luanshya. The thickness of lines and arrows indicate the intensity or proportion of change and the class into which pixels changed into the final state, respectively. The curved arrows show the proportion of pixels that persisted or remained unchanged from the initial state (2001 for Figure 4.5a and 2004 for Figure 4.5b) to the final state (2004 for Figure 4.5a and 2011 for Figure 4.5b).

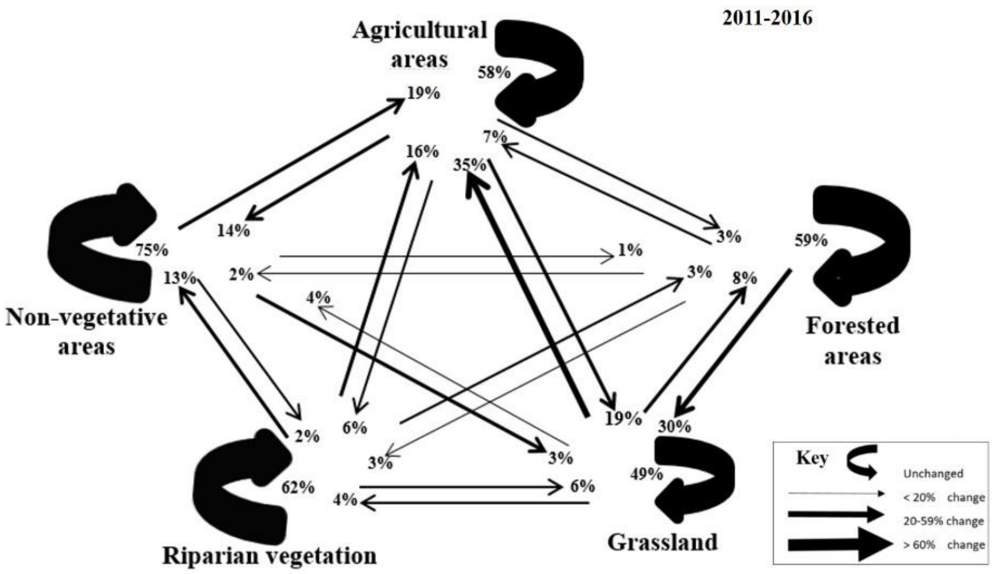

Figure 4.6: Transitional pathways associated with LULC changes for the period 2011-2016 in Luanshya. The thickness of lines and arrows indicate the intensity or proportion of change and the class into which pixels changed into the final state, respectively. The curved arrows show the proportion of pixels that persisted and remained unchanged from the initial state (2011) to the final state (2016).

4.1.1.8 Changes in secondary woodland cover in Luanshya

For each of the five observed time periods (Tables 3.2, 3.3), the spatial extent of SF cover was calculated from total dense forested areas in the final state, less wooded areas that remained unchanged. This is further illustrated in Figure 4.7, where 25 cells correspond to 100% or total area of each final state, while a single unit (both secondary and unchanged woodland cover) represent 4% of a cluster. Increased occurrence of cells for SF cover denotes enhanced forest succession and increase in the proportion of new forest cover over old cover. Given the total area of 9315 ha, 22,800 ha, 14,745 ha, 25,735 ha, and 16,699 ha and unchanged land cover of 8035 ha, 7373 ha, 11,999 ha, 12,205 ha, and 15,156 ha (Tables 3.2, 3.3), secondary forested areas constituted about 12%, 68%, 20%, 52%, and 8% of the total Miombo woodland in 1998, 2001, 2004, 2011 and 2016, respectively. This means that regeneration and forest succession was greater during the periods 1998-2001 followed by 2004-2011. Since regeneration occurred mostly along pathways of grassland→dense woodlands (Figures 4.4b, 4.5b), the lowest cell count for SF cover for the periods, 2011-2016 (2) and 1986-1998 (3) may be attributed to increased conversion of grassland to agricultural areas, which was earlier observed in Figures 4.4a and 4.6, grassland→agricultural areas (35% and 25%, respectively).

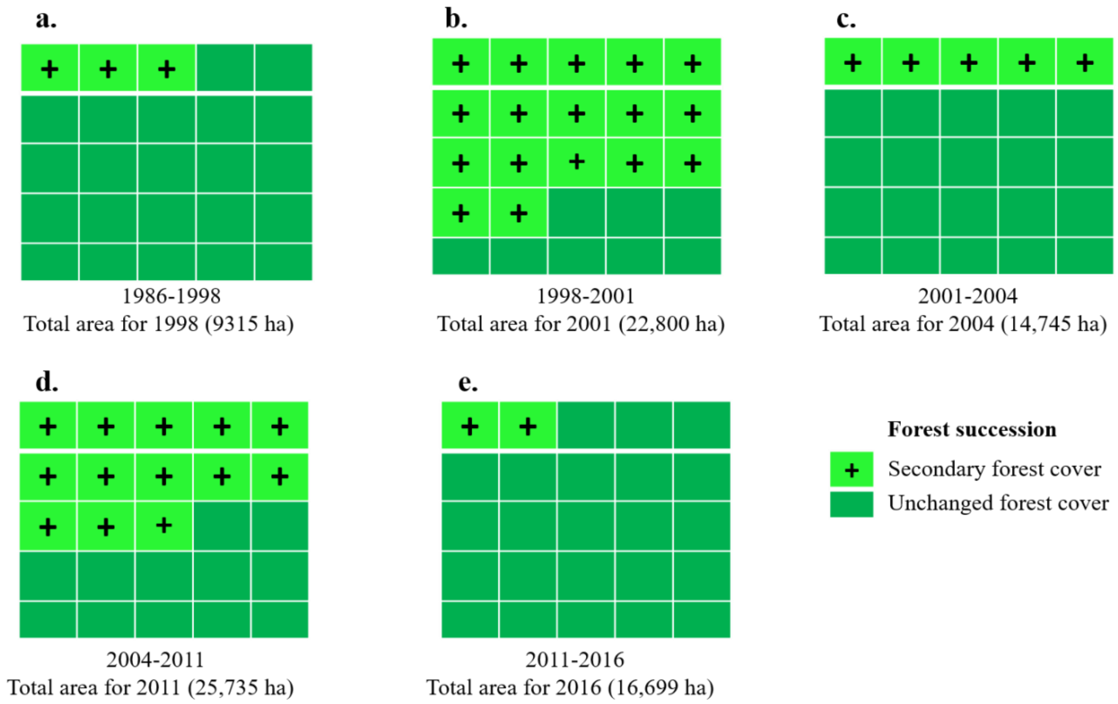

Figure 4.7: Secondary forest succession in Miombo woodland of Luanshya. A cluster of 25 cells represent the total forested areas in the final state (100%), while each unit denotes 4% (rounded to the nearest whole number) of either SF cover or unchanged forest cover for the five periods of, (a) 1986-1998, (b) 1998-2001, (c) 2001-2004, (d) 2004-2011, and (e) 2011-2016.

4.1.2 Spatial-temporal dynamics of LULC changes for Bushbuckridge

The LULC maps for Bushbuckridge showed notable LULC changes during the 24-year period from 1992 to 2016. Of the 6194 ha of the study site, the total area that changed was 3116 ha for 1992-1998, 4763 ha for 1998-2001, 2733 ha for 2001-2006, 2812 ha for 2006-2010, and 3157 ha for 2010-2016 (Figure 4.8). The changed areas therefore represented 50%, 77%, 44%, 45% and 82% of the total area or an average annual change of 8%, 26%, 9%, 11%

and 14% for the observed time periods, respectively. The differences in the magnitude and rates of land cover changes demonstrate that the number of pixels within each class of the LULC maps changed inconsistently from the observed initial state to the final state.

Reference points of between 444-730 pixels were used to assess the accuracy of the generated LULC maps for Bushbuckridge (Table 4.3). The overall accuracy of maps from SVM ranged from 91% to 97%, while Kappa coefficients was between 0.86 and 0.97. From the same reference points, Maximum Likelihood classifier reported overall accuracies and Kappa coefficients of 90-96% and 0.88-0.96, respectively (Appendix A2). The difference in the LULC maps from the two classifier was not statistically significant ($\rho = 0.00$). Similar to Luanshya, all quantitative change analysis for Bushbuckridge were calculated and reported based on the SVM method, taking an assumption that statistically similar analysis would be derived using Maximum Likelihood method.

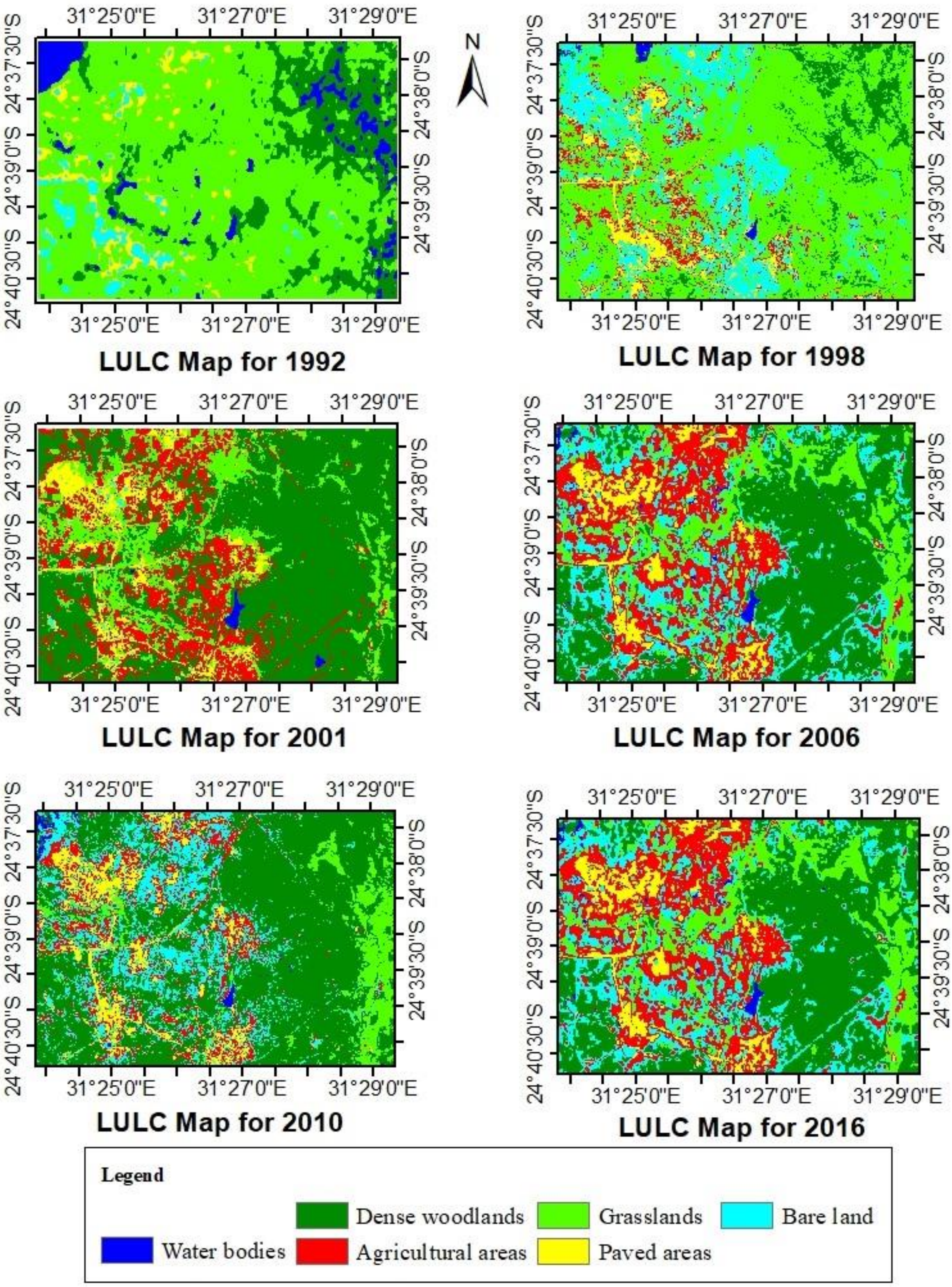

Figure 4.8: LULC for 1992, 1998, 2001, 2006, 2010 and 2016 in Bushbuckridge.

Table 4.3 - Support Vector Machine: Classification error matrices for Bushbuckridge

		Ground Truth ROI Pixels							
		Agricultural areas	**Bare land**	**Dense woodlands**	**Grasslands**	**Paved areas**	**Water bodies**	**Total**	**UA (%)**
LULC for 1992	**Agricultural areas**	-	-	-	-	-	-	-	-
	Bare land	-	56	0	0	24	0	**80**	**70**
	Dense woodlands	-	0	114	0	0	1	**115**	**99**
	Grasslands	-	0	0	182	0	0	**182**	**100**
	Paved areas	-	26	0	0	66	0	**92**	**72**
	Water bodies	-	0	0	0	0	95	**95**	**100**
	Total	**-**	**82**	**114**	**182**	**90**	**96**	**564**	
	PA (%)	**-**	**68**	**100**	**100**	**73**	**99**		
	Overall accuracy (%)		**91**						
	Kappa coefficient		**0.88**						
LULC for 1998	**Agricultural areas**	16	0	0	0	0	0	**16**	**49**
	Bare land	14	40	0	0	11	1	**66**	**61**
	Dense woodlands	0	0	52	2	0	2	**56**	**96**
	Grasslands	1	0	2	101	0	1	**105**	**98**
	Paved areas	2	26	0	0	95	0	**123**	**90**
	Water bodies	0	0	0	0	0	78	**78**	**95**
	Total	**33**	**66**	**54**	**103**	**106**	**82**	**444**	
	UA (%)	**100**	**61**	**93**	**96**	**77**	**100**		
	Overall accuracy (%)		**91**						
	Kappa coefficient		**0.88**						
LULC for 2001	**Agricultural areas**	107	1	0	0	0	0	**108**	**100**
	Bare land	0	15	0	0	1	0	**16**	**94**
	Dense woodlands	0	0	113	0	0	1	**114**	**99**
	Grasslands	0	0	0	132	0	0	**132**	**100**
	Paved areas	0	15	0	1	101	0	**117**	**86**
	Water bodies	0	0	0	0	0	143	**143**	**100**
	Total	**107**	**31**	**113**	**133**	**102**	**144**	**630**	
	PA (%)	**100**	**48**	**100**	**99**	**99**	**99**		
	Overall accuracy (%)		**97**						
	Kappa coefficient		**0.96**						
LULC for 2006	**Agricultural areas**	101	2	0	0	0	1	**104**	**97**
	Bare land	13	108	1	0	0	2	**124**	**87**
	Dense woodlands	0	0	104	0	0	0	**104**	**100**
	Grasslands	0	0	0	115	0	0	**115**	**100**
	Paved areas	0	0	0	0	107	0	**107**	**100**
	Water bodies	0	4	0	0	0	172	**176**	**98**
	Total	**114**	**114**	**105**	**115**	**107**	**175**	**730**	
	PA (%)	**89**	**95**	**99**	**100**	**100**	**98**		
	Overall accuracy (%)		**97**						
	Kappa coefficient		**0.96**						
LULC for 2010	**Agricultural areas**	94	0	0	0	0	0	**94**	**100**
	Bare land	10	106	4	0	11	11	**142**	**75**
	Dense woodlands	0	0	99	0	0	2	**101**	**98**
	Grasslands	0	0	0	110	0	0	**110**	**100**
	Paved areas	2	0	0	0	89	0	**91**	**98**
	Water bodies	0	1	0	0	0	95	**96**	**99**
	Total	**106**	**107**	**103**	**110**	**100**	**108**	**634**	
	PA (%)	**89**	**99**	**96**	**100**	**89**	**88**		
	Overall accuracy (%)		**94**						
	Kappa coefficient		**0.92**						
LULC for 2016	**Agriculture areas**	130	0	0	0	1	0	**131**	**99**
	Bare land	1	28	0	1	3	0	**33**	**85**
	Dense woodlands	0	0	37	1	0	2	**40**	**93**
	Grasslands	0	0	2	146	0	3	**151**	**97**
	Paved areas	0	10	0	0	104	0	**114**	**91**
	Water bodies	0	0	0	0	0	83	**83**	**100**
	Total	**131**	**38**	**39**	**148**	**108**	**88**	**552**	
	PA (%)	**99**	**74**	**95**	**99**	**96**	**94**		
	Overall accuracy (%)		**96**						
	Kappa coefficient		**0.95**						

4.1.2.1. Changes for the period 1992-1998

Table 4.4 and Figure 4.9a indicate that in 1992, grassland dominated the landscape of Bushbuckridge, with 4185 ha or 68% of the total area. About 62% of grassland cover for 1992 was retained in 1998. During this period, the spatial extent of grassland decreased by 512 ha, changing from 4185 ha (1992) to 3673 ha (1998) (Figure 4.9a). Because some land cover were gained from bare land (49 ha), wooded areas (807 ha), paved areas (39 ha) and water bodies (177 ha), grassland continued to dominate the landscape, covering 59% of the total area. In 1998, woodlands retained only 29% of the 1992 forest cover. Most conspicuously, about 68% of woodlands changed into grassland, 2% changed into bare land and 1% changed into agricultural areas and paved areas. This means that agricultural areas, bare land and paved areas were introduced in Bushbuckridge, largely at the expense of savanna woodland and grassland. With only about 165 ha of dense woodlands gained, the total cover of dense woodlands decreased from 1189 ha in 1992 to 506 ha in 1998, at average rate of 14.00% yr^{-1} (Table 4.4). Similar to Luanshya, Figure 4.9a also shows the absence of agricultural areas in the initial state, and its subsequent addition or presence in the final state. The introduction of agricultural fields in the area was largely from the conversion of about 325 ha of grassland cover (Table 4.4).

Table 4.4 - Change matrix in Bushbuckridge for the periods 1992-1998, 1998-2001, 2001-2006, 2006-2010 and 2010-2016 (units in hectares). Bold values indicate unchanged LULC type.

	Area (hectares)	LULC 1992						
		Agriculture areas	Bare land	Dense woodlands	Grasslands	Paved areas	Water bodies	Total
LULC 1998	**Agriculture areas**	-	43	13	325	43	4	**428**
	Bare land	-	**33**	20	959	110	82	**1203**
	Dense woodlands	-	0	**341**	118	0	47	**506**
	Grasslands	-	49	807	**2600**	39	177	**3673**
	Paved areas	-	85	6	167	**92**	4	**355**
	Water bodies	-	0	2	15	0	**12**	**28**
	Total	**-**	**210**	**1189**	**4185**	**284**	**326**	**6194**
	Changes	**-**	**177**	**848**	**1585**	**191**	**314**	**3116**

Table 4.4 (*continued*)

		LULC 1998						
LULC 2001	Agriculture areas	**144**	478	2	456	116	2	**1198**
	Bare land	0	**18**	0	0	14	0	**33**
	Dense woodlands	96	240	**501**	2536	18	12	**3403**
	Grasslands	155	225	2	**644**	91	6	**1123**
	Paved areas	32	237	0	29	**115**	0	**413**
	Water bodies	1	5	1	8	1	**9**	**24**
	Total	**428**	**1203**	**506**	**3673**	**355**	**28**	**6194**
	Changes	**285**	**1185**	**5**	**3029**	**240**	**20**	**4763**

	Area (hectares)	LULC 2001						
		Agriculture areas	Bare land	Dense woodlands	Grasslands	Paved areas	Water bodies	Total
LULC 2006	Agriculture areas	**648**	1	213	346	168	0	**1377**
	Bare land	347	**3**	631	254	17	6	**1259**
	Dense woodlands	46	0	**2134**	41	0	1	**2223**
	Grasslands	54	0	399	**442**	10	0	**905**
	Paved areas	93	28	6	38	**217**	1	**384**
	Water bodies	9	0	20	2	0	**17**	**47**
	Total	**1198**	**33**	**3403**	**1123**	**413**	**24**	**6194**
	Changes	**550**	**30**	**1269**	**681**	**196**	**7**	**2733**

	Area (hectares)	LULC 2006						
		Agriculture areas	Bare land	Dense woodlands	Grasslands	Paved areas	Water bodies	Total
	Agriculture areas	**445**	115	10	55	81	3	**708**
	Bare land	580	**344**	85	99	54	19	**1180**
	Dense woodlands	176	702	**2017**	426	3	8	**3332**
	Grasslands	43	63	99	**318**	3	2	**528**
	Paved areas	125	20	2	6	**243**	1	**397**
	Water bodies	8	14	10	1	0	**15**	**48**
	Total	**1377**	**1259**	**2223**	**905**	**384**	**47**	**6194**
	Changes	**932**	**914**	**206**	**587**	**141**	**32**	**2812**

	Area (hectares)	LULC 2010						
		Agriculture areas	Bare land	Dense woodlands	Grasslands	Paved areas	Water bodies	Total
LULC 2016	Agriculture areas	**260**	399	252	28	146	3	**1088**
	Bare land	90	**182**	476	52	39	1	**840**
	Dense woodlands	68	184	**2364**	379	6	7	**3008**
	Grasslands	156	227	206	**67**	76	2	**734**
	Paved areas	126	140	17	3	**129**	1	**416**
	Water bodies	9	48	17	0	0	**34**	**108**
	Total	**708**	**1180**	**3332**	**528**	**397**	**48**	**6194**
	Changes	**448**	**998**	**968**	**462**	**267**	**14**	**3157**

4.1.2.2 Changes for the period 1998-2001

A reversal from grassland to forest dominated landscape was observed during the period from 1998 to 2001 (Figure 4.9b). In detail, approximately 69% of grassland cover changed into dense woodlands, while only 2% of wooded areas changed into grassland (Table 4.4). In addition to retaining 99% of dense woodland, about 3-7% of new forest stand (Figure 4.8: LULC map for 2001) was established on areas that were initially (1998) classified as agricultural areas, bare land and paved area and water bodies. This suggested that agricultural areas are amenable to forest grow back, while some paved areas (residential areas) were found to be associated with mixed pixels (e.g. rooftop, grass, few individual trees, cultivated fields). This means that pixel classification of some LULC classes, especially paved areas was based on the extreme and prevailing dominant feature of the averaged spectral classes per 30 x 30 m. On the other hand, only marginal dense woodland cover of about 5 ha (0.1% of the total changes) were converted to agricultural areas, grassland and water bodies. Hence, dense woodlands increased from 506 ha in 1998 to 3403 ha in 2001. Conversely, continued increase in agricultural areas (from 428 ha to 1198 ha) and paved areas (from 355 ha to 413 ha) indicated human encroachment on savanna ecosystems (Figure 4.9b). During the same period, bare land decreased from 1203 ha to 33 ha, while water bodies with the smallest areal extent had a marginal decrease of 4 ha.

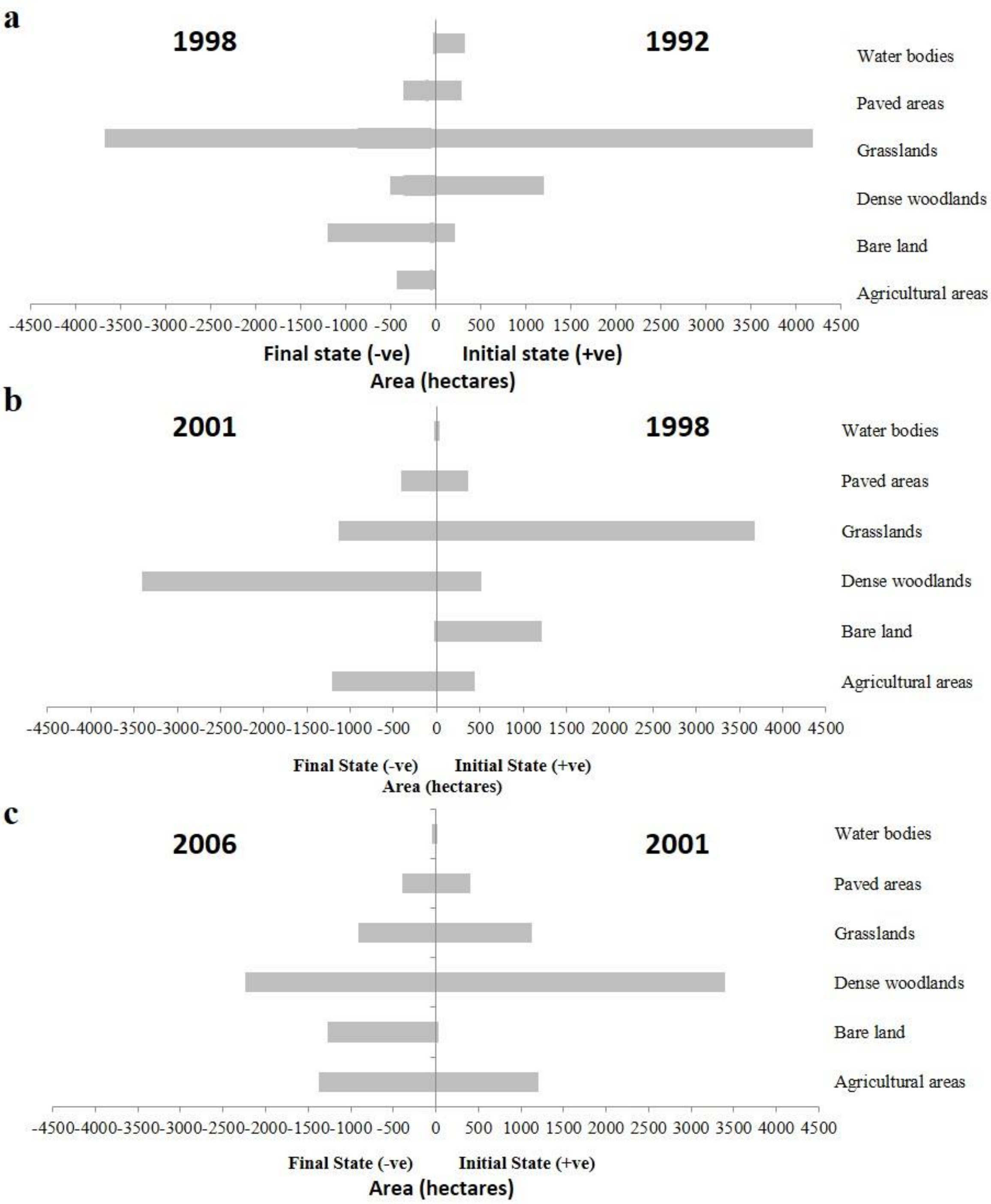

Figure 4.9: Dynamics of LULC changes for the period 1992-1998, 1998-2001 and 2001-2006 in Bushbuckridge. The graph shows the total areal changes for (a) 1992-1998, (b) 1998-2001 and (c) 2001-2006. The absolute values in the positive segment depict the different LULC types and the observed areal extent in the initial state, while the negative segments illustrate the final state.

4.1.2.3 Changes for the period 2001-2006

Just like the periods 1992-1998 and 1998-2001, spatial data exhibited continual increase in agricultural areas from 1198 ha (2001) to 1377 ha (2006), at an average rate of 2.79% yr^{-1} (Table 4.4). Bare land (2001: 33 ha; 2006: 1259 ha) expanded during this period as did water bodies (2001: 24 ha 2006: 47 ha). The reliance of agricultural activities on water availability (e.g. rainfall) is highlighted by the increase in the areal extent of agricultural areas and water bodies. By contrast, woodlands, grassland and paved areas experienced a steady decrease (Figure 4.9c). Due to increased deforestation, a total of 1269 ha of forested cover changed into: agricultural areas (17%), bare land (50%), grassland (31%), and water bodies (2%). It was evident that the total area that underwent change from 2001 to 2006 (2733 ha, at 547 ha yr^{-1}) was significantly less than the total changes observed during the previous period of 1998-2001 (4763 ha or 1588 ha yr^{-1}).

4.1.2.4 Changes for the period 2006-2010

In contrast to the earlier trends where the spatial dominance covaried between the two vegetation types (woodlands and grassland), the results indicate that savanna woodlands retained areal dominance during the period 2006-2010, covering about 36% and 54% of the total area, respectively (Table 4.4 and Figure 4.10a). This is also denoted by the retention of 2017 ha or 91% of the total forested areas (2006) into the final state (2010), while relatively smaller areas of dense woodland changed to bare land (85 ha) and grassland (99 ha). Depicting increased regeneration, a total of about 1318 ha of non-forested areas in 2006 changed to dense woodlands in 2010. The total spatial extent of dense woodlands increased from 2223 ha in 2006 to 3332 ha in 2010, at an average rate of 10.12% yr^{-1}. This findings further revealed that agricultural areas (669 ha) and bare land (79 ha) decreased during this four-year period, with the majority of land changing to dense woodlands. With less natural or human induced disturbances, the observed trend emphasised the ability of wooded areas to recuperate after clearance. Conversely, both paved areas and water bodies maintained a slight upward trend, increasing from 384 ha to 397 ha and 47 ha to 48 ha, respectively (Table 4.4).

4.1.2.5 Changes for the period 2010-2016

The period 2010-2016 showed a marginal decline but continued dominance in forested cover (3332 ha in 2010 and 3008 ha in 2016), covering 54% (2010) and 49% (2016) of the total area (Figure 4.10b). About 2364 ha of dense woodland cover was retained, whereas 476 ha, 252 ha and 206 ha changed to bare land, agricultural areas and grassland, respectively. From the converted dense woodlands and agricultural areas had the largest gains, increasing by 380 ha during the six-year period. On the other hand, agricultural fields, grassland, paved areas and water bodies increased in total area by gaining land, largely from dense woodlands and bare land. The conversion of 48 ha of bare land to water bodies suggest that during water stress periods, decrease in water bodies tend to expose some bare land (Table 4.4). Increase in water bodies also corresponded with intensification of agricultural activities, with an increase of 828 ha (agricultural areas) gained from bare land (37%), wooded areas (23%), grassland (3%), and paved areas (13%).

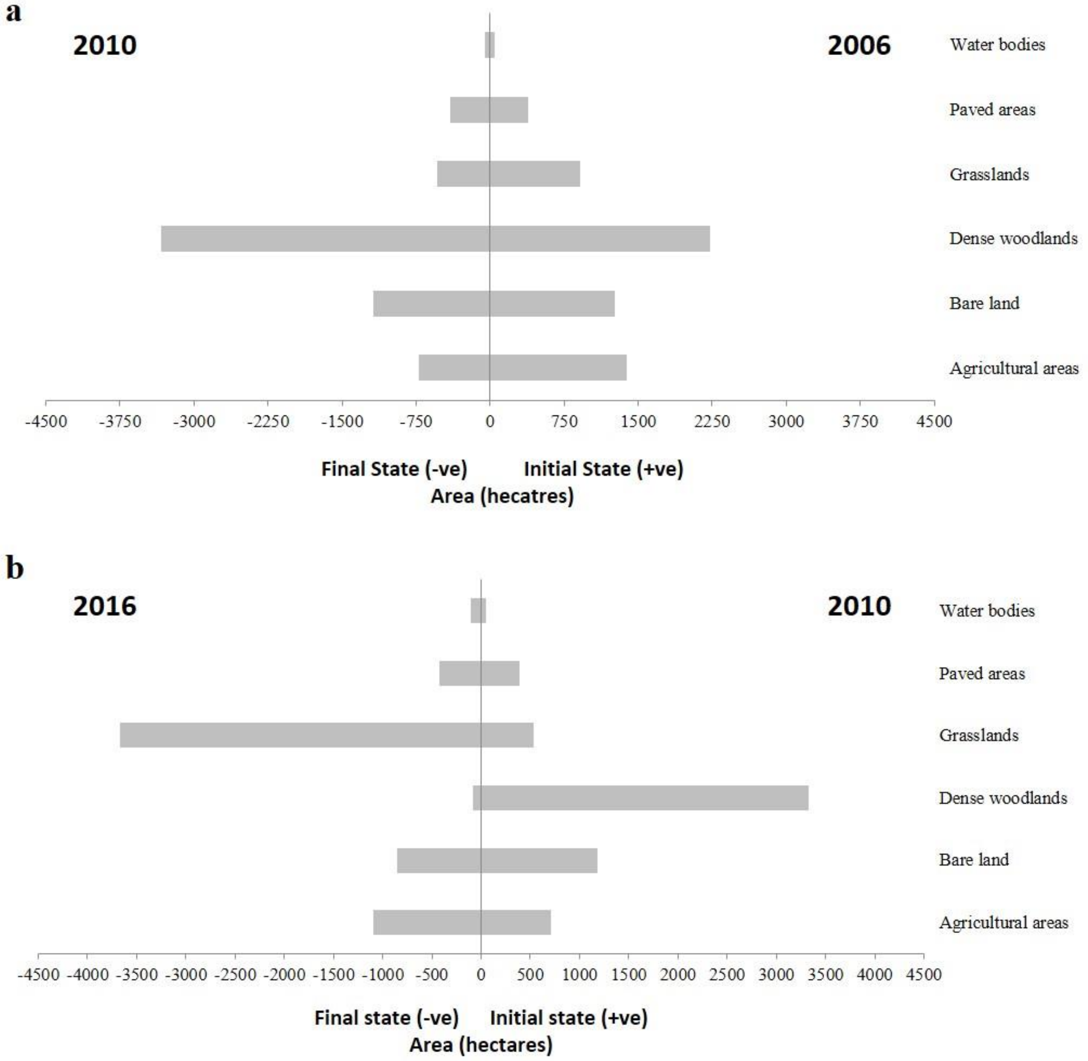

Figure 4.10: Dynamics of LULC changes for the period 2006-2010 in Bushbuckridge. The graph shows the total areal changes for (a) 2006-2010 and (b) 2010-2016. The absolute values, positive segment depict the different LULC types and the observed areal extent in the initial state, while the negative segments illustrate the final state.

4.1.2.6. Transitional pathways for 1992-1998 and 1998-2001

The unchanged (curved arrows) trajectories indicated that only 62% of grassland, 32% of paved areas, 29% of forested areas and 4% of water bodies were geographically found on the same pixels in 1992 and 1998 (Figure 4.11a). Extensive forest clearance is denoted by a two-way transitional changes, forested areas⇌grassland, which were significantly asymmetrical and not of equal magnitude, 67% (3%). Some grassland cover was directly or indirectly converted to agricultural areas along pathways of grassland→agricultural area (7%) or grassland→bare land (23%)→agricultural areas (20%). Two-way transitional pathways with departing intensities of 41% from bare land to paved areas and 39% from paved areas to bare land were also observed. Water bodies retained the smallest area among the five LULC types, and the associated change of about 25% of water bodies to bare land may suggest surface water stress, especially in the latter part of the observed time period. Cultivated fields became an established LULC type between 1998 and 2001 (Figure 4.11b). This is illustrated by 34% of agricultural areas that remained unchanged, while the trajectories denoted as, agricultural areas→grassland (36%), grassland→forested areas (69%), and agricultural areas→forested areas (22%) suggest natural revegetation due to partial or complete invasion of cultivated fields, and subsequent return to grassland community and/or wooded areas. As a result, woodland was the highest beneficiary of LULC changes among all classes.

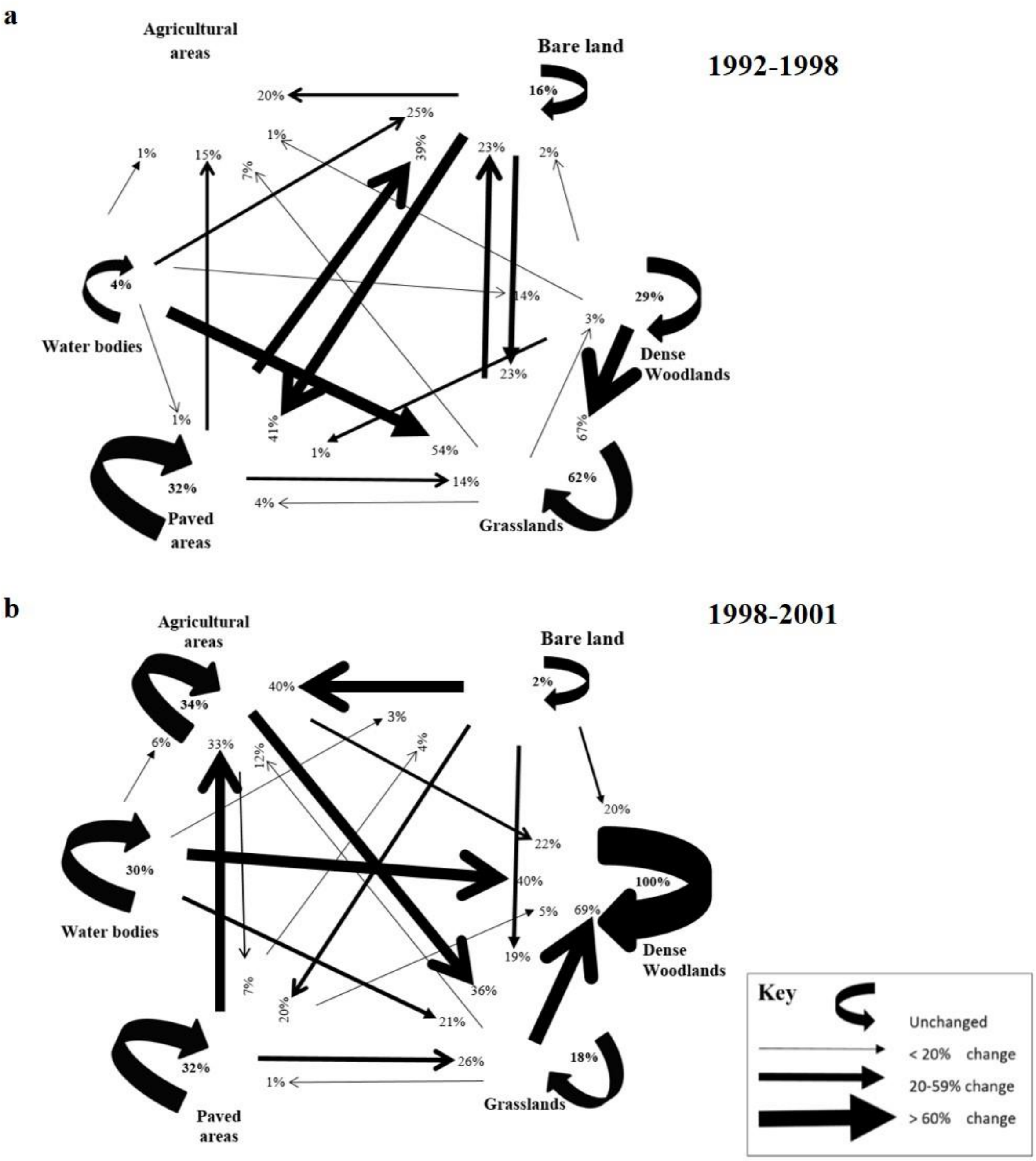

Figure 4.11: Transitional pathways associated with LULC changes for the periods 1992-1998 and 1998-2001 in Bushbuckridge. The thickness of lines and arrows indicate the intensity or proportion of change and the class into which pixels changed into the final state, respectively. The curved arrows show the proportion of pixels that persisted and remained unchanged from the initial state (1992 for Figure 4.11a and 1998 for Figure 4.11b) to the final state (1998 for Figure 4.11a and 2001 for Figure 4.11b).

4.1.2.7 Transitional pathways for 2001-2006, 2006-2010 and 2010-2016

Expansion in human settlements is evident by increase in the proportion of paved areas that remained unchanged from 32% (1992-2001) to 53% (2001-2006) and 63% (2006-2010) (Figures 4.11, 4.12). These changes occurred mostly at the expense of bare land (e.g. bare land→paved areas, 85%) (Figure 4.12a). With respect to the large total area of natural vegetation, the results indicate that land available for agriculture (from bare land) was as a result of forest (19%) and grassland (23%) clearance that left some areas with no vegetation cover. Overall, the area that remained unchanged was smallest for bare land followed by grassland (39%), while water bodies (71%), forested areas (63%) as well as paved areas retained the majority of land cover (2001 to 2006). In other words, bare land and paved areas were associated with arriving pathways of significant intensities (>20%). In addition to paved areas, forested areas retained 63% (91%) of cover in 2006 (2010), with only marginal sites changing to grassland (5%) and bare land (4%) (Figure 4.12b). Similar to the previous periods, water bodies consistently changed to bare land (2006-2010: 40%). The pathways departing from paved areas along trajectories of paved→agricultural areas, paved areas→ bare land, paved areas→forested areas, and paved areas→grassland, represent the average spectral measurements and the composition of classes that exist (per 30 x 30 m) in community settlement areas.

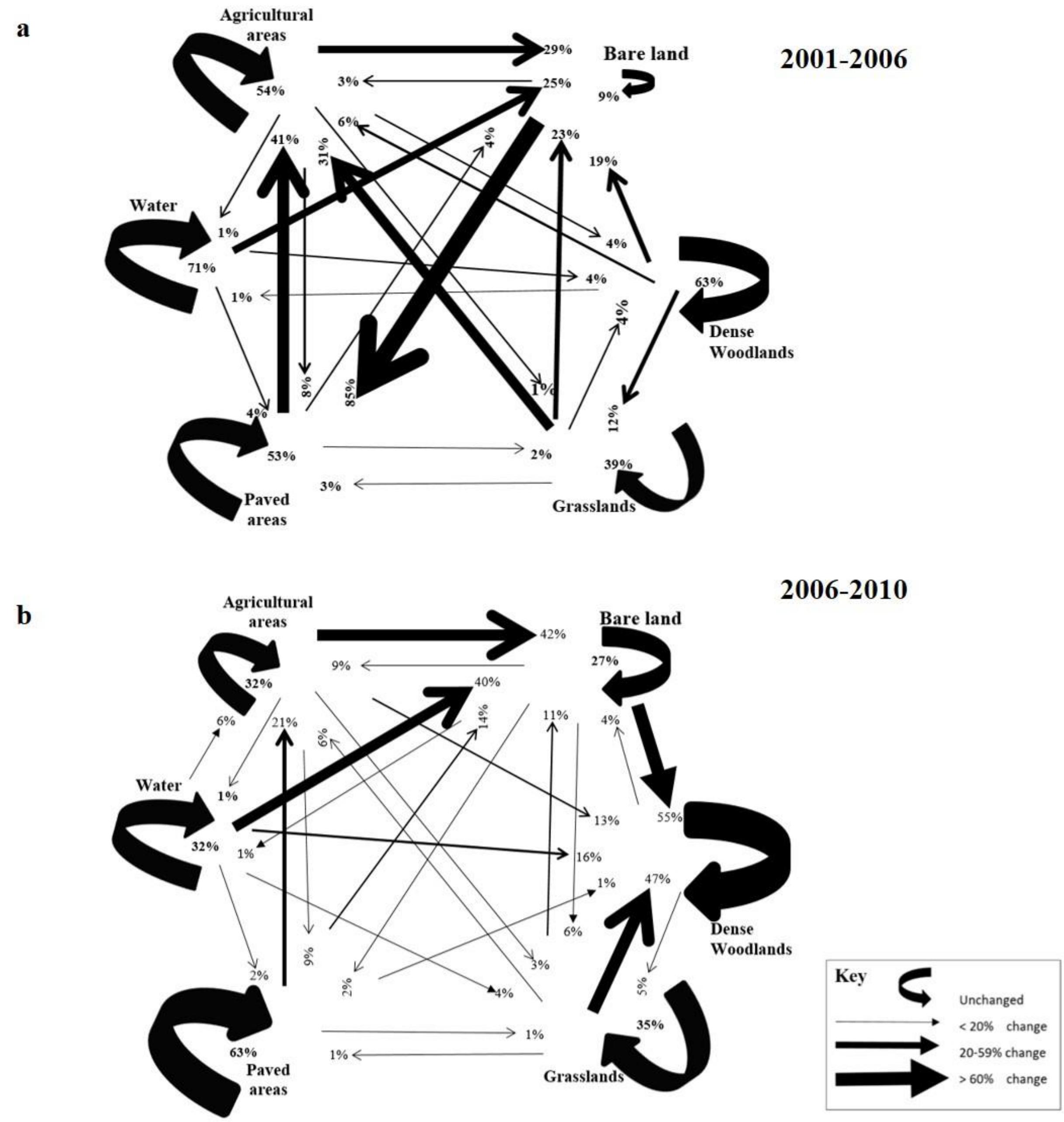

Figure 4.12: Transitional pathways associated with LULC changes for the periods 2001-2006 and 2006-2010 in Bushbuckridge. The thickness of lines and arrows indicate the intensity or proportion of change and the class into which pixels changed into the final state, respectively. The curved arrows show the proportion of pixels that persisted and remained unchanged from the initial state (2001 for Figure 4.12a and 2006 for Figure 4.12b) to the final state (2006 for Figure 4.12a and 2010 for Figure 4.12b).

Similar to the periods, 1998-2001, 2001-2006 and 2006-2010, the common occurrence of transitions from 2010 to 2016 indicate that bare land and grassland continued to act as LULC types transitional to other classes. This is depicted by the smallest proportion of unchanged area, 13% for grassland and 15% for bare land, and conversion of grassland to forested areas (71%) and bare land to agricultural areas (34%) (Figure 4.13). Due to the highest percentage of unchanged areas (71%), forested areas and water bodies were associated with the smallest departing pathways of change (depicted by the slender arrows, with <14% and <15%, respectively). Within the total area of 6194 ha for Bushbuckridge, the five periods emphasised that LULC change is not a fixed pattern, but has a large variability in specific trajectories, which results in spatial-temporal synchronous trends with continuous increases in the total area of some LULC types and decreases in other classes.

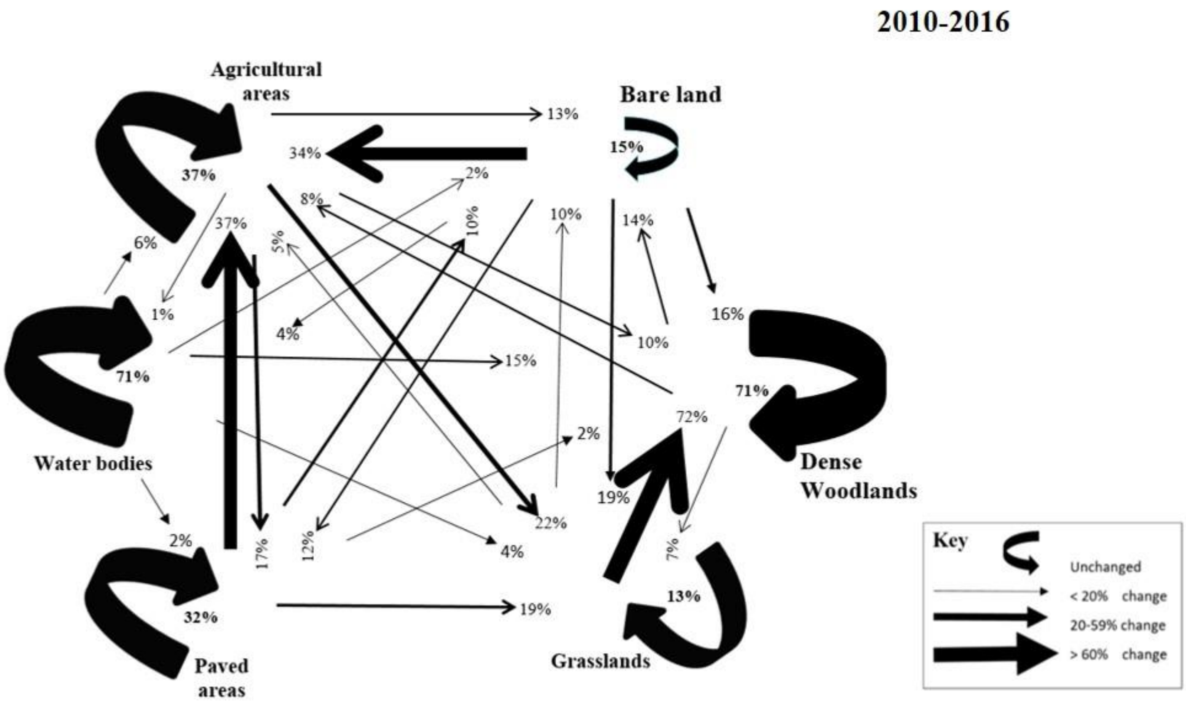

Figure 4.13: Transitional pathways associated with LULC changes for the period 2010-2016 in Bushbuckridge. The thickness of lines and arrows indicate the intensity or proportion of change and the class into which pixels changed into the final state, respectively. The curved arrows show the proportion of pixels that persisted and remained unchanged from the initial state (2010) to the final state (2016).

4.1.2.8 Changes in secondary woodland cover in Bushbuckridge

Along the observed timeline from 1992-2016, the relative mean number of 4%-sized cells for SF cover was nine and 16 for unchanged forest cover (Figure 4.14), which means that 36% of forested areas were newly recruited forest stands. In detail, regeneration and forest succession was highest from 1998-2001 (84%) and lowest during the period 2001-2006 (4%). Increased SF cover (1998-2001) compared closely with changes that occurred along transitional pathways of agricultural areas→forested areas (22%) and grassland→forested areas (69%), with both trajectories indicating establishment of new forested areas mostly on former cultivated land and grassland cover (Figure 4.11b). It may also imply that forest clearance spurred regeneration and forest succession to fill the newly created space (Figure 4.14b), but development of a more closed canopy offered less room for enhanced and continued recruitment of saplings and young trees (Figure 4.14 c,e).

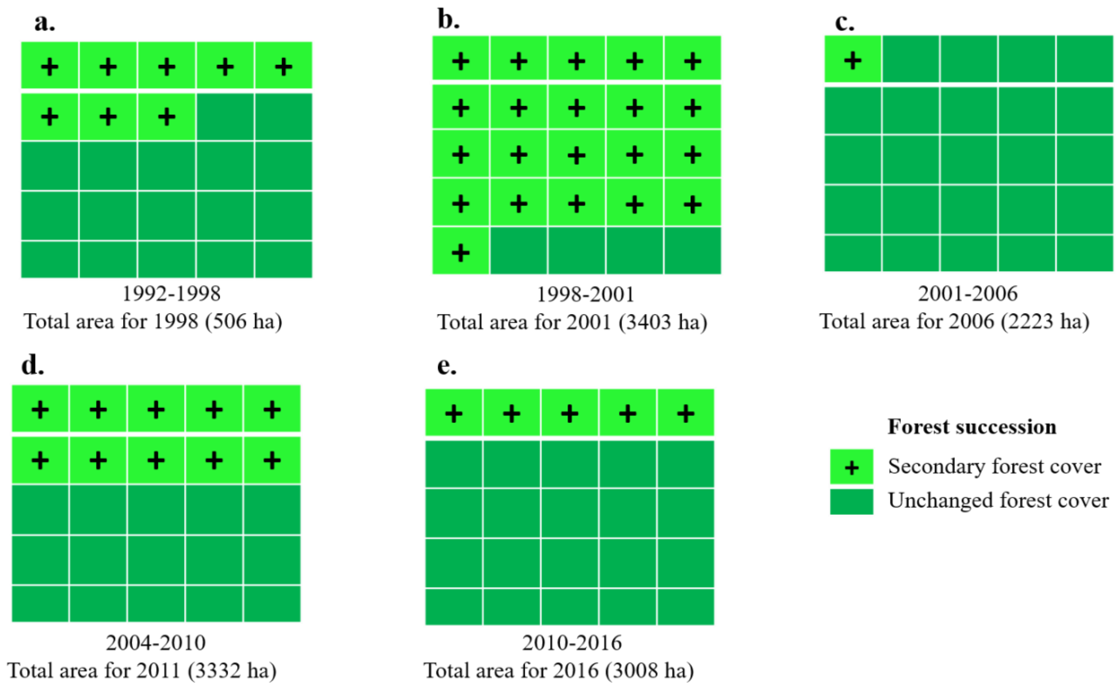

Figure 4.14: Secondary forest succession in savanna woodlands of Bushbuckridge. A cluster of 25 cells represent the total forested areas in the final state (100%), while each unit denotes 4% of either SF cover or unchanged forest cover for the five periods of, (a) 1992-1998, (b) 1998-2001, (c) 2001-2006, (d) 2006-2010 (d), and (e) 2011-2016.

4.1.3 Differences in the rate change of forest cover between Luanshya and Bushbuckridge

Estimates based on Puyravaud's (2003) equation showed an imbalance between the rate of deforestation and regeneration during the five observed periods for each study area (Table 4.5). In Luanshya (1986-2016), forest cover was lost at a relatively higher rate (3.39 yr^{-1}) than the rate at which new growths replaced the cleared stands (1.21 yr^{-1}). The largest reforestation rates were observed from 1998 to 2001 (37.63% yr^{-1}), followed by the periods 2004-2011 (10.66% yr^{-1}) and 2001-2004 (6.87% yr^{-1}). In contrast, Bushbuckridge had lower deforestation rate for the entire period from 1992 to 2016 (0.02% yr^{-1}) than the rate of forest replenishment (0.13% yr^{-1}). During this period, the largest deforestation rates were 20.82% yr^{-1} for 1992-1998, 9.33% yr^{-1} for 2001-2006, and 5.72% yr^{-1} for 2010-2016. Between the different periods, regeneration rates for 2001-2006 (0.82%) and 2010-2016 (4.02% yr^{-1}) were significantly lower than the other observed periods (63.86 yr^{-1}: 1998-2001; 12.55 yr^{-1}: 2006-2010; 6.58 yr^{-1}: 1992-1998). Between the two study areas, the differences in forest rate change highlight the difference in climate, topography, soil type and forest structure.

Table 4.5 - Comparison of dense woodland cover change based on the annual rates of deforestation and reforestation

Luanshya	**1986-1998**	**1998-2001**	**2001-2004**	**2004-2011**	**2011-2016**	**1986-2016**
Deforestation (%)	11.55	7.79	21.40	2.70	10.59	**3.39**
Regeneration (%)	1.23	37.63	6.87	10.66	1.94	**1.21**
Cover change (ha)	-22,802	13,485	-8055	10,990	-9036	**-15,478**
Bushbuckridge	**1992-1998**	**1998-2001**	**2001-2006**	**2006-2010**	**2010-2016**	**1992-2016**
Deforestation (%)	20.82	0.33	9.33	2.43	5.72	**0.02**
Regeneration (%)	6.58	63.86	0.82	12.55	4.02	**0.13**
Cover change (ha)	-683	2897	-1180	1109	-324	**1819**

Where negative and positive values imply decrease and increase in the spatial extent of forest cover, respectively.

4.2 Effects of LULC changes on forests: Characteristics and composition of sites

Figure 4.15 shows the DEM, and topographic positions, features and drainage catena that characterised the sampled forest sites of the two study areas. In Luanshya, the distance between the seven different sampling sites ranged from 1.33-13.37 km (Figure 4.15a). Site 1 and Site 3 were the two furthermost forest sites, while the closest sites were Site 6 and Site 7. The total area has an average elevation of 1234 ± 14 m above sea level (asl). Sites with lowest elevations (Site 2: 1215 m; Site 6: 1219 m; Site 7: 1228 m) were found in relatively low-lying areas (e.g. areas near streams, rivers and dams). Site 1 had the highest altitude of 1258 m asl, followed by Site 5 (1247 m) and Sites 3, 4 (1238 m). In Bushbuckridge, the distance between the sampled sites ranged between 0.28 km and 4.52 km, and had mean altitude of 416 ± 12 m asl (Figure 4.15b). Relative to Site 1, Site 3 and Site 7, with average elevations of 398 m, 404 m and 412 m asl, respectively, Site 4 (422 m), and Site 5, 6 (428 m) were upslope forested areas. The close proximity of Site 1, Site 3 and Site 7 to low-lying areas, further indicated that these sites were midslope or downslope areas.

The sampled sites were characterised by forest stands of different developmental stages which were classified as, undisturbed forest (UDF), partially disturbed forest (PDF), SF and regeneration forest (RF) plots (Table 4.6). Undisturbed forest plots were intact with no evidence of logging activities, and had relatively old tree growth and dense canopy cover (Figure 4.16). The PDF plots were similar to UDF, but were characterised by forest stands with less dense canopy cover. Further, sparse stumps were observed, which provided evidence of recent selective tree felling and logging (Figure 4.16g).

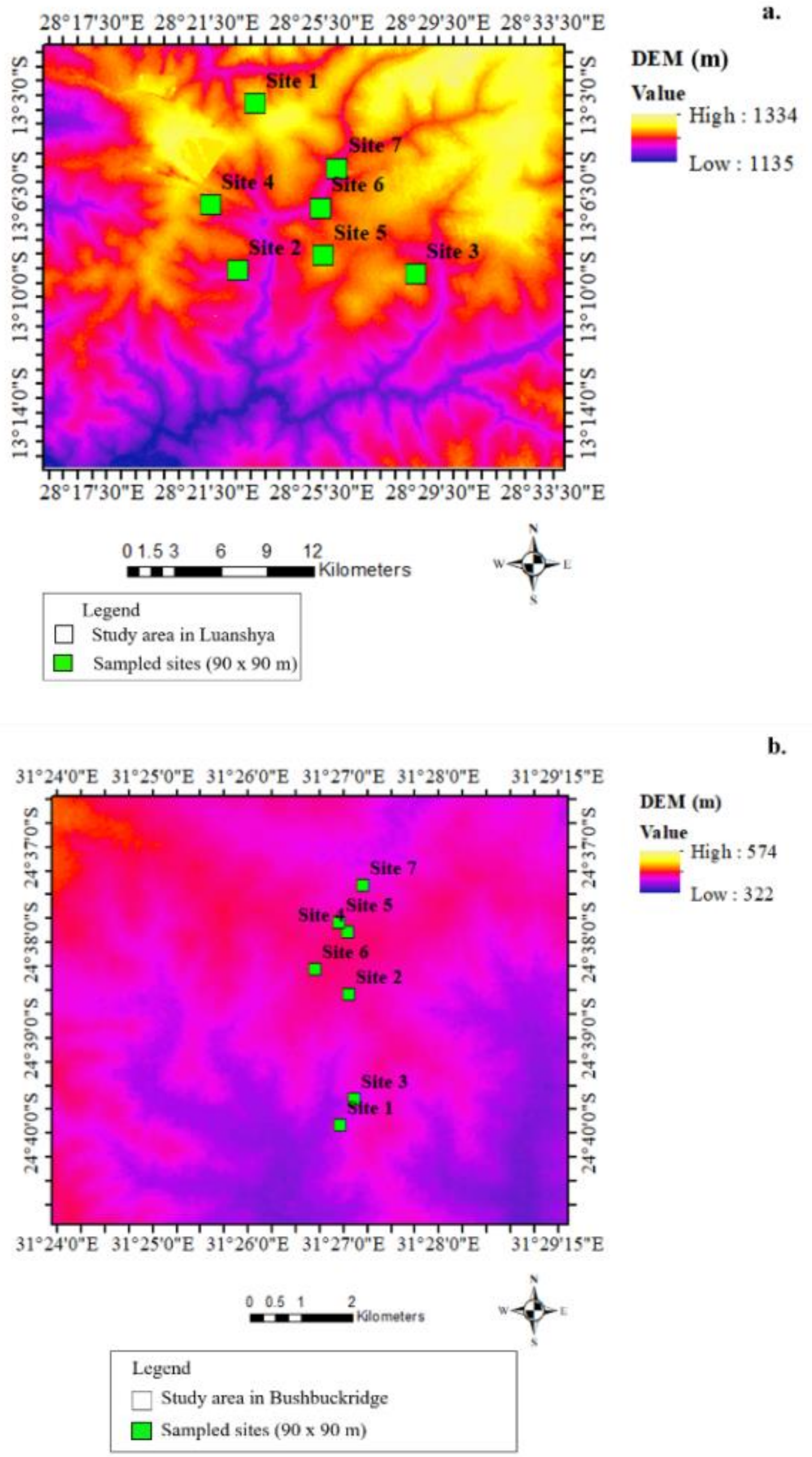

Figure 4.15: Topographic locations of the sampled forest sites (90 x 90 m) in (a) Luanshya and (b) Bushbuckridge.

Each site was nested plots measuring 30 x 30 m, which corresponded to the spatial resolution of Landsat images.

Among the four forest classes of different succession stages, SF sites were the most common type, Site 7 in Luanshya and Sites 1-3, 5, 7 in Bushbuckridge (Table 4.6). These sites were stocked with slender individual trees that coppiced and developed from stumps as multi-stems (Figure 4.16h, i). The forest floor in UDF, PDF and SF areas were partially or completely covered by herbaceous plants (e.g. grass, fern and sparse saplings) and a stratum of seed pods. The RF sites were only observed in Sites 3, 5, 6 in Luanshya and Sites 4, 6 in Bushbuckridge, and were characterised by saplings or young trees (Figure 4.16a), with DBH and tree height of less than 4.0 cm and 4.0 m, respectively (Figure 4.16d).

Table 4.6 - Classification and description of the sampled forest sites

Classification	Description	Luanshya	Bushbuckridge
UDF	: Forest plots that were consistently classified as dense forested areas (1986-2016), with no evidence of recent disturbance (e.g. stumps). These plots had no indications of critical disturbance, at least in the recent years (1986-2016; (Figure 4.16c).	Site-1	N/A
PDF	: Plots that were consistently classified as dense forested areas from (1986-2016), but sparse stumps were evident (Figure 4.16g).	Site 2, 4	N/A
SF	: Plots that were once not classified as forested areas, but were classified as dense forested in 2016. Evidence of disturbance included, increased number of stumps and multi-stems (coppiced from stumps) (Figure 4.16h, i)	Site-7	Site 1-3, 5, 7
RF	: Plots classified as forested areas, but individual saplings and young trees had DBH of less than 4.0 cm or tree height of less than 4.0 m (Figure 4.16d).	Site 3, 5, 6	Site 4, 6

Classification of forest sites was limited to the temporal variations of Landsat vegetation indices for 1986, 1998, 2001, 2004, 2011 and 2016, and the 2016 field evidence of forest disturbance. Where N/A means not applicable to the site.

Figure 4.16: Forest plots of different succession stages and structure in Luanshya (a, b and c) and Bushbuckridge (d, e and f). The photos (Figure 4.16g, h, i) also shows some notable evidence of forest disturbance in PDF and SF plots and subsequent tree succession (Figure 4.16h, i).

4.2.1 Forest species composition

A total of 52 tree species were identified across the seven forest sites in Miombo woodland (Table 4.7). Species richness (number of different species per plot, 30 x 30 m) was highest in PDF (Site-4: 35 species), followed by SF (Site-7: 23 species) and UDF (Site-1: 22 species). The RF sites had lowest richness that ranged from 12-18 species per plot. The Simpson diversity index was used to quantify species diversity or the probability associated with the occurrence of different species within each plot (Williams *et al.*, 2008; Kalaba *et al.*, 2013). For each plot, the index was calculated by: (step-1) subtracting 1 from the individual tree count of each species, (2) multiplying the answer in step-1 by the initial tree count per species, and calculating the sum, (3) dividing the answer in step-2 by the total number individual trees multiplied by the same number less than 1, and (4) subtracting the answer in step-3 from 1. Values closer to 0 represent lower species diversity, while values closer to 1 indicate higher diversity. It is evident that early recovery sites, SF (Site-7: 0.64) and RF sites (Site-3: 0.84; Site-5: 0.75; Site-6: 0.88) had the lower diversity, while higher values of the Simpson diversity index (higher species diversity) were associated with UDF (Site-1: 0.95) and PDF (Site-4: 0.93; Site-2: 0.89). These results showed that floristic composition differed significantly (ρ = 0.00) between forests sites of different succession stages.

Table 4.7 - Tree species composition of different Miombo woodland sites with the recorded number of individual trees

Tree species	Site-1 (UDF)	Site-2 (PDF)	Site-3 (RF)	Site-4 (PDF)	Site-5 (RF)	Site-6 (RF)	Site-7 (SF)
Afzelia quanzensis	-	6	-	1	-	-	-
Albizia adianthifolia	1	7	6	7	5	23	8
Albizia antunesiana	1	-	-	-	-	-	-
Albezia gummifera	-	-	1	5	7	1	-
Albezia versicolor	-	-	-	2	-	11	2
Anona longana	-	-	-	-	-	-	2
Ansophyllae boehmii	-	11	-	6	-	7	-
Baphinia bikwete	-	5	-	-	28	-	-
Bauhinia picta	-	-	10	-	-	-	-
Brachystegia boehmii	4	24	33	34	2	12	197
Brachystegia floribhuda	-	-	-	1	-	-	4
Brachystegia longifolia	-	4	-	2	-	1	1
Brachystegia spiciformis	6	17	4	12	4	-	11
Brachystegia utilis	-	-	-	1	-	-	-
Combretum fragrans	-	-	-	1	-	-	-
Combretum imberbe	4	1	26	13	-	34	2
Combretum molle	-	8	5	-	-	8	-
Combretum zeyheri	2	-	-	-	-	-	-
Dicrostachy cinerea	-	-	-	-	-	-	3
Diospyros batocana	8	-	-	16	-	-	-
Diplorhynchus condylocarpon	5	-	-	3	-	5	17
Erythrophleum africanum	5	1	7	1	-	-	1
Garcinia huillensis	1	-	-	-	-	-	-
Garcinia livingstonia	-	-	-	3	-	-	-

Table 4.7 (*continued*)

Hexalobus monopetalus	-	5	-	2	-	-	4
Hymenocardia acida	2	-	-	-	-	-	-
Julbernadia paniculata	4	24	4	22	4	19	58
Lannea discolor	3	-	1	20	2	-	9
Lantana camara	-	-	-	5	-	-	-
Mangiferra indiga	-	-	-	2	-	-	-
Marquesa macroura	1	-	-	2	-	-	-
Ochna pulcra	-	45	-	45	43	1	9
Ochna schweinfurthiana	2	-	-	9	-	-	-
Parinari curatellifolia	6	1	5	31	4	3	2
Pericopsis angolensis	2	3	-	22	-	-	1
Pseudolachynostylis maprouneifolia	5	7	2	2	-	5	5
Pterocarpus angolensis	-	7	-	-	-	2	-
Rhus longipes	4	-	1	3	-	3	-
Strychnos cocculoides	-	3	3	3	1	4	1
Swartzia madagascariensis	2	-	-	-	-	-	2
Syzygium cordatum	-	-	1	6	-	-	-
Syzygium guineense	-	7	-	2	2	-	-
Toona ciliata	-	-	1	11	-	-	-
Uapaca benguelensis	1	-	-	-	-	1	3
Uapaka kikiana	-	-	-	2	-	-	2
Vitex mombassae	1	-	-	-	-	-	-
Terminalia	-	-	1	2	-	1	-
Vitex doniana	-	-	-	1	1	-	2
n_1	**22**	**19**	**17**	**35**	**12**	**18**	**23**
N	**70**	**186**	**111**	**300**	**103**	**141**	**346**
Simpson diversity index	**0.95**	**0.89**	**0.84**	**0.93**	**0.75**	**0.88**	**0.64**
Evenness	**0.31**	**0.1**	**0.15**	**0.12**	**0.12**	**0.13**	**0.07**

Where n_1 is tree count of each specific species and N is the total number of all individual trees for Plot 5 (30 x 30 m) of each forest site (90 x 90 m).

Species evenness or dominance was estimated as a ratio of tree count for each specific species (n_1) to the total number of individual trees (N) per plot. For example, evenness of 0.12 for Site-4 was calculated as, 35 species divided by a population of 300 trees (Table 4.7). Since UDF site had the lowest population (70), the highest value of species evenness (0.31) revealed that the different tree species were more evenly distributed in Site-1 than the other sites (e.g. Site-3: 0.15, > Site-6: 0.13, and > Site-4: 0.12). In contrast, the low values of evenness revealed dominance (most frequently occurring) of a single or few species. For instance, the value of 0.07 for SF growth in Site-7 was closely associated with the dominance of *Brachystegia boehimii* (Figure 4.17a), which represented 56.94% of the population. Despite the highest richness in PDF (Site-4), the site was dominated by *Ochna pulcra*, *Brachystegia boehmii*, *Parinari curatellifolia*, *Julbernadia paniculata* and *Lannea discolor*, with cumulative percentage of 50.67% of the total trees. In sites of forest regeneration (Site-3, Site-5 and Site-6), species evenness varied between 0.12 and 0.15. Figure 4.17b shows that evenness and diversity are inversely proportional to tree density. This is evident in Site-7 (SF), where the highest tree density of 346 trees plot^{-1} was associated with the lowest species diversity (0.64) and evenness (0.07). On the other hand, UDF had the lowest density (70 trees per plot^{-1}), but had the highest diversity (0.95) and evenness (0.31) (Table 4.7 and Figure 4.17b). The PDF sites had 186 trees plot^{-1} (Site-2) and 300 trees plot^{-1} (Site-4), while sites of forest regrowth (RF) had tree density that ranged from 103-141 trees plot^{-1}. The analogous or comparable sites showed some stochastic effects of forest disturbance (e.g. selective tree felling) which include, regeneration, forest succession and increase in tree density, and reduction in species diversity and evenness.

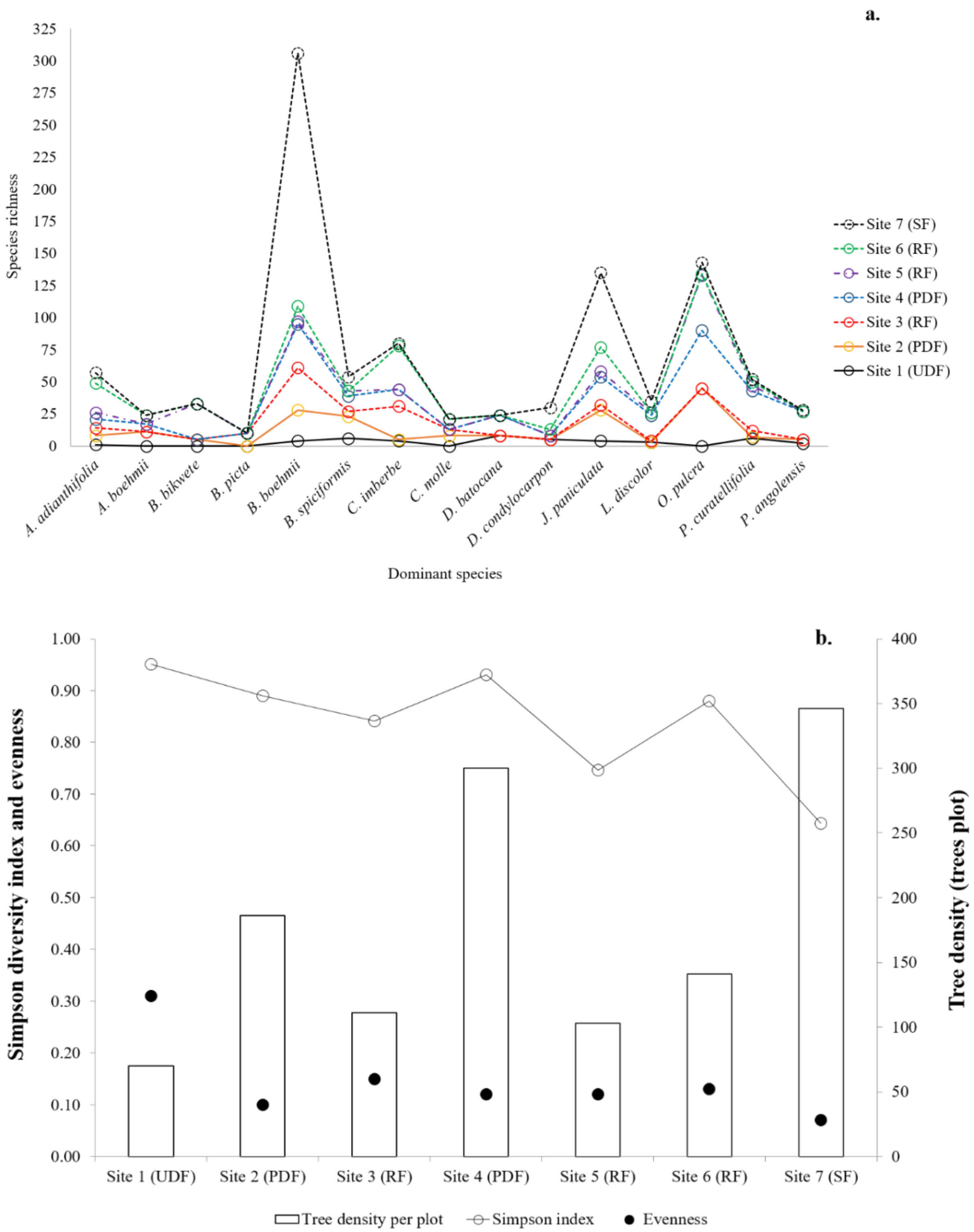

Figure 4.17: Floristic composition and tree species diversity of Miombo woodland in Luanshya. UDF, PDF, SF, and RF are forest sites of different succession stages for Luanshya. Figure 4.17a presents the dominant tree species with an average occurrence of >7 across the seven sites, while Figure 4.17b shows the variations of species diversity (Simpson diversity index) with evenness and tree density.

A total of 19 different woody species were identified in Bushbuckridge. Table 4.8 presents floristic composition, and species richness, tree count, diversity and evenness for plot-5 (30 x 30 m) of each forest sites. Of the 15 species with an average occurrence of more than two (across all sites), the three most frequently occurring species were *Dichrostachys cinerea, Ziziphus mucronata* and *Acacia mellifera* (Figure 4.18a). The quadrats with the highest species richness were, RF site in Site-4 (12 species), followed by Site-7 (11) and Site-1 (10). Relatively lower values of richness were recorded in RF site in Site-6 (3 species), and SF sites in Site-5 (8), and Site 2, 3 (9). The Simpson diversity index of 0.89, 0.84, 0.83 and 0.80, indicated higher diversity in Site-7 > Site-4 > Site-1 > Site-2, respectively.

Table 4.8 - Tree species composition of different woodland sites in Bushbuckridge with the recorded number of individual trees

Tree species	**Site-1 (SF)**	**Site-2 (SF)**	**Site-3 (SF)**	**Site-4 (RF)**	**Site-5 (SF)**	**Site-6 (RF)**	**Site-7 (SF)**
Acacia karroo	-	-	-	-	-	37	15
Acacia mellifera	13	26	8	86	-	37	15
Acacia nigrescens	19	6	17	6	15	-	8
Acacia nilotica	-	26	8	23	7	-	30
Cassine transvaalensis	-	-	-	-	7	-	-
Combretum apiculatum	50	-	8	6	7	-	38
Combretum collinum	50	-	25	6	22	-	23
Combretum kraussii	-	71	12	17	-	-	23
Combretum molle	-	6	-	-	-	-	-
Dalbergia melanoxylon	3	-	-	-	-	-	-
Dialium schlechteri	-	-	-	23	-	-	30
Dichrostachys cinerea	-	-	8	40	156	203	15
Grewia monticola	-	-	-	-	4	-	-
Euclea divinorum	35	13	-	-	-	-	-
Microberlinia brazzavillensis	25	-	-	-	-	-	-
Peltophorum africanum	3	13	-	11	4	-	-
Sclerocarya birrea	-	6	-	6	-	-	-
Terminalia sericea	3	-	25	17	-	-	46
Ziziphus mucronata	82	19	175	29	-	-	38
n_1	**10**	**9**	**9**	**12**	**8**	**3**	**11**
N	**283**	**186**	**287**	**269**	**223**	**277**	**281**
Simpson diversity index	**0.83**	**0.80**	**0.61**	**0.84**	**0.49**	**0.43**	**0.89**
Evenness	**0.04**	**0.05**	**0.03**	**0.04**	**0.04**	**0.01**	**0.04**

In contrast, the dominance of *Dichrostachy cinerea* in Site-5 (156 trees) and Site-6 (203) is described by the lowest Simpson index of less than 0.49, which showed relatively lower diversity. This means that if two individual trees were to be arbitrarily picked from Site-6 (Table 4.8), there is a <43% chance or lowest probability of selecting a different species, which indicates a lower species diversity. Figure 4.18b also indicates that species diversity and evenness were also inversely proportional to tree density. Compared to Luanshya, the lower evenness values (ranging from 0.03 to 0.05) revealed that woodlands in Bushbuckridge had a lower diversity, and its floristic composition was often dominated by trees of the same species. Owing to the effects of forest disturbance and regeneration, these results disclose that the less dominant species could be tree types that are mostly grazed by livestock or exploited by local communities.

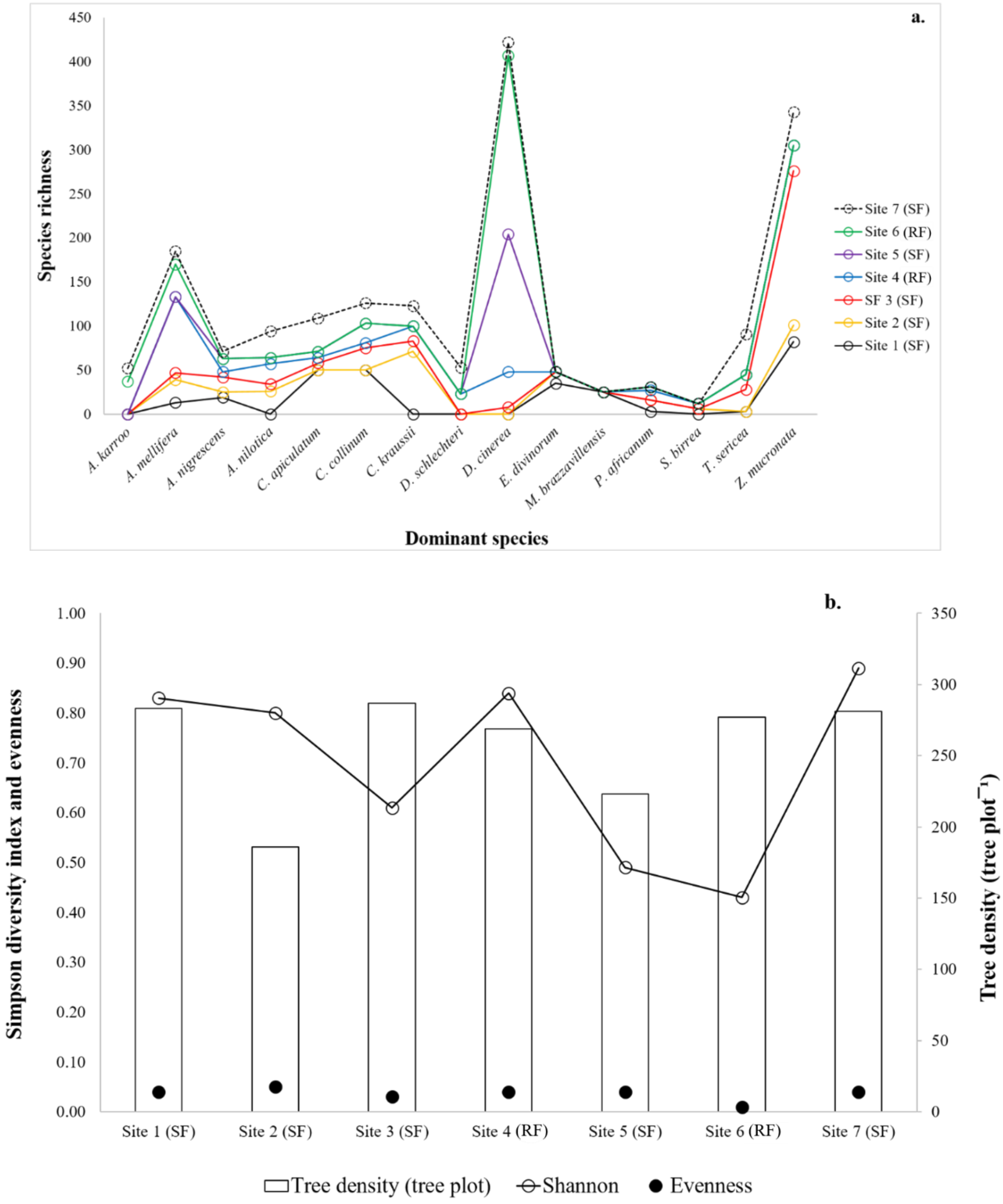

Figure 4.18: Floristic composition and tree species diversity of savanna woodland in Bushbuckridge. Figure 4.18a depicts the dominant tree species, with an average occurrence of >2 across the seven sites, while Figure 4.18b shows the variation in the Simpson diversity index, species evenness and tree density.

4.2.2 Distribution of the measured tree variables

Across the seven forests sites in Luanshya, a total of 11,275 trees were measured for their DBH and height (Table 4.9). Plots in UDF sites had the smallest tree population that ranged from 63-81 trees plot^{-1} or 778 trees ha^{-1}, while the highest tree density was observed in SF site (mean: 347 ± 11 trees plot^{-1}). The number of trees inventoried in PDF sites were between 2.7 and 4.3 times higher than that of UDF site. On the other hand, tree densities in RF sites (Site-3: 111 tree plot^{-1}, Site-5: 100 trees plot^{-1}, Site-6: 140 trees plot^{-1}) were higher than UDF, but lower than PDF and SF sites. The differences in tree populations was largely attributed to woodland clearing and subsequent increases in regeneration (e.g. multi stems) from resprouts and stumps. Since UDF site with elevation of 1258 m asl was associated with lowest tree density, whereas SF with lowest altitude of 1228 m asl had a greater tree population, the results indicates that tree density was also related to topographic positions of different forest sites.

Table 4.9 - Characterisation of trees growing in the sampled forest sites, Luanshya

Site/Plot	Measured Characteristics	Plot 1	Plot 2	Plot 3	Plot 4	Plot 5	Plot 6	Plot 7	Plot 8	Plot 9
Site-1 (UDF)	N	70	75	67	63	70	81	77	64	63
	Mean DBH (cm)	13.0	12.6	11.9	15.4	13.5	14.4	14.8	13.0	13.0
	Mean height (m)	10.2	10.00	10.5	9.6	10.4	9.9	10.7	11.1	10.9
Site-2 (PDF)	N	171	196	190	174	186	201	168	186	198
	Mean DBH (cm)	6.6	6.9	6.8	8.6	6.3	5.9	7.1	6.5	6.7
	Mean height (m)	7.7	7.3	7.6	7.6	7.7	7.9	7.6	7.4	7.4
Site-3 (SF)	N	111	98	98	106	111	119	126	109	123
	Mean DBH (cm)	3.5	4.0	4.4	3.9	3.8	3.5	4.0	4.4	3.9
	Mean height (m)	3.0	3.0	3.1	4.0	3.1	3.0	3.0	3.1	2.7
Site-4 (PDF)	N	300	290	313	278	299	318	315	311	275
	Mean DBH (cm)	5.1	6.2	6.2	6.0	5.8	5.9	6.2	5.7	6.2
	Mean height (m)	5.1	5.0	5.2	4.8	5.2	4.8	5.3	5.5	5.5
Site-5 (RF)	N	91	99	93	98	102	111	108	100	99
	Mean DBH (cm)	2.0	2.1	2.3	3.4	1.6	1.7	1.5	1.5	1.6
	Mean height (m)	2.3	2.3	2.0	2.1	2.1	2.5	2.1	1.9	2.0
Site-6 (RF)	N	137	140	129	135	141	153	160	156	111
	Mean DBH (cm)	1.8	2.6	2.2	2.0	1.8	2.6	2.0	1.8	1.6
	Mean height (m)	3.0	2.9	2.7	3.0	3.1	2.3	1.8	3.0	3.5
Site-7 (SF)	N	363	339	359	340	346	328	350	355	340
	Mean DBH (cm)	6.0	5.6	5.8	5.4	5.7	5.8	5.7	5.7	6.3
	Mean height (m)	5.4	5.5	5.6	5.5	5.5	5.3	5.4	5.6	5.2

Where N is the number of trees.

The size-class distribution of stem diameters (measured at 1.3 m above the ground) and tree heights are illustrated using boxplots (Figures 4.19, 4.20). Based on the different levels of forest disturbance within each site, the different size-class distributions reflect forest stands of different developmental stages. These patterns were extremely asymmetrical, with positive skewness indicating that mean diameters were greater than median values, and presence of a fewer number of bigger trees. The UDF site (Site-1) had individual trees with the biggest measurable characteristics. The mean tree diameter was 13.7 cm, while tree height was 10.4 m. The two PDF sites (Site 2, 4) had mean DBH and tree height of 8.0 and cm 7.6 m, respectively (Figure 4.19a).

In Figure 4.19b, the conspicuous positive skewness in Site-1, Site-2, and Site-7 corresponded to taller trees with mean heights of 10.4 ± 0.5 m for UDF, and 7.6 ± 0.2 m for PDF (Site-2), and 5.4 ± 0.1 m for SF. Normal-slightly skewed (positive) distribution, depict younger forest sites (RF) that had relatively shorter trees, with mean heights of 2.7 ± 0.41 m for Site 3, 5, 6 or areas with increased regeneration (e.g. Site-4: 5.2 ± 0.2 m). Supplementary graphs on the different distribution of stem diameter and tree height classes are provided in Appendix B1, B2. Across the seven sites, stem diameter had an average CV of 101, while tree height had 0.63. The distribution of the two measured characteristics suggested that stem diameter was more variable than tree height.

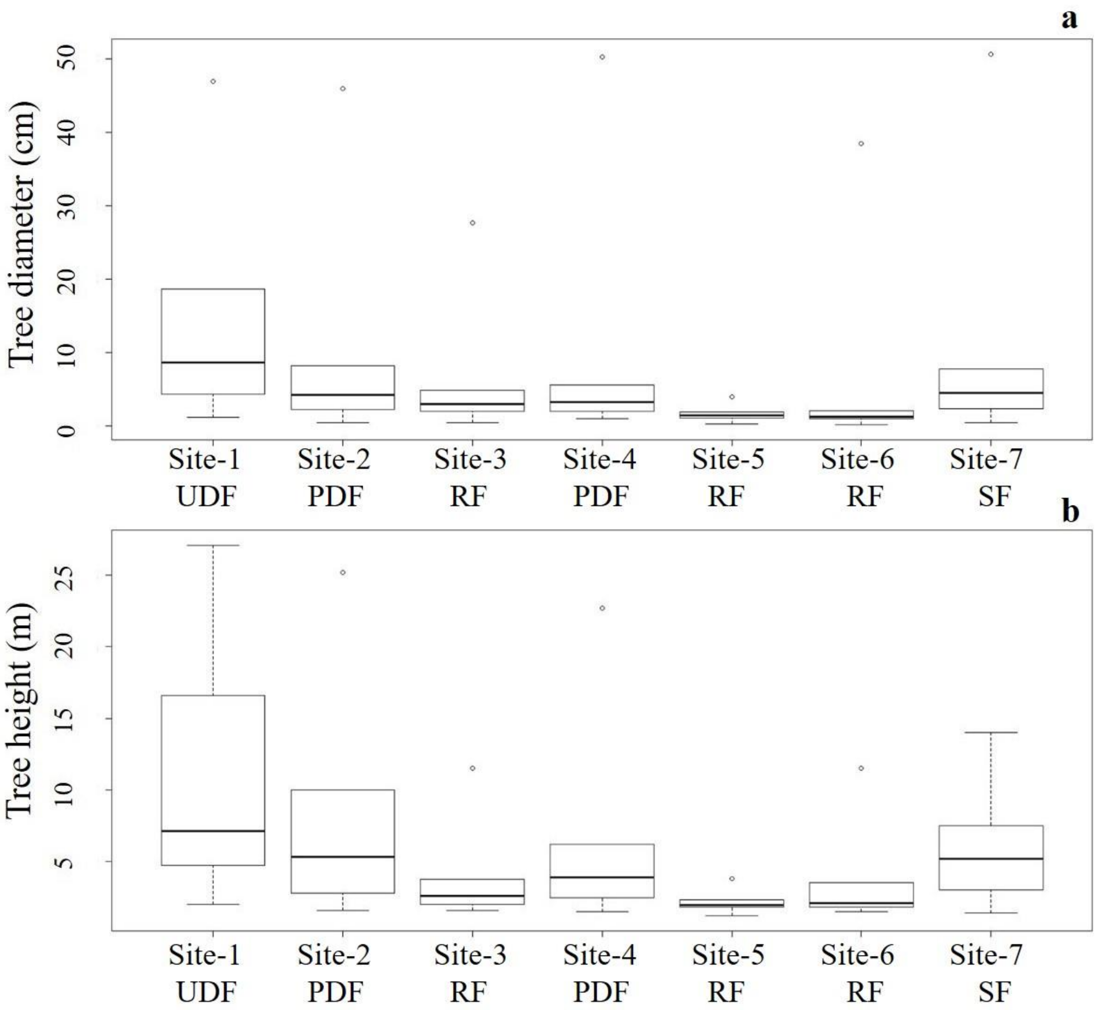

Figure 4.19: Distribution of DBH and tree height in Luanshya. The seven boxplots (1-7) of DBH (a) and tree height (b) illustrate the forest sites while each boxplot depicts the nine nested sample plots and average distribution of measured tree characteristics. The lowest whisker, lowest box margin, black-bold line, highest box margin and the highest whiskers represent the trees with the smallest DBH size, the 25th percentile, median or 50th percentile, 75th percentile and the trees with the largest DBH size, while outliers are depicted by the small circles outside the box-whiskers plot, respectively. If the black-bold line (50th percentile) is closer to the 25th percentile then the distribution was positively skewed, negatively skewed if the black-bold line is closer to the 75th percentile, and uniformly distributed if the distance from black-bold line to the 25th percentile is equal to the distance from the black-bold line to the 75th percentile.

In Bushbuckridge, tree density ranged from 215-379 trees plot^{-1} (Table 4.10), with RF sites inventoried with lowest number of individual trees (Site-4: 231 trees plot^{-1}; Site-6: 215 trees plot^{-1}). A two-way ANOVA indicated that within each site (nested with 30 x 30 m sample plots) and between different forest sites (90 x 90 m), the measured stem diameters and heights were not equally distributed (ρ <0.05). The observed lower tree density in RF sites were associated with topographic locations (higher elevations) of the forest stands (Site 4, 6: >422 m asl.). In contrast, sites with higher tree density (Site-1: 276 trees plot^{-1}; Site-3: 404 tree plot^{-1}; Site-7: 412 tree plot^{-1}) were located on downslope areas of less than 412 m asl. These variations suggested that regeneration and increased tree recruitment occurred mostly in lower catenary or low-lying areas.

Table 4.10 - Characterisation of trees growing in the sampled forest sites, Bushbuckridge

Site/Plot	Measured characteristics	Plot 1	Plot 2	Plot 3	Plot 4	Plot 5	Plot 6	Plot 7	Plot 8	Plot 9
Site-1 (SF)	N	250	266	295	282	281	243	301	280	289
	Mean DBH (cm)	4.1	3.9	3.9	4.0	3.8	3.9	3.9	4.2	3.9
	Mean height (m)	4.2	4.30	4.2	3.9	4.1	3.9	4.1	3.9	4.0
Site-2 (SF)	N	270	288	276	278	281	277	260	290	249
	Mean DBH (cm)	4.9	4.8	5.8	4.5	4.8	5.4	3.4	5.0	4.4
	Mean height (m)	4.4	3.8	4.2	4.3	4.1	4.3	3.9	4.3	4.1
Site-3 (SF)	N	270	273	281	275	290	280	284	277	270
	Mean DBH (cm)	5.0	4.5	4.5	5.6	4.9	4.4	5.1	5.1	4.6
	Mean height (m)	3.9	3.5	4.3	4.1	4.1	4.2	4.3	4.0	4.3
Site-4 (RF)	N	232	230	235	229	227	234	240	231	218
	Mean DBH (cm)	2.4	2.5	1.9	1.9	1.9	2.0	1.7	1.7	1.5
	Mean height (m)	3.8	3.6	3.7	3.7	3.8	3.7	3.7	3.9	3.9
Site-5 (SF)	N	370	388	379	364	374	360	340	376	381
	Mean DBH (cm)	5.1	5.1	5.5	5.2	5.2	5.4	5.0	5.0	4.9
	Mean height (m)	4.3	4.3	4.2	4.3	4.3	4.3	4.1	4.3	4.2
Site-6 (RF)	N	220	220	213	217	209	211	216	210	223
	Mean DBH (cm)	2.5	1.6	1.6	1.5	1.7	1.7	1.7	1.5	1.7
	Mean height (m)	4.1	4.1	4.0	4.2	4.1	4.1	4.2	3.7	3.9
Site-7 (SF)	N	312	270	257	282	281	290	262	273	305
	DBH (cm)	5.0	3.5	4.2	3.7	4.1	4.4	4.2	4.1	3.7
	Height (m)	7.2	4.3	4.4	4.4	3.7	3.7	4.0	3.8	3.8

Where N is the number of trees.

The mean measured characteristics of forest stands in Bushbuckridge, ranged from 1.7 to 5.2 cm for stem diameter and 3.8 to 4.4 m for tree height (Table 4.10). In contrast to Luanshya, these variations indicated a relatively smaller range of size classes. The average median values (black bold line at the centre of each boxplot) of 3.3 cm for DBH and 3.8 m for height were sizes of subjective measure of central tendency, which indicated that 50% of the measured trees were less than these values (Figure 4.20). For all the differing sample sites, stem diameter and height distributions were marginally positively skewed (mean > median), indicating a low but active recruiting population. The SF site in Site-5 had tree stands with biggest stem diameters (mean: 5.2 ± 2.9 cm), followed by SF sites in Site 1, 2, 3, and 7, with mean diameters of between 3.8 and 4.1 cm, while RF sites had smallest trees (mean: 1.7-1.9 cm for diameters and 3.8-4.0 m for heights). Graphs depicting the average frequency of each stem diameter and height size classes are provided in Appendix B3, B4.

Across the seven sites, the variability of stem diameter sizes was associated with a higher average coefficient of variation (0.71), while tree height had a lower measure of dispersion (0.47). This is also clearly illustrated in the boxplots where stem diameters (Figure 4.20a) were more widely distributed than tree heights (Figure 4.20b). Despite the seemingly smaller tree size classes, ANOVA indicated that the difference between the measured forest tree variables (DBH and tree height) in Luanshya and Bushbuckridge were not statistically significant ($\rho = 1.44$). This means that the same general allometric equations can be applied to accurately estimate AGLB in the two study areas.

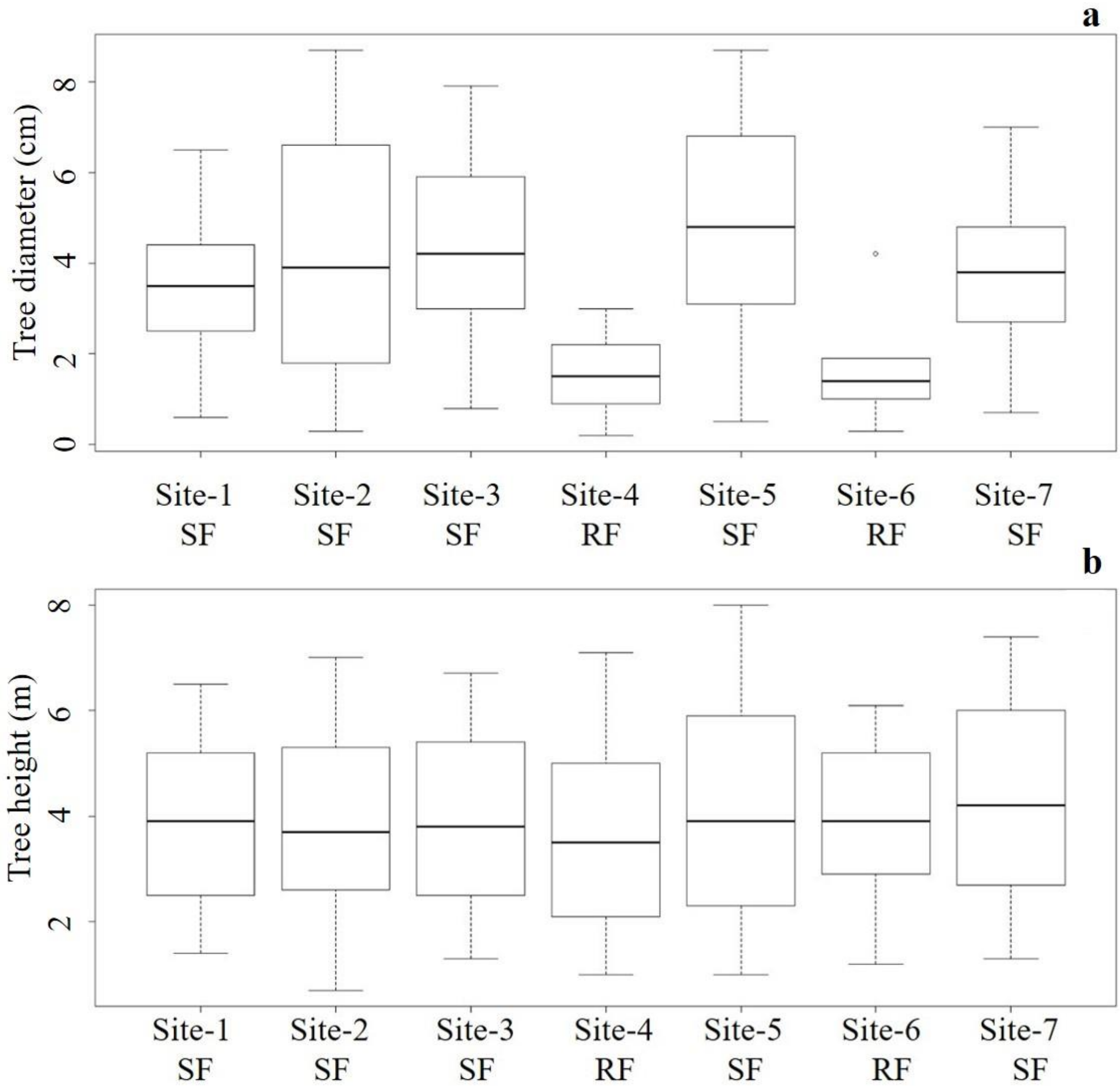

Figure 4.20: Distribution of DBH and tree height in Bushbuckridge. The seven boxplots (1-7) of DBH (a) and tree height (b) illustrate the forest sites while each boxplot depicts the nine nested sample plots and average distribution of measured tree characteristics. The lowest whisker, lowest box margin, black-bold line, highest box margin and the highest whiskers represent the trees with the smallest DBH size, the 25th percentile, median or 50th percentile, 75th percentile and the trees with the largest DBH size, while outliers are depicted by the small circles outside the box-whiskers plot, respectively. If the black-bold line (50th percentile) is closer to the 25th percentile then the distribution was positively skewed, negatively skewed if the black-bold line is closer to the 75th percentile, and uniformly distributed if the distance from black-bold line to the 25th percentile is equal to the distance from the black-bold line to the 75th percentile.

4.2.3 Estimation of AGLB

Table 4.11 and Table 4.12 show the estimated average AGLB per forest site in Luanshya and Bushbuckridge, respectively. In Luanshya, biomass ranged from 0.06-99.29 t ha^{-1} (Table 4.11). The three allometric models consistently estimated higher mean biomass in the PDF sites and secondary forests (Site-2: 92.00 to 100.83 t ha^{-1}; Site-4: 108.98 to 119.39 t ha^{-1}; Site-7: 68.76 to 76.81 t ha^{-1}). The AGLB in secondary forests were between 5% and 19% lower than the UDF areas. On the other hand, sites of forest regeneration had the lowest estimates of AGLB with mean biomass per site ranging between 0 and 19.66 t ha^{-1}. Statistically significant differences in the estimated biomass were found between the forest sites in Luanshya and Bushbuckridge ($\rho = 0.00$), and within the seven sites ($\rho = 0.00$) of each area.

For the same measured variables, the allometric equation by Stromgaard (1985) estimated the lowest biomass, while Nickless *et al*. (2011) had highest biomass estimates. Statistically, ANOVA indicated that differences in the mean AGLB estimates between the three equations were not statistically different (ρ =0.68). Relationships between tree diameter and biomass showed that estimations from Stromgaard (1985) were associated the highest average coefficient of determination (r^2 =0.91) and a lower average standard error (SE) of 9.90 t ha^{-1} (Tables 4.11, 4.12). Correspondingly, higher estimates of AGLB from the models by Chidumayo (1991) (0 to 101.51 ton ha^{-1}) and Nickless (2011) (0 to 120.19 ton ha^{-1}) were associated with comparatively lower determination of coefficients (r^2 = 0.82 and r^2 = 0.73, and higher average SE of 19.13 t ha^{-1} and 24.51 t ha^{-1}).

Owing to a two-three year forest rotational harvest practice and grazing of livestock within woodland ecosystems of Bushbuckridge, as well differences in environmental factors, the average biomass per plot was significantly lower (ρ = 0.00) than the forested areas of Luanshya. The SF sites in Site-5 had the largest AGLB of 45.07 t ha^{-1}, followed by Site-3 (10.99 t ha^{-1}), whereas regeneration forest sites had the lowest total biomass per plot (Site 4, 6: 0-0.63 t ha^{-1}). Sites with biomass of zero imply that despite being populated with trees, the individual trees were negligible or mathematically smaller than is estimated from the three allometric equations. Across the sampled sites, the variations of AGLB that was explained by DBH was higher (ranged between r^2: 0.83 and 0.98) with the Stromgaard (1985) allometric equation than Nickless *et al*. (2011) (ranged between r^2: 0.54 and r^2: 0.92) and Chidumayo (1991) (ranged between r^2: 0.42 and 0.96). Conversely, estimations using Stromgaard (1985) had the lowest SE of biomass values in Luanshya, but were higher (ranged between 1.25 t ha^{-1} and 6.95 t ha^{-1}) than the Nickless *et al*. (2011) model (ranged between 0.05 and 0.21 t ha^{-1}) in Bushbuckridge. Given that estimates of AGLB from the three allometric equations were not statistically different for each study area, the mean biomass per plot were calculated and used for regression modelling (relating ground measurements to reflectance measurements of Landsat images).

Table 4.11 - Comparison of biomass estimation using three different allometric models, Luanshya

Allometric Model			Stromgaard (1985)			Chidumayo (1991)			Nickless *et al*. (2011)			Mean	Mean
Site	**Mean DBH (cm)**	**Mean Height (m)**	**AGLB (ton plot^{-1})**	**r^2**	**SE**	**AGLB (ton plot^{-1})**	**r^2**	**SE**	**AGLB (ton/plot)**	**r^2**	**SE**	**AGLB (ton plot^{-1})**	**AGLB (ton ha^{-1})**
1	13.5 ± 2.8	10.4 ± 1.8	6.86	0.95	32.31	9.14	0.96	55.37	10.82	0.81	85.68	**8.94**	**99.29**
2	6.8 ± 1.1	7.6 ± 0.9	6.19	0.93	10.73	8.28	0.88	18.29	9.81	0.68	24.76	**8.09**	**89.91**
3	3.8 ± 0.6	3.1 ± 0.3	0.93	0.84	3.1	0.81	0.57	7.57	0.99	0.65	6.64	**0.91**	**10.12**
4	5.8 ± 0.9	5.2 ± 0.4	6.91	0.91	8.27	9.07	0.9	15.83	10.75	0.76	26.26	**8.91**	**99.01**
5	1.6 ± 0.1	2.1 ± 0.1	0	N/A	N/A	0	N/A	N/A	0.02	0.79	0.04	**0.01**	**0.06**
6	1.8 ± 0.5	3.1 ± 0.3	1.72	0.98	1.67	1.46	0.91	9.47	1.77	0.9	13.28	**1.65**	**18.31**
7	5.7 ± 0.5	5.5 ± 0.3	6.5	0.9	3.3	7.37	0.71	8.23	8.74	0.54	14.94	**7.54**	**83.74**

Table 4.12 - Comparison of biomass estimation using three different allometric models, Bushbuckridge

Allometric model			Stromgaard (1985)			Chidumayo (1991)			Nickless *et al*. (2011)			Mean	Mean
Site	**Mean DBH (cm)**	**Mean Height (m)**	**AGLB (ton plot^{-1})**	**r^2**	**SE**	**AGLB (ton plot^{-1})**	**r^2**	**SE**	**AGLB (ton/plot)**	**r^2**	**SE**	**AGLB (ton plot^{-1})**	**AGLB (ton ha^{-1})**
1	4.0 ± 0.38	4.1 ± 0.2	0.88	0.93	1.42	0.07	0.48	3.86	0.02	0.80	0.05	**0.32**	**3.57**
2	4.8 ± 1.3	4.2 ± 1.0	0.40	0.83	6.75	0.15	0.69	3.46	0.19	0.92	0.21	**0.25**	**2.74**
3	4.9 ± 0.1	4.1 ± 0.1	1.16	0.84	1.45	0.81	0.49	4.78	0.99	0.83	0.07	**0.99**	**10.99**
4	1.9 ± 0.3	3.8 ± 0.1	0.00	0.83	1.25	0.00	N/A	N/A	0.00	N/A	N/A	**0.00**	**0.00**
5	5.2 ± 0.2	4.3 ± 0.3	3.71	0.87	6.95	3.86	0.51	17.34	4.60	0.83	8.90	**4.06**	**45.07**
6	1.7 ± 0.3	4.0 ± 0.1	0.17	0.88	2.78	0.00	N/A	N/A	0.00	N/A	N/A	**0.06**	**0.63**
7	4.1 ± 0.4	4.4 ± 1.0	0.85	0.90	1.52	0.58	0.42	3.85	0.71	0.78	0.10	**0.71**	**7.93**

Due to different levels of forest disturbances and variations in topographic relief within the same study area, total AGLB was different among the sampled forest sites. Since individual tree biomass was allometrically calculated from the easily measurable tree characteristics (Tables 4.11, 4.12), the difference in total biomass per site reflect variations in species diversity, stem diameter, height and tree density. Site-1 with the biggest mean stem diameter (Site-1: 13.5 ± 2.8 cm) and height (10.4 ± 1.8 m) was associated with the highest total biomass (8.94 t plot^{-1}), whereas areas with relatively smaller measurable characteristics had lower total biomass (e.g. Site 5 with mean DBH and height of 1.6 cm and 2.1 m, respectively, had biomass of 0.01 t plot^{-1}). Even though stem diameters and heights in UDF site were at least twice bigger than the size of trees in other sites (Table 4.11), total AGLB in PDF (Site 2, 4) and SF (Site-7) sites compared quite closely with biomass in Site-1. This highlighted the importance of tree density on estimates of total biomass in different forested areas of the same spatial extent (e.g., 30 x 30 m).

In Bushbuckridge, AGLB was also observed to increase more with mean stem diameter than tree height. For example, Site-5 with mean DBH of 5.2 cm had the highest estimates of biomass (45.07 t plot^{-1}), while other sites with DBH of <4.9 cm were associated with relatively lower biomass of less than 0.99 t plot^{-1} or 10.99 t ha^{-1} (Table 4.12). Interestingly, mean estimates of forest biomass in SF sites of Bushbuckridge were significantly ($\rho = 0.00$) lower than SF areas in Luanshya, which suggested that variations (between the two areas) in AGLB was due not only to differences in tree size classes and terrain relief, but also to the different management practices and environmental factors. This is evidenced by increased multi-stem growths from stumps, especially in previously disturbed sites, which is sufficing to establish that transitions from primary to secondary forests often results in reduced total biomass due to replenishment of bigger trees by smaller trees of the same or fewer species.

This means that higher AGLB in second growth forest stands may be attributed to higher tree density and not increased allocation of photosynthate in long-lived individual trees.

4.2.4 Regression modelling of biomass using Landsat-Thematic Mapper

The acquired location coordinates of the nine sample plots per forest site were uploaded onto the 2016 pre-processed Landsat images so as to locate the corresponding individual pixels in each ROI. Five vegetation indices were calculated from the spectral reflectances of the 84 pixels from the two Landsat-TM images for Luanshya (42) and Bushbuckridge (42) which correspond to about 67% of the number of forest sample plots. The difference in the chlorophyll content, greenness and vigor of the two woodlands was indicated by the higher mean absorption (units in W m^{-1} sr^{-1} μm^{-1}) of radiation in the blue and red band in Luanshya (blue: 173 ± 54; red: 435 ± 195) than the absorption in Bushbuckridge (blue: 2312 ± 210; red: 725 ± 114). The contrast in the structure and health of forests between the two study areas was indicated by the significant difference ($\rho = 0.00$) in mean reflectance measurements (Luanshya: 2344 ± 183 W m^{-1} sr^{-1} μm^{-1}; Bushbuckridge: 457 ± 69 W m^{-1} sr^{-1} μm^{-1}) in the near infra-red (NIR) band (Table 4.13).

Table 4.13 - Estimates of vegetation indices based on forest cover spectral reflectance

Area	Site	Blue (band 2)	Red (band 4)	NIR (band 5)	SR	DV	NDVI	EVI	SAVI
Luanshya	1 (UDF)	126	252	2299	9.13	2047	0.80	1.79	1.20
	2 (PDF)	118	251	2106	8.38	1855	0.79	1.7	1.18
	3 (RF)	269	669	2232	3.34	1563	0.54	0.92	0.81
	4 (PDF)	119	243	2228	9.18	1986	0.80	1.78	1.21
	5 (RF)	212	653	2616	4.00	1963	0.60	0.99	0.90
	6 (RF)	212	653	2616	4.00	1963	0.60	0.99	0.90
	7 (SF)	158	327	2312	7.07	1985	0.75	1.6	1.13
Bushbuckridge	1 (SF)	2296	741	474	0.64	-267	-0.22	0.05	-0.33
	2 (SF)	2549	797	491	0.62	-306	-0.24	0.06	-0.36
	3 (SF)	2120	635	408	0.64	-227	-0.22	0.05	-0.33
	4 (RF)	2213	693	432	0.62	-261	-0.23	0.05	-0.35
	5 (SF)	2646	933	588	0.63	-345	-0.23	0.06	-0.34
	6 (RF)	2009	542	350	0.65	-192	-0.22	0.04	-0.32
	7 (SF)	2350	734	459	0.62	-275	-0.23	0.05	-0.35

Where the units for spectral reflectance in blue, red and NIR is W m^{-1} sr^{-1} μm^{-1}, while indices values are non-dimensional.

Linear regression models relating vegetation indices and AGLB were developed. Figure 4.21 provides the expressions of vegetation indices and illustrates the correlation between EVI per pixel and total AGLB per plot, averaged from the three estimates based on allometric equations by Stromgaard (1985), Chidumayo (1991) and Nickless *et al*. (2011). Based on the coefficient of determination, total biomass per plot was best correlated to EVI (r^2: 0.96). The model was defined by a regression equation:

$$M = 6.5743x - 4.7431 \qquad \text{(Equation 4.1)}$$

where M is total AGLB per plot and x is EVI per pixel.

Analyses were not continued with vegetation indices (SR, DVI, NDVI and SAVI) that resulted in regression models with relatively lower coefficients of determination (r^2: 0.58 to 0.90) (Appendix C).

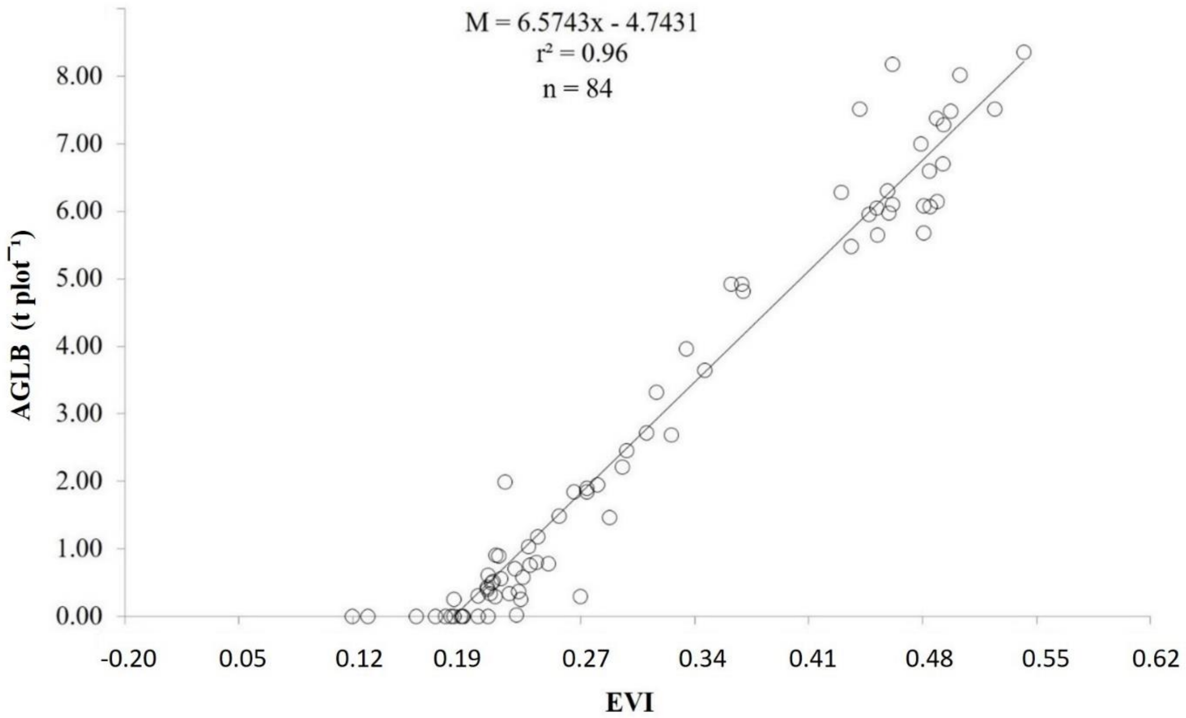

Figure 4.21: Regression models relating AGLB and EVI. The graph provides linear trend lines and the associated regression equations, coefficient of determinations (r^2) and mathematical expressions of EVI (labelled in the x-axis).

4.2.5. Relating tree measurable characteristics

A homoscedasticity exponential relationship, or a more uniform variance of measured tree characteristics, was observed between aboveground tree biomass and stem diameters, compared to those between biomass and tree heights (Figure 4.22). A lower homoscedasticity relationship between tree biomass and heights (Figure 4.22b) can be attributed to the weak positive logarithmic relationship between DBH and height (r^2 = 0.56; Figure 4.23a). These relationships demonstrates that tree height increased with diameter, but later tapered off. Biologically, this may imply that as trees grow the allocation of photosynthetic gain results in an increase in tree height and diameter, but in long-lived trees increase in height tapers off with increase in tree diameter. Given the regression equation (Equation 3.1) which relates EVI to estimates of AGLB per plot (30 x 30 m), then the correlation between EVI and DBH

(r^2 = 0.88; Figure 4.23b) should hold, provided a sensor has a high enough resolution to delineate single trees.

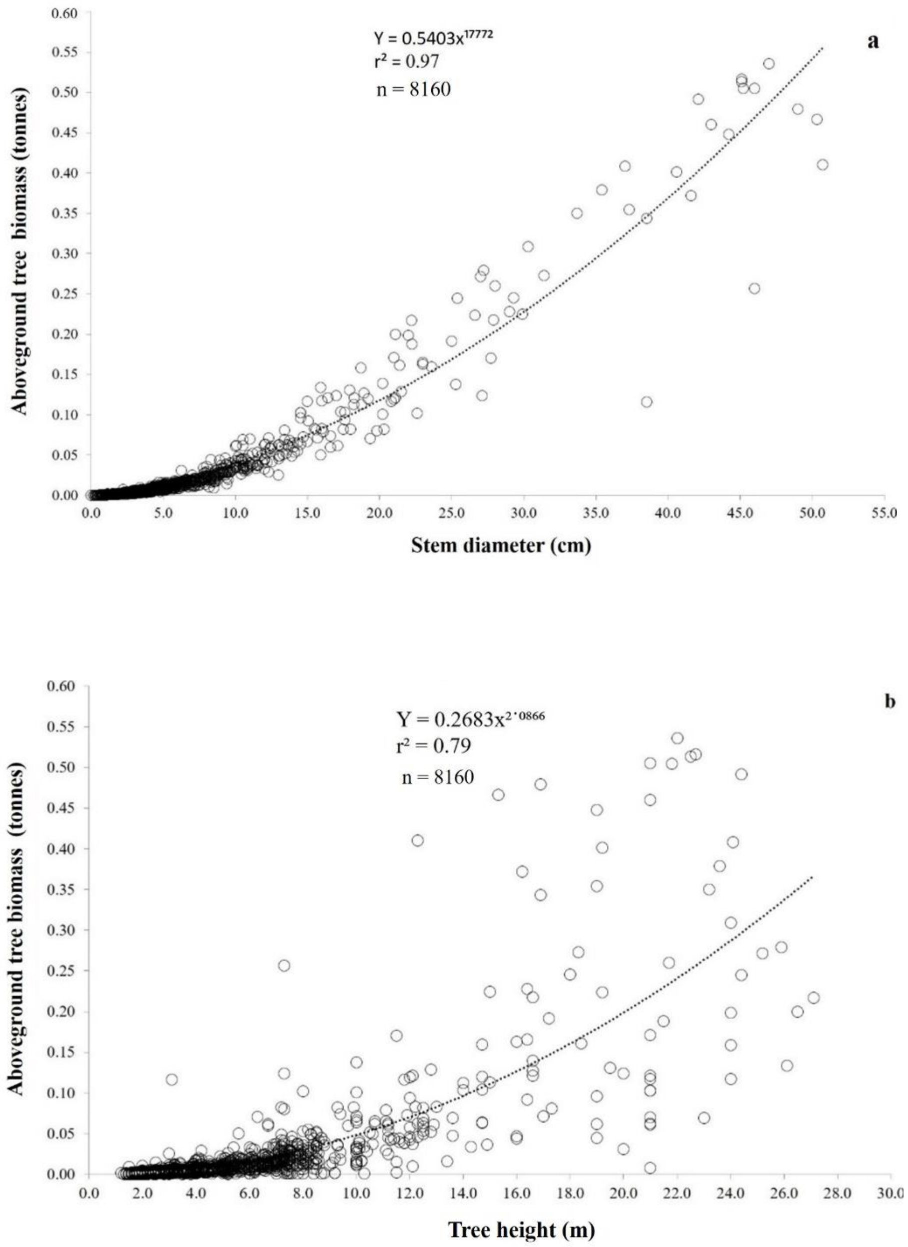

Figure 4.22: Allometric relationships between the measured characteristics and tree biomass. The graphs depict correlations between (a) stem diameter (measured at 1.3 m above ground level) and aboveground tree biomass, and (b) tree height and aboveground tree biomass.

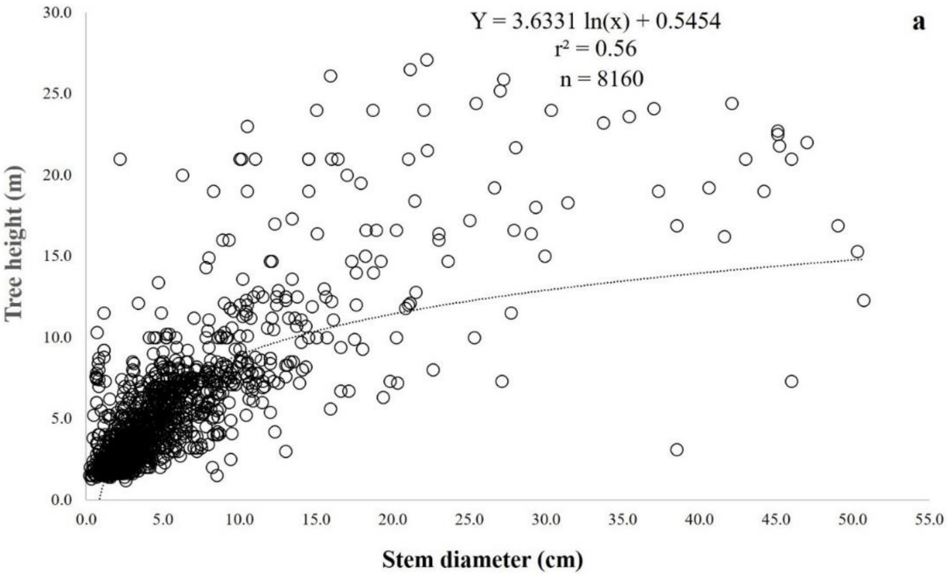

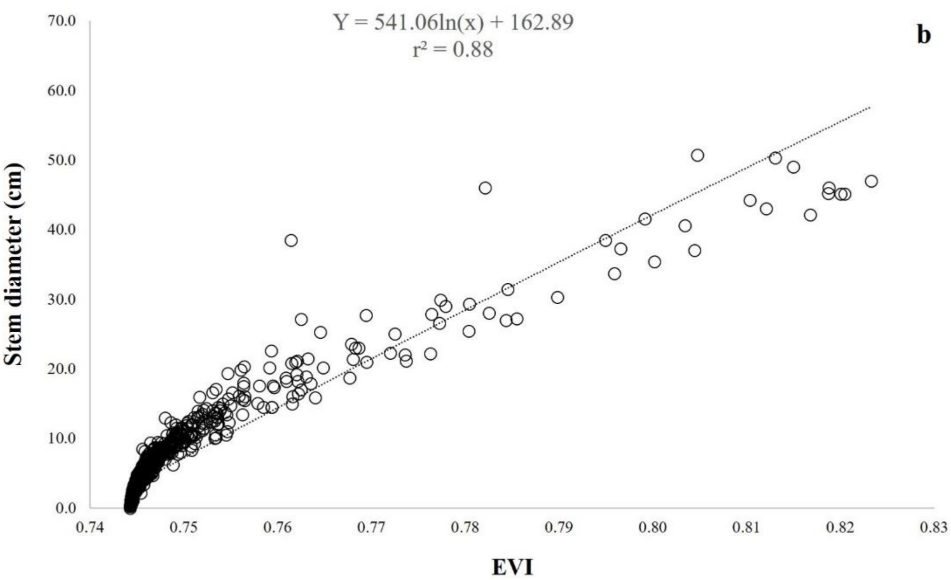

Figure 4.23: Relationships between the measured tree characteristics, and EVI. The graphs illustrate correlations between (a) stem diameters (measured at 1.3 m aboveground level) and tree height and (b) EVI and stem diameter.

4.2.6 Model validation

Model validation was performed by comparing the values of AGLB predicted using the regression model (M = 6.5743x – 4.7431) and the mean measured biomass values estimated from Stromgaard (1985), Chidumayo (1991) and Nickless *et al*. (2011). Since the model was tested on a different dataset (33%) from the one used for fitting it, the difference between the measured and predicted values provided the error associated with the applicability of the model (Table 4.14). The model was defined by the mean absolute errors (MAE), the sum of squares (SSE), mean absolute percent error (MAPE) and root mean square error (RMSE) of 0.24 tonnes, 0.06 tonnes, 9.3% and 0.24 tonnes for Luanshya, and 0.22 tonnes, 0.07 tonnes, 29.5% and 0.22 tonnes for Bushbuckridge, respectively. In Luanshya, sites of forest regeneration (Site-3 and Site-6) with less total biomass (from 0.68 to 1.52 tonnes) were associated with high MAPE (between 17.8% and 25%) and RMSE of 0.27 tonnes. Similarly, wooded areas in Bushbuckridge with biomass of less than 0.48 tonnes per plot had higher MAPE and RMSE of greater than 35.1% and biomass of 0.26 tonnes, respectively.

Table 4.14 - Relationship between predicted and measured values of forest biomass

	Site	**Number of plots**	**Measured AGLB (t plot$^{-1)}$**	**Predicted AGLB (t plot^{-1})**	**MAE**	**SSE**	**MAPE (%)**	**RMSE**
Luanshya	1	3	7.62	7.41	0.21	0.04	2.8	0.21
	2	3	6.13	5.91	0.22	0.05	3.6	0.22
	3	2	1.52	1.25	0.27	0.07	17.8	0.27
	4	3	6.69	6.47	0.22	0.05	3.3	0.22
	5	N/A	N/A	N/A	N/A	N/A	N/A	N/A
	6	3	1.08	0.81	0.27	0.07	25.0	0.27
	7	3	6.26	6.04	0.22	0.05	3.5	0.22
				Mean	**0.24**	**0.06**	**9.3**	**0.24**
Bushbuckridge	1	3	1.85	1.98	0.13	0.02	7.0	0.13
	2	3	0.71	0.35	0.36	0.13	50.7	0.36
	3	3	3.61	3.57	0.04	0.00	1.1	0.04
	4	2	0.69	0.29	0.40	0.16	58.0	0.40
	5	1	0.81	0.82	0.01	0.00	1.2	0.01
	6	2	0.74	0.48	0.26	0.07	35.1	0.26
	7	2	0.68	0.32	0.36	0.13	52.9	0.36
				Mean	**0.22**	**0.07**	**29.5**	**0.22**

Where SSE is the Sum of Squared Error, MAPE is the Mean absolute Percent Error and RMSE is the Root Mean Square Error. N/A implies that a priori site was not accessible or the measured tree characteristics were mathematically smaller than is estimated from the three allometric equations.

Figure 4.24 demonstrates a visual deviation of predicted and measured values from the reference line. For perfect prediction, all the points should lie exactly along the line. In this scenario the graph shows that the majority of scatter points were marginally positively or negatively dispersed from the line. In forest sites with biomass of less than 0.5 tonnes, the values aligned positively or above the reference line which indicates that the developed model slightly over-estimated total biomass. In the case of plots with biomass of less than 2.0 t $plot^{-1}$ (Figure 4.24), the model slightly underestimated total AGLB. The limitation of Landsat sensors to delineate saplings and young trees that continue to regenerate and grow under canopies of more mature trees, is emphasised by marginal underestimation of AGLB in forested areas with biomass of more than 4.0 t $plot^{-1}$. Analysis of variance revealed that the average divergence between predicted and measured values within forest sites of the same successional stages was not statistically significant ($\rho = 0.77$). This means that that the model ($M = 6.5743x - 4.7431$) showed a higher and acceptable prediction accuracy for mapping AGLB and tracing the changes in carbon stocks of the natural forests in both Luanshya and Bushbuckridge.

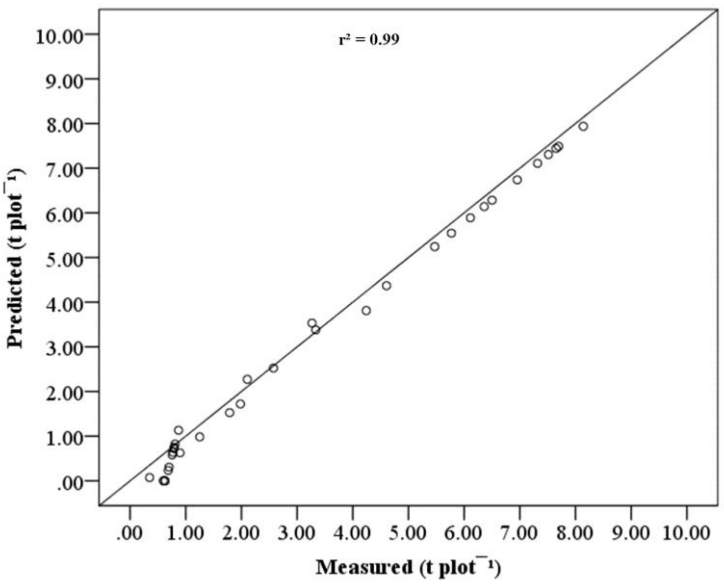

Figure 4.24: One-to-one relationship between measured and predicted AGLB. The graph shows the unequal dispersion of the values from the reference line. The scatter points above the line indicate overestimation, while points below infer underestimation of biomass that may be associated with the developed regression model relating AGLB per plot (30 x 30 m) to EVI.

4.2.7 Carbon maps: Spatial-temporal changes in forest biomass carbon stocks

The regression equation developed from the relationship between EVI and AGLB was applied in ENVI 5.3 band math tool and ArcGIS 10.3.1 to map biomass carbon stocks from the remotely sensed images for Luanshya (Figure 4.25) and Bushbuckridge (Figure 4.26). Based on the 2016 *in situ* measurements, each pixel of the choropleth maps provides a proxy for forest carbon stocks in tonnes per plot (t $plot^{-1}$). These estimates were based on the assumption that tree biomass consist of 50% carbon (Grossman, 2007; Martin and Thomas, 2011; Thomas and Martin, 2012). Spatial-temporal changes in forest carbon stocks were assessed by comparing forest carbon stocks per plot, which were represented by changes in pixel values at 10^{th}, 25^{th}, 50^{th} and 75^{th} and 90^{th} percentiles (Tables 4.15, 4.16).

With reference to the digital numbers of forest carbon stocks maps, Table 4.15 provides the corresponding number of pixels or plots (900 m^2) with lower carbon than the provided DN for each observed percentile in Luanshya. For instance, in the year 1986, a total of 356,856 pixels, representing 61.49% (32,117 ha) of the total area of 52,232 ha had plots with carbon stocks that ranged from 0 to 7.60 t $plot^{-1}$. At the 50^{th} percentile, a total of 354,492 pixels or 50% of the total pixels had carbon storage of less than 3.32 t $plot^{-1}$. In 1998 (3.56 t $plot^{-1}$) and 2001 (4.41 t $plot^{-1}$), the 50^{th} percentiles were associated with relatively increased carbon stocks, but later decreased in 2004 (4.27 t $plot^{-1}$), 2011 (3.60 t $plot^{-1}$) and 2016 (3.01 t $plot^{-1}$). Similar trends were observed for the 10^{th}, 25^{th} and 75^{th} percentiles.

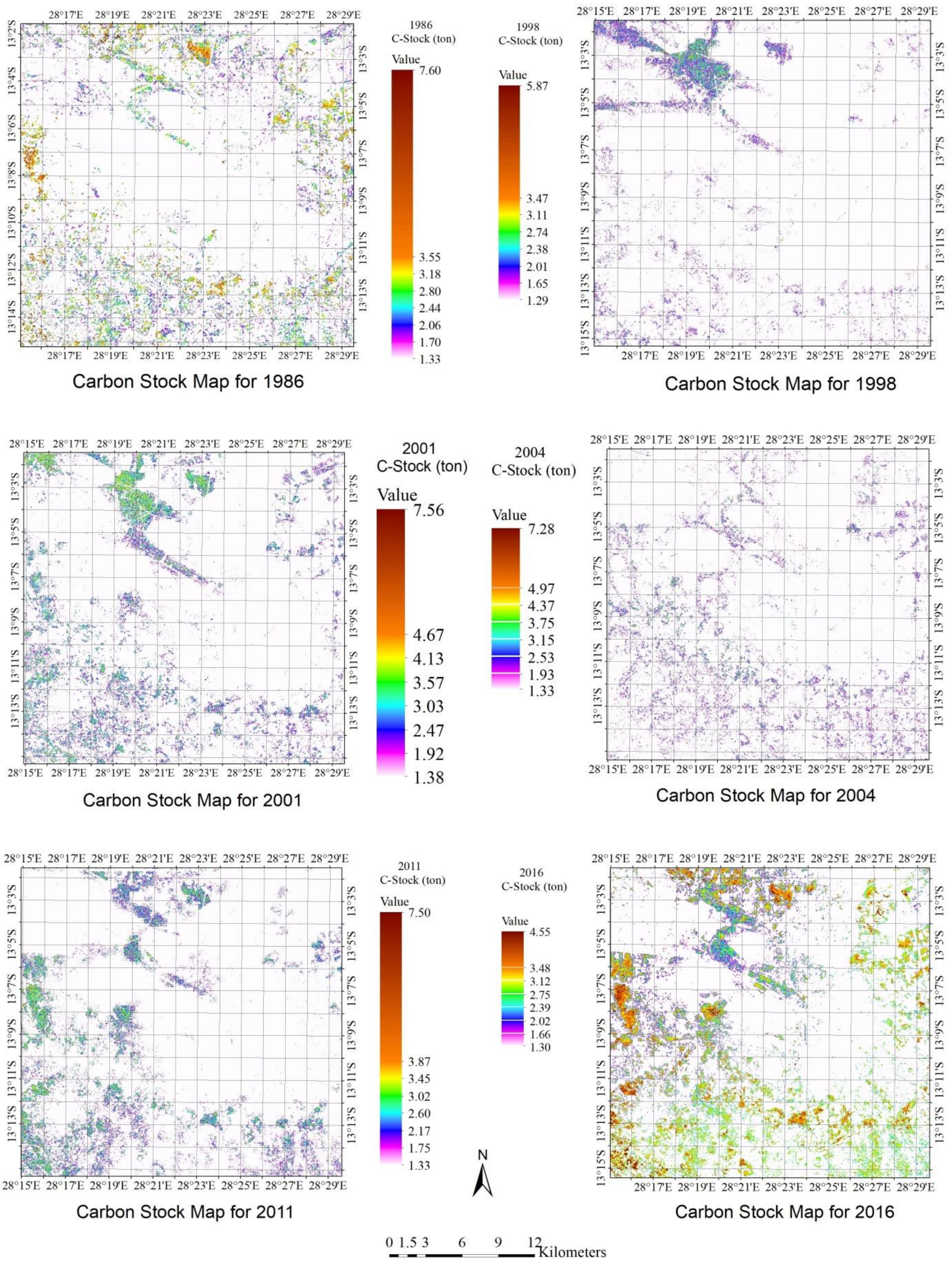

Figure 4.25: Forest carbon stock maps for 1986, 1998, 2001, 2004, 2011 and 2016 in Luanshya. For each map, the white patches in each LULC map indicates either the absence of woody forest cover or forested areas had negligible estimates of carbon stocks as per the legend.

Table 4.15 - Spatial-temporal changes in aboveground forest carbon stocks in Luanshya

	Percentile	10^{th}	25th	50^{th}	75^{th}	90^{th}	Highest
1986	**Pixel Digital Number**	1.67	2.29	3.32	4.35	5.68	**7.6**
	Number of Pixels	321,527	334,081	354,492	356,845	356,850	
	Total	536,950	765,045	1,176,913	1,552,276	2,026,908	
	C-Stock (t ha^{-1})	**18.56**	**25.44**	**36.89**	**48.33**	**63.11**	
1998	**Pixel Digital Number**	1.72	2.41	3.56	4.71	5.41	**5.87**
	Number of Pixels	99,907	102,664	103,430	103,495	103,499	
	Total	171,840	247,420	368,211	487,461	559,930	
	C-Stock (t ha^{-1})	**19.11**	**26.78**	**39.56**	**52.33**	**60.11**	
2001	**Pixel Digital Number**	1.89	2.83	4.41	5.98	6.93	**7.56**
	Number of Pixels	228,975	243,633	252,737	253,323	253,337	
	Total	432,763	689,481	1,114,570	1,514,872	1,755,625	
	C-Stock (t ha^{-1})	**21.00**	**31.44**	**49.00**	**66.44**	**77.00**	
2004	**Pixel Digital Number**	1.86	2.76	4.27	5.78	6.68	**7.28**
	Number of Pixels	162,224	162,224	163,707	163,801	163,801	
	Total C-Stock (t $plot^{-1}$)	301,737	447,738	699,029	946,770	1,094,191	
	C-Stock (t ha^{-1})	**20.67**	**30.67**	**47.44**	**64.22**	**74.22**	
2011	**Pixel Digital Number**	1.73	2.43	3.60	4.76	5.79	**7.5**
	Number of Pixels	257,837	272,260	284,652	285,883	285,927	
	Total C-Stock (t $plot^{-1}$)	446,058	661,592	1,024,747	1,360,803	1,655,517	
	C-Stock (t ha^{-1})	**19.22**	**27.00**	**40.00**	**52.89**	**64.33**	
2016	**Pixel Digital Number**	1.61	2.13	3.01	3.88	4.41	**4.55**
	Number of Pixels	151,595	152,485	174,310	185,542	185,553	
	Total C-Stock (t $plot^{-1}$)	244,068	324,793	524,673	719,903	818,289	
	C-Stock (t ha^{-1})	**17.89**	**23.67**	**33.44**	**43.11**	**49.00**	

Plots with the largest forest carbon storage are indicated by pixels with the highest digital number

An increase in carbon stocks implied increased tree density and/or increase in net primary productivity (NPP) of individual trees, while a decrease suggests forest disturbance, especially the clearance of bigger individual trees. By contrast, carbon stocks at 90^{th} percentile decreased from 5.68 t $plot^{-1}$ in 1986 to 5.41 t $plot^{-1}$ in 1998 and increased to 6.93 t $plot^{-1}$ in 2001, and subsequently decreased at an average annual rate of 19.67% from 2001 to 2016. Further, due to higher spatial extent of forest cover, the total carbon stocks was higher in 1986 (234.10 t $plot^{-1}$), > 2011 (199.58 t $plot^{-1}$) > and 2001 (191.53 t $plot^{-1}$) than the stocks for 2004 (119 t $plot^{-1}$), > 2016 (88.32 t $plot^{-1}$) > and 1998 (60.75 t $plot^{-1}$).

In Bushbuckridge, spatial-temporal changes in forest carbon stocks are clearly observed in Figure 4.26 and Table 4.16. Across the five percentiles, the carbon stocks for 1992, 1998 and 2016 were lower than the stocks for 2001, 2006 and 2011. About 50% (50^{th} percentile) of the plots had carbon stocks of 0.31 t $plot^{-1}$ for 1992, 0.67 t $plot^{-1}$ for 1998 and 1.81 t $plot^{-1}$ for 2016. The year 2001, 2006 and 2010 had higher carbon stocks of 3.11 t $plot^{-1}$, 2.70 t $plot^{-1}$ and 3.23 t $plot^{-1}$, respectively. Likewise, a similar trend was observed for the 10^{th}, 25^{th}, 75^{th} and 90^{th} percentile with the year 2001, 2006 and 2010 having higher values than 1992, 1998 and 2016. The values at 90^{th} percentiles indicates that only 10% of the forest cover (30 x 30 m) had carbon stocks of greater than 6.49 tonnes for 2001, 5.04 tonnes for 2006 and 6.48 tonnes for 2010.

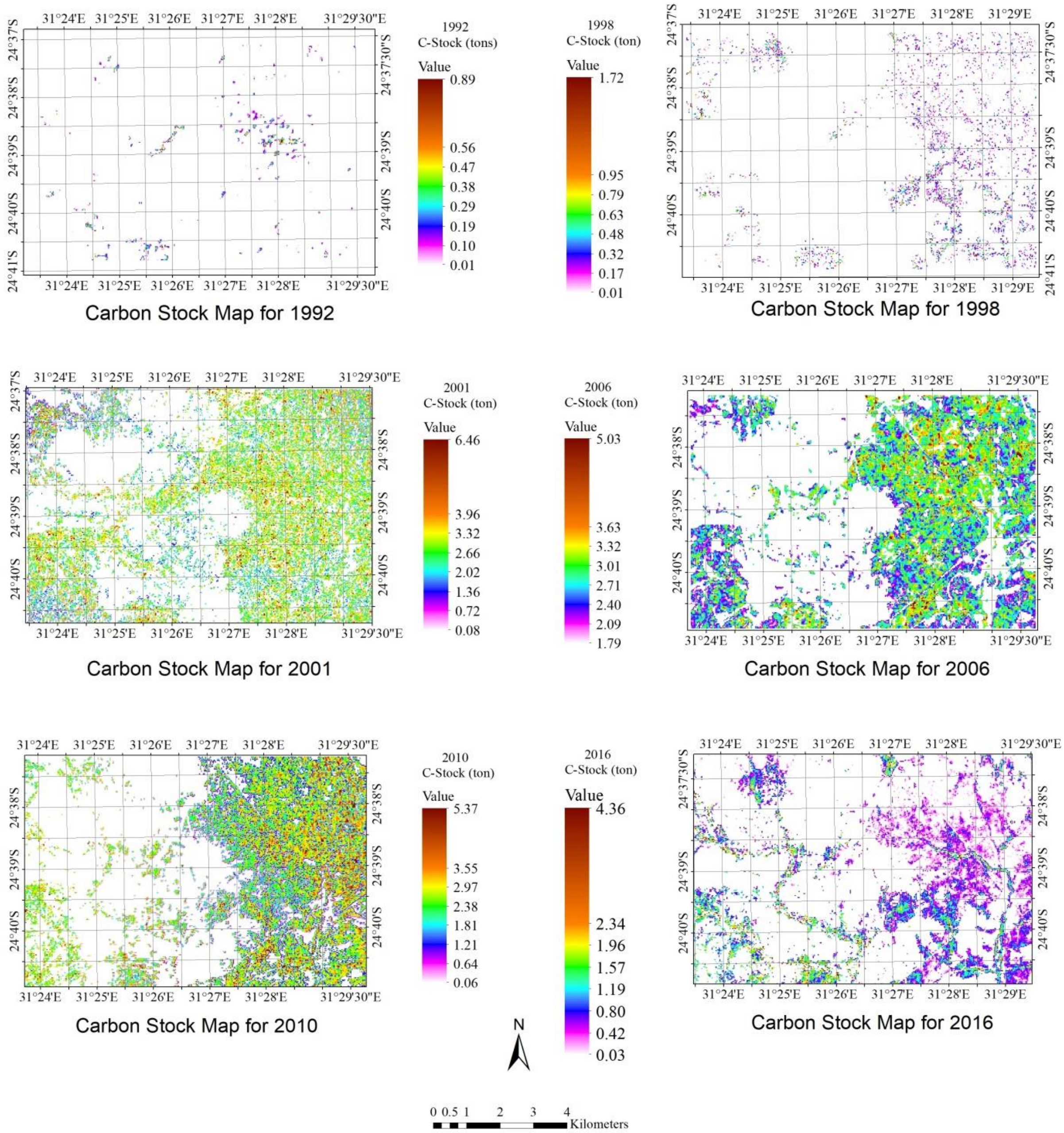

Figure 4.26: Maps of forest carbon stocks for 1992, 1998, 2001, 2006, 2010 and 2016 in Bushbuckridge. For each map, the white patches in each LULC map indicates either the absence of woody forest cover or the forested areas had negligible estimates of carbon stocks as per the legend.

Table 4.16 - Spatial-temporal changes in aboveground forest carbon stocks in Bushbuckridge

	Percentile	10th	25th	50th	75th	90th	Highest
1992	**Pixel Digital Number**	0.09	0.22	0.44	0.66	0.80	**0.89**
	Number of Pixels	77,336	77,781	78,120	78,191	78,199	
	Total	6960	17,112	34,373	51,606	62,559	
	C-Stock (t ha^{-1})	**1.00**	**2.44**	**4.89**	**7.33**	**8.89**	
1998	**Pixel Digital Number**	0.14	0.34	0.67	1.00	1.27	**1.72**
	Number of Pixels	1788	3352	4315	4560	4599	
	Total	250	1140	2891	4560	5841	
	C-Stock (t ha^{-1})	**1.56**	**3.78**	**7.44**	**11.11**	**14.11**	
2001	**Pixel Digital Number**	1.13	1.87	3.11	4.35	5.10	**6.46**
	Number of Pixels	37	1613	17,137	26,102	26,540	
	Total	41.81	3016	53,296	113,544	135,354	
	C-Stock (t ha^{-1})	**12.56**	**20.78**	**34.56**	**48.33**	**56.67**	
2006	**Pixel Digital Number**	1.09	1.77	2.70	3.64	4.20	**5.03**
	Number of Pixels	16	146	15,689	36,401	37,371	
	Total	17	258	42,360	132,500	156,958	
	C-Stock (t ha^{-1})	**12.11**	**19.67**	**30.00**	**40.44**	**46.67**	
2011	**Pixel Digital Number**	1.29	2.02	3.23	4.45	5.17	**5.37**
	Number of Pixels	1	1588	20,360	26,999	27,269	
	Total	1	3208	65,763	120,146	140,981	
	C-Stock (t ha^{-1})	**14.33**	**22.44**	**35.89**	**49.44**	**57.44**	
2016	**Pixel Digital Number**	0.37	0.91	1.81	2.71	3.3	**4.36**
	Number of Pixels	63,524	71,772	77,050	78,083	78,173	
	Total	23,504	65,313	13,9461	211,605	257,971	
	C-Stock (t ha^{-1})	**4.11**	**10.11**	**20.11**	**30.11**	**36.67**	

Plots with the largest forest carbon storage are indicated by pixels with the highest digital number

From the five percentiles of forest carbon stocks, a two-way ANOVA with replication indicated that natural forests in Luanshya have higher biomass carbon stocks (ρ = 0.00) than forests in Bushbuckridge (Figure 4.27). However, there has been a steady decrease in the average carbon stocks of forests in Luanshya. The mean aboveground stored carbon of 44.20 ± 19.41 t ha^{-1} decreased by 0.80% from 1986 to in 1998, but later increased to a peak of 54.81 ± 23.10 t ha^{-1} in 2001. From 2001 to 2016, the average carbon stocks gradually declined at an average rate of 1.25% per annum. Relating the observed old stumps to the lower tree density and higher biomass in primary forests, an increase in the mean carbon stocks from 1998 to 2001 could be attributed to the thinning effect that results from selective felling of mature trees. The effect of continuous forest disturbance on forest aboveground carbon stocks is highlighted in an exponential decline in biomass carbon density from 54.81 t ha^{-1} in 2001 to an average low of 36.67 t ha^{-1} in 2016 (Figure 4.27).

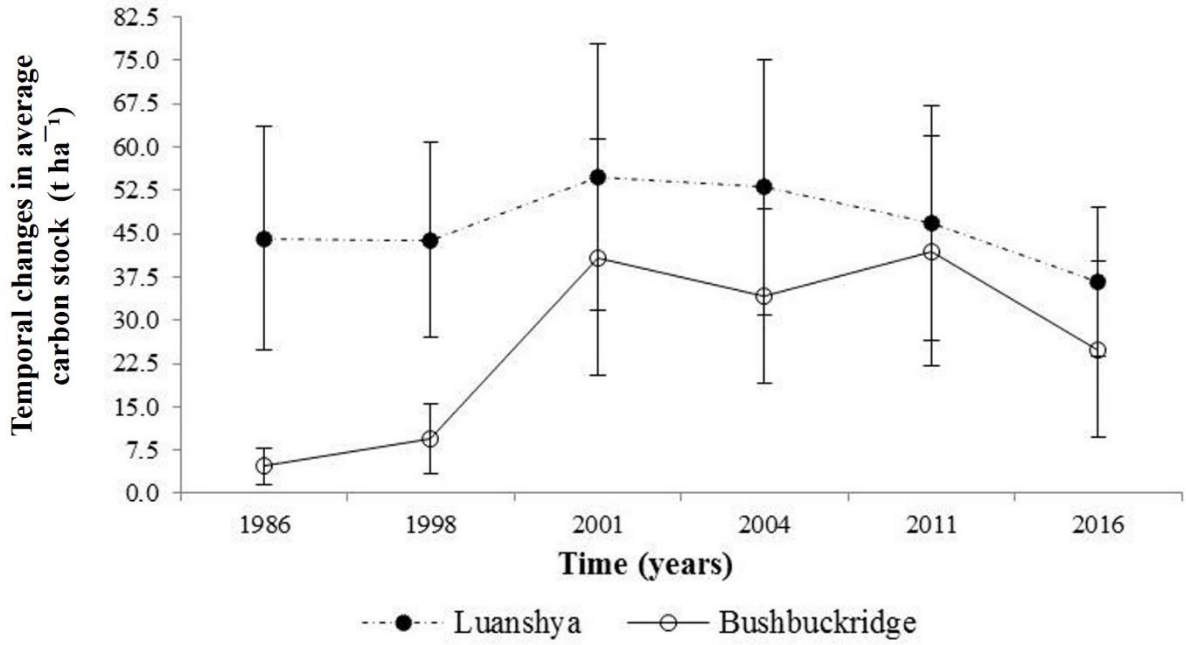

Figure 4.27: Comparison of temporal changes in aboveground carbon stocks between forests in Luanshya and Bushbuckridge. Errors bars indicate the standard deviation from the observed average carbon stock.

Unlike the forests in Luanshya, the spatial and temporal changes in Bushbuckridge showed that the stocks of biomass carbon increased from 4.67 t ha^{-1} in 1992 to 9.52 t ha^{-1} in 1998 and further increased to a peak of 40.84 t C ha^{-1} in 2001. From 2001 to 2006, 2006 to 2010 and 2010 to 2016, a decrease in average carbon stock was followed by an increase of between 16.38% and 40.48% and vice versa. The oscillating trend from 2001-2016 compared closely with forest harvest scheduling that was observed from the field survey (Figure 4.28). During the harvest periods, households harvest and buffer enough woodlots to see them through a two/three-year period of harvest restrictions. During the periods of harvest restrictions, forested areas recovered from disturbance, and increased in AGLB and carbon stocks as seen in the year 2001 and 2011 (Figure 4.27).

Figure 4.28: Storage and important utilisation of the harvested forest woodlots in Bushbuckridge. The pictures show evidence of deforestation, where (a) households harvest and gather enough woodlots to use during periods of harvest restriction. The woodlots are mainly used for (b, c) construction and maintenance of livestock fencing.

4.3 Effects of temperature and precipitation fluctuations on forests

Figures 4.29, 4.30 show the fluctuations in temperature and precipitation during the period 1986-2016 in Luanshya and 1992-2016 in Bushbuckridge. Throughout the 36-year period (Luanshya), minimum temperature varied between 13.55°C and 21.75°C, whereas maximum temperature ranged from 25.37°C to 30.33°C. Precipitation was highly inconsistent, with the observed weather stations recording mean annual rainfall of 1291 mm. Periods with rainfall less than the 1986-2016 average were 1992-1995 (887 mm), 1998-2001 (1112 mm) and 2004-2005 (951 mm) (Figure 4.29). In comparison to Luanshya, the Lowveld area of Mpumalanga experienced statistically similar temperatures ($\rho = 0.19$) ranging between 13.72°C and 29.69°C. Based on the 1992-2016 annual mean precipitation (534 mm), extreme droughts were experienced in 1992 (435 mm), 1994 (258 mm), 2002 (289 mm), 2003 (267 mm), 2015 (193 mm) and 2016 (306 mm). Generally, Bushbuckridge recorded lower rainfall ($\rho = 0.00$) for the five periods of 1992-1998, 1998-2001, 2001-2006, 2006-2010 and 2010-2016 than the observed periods (1986-1998, 1998-2001, 2001-2004, 2004-2011 and 2011-

2016) in Luanshya. Assuming that the amount of rainfall was correlated to readily available water for NPP, these differences are meaningful in understanding the observed differences in natural regeneration, extent of forest cover, size of individual trees and the amount of biomass carbon stock.

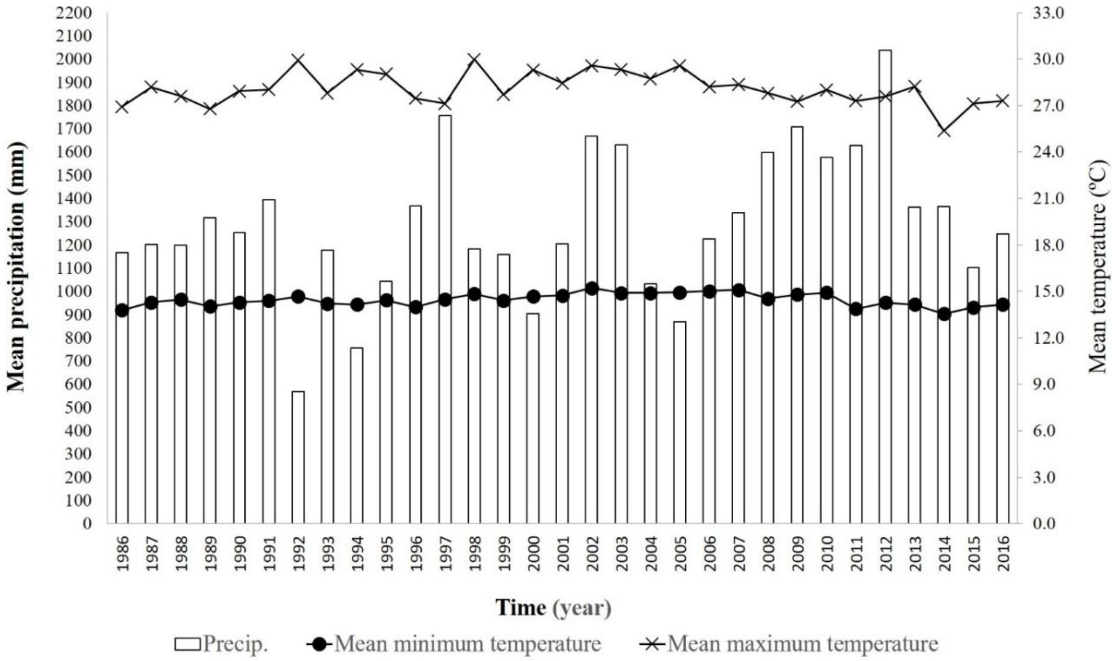

Figure 4.29: Fluctuations in temperature and precipitation for the period 1986-2016, Luanshya.

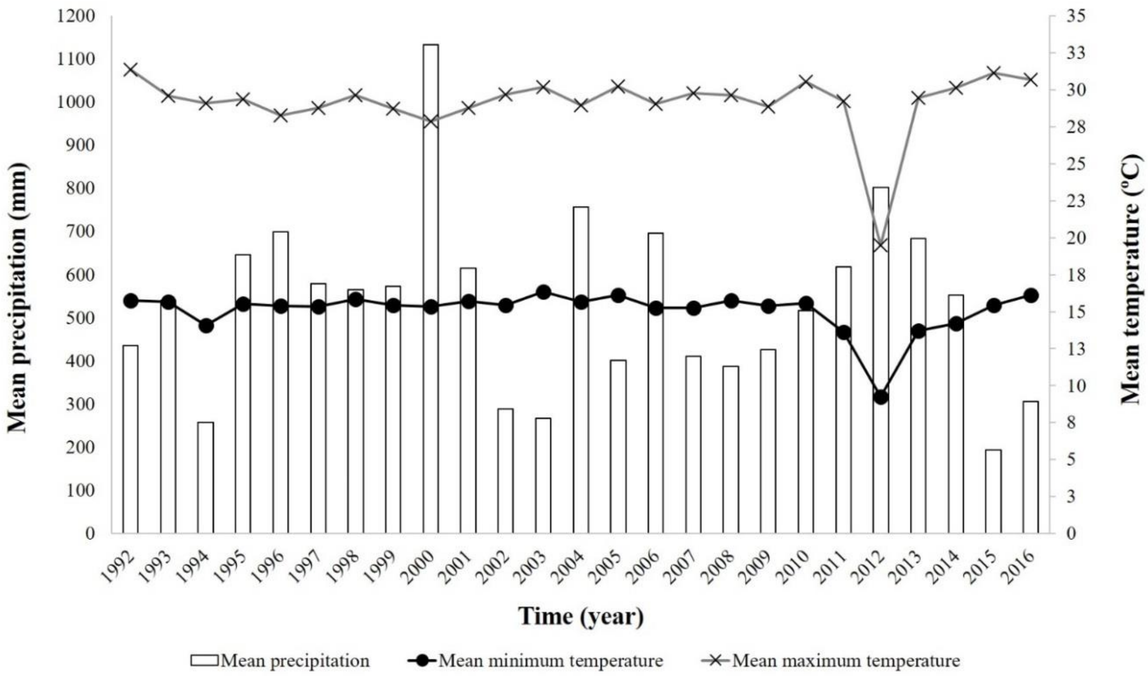

Figure 4.30: Fluctuations in temperature and precipitation for the period 1992-2016, Bushbuckridge.

4.4.1 Interannual variability of EVI with precipitation

Table 4.17 provides the time period over which precipitation most strongly influences NPP of woodlands during the preceding time periods of one to five years. During these periods, mean precipitation ranged from 1116 mm yr^{-1} to 1268 mm yr^{-1}. Precipitation of longer time durations (1268 mm yr^{-1} for a four-year time lag; 1205 mm for a five-year time lag) were associated with lower values of relative standard deviation or coefficients of variation (CV: 0.16) than average rainfall recorded over a shorter time periods (0.26 for mean precipitation averaged over two and three year time lags). Relationships between EVI of UDF site and precipitation were used as control plots (Figure 4.31), over which the overall temporal response of EVI to rainfall was evaluated (Figure 4.32).

Table 4.17 - Mean precipitation across different combinations of different preceding time periods in Luanshya.

		Previous precipitation and temperature	Year					
			1986	**1998**	**2001**	**2004**	**2011**	**2016**
Time lags	**1 year**	Mean precipitation (mm)	1290	1472	1316	813	1519	1126
		Mean minimum temperature (ºC)	15.8	17.0	16.5	17.1	16.3	21.8
		Mean maximum temperature (ºC)	26.9	28.5	28.0	29.9	27.7	30.3
	2 year	Mean precipitation (mm)	616	1453	1007	1057	1468	1095
		Mean minimum temperature (ºC)	16.0	15.4	15.3	15.7	15.4	21.8
		Mean maximum temperature (ºC)	27.1	27.9	29.0	29.4	27.7	30.3
	3 year	Mean precipitation (mm)	1230	1460	1147	884	1937	1098
		Mean minimum temperature (ºC)	14.5	14.9	15.0	15.5	16.5	21.8
		Mean maximum temperature (ºC)	27.0	27.7	28.5	29.6	27.8	30.3
	4 year	Mean precipitation (mm)	1280	1298	1228	993	1649	1157
		Mean minimum temperature (ºC)	14.5	14.7	15.0	15.2	15.0	21.8
		Mean maximum temperature (ºC)	27.4	28.1	28.5	29.2	28.0	30.3
	5 year	Mean precipitation (mm)	1292	1184	1269	813	1448	1225
		Mean minimum temperature (ºC)	14.4	14.6	14.8	17.0	15.1	14.3
		Mean maximum temperature (ºC)	27.5	28.4	28.3	29.9	27.9	27.9
		Mean EVI for UDF site	**0.53**	**0.34**	**0.40**	**0.30**	**0.38**	**0.51**
		Mean EVI for the entire forest cover	**0.27**	**0.19**	**0.25**	**0.22**	**0.25**	**0.38**

Mean EVI was calculated for UDF site (control plots) and the entire woodland cover.

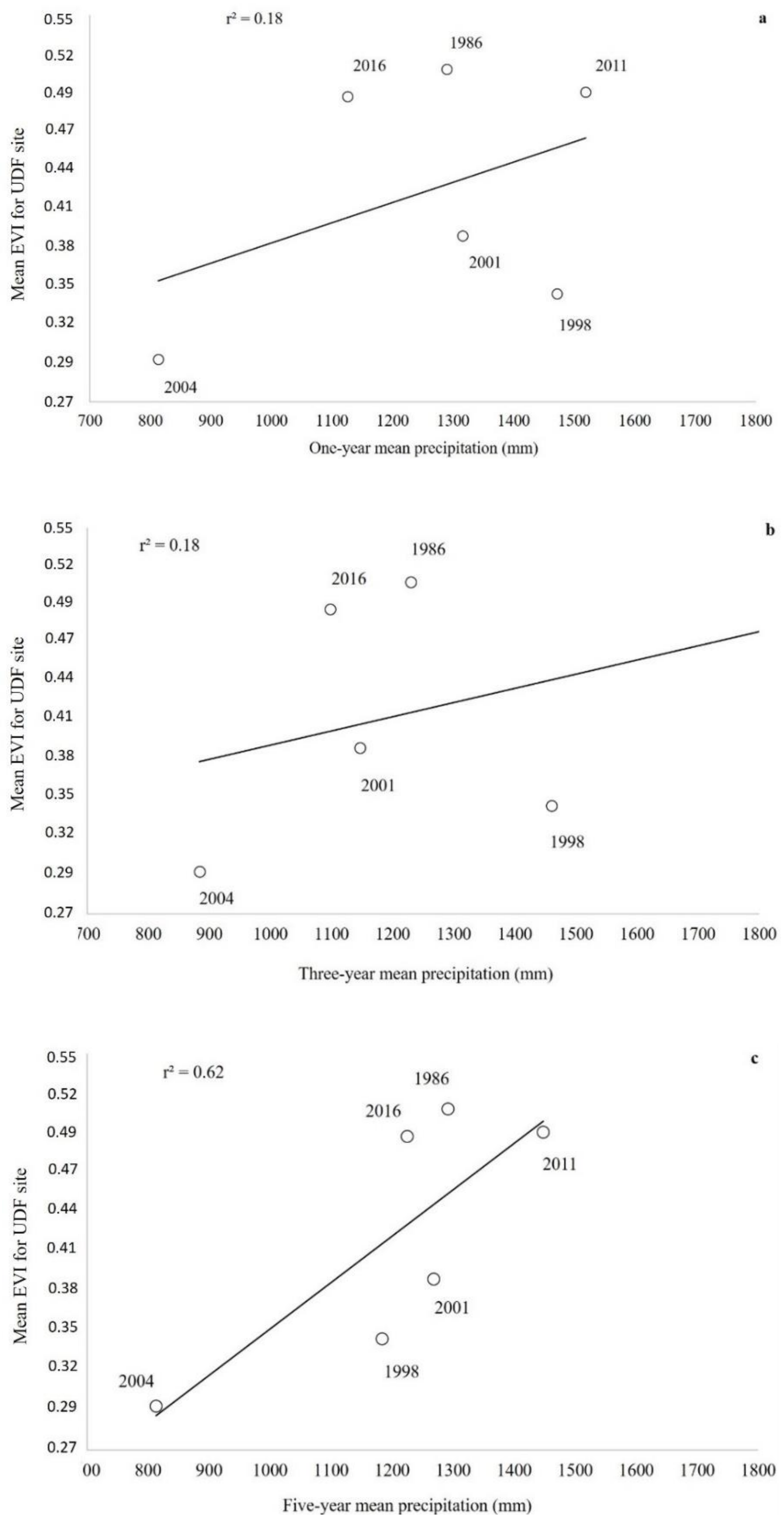

Figure 4.31: Relationships between precipitation and mean EVI of UDF site in Luanshya. Mean annual precipitation was calculated from the preceding time period spanning (a) one year, (b) three years and (c) five years.

Figures 4.31, 4.32 demonstrate how Miombo woodlands in Luanshya responded to interannual variability in precipitation. For UDF site (Figure 4.31), positive correlations between precipitation and EVI were consistently strongest for longer time lags than shorter time durations (five-year period: $r^2 = 0.62$; three-year period: r^2: 0.18; one-year period: $r^2 = 0.18$). This indicates that in the absence of forest disturbance, EVI is influenced by precipitation of not only the immediate preceding growing season, but also the amount of rainfall received over a longer time period (e.g. time lag of five years). Across the entire forested areas, Figure 4.32 shows distinct negative linear relationships between EVI and mean precipitation, averaged from different combinations of time duration and time lags (five-year period: $r^2 = -0.75$; three-year period: $r^2 = -0.30$; one-year period: $r^2 = -0.64$). In contrast to UDF sites (Figure 4.31), the negative correlation coefficients for the whole woodland cover reflect a chronosequence of forest sites, which included, UDF, PDF, SF and RF sites. Supplementary figures depicting correlations between EVI and mean precipitation averaged from time lags spanning two and four years are provided in Appendix D1.

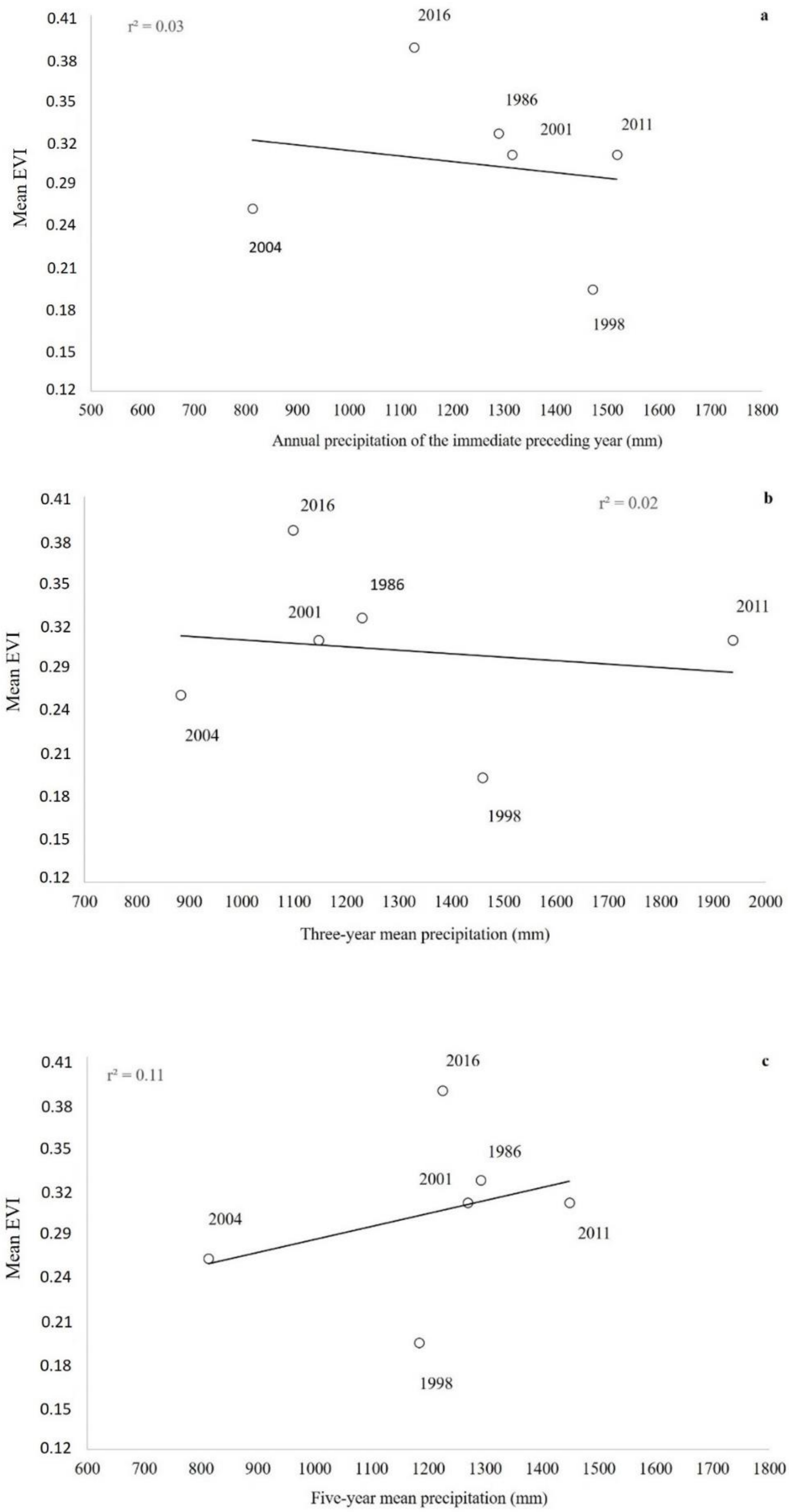

Figure 4.32: Relationships between precipitation and mean EVI of the whole study area in Luanshya. Mean annual precipitation was calculated from the preceding time period spanning (a) one year, (b) three years and (c) five years (c).

In Bushbuckridge, the relationships between EVI and precipitation also depended on the combination of time duration and time lags over which annual rainfall was integrated (Table 4.18 and Figure 4.33). Unlike the alternatingly weak positive to negative correlations for Luanshya, EVI in the adjoining woodlands of Bushbuckridge responded more strongly to variations in precipitation. Similarities can be drawn from the relationships between a five-year mean precipitation and temporal response of EVI in the UDF areas of Luanshya (especially for a five-year mean precipitation: $r^2 = 0.62$), and that of wooded areas in Bushbuckridge (r^2: 0.51-0.64). Of the five observed time lags, changes in EVI were mostly influenced by precipitation received over a longer time duration (Table 4.18). Figure 4.33 demonstrates that the highest correlation coefficient (r^2: 0.64) between EVI and mean precipitation, averaged over a five-year period preceding the dates of the acquired Landsat scenes (Figure 4.33c), was partly attributed to the relatively less variations (CV: 0.16) in the amount of rainfall received (655 ± 107 mm yr^{-1}). This suggests that a five-year period of moderate rainfall, with smaller interannual variability often resulted in a marked increase in EVI (See Appendices F the relationships between EVI and precipitation, averaged from the preceding periods spanning two and four years). By contrast, drought experienced in 2005/2006 and 2015/2016 growing seasons, led to reduced available soil MC to spur natural regeneration. This is also in agreement with the earlier observed decrease in regeneration and forest succession during the period 2001-2006 and 2010-2016 (Figure 4.14). Amid forest disturbance and LULC changes, these analyses are important in understanding forest productivity and changes that accompany rainfall variability.

Table 4.18 - Mean precipitation across different combinations of preceding time periods, in Bushbuckridge

		Previous precipitation and temperature	1992	1998	2001	2004	2011	2016
Time lags	1 year	Mean precipitation (mm)	253	556	664	568	697	193
		Mean minimum temperature (ºC)	15.0	15.5	15.6	16.0	16.0	16.0
		Mean maximum temperature (ºC)	29.8	29.1	27.6	29.0	29.0	27.0
	2 years	Mean precipitation (mm)	361	506	27.4	537	759	373
		Mean minimum temperature (ºC)	15.0	15.5	15.7	16.0	16.0	15.0
		Mean maximum temperature (ºC)	29.2	28.5	27.4	29.0	29.0	27.0
	3 years	Mean precipitation (mm)	434	598	993	509	877	476
		Mean minimum temperature (ºC)	15.1	15.4	15.7	16.0	16.0	15.0
		Mean maximum temperature (ºC)	28.9	28.2	27.7	29.0	29.0	27.0
	4 years	Mean precipitation (mm)	506	534	886	545	820	558
		Mean minimum temperature (ºC)	15.1	15.1	15.6	16.0	16.0	15.0
		Mean maximum temperature (ºC)	28.6	28.3	28.0	29.0	29.0	27.0
	5 years	Mean precipitation (mm)	611	489	800	709	748	570
		Mean minimum temperature (ºC)	15.2	15.1	15.6	16.0	16.0	15.0
		Mean maximum temperature (ºC)	28.4	28.4	28.0	28.0	29.0	29.6
		Mean EVI	**-0.20**	**0.20**	**0.42**	**0.33**	**0.42**	**0.30**

Where mean EVI values are the average greenness and quantity measure of the entire study area.

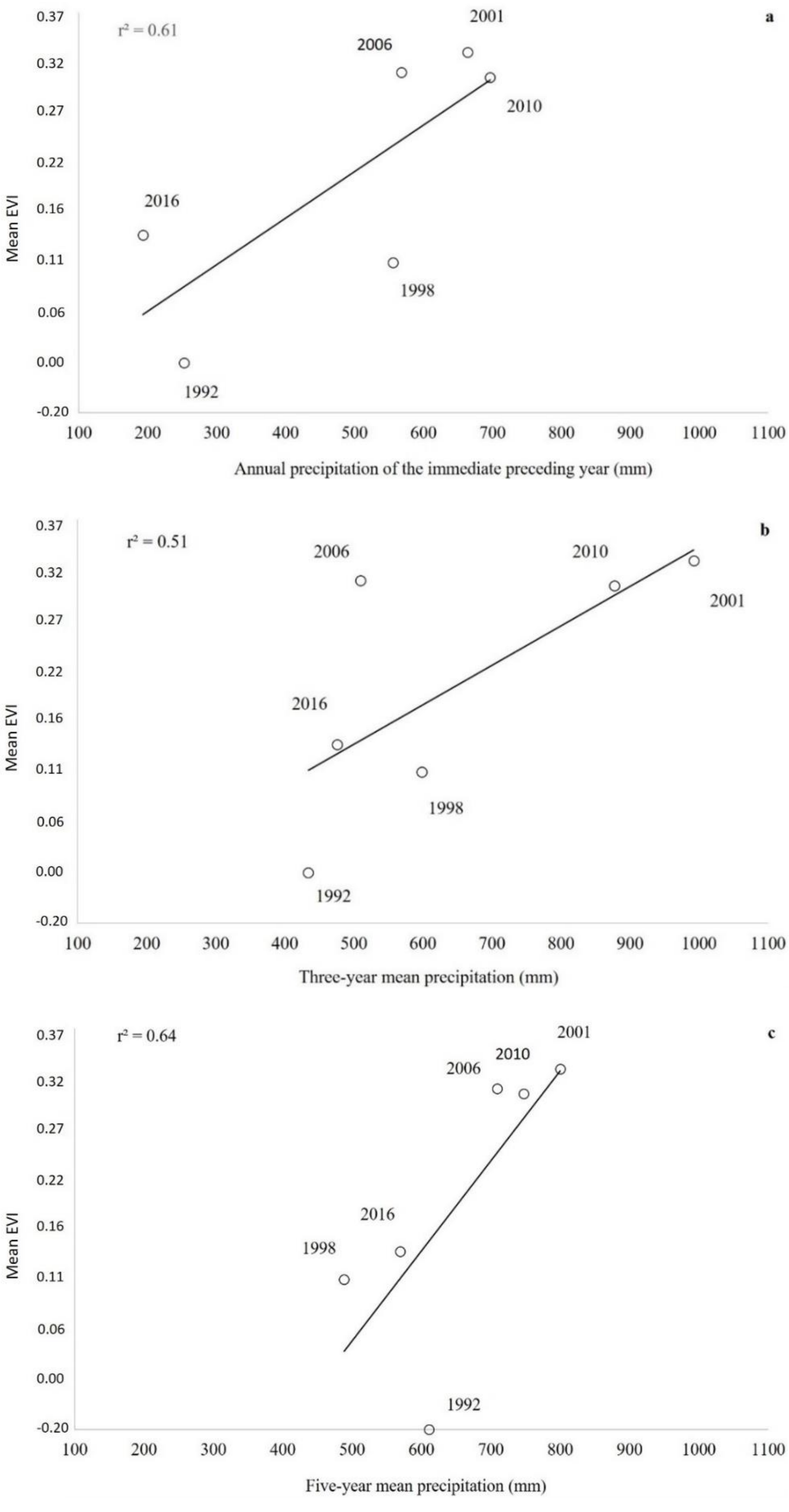

Figure 4.33: Relationships between precipitation and mean EVI of the entire woodland cover in Bushbuckridge. Mean annual precipitation was calculated from the preceding time period spanning (a) one year, (b) three years and (c) five years.

The influence of temperature on forest EVI was not as significant (ρ <0.00) as that of interannual variability in precipitation (Appendices E1, E2, G1, G2). In Luanshya, the correlation coefficients between EVI and mean minimum temperature, and mean maximum temperature varied from 0.04-0.15 and 0.01-0.03, respectively (Appendices E1, E2). These relationships were further highlighted in Bushbuckridge, where variations in minimum temperature was positively correlated with EVI (r^2 = 0.48-0.73), while there was no noticeable response of EVI to variations in maximum temperature (r^2 = -0.10 and 0.01) (See Appendices G1, G2). This was attributed to the covariance between precipitation and temperature (r^2 = -25 to -0.01), with lower temperature consistently associated with increased amount of rainfall (Appendices H1, H2).

4.4 Vertical distribution of SOM concentration by depth, Luanshya

The mean estimates of SOM concentration from the experimental procedures for loss-on-ignition (LOI) method is presented in Table 4.19. In order to quantify both smaller and bigger changes in soil weight, all estimates were reported to a precision of 0.0001g. For each of the 189 soil samples (0-10 cm: 63; 10-20 cm: 63; 20-30 cm: 63), a correction factor for structural water loss was applied to the loss in weight or the difference in weight between soil samples before and after ignition. For instance, the loss in weight of 0.6967 g for soils from 0-10 cm depth in Site-1 was multiplied by a factor of 0.96 (1-0.04) to estimate mean SOMc (0.6688g, which represent 2.75% of the total soil weight).

Table 4.19 - Loss on ignition method: Estimates of SOM concentration (of soil samples from Luanshya) from the measured weight loss at 450ºC

Soil depth	Sampled Site	Crucible weight (g)	Before ignition crucible + soil weight (g)	Soil weight (g)	After ignition crucible + soil weight (g)	Loss in weight (g) 450 °C	SOMc (g) ($1-CF_{SWL}$)	SOMc (%)
0-10 cm	Site 1 (UDF)	44.2554	69.3694	25.1140	68.6278	0.7416	0.7119	**2.83**
	Site 2 (PDF)	44.6529	67.1005	22.4477	66.1543	0.9462	0.9084	**4.05**
	Site 3 (RF)	43.7875	67.3174	23.5298	65.7794	1.5380	1.4765	**6.27**
	Site 4 (PDF)	43.8716	63.8408	19.9692	61.7468	2.0940	2.0103	**10.07**
	Site 5 (RF)	44.9772	67.9588	22.9816	66.9967	0.9621	0.9236	**4.02**
	Site 6 (RF)	42.9494	65.4667	22.5173	64.1538	1.3129	1.2604	**5.60**
	Site 7 (SF)	44.3459	67.1001	22.7541	65.7657	1.3344	1.2810	**5.63**
10-20 cm	Site 1 (UDF)	44.9246	71.3562	26.4316	70.2302	1.1259	1.0809	**4.09**
	Site 2 (PDF)	43.7362	69.9413	26.2051	69.3595	0.5818	0.5586	**2.13**
	Site 3 (RF)	43.4414	67.0636	23.6223	65.4025	1.6613	1.5948	**6.75**
	Site 4 (PDF)	43.5893	64.4946	20.9053	63.4351	1.0595	1.0172	**4.87**
	Site 5 (RF)	44.5218	68.2862	23.7645	67.2553	1.0309	0.9897	**4.16**
	Site 6 (RF)	45.0981	65.5862	20.4881	64.8866	0.6996	0.6716	**3.28**
	Site 7 (SF)	44.3234	70.9730	26.6496	69.9537	1.0193	0.9785	**3.67**
20-30 cm	Site 1 (UDF)	43.4081	70.4046	26.9965	69.7381	0.6665	0.6399	**2.37**
	Site 2 (PDF)	44.1955	67.2812	23.0857	66.7657	0.5155	0.4949	**2.14**
	Site 3 (RF)	43.2873	67.2133	23.9260	65.4053	1.8080	1.7357	**7.25**
	Site 4 (PDF)	45.1236	62.5439	17.4203	61.8152	0.7286	0.6995	**4.02**
	Site 5 (RF)	43.0798	65.5232	22.4433	64.4281	1.0950	1.0512	**4.68**
	Site 6 (RF)	44.5278	65.9538	21.4260	64.5617	1.3921	1.3364	**6.24**
	Site 7 (SF)	43.9142	67.2666	23.3524	66.4313	0.8353	0.8019	**3.43**

Where CF_{SWL} is the correction factor for structural water loss = 0.96

Results show that soil layer from 0-10 cm had the highest proportions of SOM compared to soil layers from 10-20 cm and 20-30 cm depths (Figure 4.34), ranging from 28.35 g kg^{-1} to 100.67 g kg^{-1}, 21.32 g kg^{-1} to 67.51 g kg^{-1} and 21.44 g kg^{-1} to 72.54 g kg^{-1}, respectively. In the upper most layer, Site-1 of undisturbed (UDF) stands had the lowest and least variable SOM concentration (24.50 g kg^{-1} to 33.35 g kg^{-1}), while Site-4 of the PDF site had the highest concentration of organics (71.99 g kg^{-1} to 116.88 g kg^{-1}), followed by SF in Site-7 (26.95 g kg^{-1} to 105.70 g kg^{-1}). A one-way ANOVA indicated significant differences ($\rho = 0.05$) in the mean concentration of SOM across the sampled forest sites. A further statistical analysis revealed that the mean values of SOM concentration are not significantly different between the three soil depth ($\rho = 0.35$). These findings suggest the effect of forest disturbances on the spatial and vertical distribution of SOM concentration. Further, it reveals that soil depth is an important consideration for quantifying the spatial variationof SOM concentration/stock.

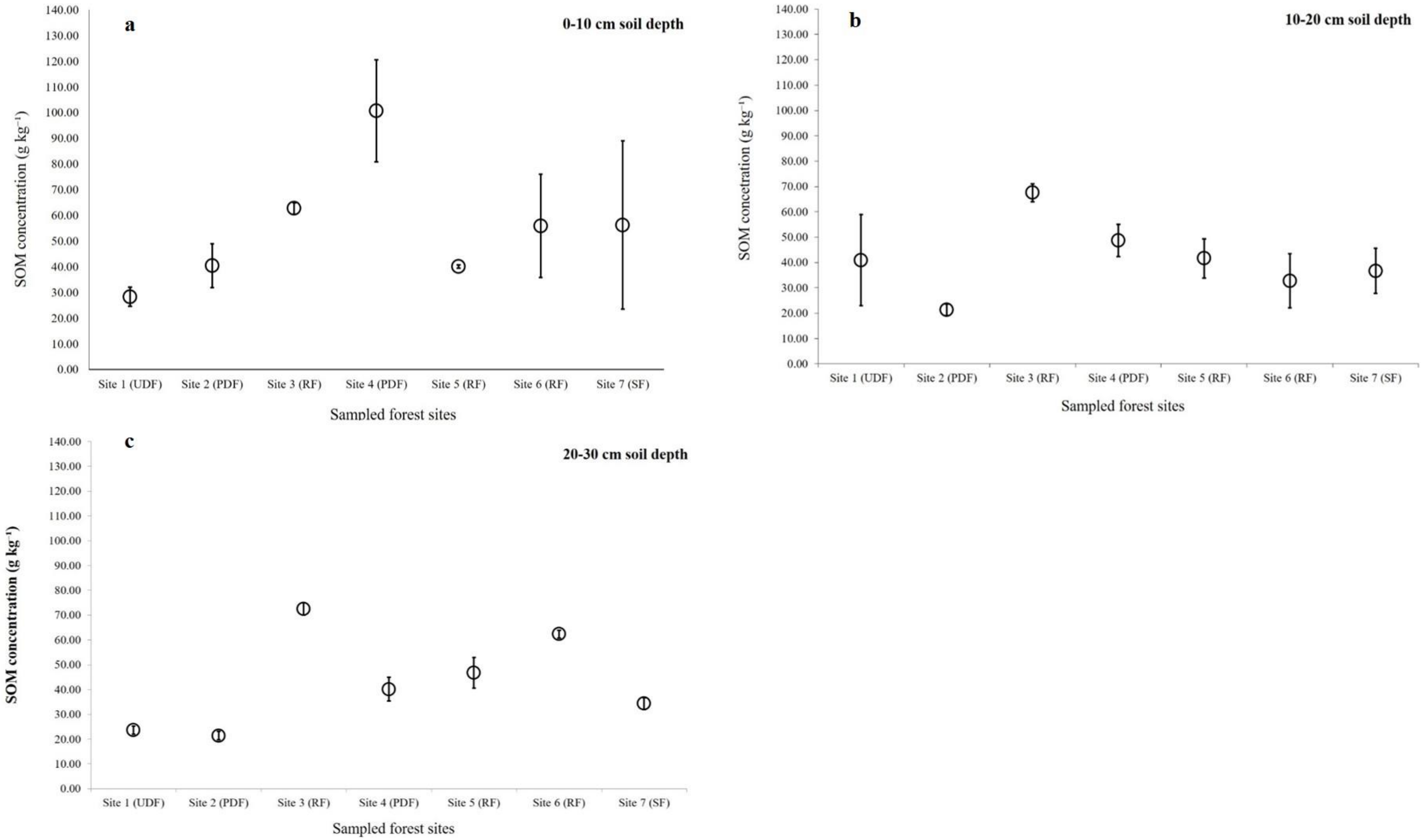

Figure 4.34: Spatial and vertical distribution of SOM concentration in Luanshya. The graphs show estimates of forest SOM concentration and its downward vertical variations with depth, 0-10 cm, 10-20cm and 20-30 cm. Site-1 is UDF site, Site-2 and Site-4 are PDF sites, Site-3, Site-5 and Site-6 are RF sites, and Site-7 is SF site. Each scatter point is the mean of nine-sample plots, and error bar is the standard deviation from the mean.

4.4.1 Laser diffraction: Granulometric soil composition

Subsamples of undisturbed and composite soils were analysed for granulometric composition using a Mastersizer 3000. Nine plots of soil particle size distributions for the UDF (Site-1), PDF (Site-4) and SF (Site-7) forest sites are shown in Figure 4.35. Classical statistics associated with the distributions were particle sizes at the 10^{th}, 50^{th} and 90^{th} percentiles, the measure of "tailedness" (kurtosis) and asymmetry (skewness) of the distributions. Further, the coefficients of variation or the ratio of standard deviation to the mean were used to classify soil types. All the samples were described by the right-leaning curves that depicted negatively skewed distributions. This means that the mean particle sizes were less than the median for the three soil profiles of the seven forest sites.

Soils sampled from Site-1 had the highest particle size values at 10^{th}, 50^{th} and 90^{th} percentile (ranging from: 6.66-7.94 µm for 0-10 cm, 164-182 µm for 10-20 cm and 483-542 µm for 20-30 cm depth, respectively) and are characterised by noticeable right-tailed skewness (Figure 4.35, Table 4.20). These patterns had heavy tails defined by higher variables of skewness (0.45-0.49), kurtosis (0.97-1.08) and coefficients of variation (ranging from 0.70 to 0.74). On the contrary, soils with lower percentile values (e.g. Site 7 of the SF site) had lower coefficients of variations, lighter tails (kurtosis: <0.88) and finely-strongly finely skewed distribution of comparatively lower skewness (<0.36).

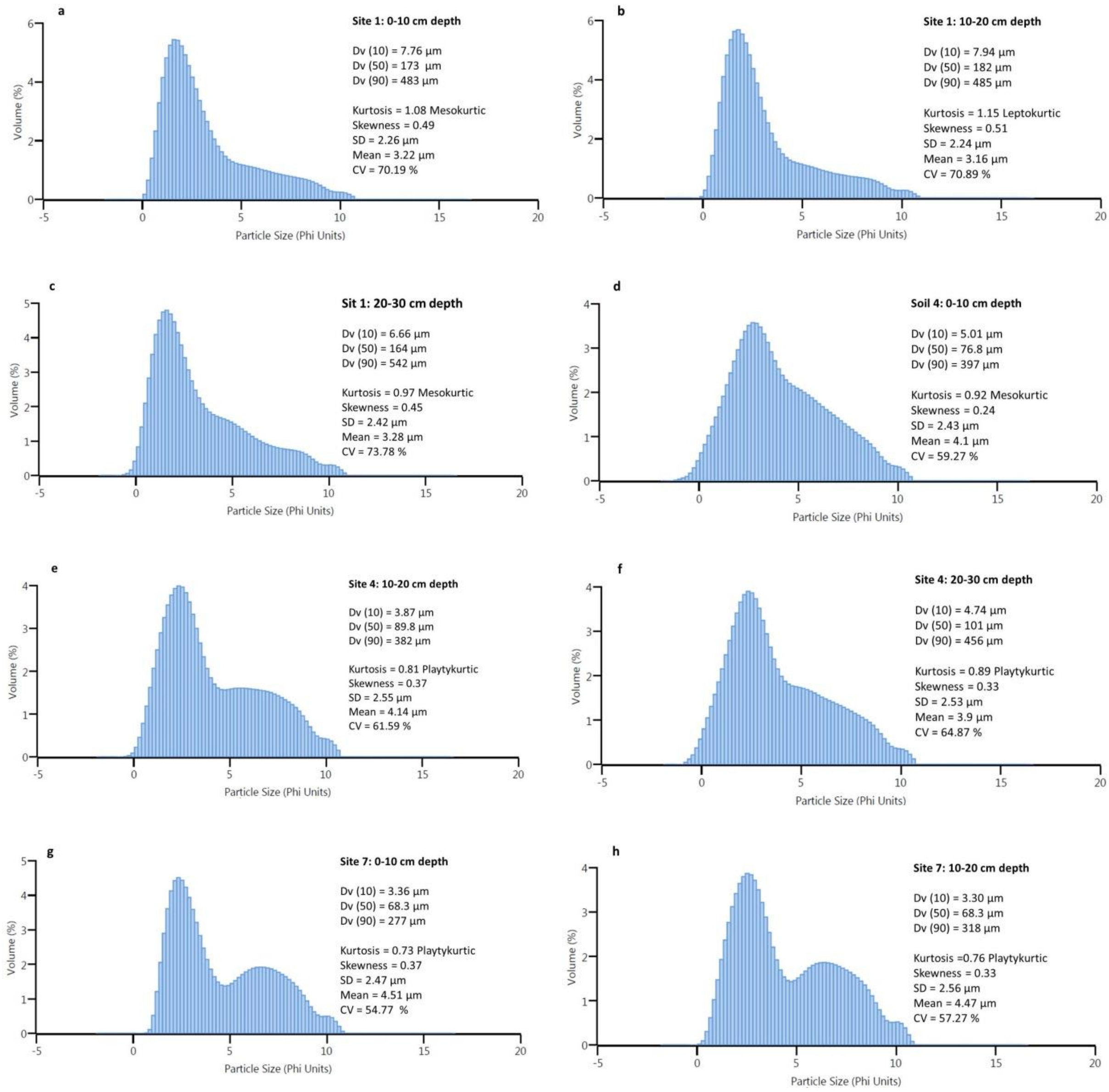

Figure 4.35: Scatter signature of selected soil samples for Luanshya. The associated legend provides a summary of relative volume-size (Phi) distribution by depth.

Table 4.20 - Average classical statistics by depth: Summary of soil particle size distribution in Luanshya

Soil profile	Dv (10) µm	Dv (50) µm	Dv (90) µm	Kurtosis	Skewness	Mean (µm)	SD (µm)	CV
0-10 cm	6.08	103.79	446.00	0.97	0.31	3.84	2.39	0.63
10-20 cm	6.19	109.94	448.70	1.01	0.32	3.79	2.41	0.64
20-30 cm	5.26	106.98	450.38	0.98	0.31	3.89	2.45	0.65

Where Dv is soil particle volume-size distributions at 10th, 50th and 90th percentile, SD is the standard deviation and CV is coefficient of variation.

From the cumulative particle size distribution and classical statistics (Figure 4.35 and Table 4.20), the forest soils were textural classified as, sandy loam and loamy sand (Figure 4.36). The cumulative volume composition in sandy loam was 2.60-5.70% clay, 24.82-41.88% silt and 53.15-71.69% sand. Irrespective of soil type and depth, the proportion of clay (e.g. decreased in particle size at 10th percentile) and coefficients of variation marginally increased with depth.

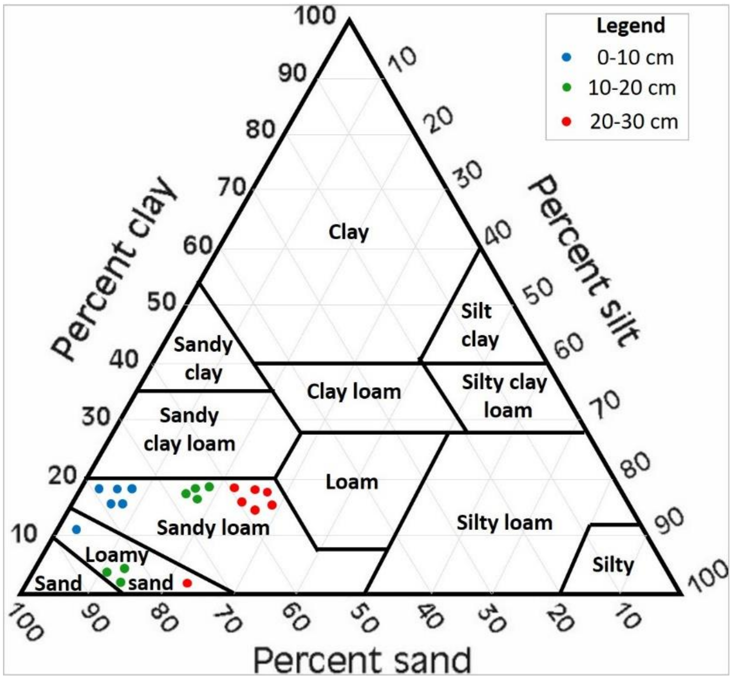

Figure 4.36: Textural classification of the forest soils in Luanshya. The different position and type of points depict classification of the cumulative (0-10 cm, 10-20 cm, 20-30 cm depth) samples from the seven soil pits of each forest site. The number of points within loam, sandy loam and loamy sand segments indicate the common occurrence of soil type.

4.4.2 Estimates of SOM stock

Table 4.21 provides SOM stock calculated from BD, SOM concentrations and thickness or depth for each of the three soil layers, 0-10 cm, 10-20 cm and 20-30 cm. For 0-10 cm depth, the UDF site (Site-1) had the lowest mean amount of SOMs (3667 g m^{-3}) followed by the PDF site (Site-2: 5178 g m^{-3}). The highest stock of SOM was recorded in Site-4 of PDF site (11,389 g m^{-3}), whereas the forest stands of secondary and regeneration growth had fairly large mean stocks of 8711 g m^{-3} and 6815 g m^{-3}, respectively. At 10-20 cm depth, the largest stocks were estimated in Site-3 (7956 g m^{-3}) and Site-5 (6711 g m^{-3}) of regeneration growth. Vertical partitioning of SOM stock changed markedly from 3667 g m^{-3} in 0-10 cm to 5667 g m^{-3} in 10-20 cm and 3722 g m^{-3} in 20-30 cm depth of the UDF site. Likewise, SOMs in forest soils of the PDF sites (Site-4) decreased noticeably by 57.4% from 0-10 cm to the underlying layers of 10-20 cm and 20-30 cm.

Soil BD was generally lower for 0-10 cm soil layers (mean: 1286 ± 114 g kg^{-3}) than the underlying layers of 10-20 cm: 1331 ± 186 g kg^{-3} and 20-30 cm: 1469 ± 204 g kg^{-3}. This was closely associated with the vertical partitioning of SOM concentration, where the proportion of organics decreased with increased soil depth. The variations in SOM concentration that is explained by BD was r^2 = -0.20 for 0-10 cm layers, r^2 = -0.23 for 10-20 cm and r^2 = -0.28 for 20-30 cm. These findings also reveal that SOM becomes stable and less variable with depth, which was attributed to the negative covariance between SOMc and BD.

Table 4.21 - Physical and chemical properties of forest soils, Luanshya

	Site	Altitude (m)	BD (kg m^{-3})	SOMc (g kg^{-1})	AGLB (ton $plot^{-1}$)	Clay (%)	Silt (%)	Sand (%)	EC (µS cm^{-1})	MC (%)	pH	Gravel (%)	SOMs (g m^{-3})
Depth : 0-10 cm	1	1260	1290	28.47	6.70	2.53	25.55	71.92	64.47	21.10	4.50	0.00	**3667**
	2	1229	1280	40.42	6.57	2.54	22.06	75.4	102.47	10.00	4.91	0.00	**5178**
	3	1213	1110	62.72	0.76	4.65	37.98	57.01	77.23	17.00	4.21	1.00	**6967**
	4	1212	1140	99.87	7.48	3.26	34.13	62.23	130.73	31.10	5.50	25.00	**11,389**
	5	1248	1340	40.20	0.12	5.59	40.94	52.97	103.25	16.00	4.55	11.00	**5389**
	6	1231	1430	56.57	0.33	3.43	29.43	66.64	74.17	14.00	4.92	13.00	**8089**
	7	1225	1410	61.77	6.03	3.82	37.91	57.71	136.80	19.80	5.21	13.00	**8711**
Depth: 10-20 cm	1	1260	1360	41.71	6.70	2.53	25.55	71.92	64.47	21.10	4.50	0.00	**5667**
	2	1229	1350	21.19	6.57	2.54	22.06	75.4	102.47	10.00	4.91	0.00	**2867**
	3	1213	1180	67.45	0.76	4.65	37.98	57.01	77.23	17.00	4.21	3.00	**7956**
	4	1212	980	49.52	7.48	3.26	34.13	62.23	130.73	31.10	5.50	57.00	**4856**
	5	1248	1600	41.98	0.12	5.59	40.94	52.97	103.25	16.00	4.55	5.00	**6711**
	6	1231	1470	33.01	0.33	3.43	29.43	66.64	74.17	14.00	4.92	15.00	**4856**
	7	1225	1380	36.82	6.03	3.82	37.91	57.71	136.80	19.80	5.21	16.00	**5078**
Depth: 20-30 cm	1	1260	1570	23.68	6.70	2.84	24.30	72.83	96.03	11.10	4.9	0.00	**3722**
	2	1229	1490	21.38	6.57	3.32	24.29	72.39	85.50	9.80	4.84	0.00	**3189**
	3	1213	1000	72.78	0.76	4.84	38.93	56.03	76.20	18.50	4.19	1.00	**7278**
	4	1212	1480	40.15	7.48	3.43	33.98	62.5	98.77	41.10	5.52	68.00	**5944**
	5	1248	1690	46.74	0.12	6.04	45.51	48.44	96.53	18.00	4.61	7.00	**7900**
	6	1231	1580	62.37	0.33	3.79	32.18	62.99	46.20	15.20	5.07	12.00	**9856**
	7	1225	1470	34.38	6.03	3.83	39.48	55.59	101.93	21.50	5.17	46.00	**5056**

Since, SOMc and soil BD are influenced by other edaphic factors, 11 different potential indictors were evaluated per forest plot and their explanatory correlations coefficients investigated. The 11 edaphic factors included the average altitude, total AGLB, soil BD, proportion of clay (%), silt (%) and sand (%), gravel (%), MC (%), EC, pH and SOMc. These factors were preferred because they have been previously studied, but only in parts, and by applying simple linear regression (Brudvig and Asbjornsen, 2009; Chaudhari *et al*., 2013; Maraseni and Pandey, 2014).

4.4.3 Vertical distribution of SOM concentration by depth, Bushbuckridge

Procedures for LOI analysis were repeated on a total of 189 forest soil samples from Bushbuckridge. Of the oven dried samples (105ºC), about 20 g of soil per crucible were combusted in a furnace at 450ºC for 12 hours. Likewise, the estimates of loss-in-weight (Table 4.22) were converted to SOM concentration by applying a correction factor for structural water loss (CF_{SWL}) (Hoogsteen *et al*., 2015). As a function of the soil weight (before ignition), the average proportion of SOM concentration was 3.76%, 3.71%, and 3.92% for 0-10 cm, 10-20 cm, and 20-30 cm depth, respectively.

Table 4.22 - Loss on ignition method: Estimates of SOM concentration (of soil samples from Bushbuckridge) from the measured weight loss at 450ºC

Sampled site	Crucible weight (g)	Before ignition crucible + soil weight (g)	Soil weight (g)	After ignition crucible + soil weight (g)	Loss in weight (g) 450°C	SOMc g ($1-CF_{SWL}$)	SOMc (%)
Site 1 (SF)	43.6815	70.4362	26.7547	69.3696	1.0666	1.0239	**3.83**
Site 2 (SF)	43.2279	63.7725	20.5447	62.8007	0.9718	0.9329	**4.54**
Site 3 (SF)	44.0005	70.4536	26.4531	69.3696	1.0840	1.0407	**3.93**
Site 4 (SF)	43.2260	63.7298	20.5038	63.0256	0.7042	0.6760	**3.30**
Site 5 (SF)	43.5584	63.8474	20.2890	63.1581	0.6893	0.6617	**3.26**
Site 6 (SF)	44.0752	61.5405	17.4653	60.8215	0.7190	0.6903	**3.95**
Site 7 (SF)	43.6825	63.0343	19.3518	62.3324	0.7020	0.6739	**3.48**
Site 1 (SF)	44.2266	67.3656	23.1391	66.4681	0.8975	0.8616	**3.72**
Site 2 (SF)	44.1344	63.4966	19.3622	62.5301	0.9665	0.9278	**4.79**
Site 3 (SF)	44.1699	67.4284	23.2585	66.4903	0.9380	0.9005	**3.87**

Table 4.22 (*continued*)

Site 4 (SF)	43.5436	62.5276	18.9840	61.9176	0.6100	0.5856	**3.08**
Site 5 (SF)	43.4401	62.4619	19.0219	61.8590	0.6029	0.5788	**3.04**
Site 6 (SF)	43.2846	60.9567	17.6720	60.3003	0.6564	0.6301	**3.57**
Site 7 (SF)	44.2275	63.7843	19.5568	62.9910	0.7933	0.7615	**3.89**
Site 1 (SF)	43.6069	61.4524	17.8455	60.8473	0.6050	0.5808	**3.25**
Site 2 (SF)	43.5822	62.7927	19.2104	61.5610	1.2317	1.1824	**6.16**
Site 3 (SF)	43.5991	61.4739	17.8749	60.8473	0.6266	0.6015	**3.37**
Site 4 (SF)	44.1834	62.5910	18.4076	61.8362	0.7548	0.7246	**3.94**
Site 5 (SF)	44.0222	62.3286	18.3064	61.5968	0.7318	0.7025	**3.84**
Site 6 (SF)	43.5017	61.4112	17.9095	60.8202	0.5910	0.5673	**3.17**
Site 7 (SF)	43.6070	62.5910	18.9839	61.8584	0.7326	0.7033	**3.70**

Where CF_{SWL} is the correction factor for structural water loss = 0.96

The concentration of SOM in the seven forest sites of Bushbuckridge was relatively lower ($\rho = 0.02$) than that of Luanshya. At the 0.05 level of signifiance, the proportion of SOMc was significantly different ($\rho = 0.02$) across the different forest sites (Table 4.22). The distribution and vertical concentration of organic matter was also observed to marginally decrease with depth, declining from an average of 37.56 ± 5.77 g kg^{-1} in the 0-10 cm depth through 37.11 ± 7.56 g kg^{-1} in the 10-20 cm layer, and increasing to 39.17 ± 5.34 g kg^{-1} in the 20-30 cm soil depth. Further, the relative standard deviation indicated that SOMc was slightly more variable in 20-30 cm depth (coefficient of variation, CV: 0.24), followed by 10-20 cm depth (CV: 0.15), and lastly, 0-10 cm soil depth (0.11). Although not as clearly evident as the forest soils in Luanshya, the distribution of SOMc was correspondingly more homogeneous or less variable in the topmost layers than the underlying layers (Figure 4.37).

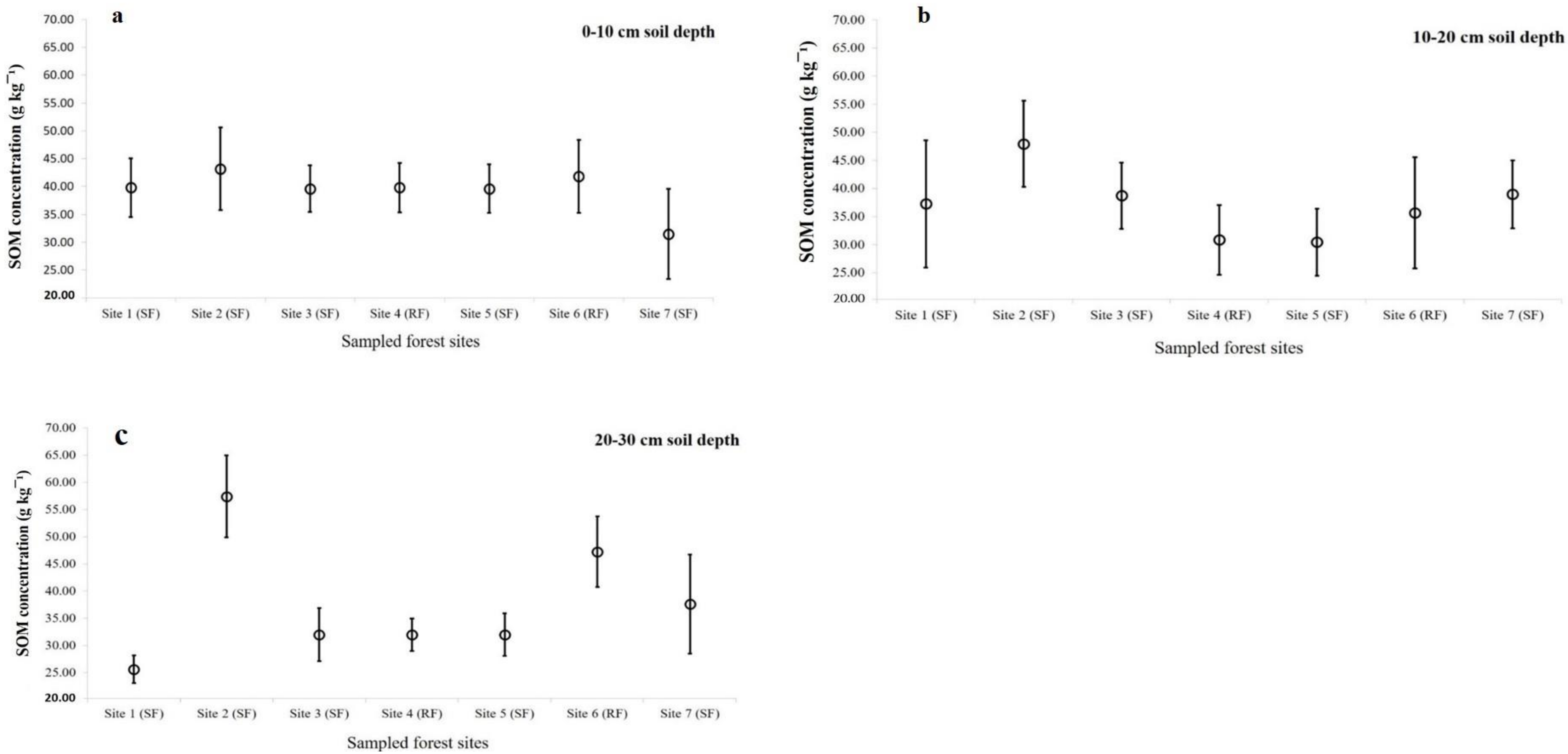

Figure 4.37: Distribution of SOM concentration by depth, Bushbuckridge. The graphs show estimates of forest SOM concentration and its downward vertical variations with depth, 0-10 cm, 10-20cm and 20-30 cm. Site-1, Site-2, Site-3, Site-5 and Site-7 were classified as SF sites, while Site-4 and Site-6 were SF sites. The scatter point and error bar indicates the mean SOM concentration and the standard deviation.

4.4.4 Laser diffraction: Granulometric soil composition

A summary of the spatial and vertical granulometric compositions of the 189 forest soil samples and some of the volume-particle size (units in Phi) distribution curves are presented in Figure 4.38. The three soil profiles were defined by negatively skewed distribution with mean particle sizes of 3.56 ± 2.71 (µm) for 0-10 cm, 3.52 ± 2.70 (µm) for 10-20 cm and 3.80 ± 2.83 (µm) for 20-30 cm depth. Accordingly, the median (86.05-107.98 µm) or 50% of the particles were significantly ($\rho = 0.00$) less than the mean values (3.52-3.80 µm). Even though the cumulative volume (%) was largely dominated by particles greater than 5Ø (31 µm), the variables at 10^{th} percentile further underscored the earlier observed trend which revealed that the proportion of fines tend to increase with depth.

Soils from Bushbuckridge were largely discriminated from that of Luanshya by bimodal distributions. These were associated with nearly symmetrical curves (skewness: <0.12) and lower mean kurtosis values of about 0.90. Higher kurtosis and skewness values were closely associated with lower percentile values and coefficients of variation vice versa. For example, soils from 20-30 cm depth of Site-2 had the lowest kurtosis (0.93), skewness (0.01) and relative standard deviation (0.59), while higher distribution values in Site-1 and Site-7 were associated with relatively higher percentile values and variability coefficients (Table 4.23). In other words, loamy sand with a higher proportion of sand (63-2000 µm) resulted in increased measure of skewness and kurtosis than sandy loam and loam (Figure 4.39).

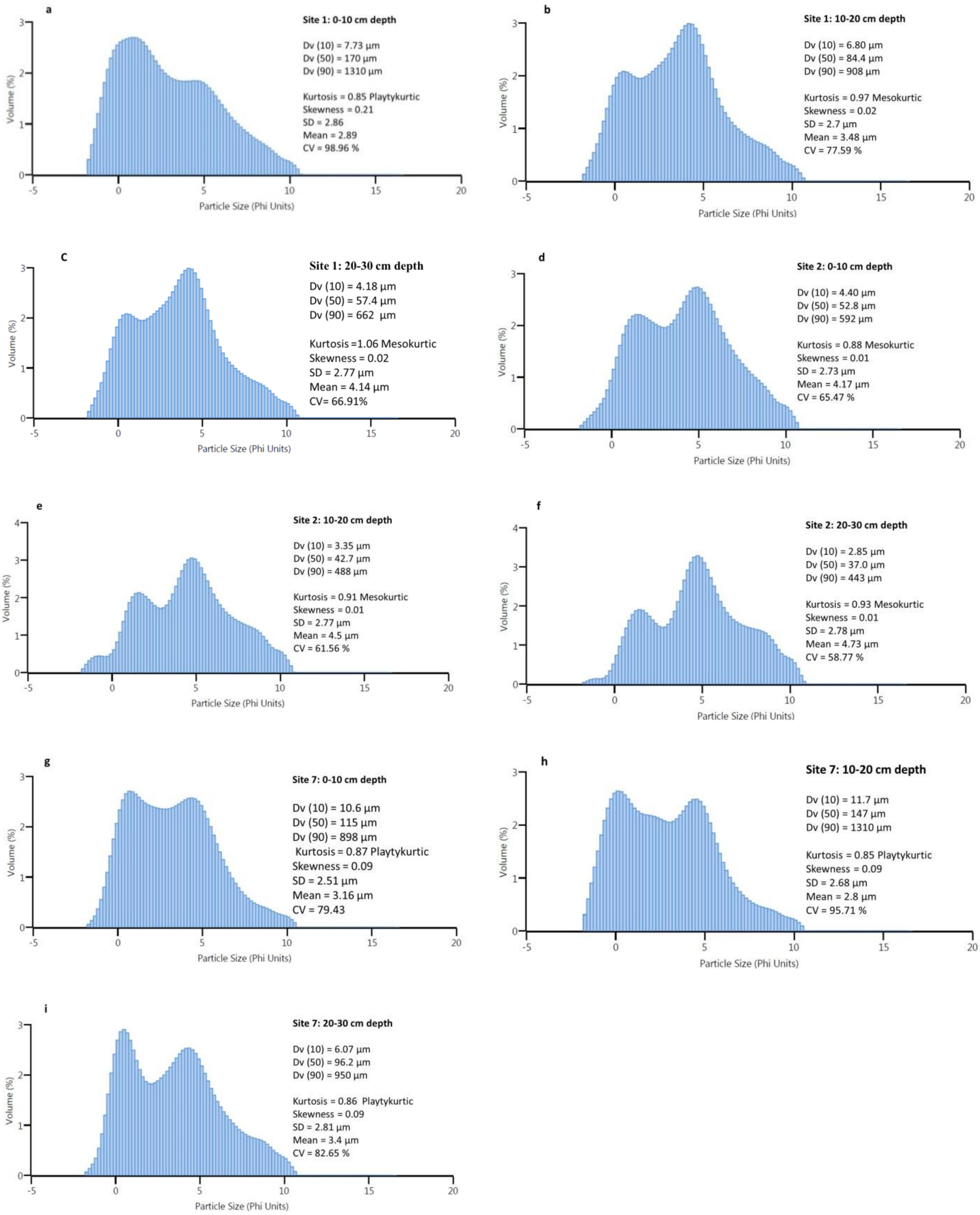

Figure 4.38: Scatter signature of selected soil samples from Bushbuckridge. The associated legends provides a summary of relative volume-size (Phi) distribution by depth.

Table 4.23 - Average classical statistics by depth: Summary of soil particle size distribution in Bushbuckridge

Soil profile	Dv (10) µm	Dv (50) µm	Dv (90) µm	Kurtosis	Skewness	Mean (µm)	SD (µm)	CV
0-10 cm	6.50	107.21	839.73	0.90	0.12	2.71	3.56	0.78
10-20 cm	6.93	107.98	891.06	0.90	0.11	2.70	3.52	0.80
20-30 cm	5.06	86.05	810.54	0.90	0.08	2.83	3.80	0.77

Where Dv is soil particle volume-size distributions at 10th, 50th and 90th percentile, SD is the standard deviation and CV is coefficient of variation.

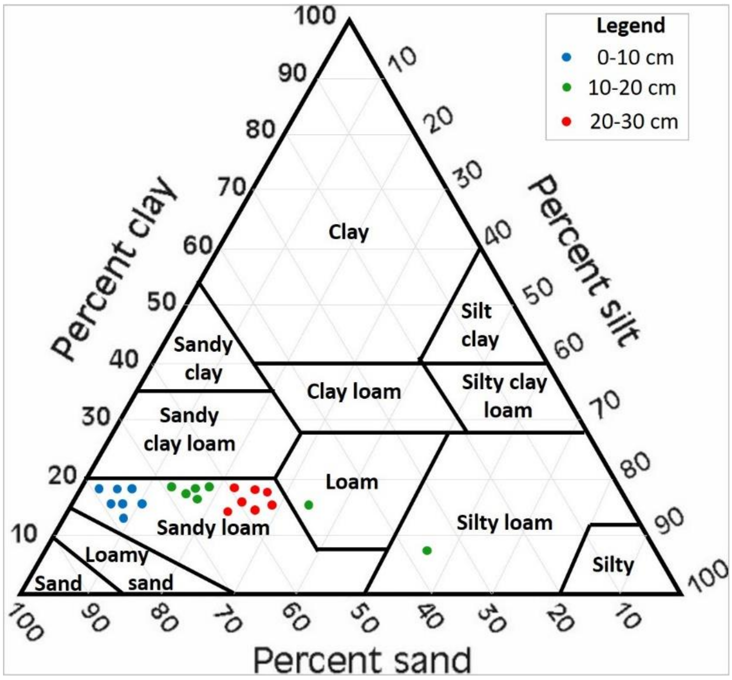

Figure 4.39: Textural classification of the forest soils in Bushbuckridge. The different position and type of points depict classification of the cumulative (0-10 cm, 10-20 cm, 20-30 cm depth) samples from the seven soil pits of each forest site. The common positional occurrence of points within sandy loam, and only one point in both silty loam indicate the most dominate soil type.

4.4.5 Estimates of forest SOM stock

Soil organic matter stock to 30 cm depth averaged about 4876 ± 1601 g m^{-3} in the surveyed wooded areas of Bushbuckridge. The largest stocks were held in the subsoil's of 0-10 cm depth (5109 ± 1088 g m^{-3}) and 10-20 cm depth (4786 ± 1334 g m^{-3}) while deeper soil (20-30 cm) were consistently associated the smallest amounts of about 4732 ± 2155 g m^{-3} (Table

4.24). The depth distributions of SOMs resembled those of SOMc only in the 0-20 cm, but not in the 10-30 cm depth. Based on the coefficients of determination (r^2: 0.61 in the 0-10 cm layer and r^2: 0.83 in the 10-20 cm layer to r^2: 0.84 in the 20-30 cm soil depth), SOMs consistently increased with SOMc. This also indicates that the overall variability of SOMs is not only contributed by SOMc, but partly influenced by BD. In contrast, the variations of SOMs explained by soil BD was largest in layer-2 ($r^2 = 0.88$) and lowest in layer-1 (0-10 cm: $r^2 = 0.43$). These findings substantiates that the amount of SOMs is largely affected by the negative covariance between BD and SOMc. In turn, estimating SOMs from BD, organic matter concentration and soil thickness is not a simple progression because of the many factors influencing the three predictor variables.

Table 4.24 - Physical and chemical properties of forest soils, Bushbuckridge

Stratum	Site	Altitude (m)	BD (kg m^{-3})	SOMc g kg^{-1}	AGLB (ton $plot^{-1}$)	Clay (%)	Silt (%)	Sand (%)	EC (µS cm^{-1})	MC (%)	pH	Gravel (%)	SOMs (g m^{-3})
Depth 0-10 cm	1	401	1410	39.81	1.20	3.04	34.69	60.53	1.10	13.21	5.41	11.50	**5613**
	2	422	1510	43.17	0.50	3.73	42.82	52.44	1.07	11.98	4.88	0.94	**6519**
	3	429	1130	39.61	1.99	2.97	35.06	60.56	1.10	13.21	5.41	11.14	**4476**
	4	422	1380	39.81	0.30	2.98	34.76	60.54	1.10	12.23	4.99	12.65	**5494**
	5	402	960	39.61	0.12	2.92	33.94	56.49	1.09	11.02	4.70	9.65	**3803**
	6	412	1440	41.83	2.97	3.21	37.00	61.03	1.32	13.21	5.41	6.04	**6024**
	7	429	1410	31.48	1.12	3.05	33.44	63.51	1.88	9.65	4.54	4.29	**4439**
Depth 10-20 cm	1	401	1540	33.96	1.20	2.88	31.49	63.51	1.60	13.77	4.99	12.54	**5230**
	2	422	1560	44.82	0.50	4.82	47.07	47.74	1.43	13.40	5.04	4.43	**6992**
	3	429	1070	35.42	1.99	3.03	33.29	62.05	1.60	13.77	4.99	7.45	**3790**
	4	422	1360	35.42	0.30	2.45	31.56	49.89	1.46	7.25	4.48	1.82	**4817**
	5	402	1030	32.98	0.12	2.52	31.63	52.03	1.48	8.34	4.57	5.54	**3397**
	6	412	1490	41.06	2.97	3.03	33.29	63.51	1.60	13.77	4.99	1.92	**6118**
	7	429	1030	30.55	0.81	2.37	31.95	63.61	2.55	6.17	4.39	12.45	**3147**
Depth 20-30 cm	1	401	750	25.61	1.20	3.52	35.60	59.40	1.83	29.15	4.88	30.72	**1921**
	2	422	1470	57.39	0.50	5.72	48.02	44.97	1.30	15.71	5.15	4.22	**8436**
	3	429	980	31.99	1.99	3.25	36.80	57.40	1.83	29.15	4.88	12.65	**3135**
	4	422	1691	31.99	0.30	3.27	35.52	50.44	1.53	11.31	4.51	4.16	**5410**
	5	402	1120	31.99	0.12	3.26	35.50	48.70	1.46	10.21	4.42	0.94	**3583**
	6	412	1490	47.23	2.97	3.28	34.45	62.78	1.72	14.74	4.99	9.46	**7037**
	7	429	960	37.61	0.81	3.29	35.46	58.70	2.50	7.85	4.22	11.14	**3611**

4.5 Preliminary data screening for PCA

Table 4.25 shows the measured edaphic variables namely, altitude, BD, SOMc, AGLB, clay (%), silt (%), sand (%), EC, MC, pH, and gravel and one dependent variable (SOMs). The overall preliminary data screening revealed that several variables were highly correlated. For example, the intersection value between column three of SOMc and the last row of SOMs provides the correlation coefficients between the two forest soil variables (Tables 4.25 and 4.26). In Luanshya, the three-10 cm layers showed that altitude was positively correlated with soil BD (r^2 = 0.32 for 0-10 cm; 0.62 for 10-20 cm; 0.93 for 20-30 cm) and sand (r^2 = 0.54 for 0-10 cm; 0.54 for 10-20 cm; 0.62 for 20-30), but negatively correlated with SOMc, clay, silt and AGLB (Table 4.25). Similar correlations (ρ >0.05) were also observed between the three strata in Bushbuckridge.

Table 4.25 - Pearson correlation matrix of the measured variables for Luanshya

		Altitude	BD	SOMc	AGLB	Clay	Silt	Sand	EC	MC	pH	Gravel	SOMs
Correlation for 0-10 cm	**Altitude**	-	0.32	-0.86	-0.29	-0.60	-0.53	0.54	-0.92	-0.30	-0.96	-0.78	-0.88
	BD	0.32	-	-0.55	-0.99	0.32	0.17	-0.18	0.01	-0.55	-0.34	-0.45	-0.37
	SOMc	-0.86	-0.55	-	0.58	0.61	0.68	-0.68	0.79	0.75	0.95	0.98	0.98
	AGLB	-0.29	-0.99	0.58	-	-0.26	-0.08	0.10	-0.01	0.65	0.34	0.51	0.40
	Clay	-0.60	0.32	0.61	-0.26	-	0.97	-0.97	0.85	0.42	0.72	0.70	0.75
	Silt	-0.53	0.17	0.68	-0.08	0.97	-	-1.00	0.77	0.62	0.71	0.79	0.79
	Sand	0.54	-0.18	-0.68	0.10	-0.97	-1.00	-	-0.78	-0.61	-0.71	-0.78	-0.79
	EC	-0.92	0.01	0.79	-0.01	0.85	0.77	-0.78	-	0.30	0.93	0.77	0.88
	MC	-0.30	-0.55	0.75	0.65	0.42	0.62	-0.61	0.30	-	0.52	0.82	0.69
	pH	-0.96	-0.34	0.95	0.34	0.72	0.71	-0.71	0.93	0.52	-	0.91	0.97
	Gravel	-0.78	-0.45	0.98	0.51	0.70	0.79	-0.78	0.77	0.82	0.91	-	0.98
	SOMs	**-0.88**	**-0.37**	**0.98**	**0.40**	**0.75**	**0.79**	**-0.79**	**0.88**	**0.69**	**0.97**	**0.98**	-
Correlation for 10-20 cm	**Altitude**	-	0.62	-0.10	-0.29	-0.60	-0.53	0.54	-0.92	-0.30	-0.96	-0.74	0.36
	BD	0.62	-	-0.65	-0.90	-0.18	-0.32	0.31	-0.41	-0.79	-0.71	-0.94	-0.09
	SOMc	-0.10	-0.65	-	0.56	0.36	0.59	-0.57	0.14	0.98	0.34	0.71	0.81
	AGLB	-0.29	-0.90	0.56	-	-0.26	-0.08	0.10	-0.01	0.65	0.34	0.71	0.05
	Clay	-0.60	-0.18	0.36	-0.26	-	0.97	-0.97	0.85	0.42	0.72	0.50	0.33
	Silt	-0.53	-0.32	0.59	-0.08	0.97	-	-1.00	0.77	0.62	0.71	0.62	0.52
	Sand	0.54	0.31	-0.57	0.10	-0.97	-1.00	-	-0.78	-0.61	-0.71	-0.61	-0.50
	EC	-0.92	-0.41	0.14	-0.01	0.85	0.77	-0.78	-	0.30	0.94	0.64	-0.15
	MC	-0.30	-0.79	0.98	0.65	0.42	0.62	-0.61	0.30	-	0.52	0.85	0.67
	pH	-0.96	-0.71	0.34	0.34	0.72	0.71	-0.71	0.94	0.52	-	0.86	-0.10
	Gravel	-0.74	-0.94	0.71	0.71	0.50	0.62	-0.61	0.64	0.85	0.86	-	0.21
	SOMs	**0.36**	**-0.09**	**0.81**	**0.05**	**0.33**	**0.52**	**-0.50**	**-0.15**	**0.67**	**-0.10**	**0.21**	-
Correlation for 20-30 cm	**Altitude**	-	0.93	-0.71	-0.29	-0.77	-0.63	0.62	-0.15	-0.74	-0.72	-0.78	-0.66
	BD	0.93	-	-0.57	0.07	-0.92	-0.69	0.70	-0.13	-0.50	-0.52	-0.65	-0.50
	SOMc	-0.71	-0.57	-	0.38	0.59	0.84	-0.81	0.76	0.95	0.98	0.99	1.00
	AGLB	-0.29	0.07	0.38	-	-0.35	-0.19	0.23	-0.04	0.65	0.57	0.37	0.41
	Clay	-0.77	-0.92	0.59	-0.35	-	0.86	-0.88	0.39	0.41	0.47	0.65	0.54
	Silt	-0.63	-0.69	0.84	-0.19	0.86	-	-1.00	0.80	0.63	0.71	0.84	0.81
	Sand	0.62	0.70	-0.81	0.23	-0.88	-1.00	-	-0.78	-0.60	-0.67	-0.82	-0.78
	EC	-0.15	-0.13	0.76	-0.04	0.39	0.80	-0.78	-	0.57	0.65	0.70	0.78
	MC	-0.74	-0.50	0.95	0.65	0.41	0.63	-0.60	0.57	-	0.99	0.95	0.95

Table 4.25 (*continued*)

pH	-0.72	-0.52	0.98	0.57	0.47	0.71	-0.67	0.65	0.99	-	0.97	0.98
Gravel	-0.78	-0.65	0.99	0.37	0.65	0.84	-0.82	0.70	0.95	0.97	-	0.98
SOMs	**-0.66**	**-0.50**	**1.00**	**0.41**	**0.54**	**0.81**	**-0.78**	**0.78**	**0.95**	**0.98**	**0.98**	-

Values in bold indicate significant correlations at the 0.05 level (1-tailed).

Table 4.26 indicates inverse relationships between altitude and SOMc, AGLB, and clay, while BD and sand correlated positively with the topographic altitudes of forest plots, especially at 0-10 cm depth (r^2: 0.65 and 0.11, respectively). Higher SOMs resulted from increased SOMc and were largely discernable in soils with higher proportions of clay and silt. This is recognised by the strong positive correlations for SOMs-SOMc, SOMc-clay and SOMc-silt. On the other hand, high SOMc consistently resulted in low BD thereby reducing the ability of forest soils to accumulate or retain organic matter (Tables 4.25, 4.26). Corresponding to the forest sample plots, the 63 observations from Luanshya and Bushbuckridge were pooled into single datasets (126 observations) of 0-10 cm, 10-20 cm and 20-30 cm soil depth. In order to reduce the dimensionality of data and avoid collinearity between the measured variables, the suitability of the datasets for PCA was tested using Kaiser-Meyer-Olkin (KMO) test for sampling adequacy and Bartlett's test of sphericity. The datasets retained KMO values of 0.68 for layer-1, 0.56 for layer-2 and 0.54 for layer-3. Further, the Bartlett's test suggested that there was a significant difference ($\rho = 0.00$) between the correlation matrices of the measured variables. The test motioned that some measured variables were identical, explaining similar variability within the datasets.

Table 4.26 - Pearson correlation coefficient matrix of the measured variables for Bushbuckridge

		Altitude	BD	SOMc	AGLB	Clay	Silt	Sand	EC	MC	pH	Gravel	SOMs
Correlation for 0-10 cm	**Altitude**	-	0.65	-0.30	-0.10	-0.08	-0.10	0.11	0.45	-0.14	-0.72	-0.54	-0.18
	BD	0.65	-	-0.48	0.35	-0.49	-0.53	0.53	0.64	-0.06	-0.63	-0.13	-0.31
	SOMc	-0.30	-0.48	-	-0.13	0.61	0.90	-0.88	-0.83	0.58	0.58	0.60	0.98
	AGLB	-0.10	0.35	-0.13	-	-0.25	-0.29	0.29	0.16	0.45	-0.06	0.11	-0.06
	Clay	-0.08	-0.49	0.61	-0.25	-	0.83	-0.88	-0.85	-0.09	0.43	-0.03	0.55
	Silt	-0.10	-0.53	0.90	-0.29	0.83	-	-0.99	-0.88	0.32	0.49	0.31	0.86
	Sand	0.11	0.53	-0.88	0.29	-0.88	-0.99	-	0.88	-0.26	-0.53	-0.25	-0.83
	EC	0.45	0.64	-0.83	0.16	-0.85	-0.88	0.88	-	-0.24	-0.75	-0.34	-0.76
	MC	-0.14	-0.06	0.58	0.45	-0.09	0.32	-0.26	-0.24	-	0.31	0.54	0.62
	pH	-0.72	-0.63	0.58	-0.06	0.43	0.49	-0.53	-0.75	0.31	-	0.36	0.48
	Gravel	-0.54	-0.13	0.60	0.11	-0.03	0.31	-0.25	-0.34	0.54	0.36	-	0.63
	SOMs	**-0.18**	**-0.31**	**0.98**	**-0.06**	**0.55**	**0.86**	**-0.83**	**-0.76**	**0.62**	**0.48**	**0.63**	-
Correlation for 10-20 cm	**Altitude**	-	0.50	-0.15	-0.07	-0.19	-0.06	0.09	0.39	-0.54	-0.32	-0.51	-0.14
	BD	0.50	-	-0.67	0.46	-0.86	-0.81	0.82	0.65	-0.77	-0.50	0.35	-0.65
	SOMc	-0.15	-0.67	-	-0.25	0.87	0.86	-0.88	-0.65	0.52	0.66	-0.25	1.00
	AGLB	-0.07	0.46	-0.25	-	-0.43	-0.48	0.49	0.03	-0.29	-0.40	0.28	-0.24
	Clay	-0.19	-0.86	0.87	-0.43	-	0.97	-0.99	-0.73	0.58	0.48	-0.44	0.85
	Silt	-0.06	-0.81	0.86	-0.48	0.97	-	-0.99	-0.63	0.53	0.50	-0.48	0.85
	Sand	0.09	0.82	-0.88	0.49	-0.99	-0.99	-	0.67	-0.53	-0.52	0.47	-0.87
	EC	0.39	0.65	-0.65	0.03	-0.73	-0.63	0.67	-	-0.35	-0.07	0.27	-0.64
	MC	-0.54	-0.77	0.52	-0.29	0.58	0.53	-0.53	-0.35	-	0.69	-0.12	0.50
	pH	-0.32	-0.50	0.66	-0.40	0.48	0.50	-0.52	-0.07	0.69	-	0.09	0.65
	Gravel	-0.51	0.35	-0.25	0.28	-0.44	-0.48	0.47	0.27	-0.12	0.09	-	-0.24
	SOMs	**-0.14**	**-0.65**	**1.00**	**-0.24**	**0.85**	**0.85**	**-0.87**	**-0.64**	**0.50**	**0.65**	**-0.24**	-
Correlation for 20-30 cm	**Altitude**	-	-1.00	-0.19	-0.07	-0.13	-0.08	0.04	0.31	-0.92	-0.32	-0.70	0.15
	BD	-1.00	-	-0.22	0.07	0.09	0.05	-0.01	-0.29	0.92	0.32	0.74	-0.18
	SOMc	0.19	-0.22	-	-0.44	0.86	0.94	-0.93	-0.54	-0.22	0.58	-0.51	1.00
	AGLB	-0.07	0.07	-0.44	-	-0.40	-0.48	0.50	0.35	-0.09	-0.37	0.21	-0.44
	Clay	-0.13	0.09	0.86	-0.40	-	0.95	-0.96	-0.58	0.17	0.50	-0.40	0.87
	Silt	-0.08	0.05	0.94	-0.48	0.95	-	-0.99	-0.53	0.06	0.55	-0.35	0.95
	Sand	0.04	-0.01	-0.93	0.50	-0.96	-0.99	-	0.57	-0.07	-0.56	0.40	-0.94
	EC	0.31	-0.29	-0.54	0.35	-0.58	-0.53	0.57	-	-0.32	-0.73	0.11	-0.56
	MC	-0.92	0.92	-0.22	-0.09	0.17	0.06	-0.07	-0.32	-	0.31	0.60	-0.18
	pH	-0.32	0.32	0.58	-0.37	0.50	0.55	-0.56	-0.73	0.31	-	0.09	0.60
	Gravel	-0.70	0.74	-0.51	0.21	-0.40	-0.35	0.40	0.11	0.60	0.09	-	-0.49
	SOMs	**0.15**	**-0.18**	**1.00**	**-0.44**	**0.87**	**0.95**	**-0.94**	**-0.56**	**-0.18**	**0.60**	**-0.49**	-

Values in bold indicate significant correlations at the 0.05 level (1-tailed).

4.5.1 Determining the number of eigenvector components

The optimal number of components characterised by the highest cumulative proportion of variance were determined by the eigenvalue (estimated by squaring the variance) analysis method. The eigenvalue decomposition curves show the elbow or point of marked change in variance explained by individual components (Figure 4.40). Based on the eigenvalue cut-off rule of "1", the complexity associated with the 11 measured variables was considerably reduced by discriminating components (principal components) explaining the highest variability from redundant or unimportant components. The extracted principal components (PC) were used to fit multiple linear principal component regression (MLPCR) and predict

SOM stock, while redundant components were disregarded from the analysis. For layer-1 and layer-2, two PC were determined (Figures 4.40 a, b), whereas four PC were extracted for layer-3 (Figure 4.40 c). In layer-1, the two optimal components accounted for 80% of the total variance. The extracted solution for layer-2 (PC1 and PC2) explained 81% of the cumulative variance, while the four important components in layer-3 (PC1, PC2, PC3 and PC4) had an overall proportion variance of 93% (Table 4.27).

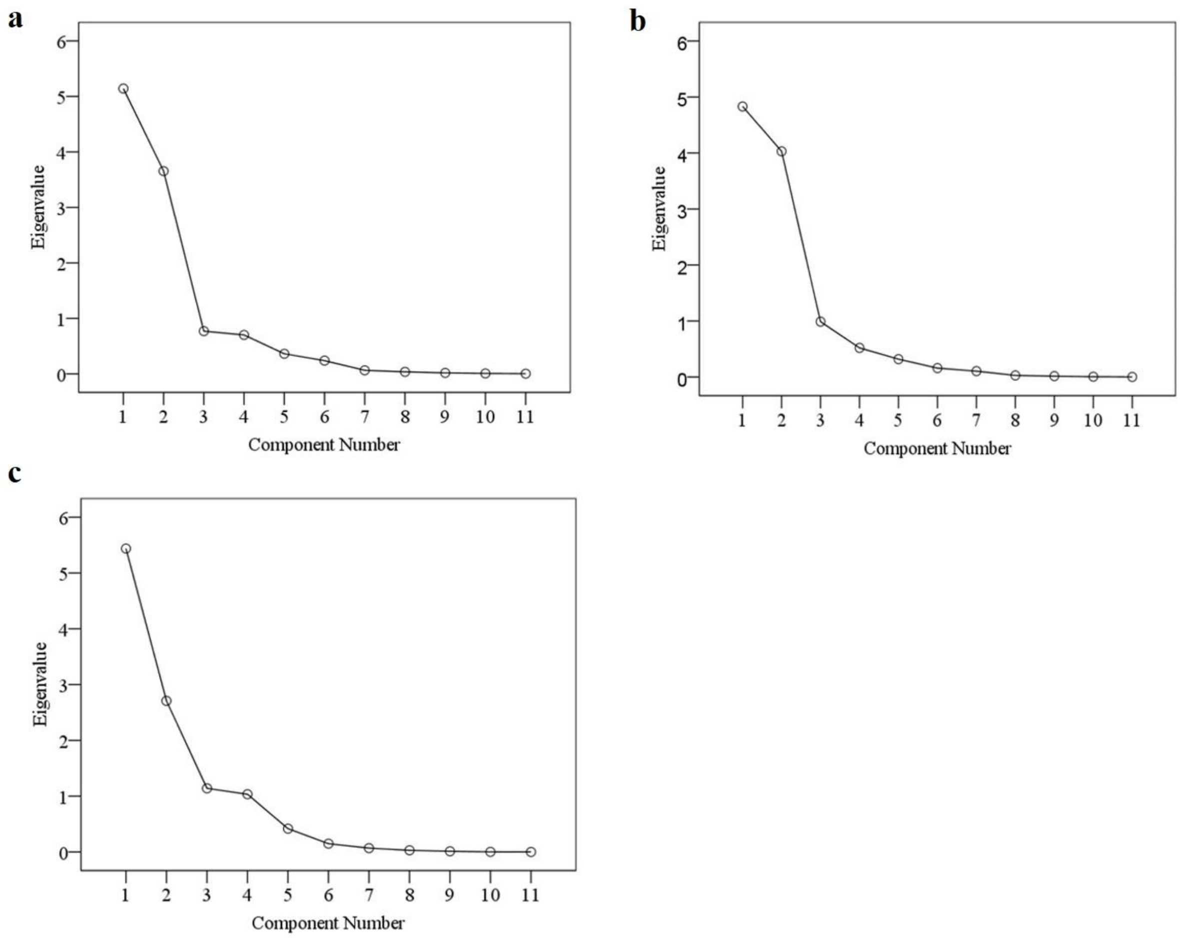

Figure 4.40: Eigenvalues decomposition curves for (a) layer-1, (b) layer-2 and (c) layer-3. The curves show the decline in the importance of the 11 components. Unlike principal components (eigenvalue > 1), components with eigenvalues of less than 1 ($variance^2$) explained the smallest and unimportant variation in the datasets.

4.5.2 Principal component analysis and regression of forest soils

Table 4.27 presents detailed rotated loadings or weightings of the measured variables in each of the extracted principal components. Most notably, the loadings of clay and silt closely compared across the three layers, while sand represented contrasting or opposite loadings. In layer-1, altitude, SOMc, AGLB, EC, MC and gravel had the largest positive loadings in PC1, whereas clay, silt and sand had the largest mixed or absolute loadings in PC2. Further, AGLB was observed to have large positive weightings in both PC1 and PC2 of 0-10 cm and 10-20 cm soil depth, but changed to negative loadings at 20-30 cm depth.

Table 4.27 - Rotated component matrix loadings

	0-10 cm depth		10-20 cm depth		20-30 cm depth			
	PC1	**PC2**	**PC1**	**PC2**	**PC1**	**PC2**	**PC3**	**PC4**
Altitude	**0.37**	0.22	**0.41**		**-0.36**	-0.22	-0.26	0.257
BD	-2.83		**-0.33**	0.19	-0.14		0.78	**0.377**
SOMc	**0.38**	-0.22		-0.45	**0.36**	0.25	-0.19	0.123
AGLB	**0.38**	0.22	**0.42**		**-0.38**	0.19	-0.22	0.156
Clay		**-0.45**		**-0.44**	**0.32**	0.29		**0.305**
Silt		**-0.51**	-0.20	**-0.44**	**0.38**	0.27		
Sand		**0.51**	0.21	**0.43**	**-0.39**	-0.23		
EC	**0.40**	0.12	0.42		**-0.36**	0.24	-0.25	0.2
MC	**0.38**		**0.36**	-0.24	-0.12	**0.43**	**0.41**	**-0.413**
pH	0.29	0.25	0.18	-0.31		**0.49**		**0.304**
Gravel	**0.32**	-0.24	**0.33**	-0.16	-0.18	**0.40**		**-0.596**
Eigenvalues	**27**	**13**	**23**	**16**	**29**	**7**	**1**	**1**
% of variance	**47**	**33**	**44**	**37**	**49**	**25**	**10**	**9**
Cumulative (%)	**80**		**81**		**93**			

Where the largest loadings are represented in bold values. The empty cells indicate absolute loadings of less than 10.

The PCA ordination diagrams or biplots illustrate the vectors (magnitudes and directions) of the 11 measured variables with respect to the extracted principal components (Figure 4.41). Negatively correlated variables were defined by obtuse angles, while acute angles corresponded to positively correlated variables with similar ordination and component loadings. The graphs indicate that the cosine angles (acute) between SOMc and clay, and silt decreased with soil depth. This agrees with correlation matrices which suggest that the proportion of smaller sized particles (<63 µm) was greater in underlying layers and that this proportionality resulted in increased concentration of organic matter. By contrast, SOMc was consistently opposed by BD and sand (obtuse angle) across the three soil layers. Figure 4.41a indicates that the highest SOMs recorded in observation-21 combined highest attributes of SOMc and gravel, and lowest values of BD (1140 g kg^{-1}). Observation-42 had reverse trait profiles to observation-21, characterised by the lowest SOMc and gravel, and highest scores of BD (1410 g kg^{-1}).

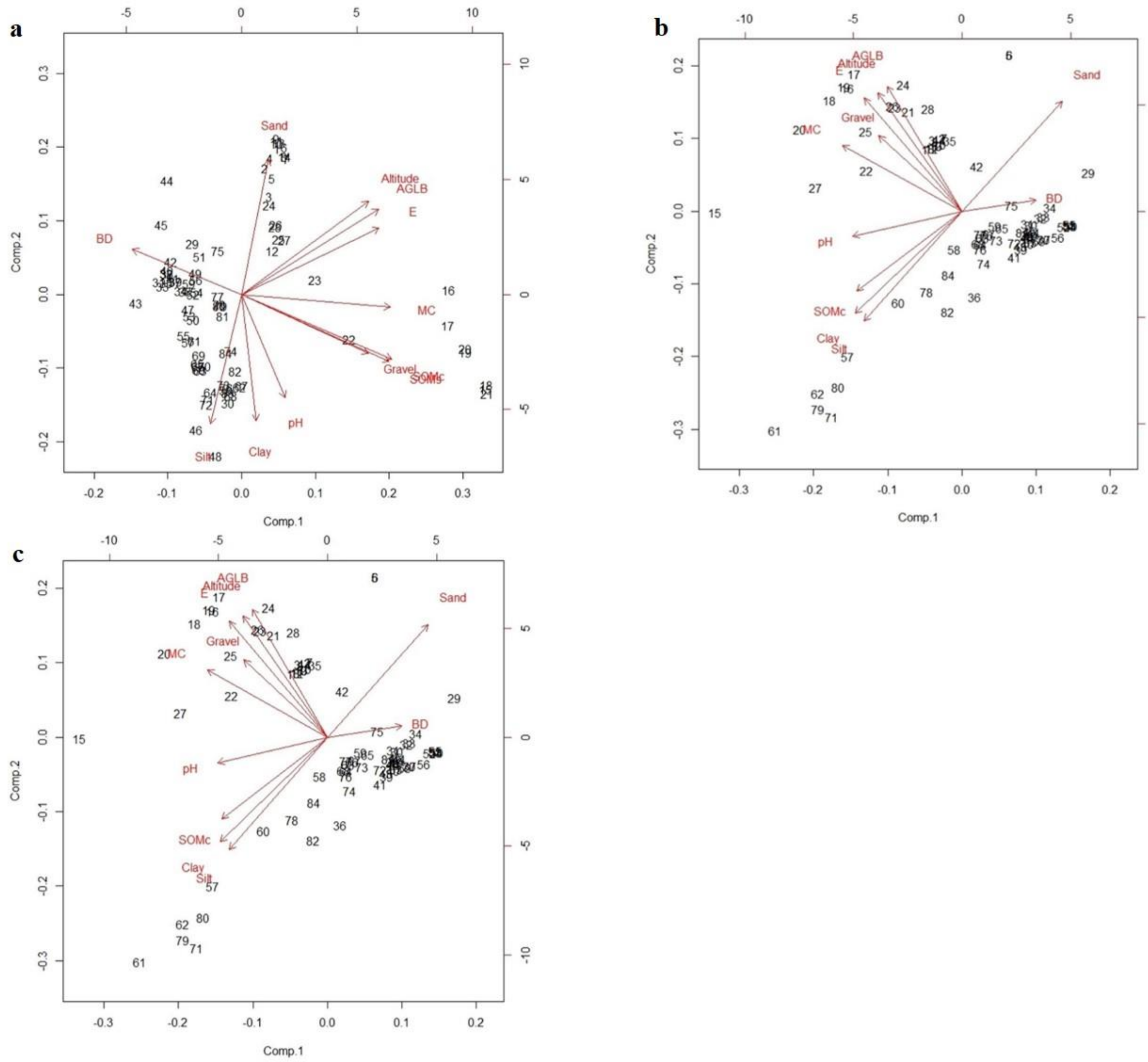

Figure 4.41: The PCA ordination diagram of the measured variables in PC1-PC4 for (a) 0-10 cm, (b) 10-20 cm and (c) 20-30 cm soil depth. The vectors of the arrows represent the magnitude and directions of the variables with respect to the principal components. The numbers within the biplots indicate different observations for each of the 11 measured variables.

In reference to the displayed principal components (PC1 and PC2) for 10-20 cm soil depth (Figure 4.41b), the 11 variables maybe discriminated into two groups. The first group of silt, clay and SOMc was characterised by negative ordination in PC1 and PC2. Secondly, BD and sand defined the second group with positive ordination in both PC1 and PC2. Closely associated ordination and loadings between SOMc, clay and silt were also observed in PC1, PC2, PC3 and PC4 of layer-3 (Figure 4.41c). In agreement with the correlation matrices and the decrease in the coefficients of determination with depth, the cosine angle between AGLB and SOMc changed with depth from acute (upper layer) to obtuse angles (underlying layer). Based on the PC (dependent variables) and SOMs (dependent variable), the datasets were fitted using multiple linear principal component regression (MLPCR) (Figure 4.42). The resulting MLPR models was associated with correlation coefficients (r^2) of 0.91 for layer-1, 0.70 for layer-2 and 0.95 for layer-3, which were statistically significant ($\rho = 0.00$).

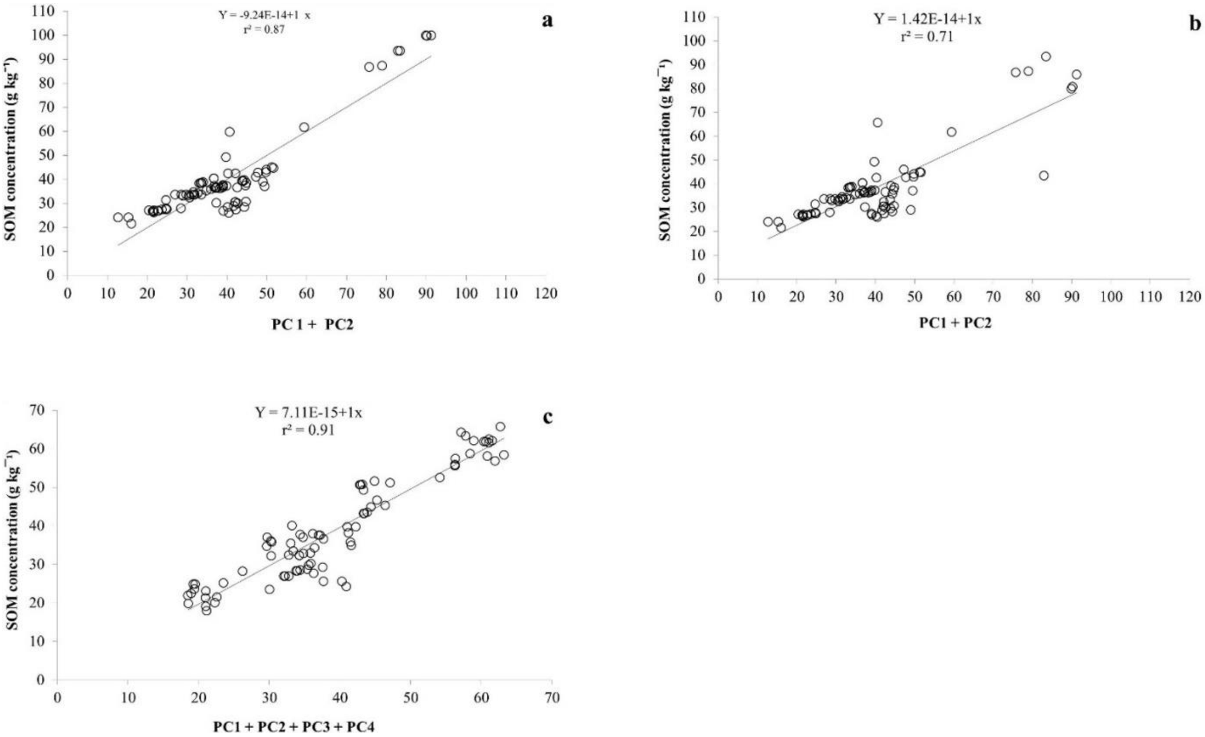

Figure 4.42: Fitted principal component regression (PCR) for layer-1, layer-2 and layer-3. The graphs show that variations in SOM content was explained by different principal components (PC's), with correlation coefficients of 87%, 71% and 91% for (a) 0-10 cm, (b) 10-20 cm and (c) 20-30 cm soil depth, respectively.

4.5.3 Leave-one-out cross validation

Leave-one-out cross validation method was used to evaluate the average prediction error of the MLPCR models. The technique involved running 126 iterations while holding-out a different row of observations for each of the trainings. Residuals were estimated from the standard error (SE) of the fitted MLPCR model less the SE of the left-out observations. Table 4.28 presents the root mean square error (RMSE) associated with the three MLPCR models for 0-10 cm, 10-20 cm and 20-30 cm depth. The model for 20-30 had an average RMSE of 0.49 g kg^{-1}, while layer-1 and layer-2 had relatively higher values of 0.68 g kg^{-1} and 0.53 g kg^{-1}, respectively. Given the lower variability in the concentration of organics especially in 20-30 cm soil depth, the combined PCA and MLPCR method predicted forest SOMs with acceptable level of accuracy.

Table 4.28 - Multiple linear principal component regression: Accuracy assessment of PCA

MLPCR Model	Number of iterations	Correlation coefficients	Standard error of estimate	Significance at 0.05	RMSE
0-10 cm	126	0.87	7.19	0.000	0.68
10-20 cm	126	0.71	5.88	0.001	0.53
20-30 cm	126	0.91	5.13	0.000	0.49

Where RMSE (g kg^{-1}) is root mean square error associated with the prediction SOM concentration from PC.

CHAPTER 5 - DISCUSSION

5.1 Estimates of LULC changes

The spatial extents of the adjoining woodlands of Luanshya, Zambia, and Bushbuckridge, South Africa, have been dynamic over the last two to three decades in response to LULC changes and climatic variability. Different forest management practices and conservation models such as assisted forest restoration are continuously being initiated to reduce deforestation and forest degradation (Robinson *et al*., 2013; Syampungani *et al*., 2014; Goetz *et al*., 2015). Based on the assessment of the spatial-temporal changes in forest cover, and aboveground and belowground carbon stocks, the discussion herein informs a methodological approach for evaluating long term changes in carbon storage from an integrated approach that combined remotely sensed imagery and *in situ* measurements. Within woodlands of similar structure, the study also provides counterfactual scenarios for monitoring, evaluating and reporting forest changes consistent with REDD+.

Although some studies have explored the environmental, social and economic factors driving LULC changes, particularly deforestation of woodlands (Chidumayo, 1993; Dovie *et al*., 2002; Thomas and Pacham, 2007; Strömquist and Backéus, 2009; Syampungani *et al*., 2009; Cabral *et al*., 2010; Jew *et al*., 2017), there are fewer studies that have applied remote sensing and landscape metrics methods to quantify the dynamics of forest changes (Prins and Kikula, 1996; Mayes *et al*., 2015; Schneibel *et al*., 2016, 2017; Lobora *et al*., 2017; Mapfumo *et al*., 2017). These previous studies have mainly focused on comparison between two or three time periods, not a longitudinal analysis of the duration examined in this study. The latter approach shows that there are complex net and gross changes in different LULC types within the study area and over the five time periods examined (1986–1998, 1998–2001, 2001–2004, 2004–2011, 2011–2016 in Luanshya; Figure 4.1, and 1992-1998, 1998-2001, 2001-2006, 2006-2010, 2010-2016 in Bushbuckridge; Figure 4.8).

5.1.1 LULC maps: Estimates of multi-temporal changes in Luanshya

The simplified figure of the LULC composition demonstrate that the landscape of Luanshya is a mosaic of different LULC classes that are in continuous change (Figure 5.1). The main LULC changes that occurred from the initial state (1986) to the final state (2016) were directly related to the declining total area of forest cover from 32,117 ha to 16,699 ha. This is portrayed in the detailed LULC maps (Figure 4.1), which showed changes from continuous forest cover to highly fragmented forested areas. Intermediate LULC maps (1998, 2001, 2004 and 2010) showed that changes in woodland cover were inconsistent and significantly asymmetrical from one time period to the next. This was attributed to different rates of deforestation and regeneration. In some scattered areas, increased forest clearance induced further conversions of forests to other LULC types such as agricultural fields, paved areas and built-up areas, which resulted in notable decrease in the total area of forest cover (1986-1998: 32,117 ha to 9315 ha; 2001-2004: 22,800 ha to 14,745 ha in 2004; 2011-2016: 25,735 ha to 16,699 ha) (Tables 4.2, 4.4). For the periods 1998-2001 and 2004-2011, the total area of forest cover increased through stochastic natural regeneration, from 9315-22,800 ha and 14,745-25,735 ha, respectively. This result is consistent with Flamenco-Sandoval *et al*. (2007) who noted that adding intermediate time periods to LULC analysis often results in contrasting scenarios, but provides more precise information of change dynamics.

In contrast to spatially-limited studies that have studied the resilience of woodlands to withstand forest disturbance (Stromgaard, 1985; Chidumayo, 1993; McNicol *et al*., 2015), this study established an average deforestation rate of 3.39 yr^{-1} over the time periods examined, which was higher than the rate or forest regeneration (1.21% yr^{-1}; Table 4.5). This implies that natural regeneration does not mirror the rate of woodland exploitation. This is in agreement with Luoga *et al*. (2002) who found that wood harvesting of 6.4 m^3 ha^{-1} yr^{-1} from natural forests in eastern Tanzania exceeded regeneration rates of 4.4 m^3 ha^{-1} yr^{-1}.

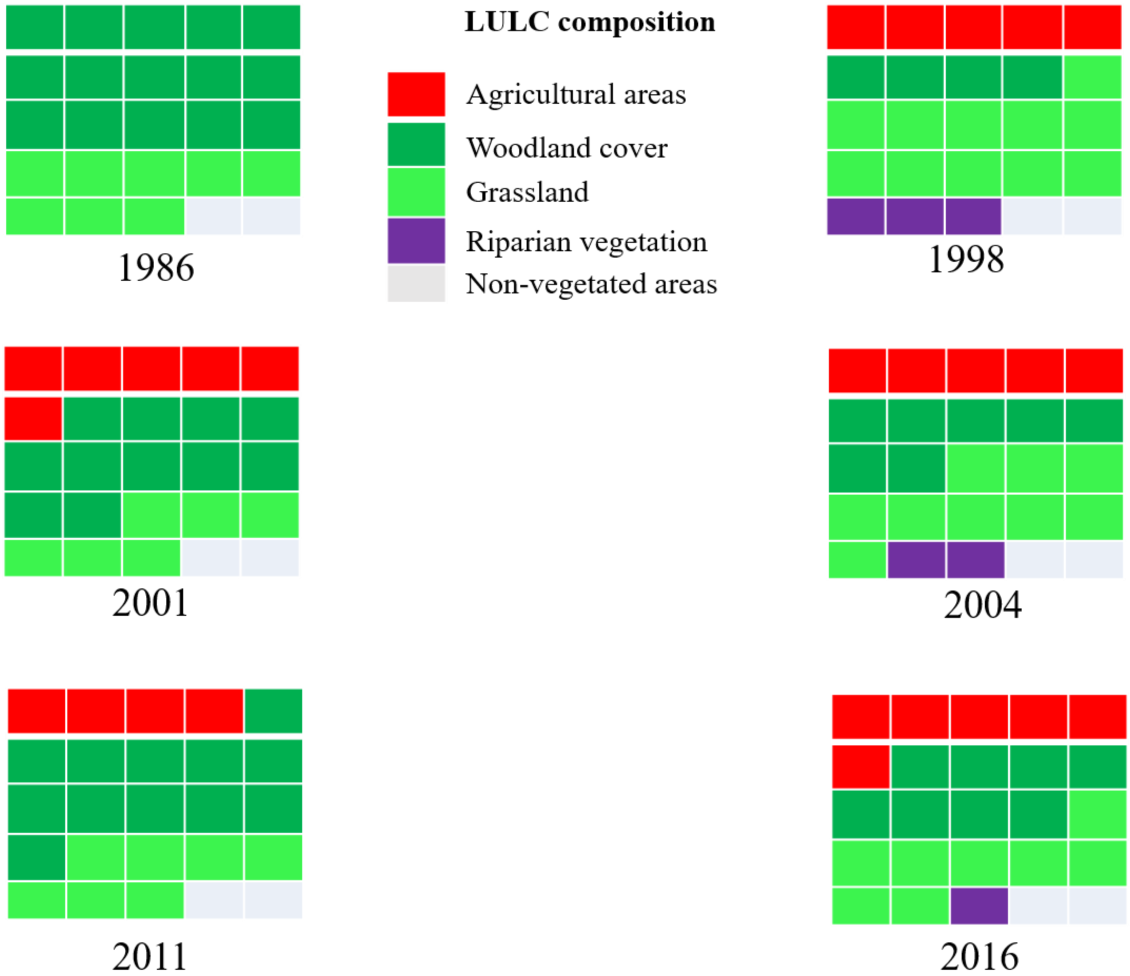

Figure 5.1: Simplified LULC composition for Luanshya. Each cell represent 4% (rounded to the nearest whole number) of the total study area (54,232 ha).

In detail, there was a spatial covariation between Miombo woodland and grassland, in which woodland disturbance by deforestation resulted in the development of grassland, which was often followed by regeneration of secondary woodlands on grassland and/or abandoned agricultural areas. A covariance in the spatial extent of the two vegetation types can been seen in Figures 4.2, 4.3, where the total area of forest cover (grassland) for the periods 1986, 1998, 2001, 2004, 2011 and 2016 were 32,117 ha (16,893 ha), 9315 ha (23,349 ha), 22,800 ha (12,352 ha), 14,745 ha (20,918 ha), 25,735 ha (15,744 ha), and 16,699 ha (17,210 ha), respectively. Extensive deforestation in the period 1986–1998 was closely associated with the introduction and increase in agricultural areas (from 0 to 10,430 ha; Table 4.2). Agricultural activities can also be seen in the 2001 LULC map by an increase in the fragmented rectilinear landscapes with regular boundaries (Figures 4.1 and 4.2). These findings compares closely with several other studies that report that nearly <80% of the net increase in agricultural areas between 1980 and 2000 in the tropics came from previously intact or disturbed forested areas (Dewan and Yamaguchi, 2009; Gibbs *et al*., 2010; Pielke *et al*., 2011). This demonstrates a pattern where fragmented wooded areas are considered as readily available land for other LULC types (Chidumayo, 1993; Ward, 2005; Wigley *et al*., 2009). However, in the period 2001-2004, some agricultural fields were abandoned as shown by the decrease in extent (from 13,562 ha to 10,041 ha; Table 4.2) of the fragmented rectilinear landscapes. A similar trend was also observed from 2004-2011, where 30.28% and 5.64% of agricultural fields changed to grassland and Miombo woodland, respectively.

Existing literature reveals that prior to 1998, the economy of Luanshya hinged on the mining industry (Craig, 2001; Lungu, 2008; Mususa, 2010). The mining firms provided employment, medical aid, education incentives, recreational and municipal facilities such as electricity, water and sewerage services to its employees and their registered dependents. However, the mining sector became increasingly uneconomical which resulted in the loss of over 696 jobs in Luanshya (Craig, 2000, 2001; Lungu, 2008; Mususa, 2010). The majority of households rented out their houses and left to establish new settlements and farming fields in the adjoining Miombo woodlands (Chidumayo, 1997; Mususa, 2010). Efforts were initiated to revive the mines through privatisation and other operational strategies, but with less success. During the periods of envisaged employment and economic growth, some agricultural lands were abandoned thereby providing an opportunity for forest recovery or forest secondary succession.

Recent studies also indicate that pressure on Miombo woodlands will continue to exacerbate because of population increase which has not been commensurate with the economic growth of most developing countries (Dewees *et al*., 2010; Pielke *et al*., 2011). As a result of the imbalance between deforestation and regeneration, Miombo woodlands are in significant decline (Syampungani *et al*., 2009) with possible decrease in their capacity to provide ecosystems services. The difference between the total area of woodland and the land that remained unchanged between successive time periods (Tables 3.2, 3.3) indicates the dominance of second-growth forests. Even though woodland regeneration mainly results from grassland conversion (Figures 4.4, 4.5), the ability of forest regrowth may be circumscribed by grassland conversion to agricultural fields and other non-vegetated LULC types (McNicol *et al*., 2015). Further, because successful natural regeneration is largely determined by the extent of soil degradation concomitant with deforestation (Aide *et al*., 2000; Chazdon, 2008), secondary forests recovering in human-altered landscapes have failed to match the areal extent of natural forests observed in 1986 (Figure 4.1). Similar to studies by Hirota *et al*. (2011) and Poorter *et al*. (2016), this may suggest that once a certain threshold of deforestation and/or land degradation has been reached, Miombo woodlands may collapse or change to an alternative stable state, secondary forests. Opportunities to increase forest cover and aboveground carbon stocks in the area through forest restoration and reforestation initiatives are highlighted by the LULC change dynamics for 1998–2001 (Figures 4.4, 4.5, 4.6) and the proportion of SF succession (Figure 4.7), which showed that over 68% of forested areas are second-growth Miombo woodlands.

5.1.2 LULC maps: Estimates of multi-temporal changes in Bushbuckridge

The land cover structure of Bushbuckridge was classified into six different LULC types, namely, agricultural areas, bare land, woodlands, grassland, paved areas and waters bodies (Figures 4.8, 5.2). During the observed periods, there were some similarities in LULC dynamics with that of Luanshya, the most notable being increases in the total area of paved areas from 284 ha in 1992 to 416 ha in 2016, and spatial covariations between woodlands and grasslands. This was evident in the LULC maps for 1992, 1998, 2001, 2006, 2010 and 2016, where woodlands (grasslands) covered about 19%(68%), 8%(59%), 55%(18%), 36%(15%), 54%(89%) and 49%(12%) of the study area (Tables 3.5, 3.6). Being a remote area with little formal employment, the communities depend on woodlands to provide resources such as wild fruits, edible vegetables and insects (e.g. crickets and grasshoppers), medicinal plants, woodlots and palatable understorey forage for livestock (Dovie *et al*., 2002). Raising of domestic livestock provides an addition source of household nutritional requirements while contributing to social-economic growth. This was demonstrated by the extensive use of timber poles for construction and maintenance of kraals and livestock fencing (Figure 4.28).

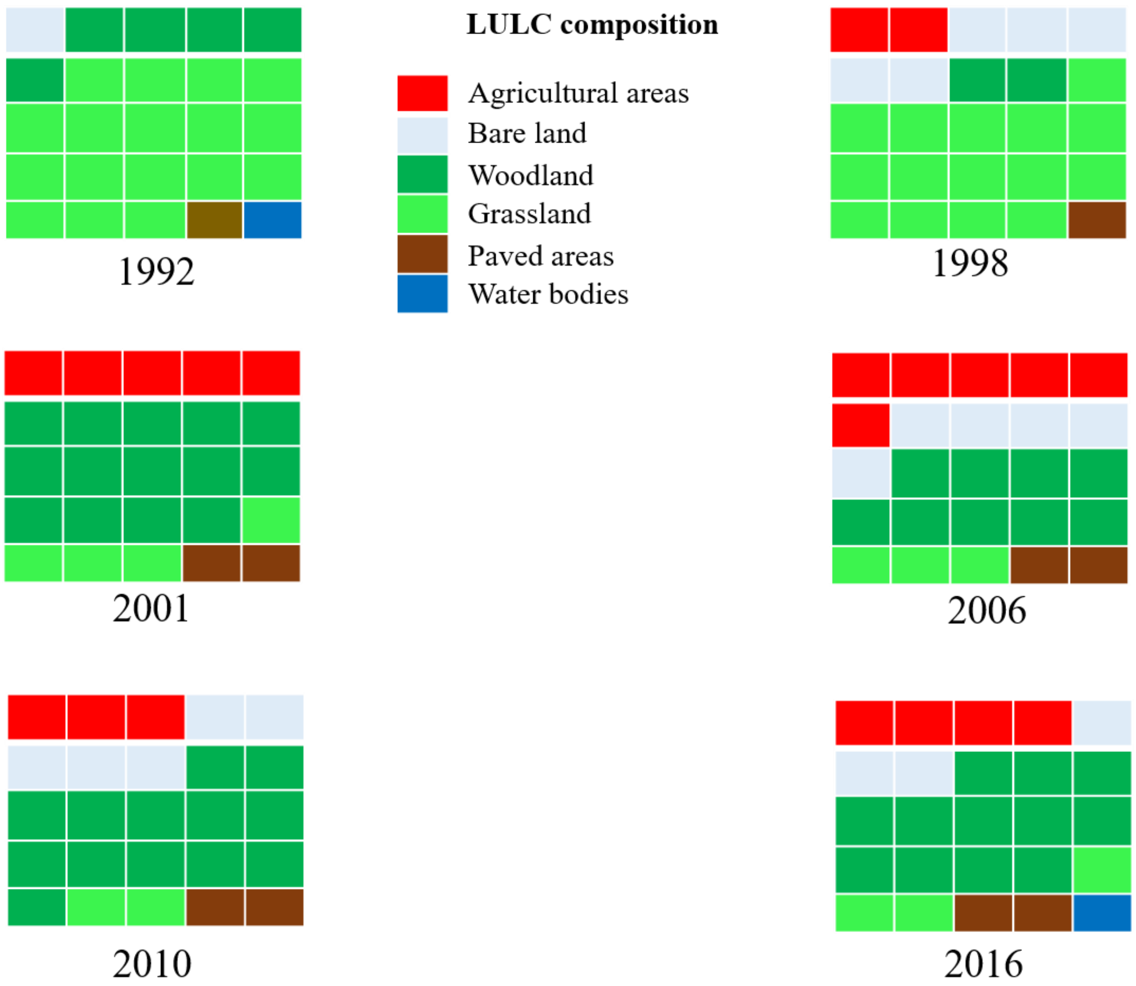

Figure 5.2: Simplified LULC composition for Bushbuckridge. Each cell represent 4% (rounded to the nearest whole number) of the total study area (6194 ha).

Field evidence (i.e., observations and informal interviews) revealed that forest harvest scheduling was initiated in the area in order to minimise the declining woodland cover that was observed, changing from approximately 20% (1992) to 8% (1998) of the total study area (Figure 5.2). During the harvest months, households gathered and stocked enough woodlots to see them through a three-year period of harvest restrictions (Figure 4.28). On the flip side, the periods of harvest restrictions allowed increased coppicing and forest regeneration, and a shift in vegetation regime from grasslands to woodlands (Scholes and Archer, 1997; Brudvig and Asbjornsen, 2009). This may partly explain the observed increase in regeneration and forest succession from 1998 to 2001 (Figure 5.2), which also demonstrates the high regenerative capacity of the forests in the Lowveld of Bushbuckridge. The other important transitional pathways occurred between grasslands and agricultural areas. However, regeneration or woody encroachment in both grasslands and agricultural areas were relatively lower than Luanshya. This supports earlier studies by Banda *et al*. (2006) and Wigley *et al*. (2009) that reported that forest regrowth tend to be slowest in woodlands that are close to communal areas, as both old trees and young trees are continuously disturbed by human activities and the grazing livestocks.

The commonalities in LULC change between the two study areas, particularly changeovers between woodlands, grasslands and agricultural fields indicated that grassland acted as a LULC type transitional to other types (Figures 4.11, 4.12 and 4.13). In Tanzania, similar changes in the community areas bordering Katavi National Park were observed, where forest cover was firstly converted into grassland before being converted to crop fields and other non-vegetated land (Kanowski *et al*., 2011). Conversely, existing literature also recognises fire as another key factor that regulate forest regeneration in savanna (Desanker and Prentice., 1994; Wigley *et al*., 2009; Saito *et al*., 2014). Even though this component was not within the scope of the present study, it was discerned from the three villages of Bushbuckridge that the communities use grazing as strategy to minimise intense forest fires.

Given the extensiveness of tropical dry forests in southern Africa (Campbell, 1996; Syampungani *et al*., 2009), the observed imbalance between deforestation and forest regrowth potentially has significant consequences for the extent to which secondary woodlands provide ecosystem services (Poorter *et al*., 2016; Ryan *et al*., 2016; Sonter *et al*., 2017; Syampungani *et al*., 2017). It also means that transitional periods between clearance of old growth woodland and switch to secondary woodland entails net CO_2 emissions (Foley *et al*., 2005; Pielke *et al*., 2011), as well as changes in forest composition and structure (Williams *et al*., 2008; Chidumayo, 2013; Kuyah *et al*., 2014; Shirima *et al*., 2015b). Chidumayo (1993) noted that unlike newly established seedlings, samplings of secondary succession woodlands already have well-established root systems which favour quick ecosystem recovery. Thus, highly productive natural forest ecosystems could play an important role in restoring natural environmental services and advancing carbon based payments for ecosystem services. An outcome is that reforestation models as well as monitoring, reporting and validation of changes in forest cover should clearly distinguish between different changes of forest succession (e.g. natural processes from assisted natural regeneration and forest succession) (Chidumayo, 1993; Chazdon, 2008).

5.2 Effects of LULC changes on species composition and forest structure

The floristic composition varied significantly across forest plots of different developmental stages. The SF plots (Site-7) with the highest tree density of 3844 trees ha^{-1} had species diversity index of 0.64, which was lower than the index for the UDF (0.95) and PDF (0.84-0.89) sites (Table 4.7). *Brachystegia boehmii*, *Combretum imberbe, Julbernardia paniculata* and *Ochna pulcra* were the most frequently occurring species in regrowth sites in Luanshya. These species represented 57% (Site-3), 48% (Site-5), 47% (Site-6) and 76% (Site-7) of the total number of individual trees per plot, respectively (Figure 4.17). This is in contrast to the UDF plots, where the four most occurring species of *Diospyros batocana*, *Brachystegia speciformis*, *Parinari curatellifolia*, and *Pseudolachynostylis maprouneifolia* cumulatively accounted for only 36% of the total trees. Similar to studies by Williams *et al*. (2008) and Kalaba *et al*. (2013), it was evident that forest disturbance alters the floristic composition from a more evenly occurrence of species to the dominance of a single or few tree species.

The dominant species in sites of forest regrowth indicated tree types that are more resilient to disturbance, and from a forest conservation perspective, these species could be used to identify secondary growth Miombo woodlands. In Bushbuckridge, the average species evenness or how evenly the individual trees are distributed over the different species, was 3.6% lower than that of Luanshya (Table 4.8). *Dichrostachys cinerea*, *Ziziphus mucronata*, *Acacia mellifera*, *Combretum collinum*, and *C. kraussii* were the most dominant species with an average of more than 20 individual trees per plot (Table 4.8). The floristic composition of the adjoining woodlands of Bushbuckridge is similar to the observed species composition of the forested areas in Luanshya, where second growth stands had lower species diversity than the less disturbed sites. This pattern agrees with studies by Jew *et al*. (2017) and Shrima *et al*. (2011), that tree recruitment in previously disturbed areas is often characterised by a decrease species diversity and evenness.

Enumerating species richness, evenness and diversity was important in understanding the dominal effects of forest disturbance on species composition and forest structure (Hirota *et al.*, 2011; Poorter *et al.*, 2016). For instance, the higher species diversity in the UDF site was associated with lower tree density of bigger trees. The results also indicated that dense canopies (e.g. UDF plots) do not favour natural regeneration and tree recruitment (Figure 4.16). Chidumayo and Frost (1996), and Kalaba *et al*. (2013) attributed this type of distribution to the suppressive effects of dense canopy on saplings and young trees. The observed sparse stumps and higher tree density in the PDF sites showed that when the forest canopy becomes less dense due to selective tree felling, enhanced regeneration is followed as enough sunlight reaches the herbaceous layer and the forest floor (Chidumayo, 1993; Kalaba *et al*., 2013). This was also shown in Bushbuckridge, where the secondary woodlands had higher tree density of smaller sized trees (mean DBH: 3.77 ± 1.32 cm; height: 4.13 ± 0.18 m)

(Table 4.10). The observation compared well with the field investigations which revealed that bigger sized tree boles are highly demanded, especially for the construction and maintenance of enclosures for livestock and fencing of agricultural fields (Figure 4.28). Within each boxplot depicting the distribution of stem diameters and heights (Figure 4.20), the observed outliers were consistent with the occurrence of large Marula trees (*Sclerocarya birrea*) that are often conserved to provide edible, saleable fruits and other ecological importance (Dovie *et al*., 2007; Kuyah 2014; Mograbi *et al.*, 2015).

Overall, forest disturbance resulting from the harvesting of woodlots in both study sites suggested that selective tree felling, particularly in less disturbed forested areas, act as a 'forest thinning' mechanism. The immediate effects include, decrease in species diversity, increased regeneration and tree density, and development of smaller trees (Figure 4.16, Tables 3.9, 3.10). The distribution of stem diameters and tree heights in second growth forest sites indicated that in the absence of disturbance on saplings and young trees, regeneration often results in forest succession, but with comparatively different tree size class distribution and forest structure than the older trees they replaced (Chazdon, 2008; Hirota *et al.*, 2011; Banks-Leite *et al.*, 2014). According to Chidumayo (1993), tree density increases to about five-times higher in regrowth forests sites than old growth. This is echoed by Williams *et al*. (2008), Mograbi *et al*. (2015) and Pelletier *et al*. (2017) who observed an increase in regenerations and stocking density following intermediate levels of forest disturbance. Consequently, large or increased AGLB per plot (30 x 30 m) was attributed to two key forest characteristics, size of individual trees and/or tree density. In Luanshya, UDF site held large AGLB (76.18 ± 49.45 t ha^{-1}) because the lower tree densities allowed development of bigger individual trees (Figures 4.16, 4.19). The higher mean biomass in the PDF sites (ranged from 68.76 t ha^{-1} to 76.81 t ha^{-1}) and SF stands (72.18 ± 5.05 t ha^{-1}) was due to increased tree density of smaller trees. By contrast, forest stands in Bushbuckridge had relatively lower biomass than Luanshya despite the higher tree density. Therefore, forest disturbance, does not only decrease the overall spatial extent of forest cover, but also reduces forest biomass (Picard *et al.*, 2012). This emphasises the need to devise site specific conservation models that optimises total biomass from the lowest number of trees while sustainably harvesting woodlots through the 'forest thinning' mechanism. This would ensure that forests continue to offer provisioning ecosystem services (e.g. timber and non-forest timber products) without impairing their capacity to provide regulating services (e.g. carbon sequestration and storage).

5.2.1 Regression model relating AGLB and EVI

Estimates of AGLB were significantly variable across the different individual forest sample plots (expressed as tonnes per 30 x 30 m plot). These estimations also differed depending on the allometric equation used. In Luanshya, biomass estimates based on the equation by Nickless *et al*. (2011) was 0.97 t plot^{-1} higher than Chidumayo (1991), and 1.97 t plot^{-1} higher than estimates based on Stromgaard (1985) equation (Table 4.11). In Bushbuckridge, the difference in biomass averaged 0.09 t plot^{-1} between estimates using Stromgaard (1985) and Nickless *et al*. (2011) equation, and 0.15 t plot^{-1} between Nickless *et al*. (2011) and Chidumayo (1991) (Table 4.12). The obvious explanation for the differences is mainly because the allometric equation by Stromgaard (1985) was developed from a combination of two predictor variables, DBH and tree height, while Chidumayo (1991) and Nickless *et al*. (2011) only used DBH. The other reason may be attributed to the different predictive power and how well each model was validated. In order to avoid significant underestimation or overestimation of AGLB in the two study sites, mean estimates ranging from 0.01-8.94 t plot^{-1} in Luanshya, and 0.00-4.06 t plot $^{-1}$ in Bushbuckridge were calculated from the three allometric models (Tables 3.13, 3.14). The principle of tree allometry was illustrated in Figures 4.22, 4.23, where individual tree biomass strongly correlated with stem diameters (r^2: 0.94) than tree heights (r^2: 0.62). These relationships indicate that net primary productivity increases more exponentially with tree cross-sectional area or tree girth than tree height. It also shows that DBH alone is an effective predictor variable for estimating tree/forest biomass (Negasi *et al*., 2017). This ontogeny explains why most allometric equations do not include tree height, or use height as an independent variable for estimating AGLB (Chave *et al*., 2005; Picard *et al*., 2012; Handavu *et al*., 2017). Further, because tree tops are often hidden by the canopy layer, tree heights are not always available in most forest field inventories (Chave *et al*., 2005).

Different mathematical combinations of pixel spectral reflectance measurements or vegetation indices were calculated and used as independent variables, and were regressed against the corresponding field estimates of total AGLB per plot (averaged from the three allometric equations). The linear regression model relating AGLB to EVI was: M= 6.5743x-4.7431. The factor "M" and "x" in the equation is the total AGLB per forest plot (30 x 30 m) and EVI values, respectively. This model was selected because it was characterised by the highest correlation coefficient (CV; r^2: 0.96) and lowest RMSE (0.22-0.24 t $plot^{-1}$) (Figure 4.21 and Appendix C). The relative standard deviation for EVI values (0.27 for Luanshya and 0.12 for Bushbuckridge) were higher than the other vegetation indices, for example, the CV values for normalised difference vegetation index (NDVI) was 0.15 in Luanshya and <0.00 in Bushbuckridge. This shows that NDVI tend to saturate in dense forested areas (Birth *et al*., 1968; Rouse *et al*., 1974). In comparison to other similar studies in Sub-Saharan Africa, this study found higher correlation coefficients between AGLB and EVI than those reported in tropical dry forests of Zimbabwe (r^2: 0.68 to 0.70; Gara *et al*., 2016) and Ethopia (r^2: 0.90;

Negasi *et al*., 2017). Although the study by Gara *et al*. (2016) was conducted in forests of similar structure, high resolution satellite data, WorldView-2 was used. The other observed difference may be attributed to the fact that Gara *et al*. (2016) did not include EVI, but only regressed biomass against SR ratio, NDVI and soil adjusted vegetation index. Given that the model in this study encompasses forest sites of different developmental stages, and was validated using 33 forest plots from forested areas of different climatic zone and structure, the biomass-EVI regression model (M= 6.5743x - 4.7431; with mean absolute error of 0.22-0.24 t $plot^{-1}$) is satisfactory for estimating aboveground forest biomass in natural forests of similar structure in the region. In addition to existing forest inventories and use of allometric equations, the biomass-EVI model offers a reliable and alternative technique for timely estimates of forest biomass in remote. It also forms a basis for monitoring, reporting and verifying (MRV) changes resulting from reforestation initiatives, and conversions of non-intervened or woodlands under unknown management practices to managed woodlands.

5.2.2 Spatial-temporal changes in forest carbon stocks

Based on the 2016 field estimates of the total AGLB per plot, and a biomass-to-carbon conversion factor of 0.50 (Grossman, 2007; Martin and Thomas, 2011; Thomas and Martin, 2012), historic forest carbon stocks were mapped, taking the assumption that Landsat reflectance measurements mirrored *in situ* variations in forest inventories (Aggarwal, 2004; Mayes *et al*., 2015). From one Landsat scene to the next, the spatial pattern of carbon storage in Luanshya showed marked temporal variation. For instance, at 10^{th}, 25^{th}, 50^{th} and 75^{th} percentiles, forest carbon storage in Luanshya increased from 1986 to 2001 (Table 4.15). Because sites of older growth are associated with bigger individual trees, there was a decrease in carbon stocks at 90^{th} percentile from 5.68 t C $plot^{-1}$ in 1986 to 5.41 t C $plot^{-1}$ in

1998. The effect of increased forest disturbance is highlighted in a downward trend in carbon storage from 2001 to 2016, with 90% of the plots having less than 4.41 t C plot^{-1} or 36.67 t ha^{-1} (Figure 4.27). Some studies suggest that when a certain threshold of disturbance is reached, natural forests may fail to revert to the initial state (Hirota *et al.*, 2011; Banks-Leite *et al.*, 2014; Poorter *et al.*, 2016). Even though these forests have the ability to retain their structure and vigor (Hirota *et al.*, 2011; Kalaba *et al.*, 2013), it remains to be seen whether Miombo woodlands in Luanshya would recover, and sequestrate and store carbon stocks similar to that of 1986 and 2001. In Bushbuckridge, the potential of increasing aboveground forest carbon storage was seen by the response of woodlands to harvest scheduling. After initiating sustainable harvesting practices, where woodlots are only selectively harvested after a three-year period, carbon stocks increased to higher values of 40.84 ± 20.52 t C ha^{-1} in 2001 and 41.92 ± 19.91 t C ha^{-1} in 2011 (Figure 4.27). These increases coupled with accurate methodology for MRV changes in forest carbon storage highlight the potential of integrating community based conservation projects within the nascent carbon based payments for environmental services and REDD+ (Chazdon, 2008; Burgess *et al.*, 2010; van Rooyen *et al*., 2013).

The United Nations REDD+ programme is envisaged to provide incentives for increases in forest carbon stocks while sinking and reducing atmospheric CO_2 concentration through assisted reforestation and forest carbon sequestration (Blom *et al*., 2010; Burgess *et al.*, 2010; Dewees *et al.*, 2010). Assessing the equitability and effectiveness of reforestation projects and their contribution to the global carbon cycle require long term monitoring (Blom *et al*., 2010). Field based sample surveys, such as national forest inventories have traditionally been used to quantify forest cover change, and estimates of AGLB and carbon stocks (Næsset *et al.*, 2016). The application of remote sensing has been integrated into traditional methodological approaches to satisfy national and regional reporting requirements (Næsset *et al.*, 2016; Schneibel *et al*., 2017b). In recent times, high spatial resolution remotely sensed information from both space borne and airborne laser scanners provide unique opportunities for quick and improved precision in biomass estimates (Ene *et al.*, 2016; Halperin *et al.*, 2016; Næsset *et al.*, 2016). However, these high volume datasets (e.g. RapidEye, WorldView-2, LiDAR, Radar etc.) are expensive to acquire and requires specialised expertise to process and analyse, which presents challenges in obtaining homogenous data over large areas (Puliti *et al*., 2017). On the other hand, this study advances the robustness of the freely available remotely sensed imagery to provide accurate, reliable and acceptable information for assessing forest carbon inventories in community forest management (Blom *et al*., 2010; Ghazoul *et al.*, 2010; Herold and Skutsch, 2011; Dube *et al*., 2016). Granted the Landsat temporal resolution of 16 days (Gleason and Im, 2011), the study also promotes the use of medium spatial resolution imagery to provide repeatable estimates of forest carbon stocks.

5.3 Effects of temperature and precipitation interannual variability on EVI

Fluctuations in climatic factors, especially precipitation and temperature, have a strong influence on the variation of EVI in Luanshya (Figures 4.31, 4.32, 4.33). From year to year, precipitation was characterised by a high degree of variability than temperature (Figures 4.29, 4.30), which indicated that rainfall was the overriding factor that characterised the different floristic composition and natural regeneration in the two different study areas. However, the strength of the relationships varied depending on the accompanying degree of forest disturbances and conversions to other LULC types (Figures 4.31, 4.32), as well as the time duration and time lag over which precipitation was integrated (Tables 3.19, 3.20). Based on the correlations between precipitation and EVI of the UDF plots, it was substantiated that rainfall is a primary factor that govern woodland productivity (r^2: 0.18-0.62). Taking into account the forest chronosequence in Luanshya, the observed negative correlations between precipitation and mean EVI of the entire forest cover suggested that some young trees tend to regenerate and grow under the canopies of more mature trees, such as PDF sites (Figure 4.31), which may not be captured by the Landsat sensors. This was evident by the positive correlations between precipitation and EVI (r^2: >0.51) in woodlands of similar forest succession stage in Bushbuckridge (Figure 4.33).

By analysing the relationships between EVI and mean precipitation of different time lags, it was established that regeneration and forest succession became evident only after five years of sustained moderate annual precipitation. These findings are in agreement with Wang *et al*. (2003) who observed that forests are buffered from climatic fluctuations and respond slowly to interannual variations in precipitation because of the deep rooted trees. The analyses also showed that temperature is equally an important factor for forest productivity, with EVI better correlated with mean minimum temperature (e.g., r^2 = -0.12 to 0.51 in Luanshya; 0.48 to 0.73 in Bushbuckridge) than maximum temperature (e.g., r^2 = -0.22 to 0.03 in Luanshya; r^2 = -0.10 to 0.01 in Bushbuckridge). Generally, as temperature increases, EVI reduced (Appendices E2, G2), mainly because of increases in forest evapotranspiration (Wang *et al*., 2003; Edoga and Suzzy, 2008). This implies that the ratio of precipitation to evapotranspiration, and available water for forest productivity increased with precipitation (Appendices H1, H2). The study established that the negative correlations between EVI and precipitation was not because of environmental constraints, but human disturbance, otherwise all forested areas (e.g., UDF sites; Figure 4.31) would have responded quite similar to fluctuations in climate. In the absence of forest disturbances, forest carbon stock in both study sites followed the annual rainfall trend. This increased tree cover, AGLB and carbon stock until forest succession or the development of saplings into mature trees is limited by tree-tree competition.

5.4 Estimates of downward vertical distribution of forest SOM concentration

Soil organic matter content or concentration (SOMc) in 0-30 cm depth, ranged from 21.19 g kg^{-1} to 99.87 g kg^{-1} for forest soils in Luanshya (Table 4.19), and 25.61 g kg^{-1} to 57.39 g kg^{-1} in Bushbuckridge (Table 4.22). This represented SOM concentration of between 2.76% and 6.54%, and 3.10% and 4.48% of the total soil weight (per sample) before ignition, respectively (Tables 3.21, 3.24). The mean SOMc in layer-1 (0-10 cm: 2.83%) of the UDF areas in Luanshya was very close to the organic concentration of 2.31% stored in the forest soils of Miombo woodlands in Malawi, as reported by Walker and Desanker (2004). Organics in layer-2 and layer-3 (2.13% to 6.75%; 2.14% to 7.25% in Luanshya and 3.04% to 4.79%; 3.17% to 6.16% in Bushbuckridge, respectively), were much higher when compared to the proportion of organics in 10-20 cm depth (1.16%) and 20-30 cm (0.62%) reported in Malawi (Walker and Desanker, 2004). In the underlying layers (10-20 cm and 20-30 cm depth) of the SF plots, SOMc (3.89%; Tables 3.21, 3.24) was in a comparable range to the previous mean estimates of soil organics (that ranged from 1.40% to 3.80%) in 0-30 cm depth of the Miombo woodland in central Zambia (Chidumayo, 2004). Comparing spatial and vertical downward distributions of SOM content in forest sites of different developmental stages was important in understanding forest degradation that are concomitant with forest disturbance. This current study is different from the few previous studies on forests soils in that, field sampling was done in woodland sites of different chronosequence, which were identified as, UDF sites, PDF, SF and RF forest sites (Table 4.6 and Figure 4.16). Further, the methodology used in quantifying SOMc (loss-on-ignition method) is clearly described, which makes it comparable and integratable into future studies.

In Luanshya, SOM stock (SOMs) was different across the different forests sites, and was highest and more variable in the top most layers (7056 ± 2402 g m^{-3}), followed by layer-3 (6135 ± 2203 g m^{-3}) and lowest in layer-2 (5427 ± 1485 g m^{-3}) (Table 4.21). In Bushbuckridge, SOM stock was also highest and more variable in 0-10 cm soil depth (5195 ± 905 g m^{-3}), but decreased with depth, from 4784 ± 1333 g m^{-3} in layer-2 to 4733 ± 2155 g m^{-3} in layer-3 (Table 4.24). In both study areas, SOM stock was highly heterogeneous due to spatial and downward vertical variations in SOM concentration and BD. In Luanshya, the difference between the highest (PDF in Site-4: 99.87 g kg^{-1}) and lowest (UDF in Site-1: 28.47 g kg^{-1}) SOMc in 0-10 cm depth was 71.40 g kg^{-1}. This was somewhat unexpected given that AGLB only differed by 0.03 tonnes, with the UDF plots having the highest total biomass (8.94 t $plot^{-1}$) than the PDF (8.91 t $plot^{-1}$; Table 4.11). One of the obvious explanation for the considerable variation was differences in topographic elevations of the sampled forest sites, and implications for soil thickness and moisture availability (Figure 4.15a). Site-4 of the PDF stands was located at a relatively lower altitude (1238 m asl.) than Site-1, which had an average elevation of 1258 m asl. Due to the high flat to gently undulating landscape (smaller variations in altitude) in Luanshya, variations in SOM concentration was largely regulated by altitude differences or the catenary positions of forest sites, where soil organics decreased from upslope to downslope. This was also highlighted by the higher SOM concentration (61.77 g kg^{-1}) in the SF site (Site-7), which was located in a low-lying area (higher MC) with an average altitude of 1228 m asl. The correlation coefficient matrices indicated that SOM concentrations were consistently negatively correlated to topographic altitudes of the forested areas (Tables 3.27, 3.28). The effect of this pattern was also seen by the increased particle size distribution of clay (<2 µm) for forest sites at lower altitudes. For instance, the lower SOM content in 0-10 cm depth of the UDF site was associated with clay content of between 2.53% and 2.84%, which were noticeably lower than the PDF sites (3.26-3.43%), and SF site (3.82-3.83%). The Lowveld forested areas of Bushbuckridge also showed similar correlations between SOM concentration and granulometric composition of soils, particularly the proportion of clay (r^2: >0.61) and silt (r^2: 0.86) (Table 4.26). These patterns revealed that forest SOM content and particles less than 50 µm exist as soil colloids with an interdependent and/or combined ability to adsorb, aggregate and retain soil nutrients (Lal, 2005; Dungait *et al.*, 2012; Saiz *et al.*, 2012; Weil and Brady, 2016).

Considering the differences in forest tree density, tree size classes and species composition, it is apparent that different intensities of forest utilisation result in different degree of soil compaction. The mean soil BD of 1286 kg m^{-3} in 0-10 cm, 1331 kg m^{-3} in 10-20 cm and 1468 kg m^{-3} in 20-30 cm compared closely with earlier studies (e.g., Chidumayo and Kwibisa, 2003). Chidumayo and Kwibisa (2003) reported BD of about 1300 kg m^{-3} in loamy sand soil of 0-10 cm soil depth, and 1400 kg m^{-3} in sandy clay loam of 11-30 cm depth. Generally, this means that soil BD of the Miombo soils increased with depth. Conversely, soil BD in woodlands of Bushbuckridge did not show any explicit trend with depth. Instead soils were mostly compacted in 10-20 cm depth (mean: 1297 kg m^{-3}) followed by the 0-10 cm depth, while the underlying layer of 20-30 cm had the lowest soil BD (1209 kg m^{-3}). This contrasts the findings by Coetsee *et al*. (2013) on encroached woodlands of South Africa, where subsoil of 0-15 cm had lower soil BD (1020 ± 100 kg m^{-3}) than the underlying soil layers, 15-30 cm (1150 ± 70 kg m^{-3}). In this current study, the reverse downward vertical compaction of soil may be associated with soil compaction prompted by grazing. This echoes earlier studies by Kotzé *et al*. (2013) and Holdo and Mack (2014) which established variations of BD with soil depth, and the resulting perturbations that may be associated with overgrazing.

Despite extensive forest utilisation and its net effect on soil BD, forest soil in Luanshya and Bushbuckridge have continued to retain at least minimum SOM content of above 2.1% and 2.56%, respectively. According to Lal (2005) and Banks-Leite *et al*. (2014), 2% of SOM concentration is the acceptable threshold value below which soil function is impaired. Even if a different threshold may be apparent for the two areas, the observed regeneration and recruitment of saplings indicate the heath and fertility condition of the forest soil. This was also demonstrated by the resilience of woodlands to climatic variabilities and critical LULC changes (Lal, 2005). Figure 5.3 summarises the described effects of climate change and LULC changes on forest carbon storage. Based on the multi-temporal variations in the spatial extent and landscape composition of the two study areas, woodlands were the most cleared and converted LULC types (changing to: grasslands, crop fields and non-vegetated land cover types.).

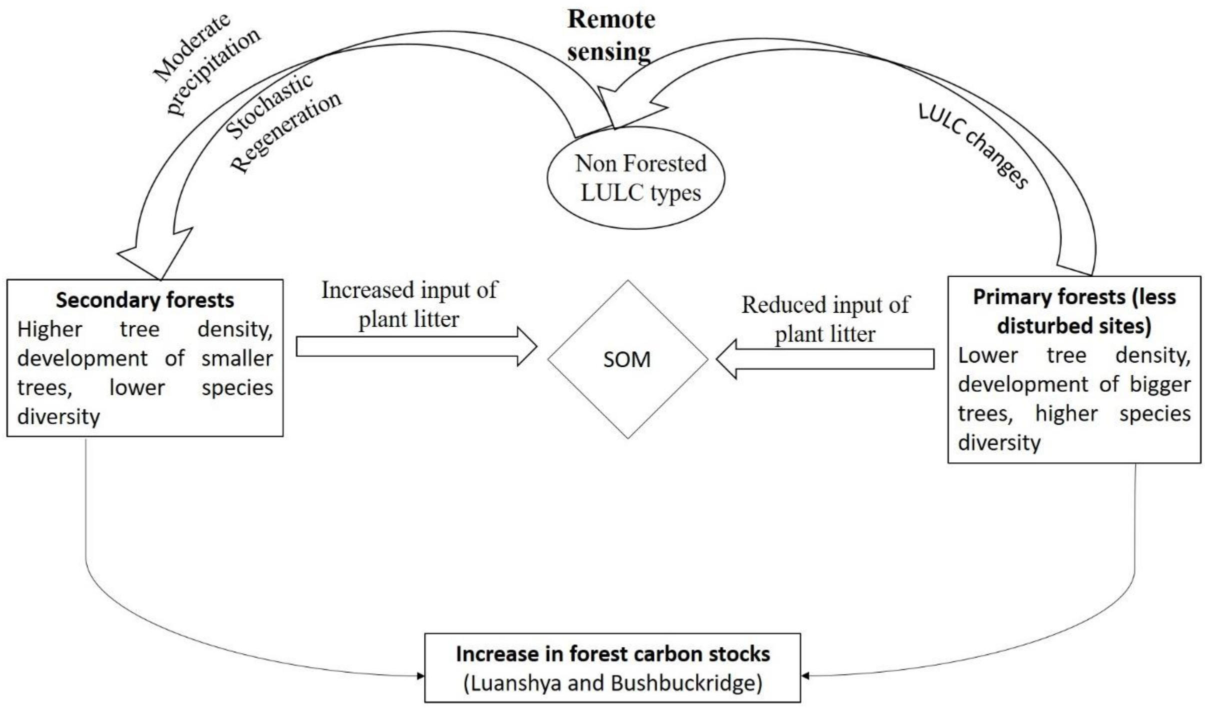

Figure 5.3: Model for system dynamics on the effects of climate change and LULC changes on the carbon sequestration capacity of natural forests.

The graph (Figure 5.3) shows that moderate precipitation of longer preceding years coupled with the reduced demand for forest land resulted in increased natural regeneration and forest succession in scattered areas. Even though second growth forest sites delivered similar ecosystem services as that of primary forests, increase in carbon storage was associated with the reduced species diversity, but increased tree density of smaller individual trees (Figure 5.3). Increased SOM in disturbed forest sites suggested that intermediate forest disturbance resulted in increased addition of plant litter into the soil, an observation which must be interpreted with caution. This is because the accumulation of SOM was influenced by other factors that included, variations in altitude, BD, AGLB, proportions of clay, silt, sand, gravel, MC, soil pH, and EC.

5.5 Application of PCA for managing soil health and security

The difficulties in assessing SOM with definitive accuracy has been acknowledged by different researchers (Dungait *et al.*, 2012; Holdo and Mack, 2014). The main reason for this paradoxical complexity is the higher dimensionality of the interactive edaphic factors and the multicollinearity and feedbacks between SOM-clay content (Dungait *et al.*, 2012; Holdo and Mack, 2014), SOM-altitude (Dungait *et al.*, 2012; Holdo and Mack, 2014), SOM-MC (Dungait *et al.*, 2012; Holdo and Mack, 2014) etc. The three PCA ordination diagrams for 0-10 cm, 10-20 cm and 10-20 cm demonstrated that soils at different depth are associated with different principal components (Figure 4.41). The contrasting ordination (obtuse angle) between SOM and sand, and BD demonstrated a negative correlations that offered physical and granulometric impedance to the accumulation of SOM and long term storage of SOC. Increased BD tend to reduce soil aeration, aggregate stability and water holding capacity, which in turn, lead to increased runoff of nutrients (e.g. organics), especially from upslope to downslope forested areas (Dungait *et al.*, 2012; Esmaeilzadeh and Ahangar, 2014). Unlike clay which acts interdependently or together with SOM to hold exchangeable cations (Dungait *et al.*, 2012; Holdo and Mack, 2014), PCA clearly proved that increase in sand content results in soil poor retention of organic matter (Dungait *et al.*, 2012; Holdo and Mack, 2014). This is consistent with the scatter signatures and particle size distribution (PSD) at 10^{th}, 50^{th} and 90^{th} percentile (Figures 4.35, 4.38), which showed higher SOM and PSD values (7.76 µm, 173 µm and 483 µm) in the UDF plots (Site-1) than in the SF plots (Site-7; 3.36 µm, 68.3 µm and 277 µm), respectively. In simple terms, for any given percentile, soils with higher PSD values had greater proportion of sand, and lower SOM content. This is because sandy soil has a loose structure which is characterised by large heterogeneous pores, which means that soil with increased volume of sand grains drained better and retained lower nutrients than clayey soil (Walczak *et al*., 2002; Dungait *et al.*, 2012; Holdo and Mack, 2014; Weil and Brady, 2016).

The ordination of AGLB and SOMc with respect to PC1 and PC2 was defined by acute (0-10 cm depth) and obtuse angles (10-30 cm depth). Due to increased input of plant matter with long mean residence time, previous work have shown that increase in AGLB ensures increased addition and stabilisation of SOM into soils (Jenkinson *et al*., 1999; Barančíková *et al*., 2010; Johnson *et al*., 2011; Coetsee *et al.*, 2013). The observed widening of the angle with depth indicated that AGLB largely influenced the accumulation of SOM in subsoil than the deeper soils. In Bushbuckridge (Table 4.26), a negative relationship existed between forest biomass and SOMs (0-10 cm: r^2 = -0.06; 10-20 cm: r^2 = -0.24; 20-30 cm: r^2 = -0.44). Even though the study did not find the underlying reason for the negative correlation, Chidumayo (1993) and Stahle *et al*. (1999) suggested that secondary forests grow by first allocating more biomass to the root growth before shoot growth becomes evident. A comparison of annual ring counts in established shoots and root stocks reveal that after disturbance it takes up to 10 years for natural forests to reach sapling phase (Lees, 1962; Chidumayo, 1993). During this period, organic matter accumulates in forest soil with little evidence from vegetation cover and AGLB.

The spatial-temporal and vertical heterogeneity of SOM exacerbates the complexity of monitoring, evaluating and reporting SOM (Peichl and Arain, 2006; Ravindranath and Osward, 2008; Bartholomeus *et al*., 2011; Nussbaum *et al*., 2014). Reducing the dimensionality of the key drivers of SOM to less than four principal components greatly minimised the difficulties that mask accurate assessment and management of SOM. This study demonstrates that PCA can be applied to discern the effects of land-use management practices on soil health. The analysis was not compared with other literature due to lack of modelling studies on SOM in the region. Nevertheless, the accuracy of PCA was checked by developing multiple linear principal regressions (MLPR) and testing its precision by using leave-one-out cross-validation (LOOCV). The high correlation coefficients (r^2: 0.70-0.95) and the low mean absolute percentage error (<15.06%) advances the importance of using PCA in assessing and understanding the dynamics of SOM. In the context of reducing deforestation and forest degradation, this study assumes added importance in that it provides different change dynamics, and baseline information that can be used for monitoring changes in forest cover extent, aboveground carbon stocks and SOM.

CHAPTER 6-CONCLUSIONS AND RECOMMENDATIONS

Multi-temporal Landsat remotely sensed images were used to map and quantify changes associated with natural forests of different climatic zones and harvesting intensities in Luanshya, Zambia, and the Lowveld of Bushbuckridge in South Africa. Owing to the extensiveness of natural forests in Africa, the methodological consideration and dynamics of LULC changes and storage of carbon can be extended to tropical dry forests of similar structure. The study illustrated the robustness of satellite imagery in evaluating the capacity of tropical dry forests to deliver ecosystem services (e.g. carbon sequestration and storage) that are linked to the resilience of these ecosystems. Through reflectance spectral signatures or pattern recognition, the preprocessed imageries were convincingly able to recognise forest sites of different attributes, where the spatial dynamics of SOM was assessed and modelled. Amid advancements in remote sensing, the study showed that Landsat Earth observation data remain a viable tool for assessing environmental conditions and functionality of forest ecosystems.

The aim of this study was underpinned by five objectives. Firstly, LULC changes that took place from 1986-2016 in Luanshya, Zambia, and from 1992-2016 in the Lowveld of Bushbuckridge, South Africa were quantified (objective i). This involved generating LULC maps from Landsat images, and using change detection methods to quantify multi-temporal changes in land cover composition. Results of the observed time periods indicated that the annual deforestation rates consistently exceeded the rate at which natural regeneration and forest succession occurred. This phenomenon precipitated changes in forest structure, from primary forests to second growth forest stands. Before forest disturbances became clearly discernable (e.g. decreasing canopy cover and AGLB), it first started as selective tree felling (e.g., PDF), which spurred forest regeneration in old growth forest stands. Under favourable climatic conditions, natural regeneration occurred in scattered areas, which resulted into forest succession and fragmented SF sites with stocks of smaller trees, increased tree density and reduced species diversity. Due to the high demand for forested areas, some forest sites were converted to agricultural fields and other non-vegetated LULC types. These conversions gave rise to different LULC types that were interlinked by transitional pathways of different intensities. These change dynamics have a wider implications, particularly for strategic identification and selection of areas for conservation and appropriate forest management that can accelerate the recovery of forests, such as, afforestation and assisted natural regeneration.

Secondly, two methodological considerations, a remote sensing and ground-based measurements were used to assess the effects of LULC changes on the spatio-temporal changes of forest carbon storage (objective ii). The best fitting linear regression model was developed by regressing the 2016 estimates of total forest biomass per plot against EVI and was used for mapping and assessing historic forest carbon stocks (biomass x 0.5) at 30 m spatial resolution. The study established that Miombo woodlands in Luanshya had higher carbon storage than the woodlands in Bushbuckridge. However, due to the implementation of harvest scheduling practices, there was a slight decrease at the rate at which aboveground forest carbon storage per unit area declined in Bushbuckridge, while LULC changes in Luanshya resulted in an increased decline in biomass carbon. Assessments of temporal forest carbon stocks at 10^{th}, 25^{th}, 50^{th}, 75^{th} and 90^{th} percentiles, revealed that the declining aboveground carbon storage was attributed to the continuous replenishment of bigger individual trees by smaller trees. This emphasises the need to devise conservation models and sustainable forest management practices that can increase forest growth rate and carbon stocks of residue trees and SF stands. Both the empirical model and the baseline data presented herein, can be used as counterfactual scenarios for evaluating the feasibility of forest management interventions that aim at increasing forest cover and biomass carbon, against which PESs and REDD+ payments can be made.

Thirdly, the effects of climate fluctuations on forest carbon storage was evaluated by developing simple linear correlations between EVI, and mean precipitation and temperature of different time durations and time lags (objective iii). In the absence of critical LULC changes, forest carbon stock in Luanshya and Bushbuckridge conspicuously followed the annual rainfall trend. This provided favourable condition for NPP which in turn increased tree cover, AGLB and carbon stock until forest succession or the development of saplings into mature trees was limited by tree-tree competition. Fourthly, the spatial and downward vertical distribution of forest SOM was assessed by quantifying forest soil BD and using loss-on-ignition method to evaluate organic matter concentration in three soil depth from 0-30 cm depth (objective iv). In dense forested sites, higher SOM concentrations were noticeably distributed in the topmost layers, but decreased inconsistently with soil depth. The fact that forest stands that had evidence of recent disturbance (e.g. stumps) were richer in SOM content than the undisturbed stands, raises important issues for belowground carbon sequestration strategies. In the less dense forest stands (regeneration sites), an opposite trend was observed, where SOM content increased with soil depth. Even though there is no published evidence for this contrasting distribution, the findings emphasised the consequences of aboveground biomass removal on the addition of plant litter and subsequent accretion of soil carbon stocks.

Lastly, the study revealed that the observed spatial variations in the downward vertical distributions of SOM concentration are influenced by several abiotic and biotic factors (Jobbagy and Jackson, 2000; Dungait *et al*., 2012; Nussbaum *et al*., 2014). Thus, PCA provided an efficient approach for determining the relationships SOM concentration and the edaphic factors that exist within the different hierarchical spatial scale of natural forest ecosystems (objective v). Given the positive correlations, the analysis showed that clay% and silt% should be considered alongside SOM concentration as they may be used as a proxy for SOM content. The patterns and strength of relationships can (1) be used as input or as independent validation for improving soil carbon models (e.g. RothC model; Barančíková *et al*., 2010), (2) help understand the consequences of forest disturbance, and (3) help devise more efficient strategies for forest management.

One of the limitations of the study was that the priori images for specific dates were of poor quality due to persistent cloud cover that obscured some ground features. As a result, some Landsat scenes of apriority dates (e.g. with a five year interval or uniform intervals), with cloud cover of <10% were not available, which resulted in inconsistencies in the dates of the acquired Landsat scenes and intervals overs which LULC changes were quantified. The other limiting factor is that forest field measurements at 30 m spatial resolution were quite a large spatial extent to sample more forest sites than what was enumerated in this study. Conversely, mapping of forest carbon stocks was based on the assumption that the mean estimates of AGLB averaged from the three general allometric equations reflected the total true biomass in each sampled plot. Due to lack of site specific allometric models and uncertainty (e.g. appropriateness of the equations) with regard to which model to use, estimates of biomass from both allometric equations is inherently associated with residual errors. Thus, developing empirical models that directly relate tree biomass and reflectance measurements from high resolution remotely sensed imagery, and calibrating measurements to Landsat datasets is an avenue for future research. In the context of the UNFCCC to provide financial incentives for reducing emissions from deforestation and forest degradation, such a methodology would ensure robustness in the governance REDD+ incentives.

Changes in the spatial-temporal patterns of woodlands and other LUCL types over a 25-year period (Bushbuckridge) and 30-year period (Luanshya), provides scientific evidence that these natural forests are in decline despite their resilience through natural regeneration. These trends have implications for ecosystem functions and strategies for assisted natural regeneration, and empowering local communities in sustainable environmental stewardship. Based on the rate change of woodland cover as well as other LULC types, the study provides a methodology for monitoring the performance of forest restoration strategies and evaluating the impacts of future LULC change scenarios. This is in line with recent studies that have advocated the inclusion of Miombo woodlands into the REDD+ mechanisms. The study highlights the need to promote decentralised natural forest management strategies in developing countries, and the effectiveness of applying remote sensing in designing monitoring mechanisms for assisted natural regeneration under different conservation models, with the aim of including tropical dry woodlands into UNFCCC mechanisms. It also provides reference scenarios on which REDD+ would reward actual reductions in deforestation rates.

For future studies, (1) it would be useful to further validate the regression model (relating AGLB and EVI) developed in this present study, particularly in sites of different climates and forest types. (2) There is also a need to use the counterfactual scenarios of this research as input variables for soil carbon model, such as RothC etc., so as to model and predict the SOM turnover times that are associated with the afforestation and reforestation initiatives in southern Africa. (3) The other research prospect is to use hyperspectral and high resolution sensors to map the species composition of natural forest ecosystems in the region. In the context of biodiversity conservation, this will enhance a fundamental understanding of the spatial distribution of species quality which could lead to the development of early warning systems to detect any subtle forest changes.

REFERENCES

Abbot, P., Lowore, J., Werren, M., 1997. Models for the estimation of single tree volume in four Miombo woodland types. Forest Ecology and Management 97: 25–37.

Adam, E., Mutanga, O., Abdel-Rahman, E.M., Ismail, R., 2014. Estimating standing biomass in papyrus (*Cyperus papyrus L.*) swamp: exploratory of in situ hyperspectral indices and random forest regression. International Journal of Remote Sensing 35: 693–714.

Adam, E., Mutanga, O., Rugege, D., 2010. Multispectral and hyperspectral remote sensing for identification and mapping of wetland vegetation: a review. Wetlands Ecology and Management 18: 281–296.

Aggarwal, S., 2004. Principles of Remote Sensing. Indian Institute of Remote Sensing, Dehra Dun, 23-38pp.

Aide, T., Zimmermann, J., Pascarella, J., Rivera, L., Marcano-Vega, H., 2000. Forest regeneration in chronosequence of tropical abandoned pastures: Implications for restoration ecology. Restoration Ecology 8: 328–338.

Akinyemi, F.O., 2017. Land change in the central Albertine rift: Insights from analysis and mapping of land use-land cover change in north-western Rwanda. Applied Geography 87: 127-138.

Archibald, S., Bond, W.J., 2003. Growing tall vs growing wide: tree architecture and allometry of Acacia karroo in forest, savanna, and arid environments. OIKOS 102: 3–14.

Aynekulu, E., Vagen, T-G., Shepherd, K., Winowiecki, L.A., 2011. A Protocol for Measurement and Monitoring Soil Carbon Stocks in Agricultural Landscapes. World Agroforestry Centre, Nairobi.

Ball, D.F., 1964. Loss-on-ignition as an estimate of organic matter and organic carbon in non-calcareous soils. European Journal of Soil Science 15: 84–92.

Banda, T., Schwartz, M.W., Caro, T., 2006. Woody vegetation structure and composition along a protection gradient in a miombo ecosystem of western Tanzania. Forest Ecology and Management 230: 179–185.

Banks-Leite, C., Pardini, R., Tambosi, L.R., Pearse, W.D., Bueno, A.A., Bruscagin, R.T., Condez, T.H., Dixo, M., Igari, A.T., Martensen, A.C., Metzger, J.P., 2014. Using ecological thresholds to evaluate the costs and benefits of set-asides in a biodiversity hotspot. Science 345: 1041–1045.

Barančíková, G., Halás, J., Gutteková, M., Makovníková, J., Nováková, M., Skalský, R., Tarasovičová, Z., 2014. Application of RothC Model to predict soil organic carbon stock on agricultural soils of Slovakia. Soil and Water Research 5: 1–9.

Bartholomeus, H., Kooistra, L., Stevens, A., van Leeuwen, M., van Wesemael, B., Ben-Dor, E., Tychon, B., 2011. Soil organic carbon mapping of partially vegetated agricultural fields with imaging spectroscopy. International Journal of Applied Earth Observation and Geoinformation 13: 81–88.

Birth, G.S., McVey, G.R., 1968. Measuring the color of growing turf with a reflectance spectrophotometer. Agronomy Journal 60: 640–643.

Blanco-Canqui, H., Lal, R., Post, W.M, Izaurralde, R.C, Shipitalo, M.J, 2006. Organic carbon influences on soil particle density and rheological properties. Soil Science Society of America Journal 70: 1407-1414.

Blom, B., Sunderland, T., Murdiyarso, D., 2010. Getting REDD to work locally: lessons learned from integrated conservation and development projects. Environmental Science & Policy 13: 164–172.

Bockheim, J.G., Gennadiyev, A.N., Hartemink, A.E., Brevik, E.C., 2014. Soil-forming factors and soil taxonomy. Geoderma 226–227: 231–237.

Bond, I., Chambwera, M., Jones, B., Chundama, M., Nhantumbo, I., 2010. REDD+ in dryland forests: issues and prospects for pro-poor REDD in the miombo woodlands of southern Africa. IIED, London. Natural Resource Issues 21.

Brown, M., Gunn, S.R., Lewis., H.G., 1999. Support Vector Machines for optimal classification and spectral unmixing. Ecological Modelling 120: 167–179.

Brudvig, L.A., Asbjornsen, H., 2009. The removal of woody encroachment restores biophysical gradients in Midwestern oak savannas. Journal of Applied Ecology 46: 231–240.

Burges, C.J.C., 1998. A tutorial on Support Vector Machines for pattern recognition. Data Mining and Knowledge Discovery 2: 121–167.

Burgess, N.D., Bahane, B., Clairs, T., Danielsen, F., Dalsgaard, S., Funder, M., Hagelberg, N., Harrison, P., Haule, C., Kabalimu, K., Kilahama, F., Kilawe, E., Lewis, S.L., Lovett, J.C., Lyatuu, G., Marshall, A.R., Meshack, C., Miles, L., Milledge, S.A.H., Munishi, P.K.T., Nashanda, E., Shirima, D., Swetnam, R.D., Willcock, S., Williams, A., Zahabu, E., 2010. Getting ready for REDD+ in Tanzania: a case study of progress and challenges. Oryx 44: 339–351.

Cabral, A.I.R., Vasconcelos, M.J., Oom, D., Sardinha, R., 2010. Spatial dynamics and quantification of deforestation in the central-plateau woodlands of Angola. Applied Geography 31: 1185–1193.

Caplow, S., Jagger, P., Lawlor, K., Sills, E., 2011. Evaluating land use and livelihood impacts of early forest carbon projects: Lessons for learning about REDD+. Environmental Science & Policy 14: 152–167.

Carreiras, J.M.B, Melo, J.B., Vasconcelos, M.J., 2013. Estimating the Above-Ground Biomass in Miombo Savanna Woodlands (Mozambique, East Africa) Using L-Band Synthetic Aperture Radar Data. Remote Sensing 5: 1524-1548.

Chaudhari, P.R., Ahire, D.V, Ahire, V.D., Chkravarty, M., Maity, S., 2013. Soil bulk density as related to soil texture, organic matter content and available total nutrients of Coimbatore soil. Internal Journal of Scientifc and Research Publications 3: 2250–3153.

Chave, J., Andalo, C., Brown, S., Cairns, M.A., Chambers, J.Q., Eamus, D., Fölster, H., Fromard, F., Higuchi, N., Kira, T., Lescure, J.-P., Nelson, B.W.., Ogawa, H., Puig, H., Riéra, B., Yamakura, T., 2005. Tree allometry and improved estimation of carbon stocks and balance in tropical forests. Oecologia 145: 87–99.

Chazdon, R.L., 2008. Beyond deforestation: restoring forests and ecosystem services on degraded lands. Science 320: 1458–1460.

Chidumayo, E., 1990. Above-ground woody biomass structure and productivity in a Zambezian woodland. Forest Ecology and Management 36: 33–46.

Chidumayo, E.N., 1991. Woody biomass structure and utilisation for charcoal production in a Zambian Miombo woodland. Bioresource Technology. 37: 43–52.

Chidumayo, E.N., 1993. Zambia Charcoal Production. Energy Policy 21: 586–597.

Chidumayo, E.N., Frost, P., 1996. Population biology of Miombo trees. In: Campbell, B.M (Ed.). The Miombo in Transition: Woodlands and Welfare in Africa. Center for International Forestry Research, Bogor, Indonesia.

Chidumayo, E.N., 1997. Miombo Ecology and Management: An Introduction. Stockholm Environment Institute, Stockholm, Sweden.

Chidumayo, E.N., Mbata, K.J., 2002. Shifting cultivation, edible caterpillars and livelihood in the Kopa area of northern Zambia. Forests, Trees and Livelihoods 12: 175–193.

Chidumayo, E.N., Kwibisa, L., 2003. Effects of deforestation on grass biomass and soil nutrient status in Miombo woodland, Zambia. Agriculture, Ecosystem and Environment 96: 97–105.

Chidumayo, E.N., 2004. Development of *Brachystegia-Julbernardia* woodland after clear-felling in central Zambia: Evidence for high resilience. Applied Vegetation Science 7: 237-242.

Chidumayo, E.N., Gumbo, D., 2010. The Dry Forests and Woodlands of Africa: Managing for Products and Services. Earthscan, London.

Chidumayo, E.N., 2013. Estimating tree biomass and changes in root biomass following clear-cutting of *Brachystegia-julbernardia* (miombo) woodland in central Zambia. Environmental Conservation 41: 54–63.

Chidumayo, E.N., 2013. Forest degradation and recovery in a miombo woodland landscape in Zambia: 22 years of observations on permanent sample plots. Forest Ecology and Management 291: 154–161.

Chidumayo, E.N., 2015. Dry season watering alters the significance of climate factors influencing the phenology and growth of saplings of savanna woody species in central Zambia, southern Africa. Austral Ecology: A Journal of Ecology in Southern Hemisphere 40: 794–805.

Ciais, P., Sabine, C., Bala, G., Bopp, L., Brovkin, V., Canadell, J., Chhabra, A., DeFries, R., Galloway, J., Heimann, M., 2014. Carbon and other biogeochemical cycles, in: Climate Change 2013: The Physical Science Basis. Contribution of Working Group I to the Fifth Assessment Report of the Intergovernmental Panel on Climate Change. Cambridge University Press, 465–570 pp.

Coetsee, C., Gray, E.F., Wakeling, J., Wigley, B.J., Bond, W.J., 2013. Low gains in ecosystem carbon with woody plant encroachment in a South African savanna. Journal of Tropical Ecology 29: 49–60.

Cortes, C., Vapnik, V., 1995. Support-Vector Networks. Machine Learning 20: 273–297.

Council for Geoscience (CGS), 1997. Geological Map of South Africa. Available from http://geoscience.org.za, accessed 28 February 2018.

Craig, J., 2000. Evaluating privatisation in Zambia: a tale of two processes. Review of African Political Economy 27: 357–366.

Craig, J., 2001. Putting privatisation into practice: the case of Zambia Consolidated Copper Mines Limited. Journal of Modern African Studies 39: 389-410.

Croft, H., Kuhn, N.J., Anderson, K., 2012. On the use of remote sensing techniques for monitoring spatio-temporal soil organic carbon dynamics in agricultural systems. Catena 94: 64–74.

de Andrade, R.B., Balch, J.K., Parsons, A.L., Armenteras, D., Roman‐ Cuesta, R.M., Bulkan, J., 2017. Scenarios in tropical forest degradation: carbon stock trajectories for REDD+. Carbon Balance Manage 12, doi: 10.1186/s13021-017-0074-0.

Department of Agriculture and Development (DAD), 1991. Soil Classification A Taxonomic System for South Africa. Soil and Irrigation Research Institute, Department of Agriculture and Development, Pretoria.

Department of Environmental Affairs (DEA), 2014. South Africa's Greenhouse Gas (GHG) Mitigation Potential Analysis. Mitigation Report. Department of Environmental Affairs, Pretoria.

Desanker, P.V., Prentice, I.C., 1994. Miombo-a vegetation dynamics model for the miombo woodlands of Zambezian Africa. Forest Ecology and Management 69: 87-95.

Dewan, A.M., Yamaguchi, Y., 2009a. Using remote sensing and GIS to detect and monitor land use and land cover change in Dhaka Metropolitan of Bangladesh during 1960–2005. Environmental Monitoring and Assessment 150: 237–249.

Dewan, A.M., Yamaguchi, Y., 2009b. Land Use and Land Cover Change in Greater Dhaka, Bangladesh: Using remote sensing to promote sustainable urbanisation. Applied Geography 29: 390–401.

Dewees, P.A., Campbell, B.M., Katerere, Y., Sitoe, A., Cunningham, A.B., Angelsen, A., Wunder, S., 2010. Managing the Miombo woodlands of southern Africa: policies, incentives and options for the rural poor. Journal of Natural Resources Policy Research 2: 57–73.

Dinka, T.M., Morgan, C.L.S., McInnes, K.J., Kishné, A.S., Daren, H.R., 2013. Shrink–swell behavior of soil across a Vertisol catena. Journal of Hydrology 476: 352–359.

Don, A., Schumacher, J., Scherer-Lorenzen, M., Scholten, T., Schulze, E., 2007. Spatial and vertical variation of soil carbon at two grassland sites-Implications for measuring soil carbon stocks. Geoderma 141: 272–282.

Dovie, D.B.K., Shackleton, C.M., Witkowski, E.T.F., 2002. Direct-use values of woodland resources consumed and traded in a South African village. International Journal of Sustainable Development & World Ecology 9: 269–283.

Dovie, D.B.K., Shackleton, C.M., Witkowski, E.T.F., 2007. Conceptualizing the human use of wild edible herbs for conservation in South African communal areas. Journal of Environmental Management 84: 146–156.

Dube, T., Mutanga, O., Ismail, R., 2016. Quantifying aboveground biomass in African environments: A review of the trade-offs between sensor estimation accuracy and costs. Tropical Ecology 57: 393–405.

Dungait, J.A.J., Hopkins, D.W., Gregory, A.S., Whitmore, A.P., 2012. Soil organic matter turnover is governed by accessibility not recalcitrance. Global Change Biology 18: 1781–1796.

Eckert, D., Sims, J.T., 1995. Recommended soil pH and lime requirement tests. Recommended Soil Test Procedure for the Northeasten United. Northeast Region Bulletin 493: 11–16.

Edoga, R.N., Suzzy, A.B.U., 2008. Effect of temperature changes on evapotranspiration in Minna, Niger, State. Journal of Engineering and Applied Sciences 3: 482-486.

Ene, L.T., Næsset, E., Gobakken, T., Mauya, E.W., Bollandsås, O.M., Mauya, E.W., Zahabu, E., 2016. Large-scale estimation of aboveground biomass in miombo woodlands using airborne laser scanning and national forest inventory data. Remote Sensing of Environment 188: 106-117.

Ernst, W.H.O., 1988. Seed and seedling ecology of *Brachystegia spiciformis*, a predominant tree component in Miombo Woodlands in South central Africa. Forest Ecology and Management 25: 195-210.

Esmaeilzadeh, J., Ahangar, A.G., 2014. Influence of soil organic matter content on soil physical, chemical and biological properties introduction. Intenational Journal of Plant, Animal and Environmental Sciences 4: 244-252.Fey, M.V., 2010. A short guide to the soils of South Africa, their distribution and correlation with World Reference Base soil groups. 19th World Congress of Soil Science, Soil Solutions for a Changing World. Brisbane, Australia.

Flamenco-Sandoval, A., Ramos, M.M., Masera, O.R., 2007. Assessing implications of land-use and land-cover change dynamics for conservation of a highly diverse tropical rain forest. Biological Conservation 138: 131–145.

Foley, J.A., DeFries, R., Asner, G.P., Barford, C., Bonan, G., Carpenter, S.R., Chapin, F.S.., Coe, M.T., Daily, G.C., Gibbs, H.K., 2005. Global consequences of land use. Science 309: 570–574.

Food Agriculture Organisation (FAO), 2001. Global Forest Resources Assessment 2000. Food Agriculture Organisation of the United Nations. Rome, Italy.

Food Agriculture Organisation (FAO), 2005. The Importance of Soil Organic Matter: Key to Drought-Resistant Soil and Sustained Food Production. FAO Soils Bulletin No. 80. Food Agriculture Organisation of the United Nations. Rome, Italy.

Food Agriculture Organisation (FAO), 2010. Global Forest Resources Assessment 2010. Food Agriculture Organisation of the United Nations. Rome, Italy.

Food and Agriculture Organisation (FAO), 2012. State of the World's Forests. Food Agriculture Organisation of the United Nations. Rome, Italy.

Food Agriculture Organisation (FAO), 2015. Action Points for Forests and Forestry (Forests and People: Investing in a Sustainable Future. FAO World Forestry Congress No. WFC2015 XIV, Durban, South Africa.

Food Agriculture Organisation (FAO), 2015. Global Forest Resources Assessment 2015. How are the World Forests Changing? (Second Edition). Rome, Italy.

Frost, P., 1996. The ecology of Miombo woodlands In: Campbell, B.M., 1996. The Miombo in Transition: Woodlands and Welfare in Africa (Ed.). Center for International Forestry Research, Bogor, Indonesia, 11-57 pp.

Gandhi, G.M., Parthiban, S., Thummalu, N; Christy, A., 2015. NDVI: Vegetation change detection using remote sensing and GIS- A case study of Vellore District. Procedia Computer Science 57: 199–1210.

Gara, T.W., Murwira, A., Ndaimani, H., 2016. Predicting forest carbon stocks from high resolution satellite data in dry forests of Zimbabwe: exploring the effect of the red-edge band in forest carbon stocks estimation. Geocarto International 31: 176–192.

Geoterraimage, 2010. 2013-2014 South African National Land Dat User Report and Metadata User Report and Metadadta 2014 South African National. Available from http:// www.geoterraimage.com, accessed 11th April 2018.

Ghazoul, J., Butler, R.A., Mateo-Vega, J., Koh, L.P., 2010. REDD: a reckoning of environment and development implications. Trends Ecol. Evol. 25 (7): 396–402.

Gibbs, H.K., Brown, S., Niles, J.O., Foley, J.A., 2007. Monitoring and estimating tropical forest carbon stocks: making REDD a reality. Environmental Research Letters 2, doi: 10.1088/1748-9326/2/4/045023.

Gibbs, H.K., Ruesch, A.S., Achard, F., Clayton, M., Holmgren, P., Ramankutty, N., Foley, J.A., 2010. Tropical forests were the primary sources of new agricultural land in the 1980s and 1990s. Proceedings of the National Academy Science 107: 16732–16737.

Gitelson, A.A., Gritz, Y., Merzlyak, M.N., 2003. Relationships between leaf chlorophyll content and spectral reflectance and algorithms for non-destructive chlorophyll assessment in higher plant leaves. Journal of Plant Physiology 160: 271–282.

Gleason, C.J., Im, J., 2011. A review of remote sensing of forest biomass and biofuel: Options for small-area applications. GIScience Remote Sensing 48: 141–170.

Goetz, S., Dubayah, R., 2011. Advances in remote sensing technology and implications for measuring and monitoring forest carbon stocks and change. Carbon Management 2: 231–244.

Gould, S.J., 1966. Allometry and size in ontogeny and phylogeny. Biological Reviews 41: 587–638.

Grau, O., Penuelas, J., Ferry, B., Freycon, V., Blanc, L., Desprez, M., Baraloto, C., Chave, J., Descroix, L., Dourdain, A., Guitet, S., Janssens, I.A., Sardans, J., Herault, B., 2017. Nutrient-cylcing mechanisms other than the direct absorption from soil may control forest structure and dynamics in poor Amazonian soils. Scientific Reports 7, doi: 10.1038/srep45017.

Grossman, J.M., 2007. Carbon in terrestrial systems: A review of the science with specific reference to central American ecotypes and locations. Journal of Sustainable Forestry 25: 17–41.

Halperin, J., LeMay, V., Coops, N., Verchot, L., Marshall, P., Lochhead, K., 2016. Canopy cover estimation in miombo woodlands of Zambia: Comparison of Landsat 8 OLI versus RapidEye imagery using parametric, nonparametric, and semiparametric methods. Remote Sensing of Environment 179: 170-182.

Handavu, F., Chirwa, P.W., Syampungani, S., Mahamane, L., 2017. A review of carbon dynamics and assessment methods in miombo woodlands. A Journal of Forest Science 79: 95-102.

Hartmann, D.L., Klein Tank, A.M.G., Rusticucci, M., Alexander, L.V., Brönnimann, S., Charabi, Y., Dentener, F.J., Dlugokencky, E.J., Easterling, D.R., Kaplan, A., Soden, B.J., Thorne, P.W., Wild, M., Zhai, P.M., 2013. In: Climate Change 2013: The Physical Science Basis. Contribution of Working Group I to the Fifth Assessment Report of the Intergovernmental Panel on Climate Change. Cambridge University Press, Cambridge, United Kingdom and New York, NY, US.

Hegazy, I.R., Kaloop, M.R., 2015. Monitoring urban growth and land use change detection with GIS and remote sensing techniques in Daqahlia Governorate Egypt. International Journal of Sustainable Built Environment 4: 117-124.

Herold, M., Skutsch, M., 2011. Monitoring, reporting and verification for national REDD + programmes: two proposals. Environmental Research Letters 6, doi: 10.1088/1748-9326/6/1/014002.

Hirota, M., Holmgren, M., Van Nes, E.H., Scheffer, M., 2011. Global resilience of tropical forest and savanna in critical transitions. Science 334: 232–235.

Hoffman, M.T., Barr, G.D., Cowling, R.M., 1990. Vegetation dynamics in the semi arid eastern Karro, South Africa: the effect of seasonal rainfall and competition on grass and shrub basal cover. South African Journal of Science 86: 462–463.

Holdo, R.M., Mack, M.C., 2014. Functional attributes of savanna soils: contrasting effects of tree canopies and herbivores on bulk density, nutrients and moisture dynamics. Journal of Ecology 102: 1171–1182.

Hollis, J.M., Jones, R.J.A., Palmer, R.C., 1977. The effects of organic matter and particle size on the water-retention properties of some soils in the west midlands of England. Geoderma 17: 225–238.

Hoogsteen, M.J.J., Lantinga, E.A., Bakker, E.J., Groot, J.C.J., Tittonell, P.A., 2015. Estimating soil organic carbon through loss on ignition: effects of ignition conditions and structural water loss: Refining the loss on ignition method. European Journal of Soil Science 66: 320–328.

Huang, C., Davis, L.S., Townshend, J.R.G., 2002. An Assessment of Support Vector Machines for land cover classification." International Journal of Remote Sensing 23 : 725–749.

Huete, A.R., 1988. A soil-adjusted vegetation index (SAVI). Remote Sensing of Environment 25: 295–309.

Huete, A.R., Didan, K., Miura, T., Rodriguez, E.P., Gao, X., Ferreira, L.G., 2002. Overview of the radiometric and biophysical performance of the MODIS vegetation indices. Remote Sensing of Environment 83: 195–213.

Im, J., Jensen, J.R., 2008. Hyperspectral remote sensing of vegetation. Geography Compass 2 : 1943–1961.

Intergovernmental Panel on Climate Change (IPCC), 2003. Practice Guidance for Land Use, Land-Use Change and Forestry. Institute for Global Environmental Strategies (IGES), Japan.

Intergovernmental Panel on Climate Change (IPCC), 2007. Climate Change 2007: The Physical Science Basis. Contribution of Working Group I to the Fourth Assessment

Report of the IPCC. Available from http://www.ipcc.ch/ipccreports/ar4-wg1.htm, accessed 5 February 2016.

Intergovernmental Panel on Climate Change (IPCC), 2014. Climate Change Synthesis Report. Contribution of Working Groups I, II and III to the Fifth Assessment Report of the Intergovermental Panel on Climate Change. IPCC, Geneva, Switzerland.

Jansson, C., Wullschleger, S.D., Kalluri, U.C., Tuskan, G.A., 2010. Phytosequestration: Carbon Biosequestration by Plants and the Prospects of Genetic Engineering. BioScience 60: 685–696.

Jenkinson, D.S., Meredith, J., Kinyamario, J.I., Warren, G.P., Wong, M.T.F., Harkness, D.D., Bol, R., Coleman, A.K., 1999. Estimating net primary production from measurements made on soil organic matter. Ecology 80: 2762-2773.

Jew, J.R., 1986. Introductory Digital Processing. Prentice-Hall, Englewood Cliffs, New Jersey.

Jew, E.K.K., Dougill, A.J., Sallu, S.M., O'Connell, J., Benton, T.G., 2016. Miombo woodland under threat: Consequences for tree diversity and carbon storage. Forest Ecology and Management 361: 144-153.

Jew, E.K.K., Dougill, A.J., Sallu, S.M., 2017. Tobacco cultivation as a driver of land use change and degradation in miombo woodlands of south-west Tanzania. Land Degradation and Development 28: 2636–2645.

Jobbagy, E.G., Jackson, R.B., 2000. The vertical distribution of soil organic carbon and its relation to climate and vegetation. Ecological Applications 10: 423–436.

Johnson, K.D., Scatena, F.N., Silver, W.L., 2011. Atypical soil carbon distribution across a tropical steepland forest catena. Catena 87: 391–397.

Kachamba, D.J., Eid, T., Gabakken, T., 2016. Above-belowground biomass models for trees in the Miombo woodlands of Malawi. Forests 7, 38, doi: 10.3390/f7020038.

Kajembe, G.C., Monela, G.C., Mvena, Z.S.K. (Eds.), 2003. Making Community-Based Forest Management Work: A Case Study of Duru-Haitemba Village Forest Reserve, Babati, Tanzania. Policies and Governance Structures in Woodlands of Southern Africa. CIFOR, Bogor.

Kalaba, F.K., Quinn, C.H., Dougill, A.J., Vinya, R., 2013. Floristic composition, species diversity and carbon storage in charcoal and agriculture fallows and management implications in Miombo woodlands of Zambia. Forest Ecology and Management 304: 99–109.

Kanowski, P.J., McDermott, C.L., Cashore, B.W., 2011. Implementing REDD+: lessons from analysis of forest governance. Environmental Science and Policy 14: 111–117.

Karatzoglou, A, Meyer D, Hornik K. 2006. Support vector machines in R. Journal of Statistical Software 15: 1–28.

Karhu, K., Mattila, T., Bergström, I., Regina, K., 2011. Biochar addition to agricultural soil increased CH_4 uptake and water holding capacity – Results from a short-term pilot field study. Agriculture, Ecosystems and Environment 140: 309–313.

Kasozi, G.N., Nkedi-Kizza, P., Harris, W.G., 2009. Varied carbon content of organic matter in Histosols, Spodosols, and Carbonatic soils. Soil Science Society of America Journal 73: 1313-1318.

Kaufman, Y.J., Wald, A.E., Remer, L.A., Gao, B., Li, R., Flynn, L., 1997. The MODIS 2.1-mu;m channel-correlation with visible reflectance for use in remote sensing of aerosol. IEEE Trans. Geoscience and Remote Sensing 35: 1286–1298.

Kavzoglu T, Colkesen I. 2009. A kernel functions analysis support vector machines for land cover classification. International Journal of Applied Earth Observation and Geoinformation 11: 352–359.

Keller, T., Dexter, A.R., 2012. Plastic limits of agricultural soils as functions of soil texture and organic matter content. Soil Research 50: 7-17.

Kern, J.S., 1995. Evaluation of soil water retention models based on basic soil physical properties. Soil Science Society of America Journal 59: 1134–1141.

Kindt, R., van Breugel, P., Lillesø, J.-P.B., Bingham, M., Demissew, S., Dudley, C., Friis, I., Gachathi, F., Kalema, J., Mbago, F., Minani, V., Moshi, H.N., Mulumba, J., Namaganda, M., Ndangalasi, H.J., Ruffo, C.K., Jamnadass, R., Graudal, L., 2011. Potential Natural Vegetation of Eastern Africa. Description and Tree Species Composition for Woodland and Wooded Grassland Potential Natural Vegetation Types. World Agroforestry Centre and Forest and Landscape Denmark, University of Copenhage.

Kirsten, M., Kaaya, A., Klinger, T., Feger, K.H., 2016. Stocks of soil organic carbon in forest ecosystems of the eastern Usambara Mountains, Tanzania. Catena 137: 651–659.

Kissel, D.E., Sonon, L., Vendrell, P.F., Isaac, R.A., 2009. Salt Concentration and Measurement of Soil pH. Communications in Soil Science and Plant Analysis 40: 179–187.

Kotzé, E., Sandhage-Hofmann, A., Meinel, J.-A., du Preez, C.C., Amelung, W., 2013. Rangeland management impacts on the properties of clayey soils along grazing gradients in the semi-arid grassland biome of South Africa. Journal of Arid Environments. 97: 220–229.

Kuyah, S., Sileshi, G.W., Njoloma, J., Mng'omba, S., Neufeldt, H., 2014. Estimating aboveground tree biomass in three different Miombo woodlands and associated land use systems in Malawi. Biomass and Bioenergy 66: 214–222.

Kuyah, S., Sileshi, G.W., Rosenstock, T.S., 2016. Allometric models based on Bayesian frameworks give better estimates of aboveground biomass in the Miombo woodlands. Forests 7, 13, doi: 10.3390/f7020013.

Lal, R., 1978. Physical properties and moisture retention characteristics of some Nigerian soils. Geoderma 21: 209–223.

Lal, R., 2004. Soil carbon sequetration. SOLAW Background Thematic Report NO. TR04B. Food Agriculture Organisation. Rome, Italy.

Lal, R., 2005. Forest soils and carbon sequestration. For. Ecol. Manag. 220: 242–258.

Lal, R., 2008. Carbon sequestration. Biological Sciences 363: 815–830.

Lees, H., 1962. Working plan for the forests supplying the Copperbelt, Western Province. Government Printer, Lusaka, Zambia.

Li, Z., Wu, H., Wang, N., Qiu, S., Sobrino, J.A., Wan, Z., Tang, B., Yan, G., 2013. Land surface emissivity retrieval from satellite data. International Journal of Remote Sensing 34: 3084–3127.

Lillesand, T., Kiefer, R.W., Chipman, J., 2014. Remote Sensing and Image Interpretation (7th Ed.). John Wiley & Sons, USA.

Liu, S., Zhang, W., Wang, K., Pan, F., Yang, S., Shu, S., 2015. Factors controlling accumulation of soil organic carbon along vegetation succession in a typical karst region in Southwest China. Science of the Total Environment 521–522: 52–58.

Lund, J.F., Treue, T., 2008. Are we getting there? Evidence of decentralized forest management from the Tanzanian miombo woodlands. World Development 36: 2780–2800.

Lungu, J., 2008. Socio-economic change and natural resource exploitation: a case study of the Zambian copper mining industry. Development Southern Africa 25: 543–560.

Luoga, E.J., Witkowski, E.T.F., Balkwill, K., 2002. Harvested and standing wood stocks in protected and communal miombo woodlands of eastern Tanzania. Forest Ecology and Management 164: 15–30.

MacCracken, M.C., 2009. The increasing pace of climate change. Strategic Planning for Energy and the Environment 28: 8–25.

Magurran, A.E., 1998. Ecological Diversity and Its Measurement. Great Britain University Press, Cambridge, UK.

Mapfumo, R.B., Murirwa, A., Mosocha, M., Andriani, R., 2017. Detection of subtle deforestation due to logging using satellite remote sensing in wet and dry savanna woodlands of southern Africa. Geocarto International 32: 514-530.

Maraseni, T.N., Pandey, S.S., 2014. Can vegetation types work as an indicator of soil organic carbon? An insight from native vegetations in Nepal. Ecological Indicators 46: 315–322.

Martin, A.R., Thomas, S.C., 2011. A Reassessment of Carbon Content in Tropical Trees. PLoS ONE 6, e23533, doi: 10.1371/journal.pone.0023533.

Mate, R., Johansson, T., Sitoe, A., 2014. Biomass equations for tropical forest tree species. Forests 5: 535-556.

Mayes, M.T., Mustard, J.F., Melillo, J.M., 2015. Forest cover change in Miombo Woodlands: Modeling land cover of African dry tropical forests with linear spectral mixture analysis. Remote Sensing of Environment 165: 203-215.

Mayes, M., Mustard, J., Melillo, J., Neill, C., Nyadzi, G., 2017. Going beyond the green: Senesced vegetation material predicts basal area in remote sensing of tree cover conditions in an African tropical dry forest (Miombo woodland) landscape. Environmental Research Letters 12, doi: 10.1088/1748-9326/aa7242.

McNicol, I.M., Ryan, C.M., Williams, M., 2015. How resilient are African woodlands to disturbance from shifting cultivation. Ecological Applications 25: 2320-2336.

Ministry of Environment and Natural Resources (MENR), 1994. National Environmental Action Plan. Ministry of Environment and Natural Resources, Lusaka, Zambia, 168 pp.

Mograbi, P.J., Erasmus, B.F.N., Witkowski, E.T.F., Asner, G.P., Wessels, K.J., Mathieu, R., Knapp, D.E., Martin, E., Main, R., 2015. Biomass increases go under cover: Woody vegetation dynamics in South African rangelands. PLoS ONE 10, doi: 10.1371/journal. pone.0127093.

Mtui, D.T., Lepczyk, C.A., Chen, Q., Miura, T., Cox, L.J., 2017. Assessing multi decadal land- cover-land-use change in two wildlife protected areas in Tanzania using Landsat imagery. PLOS ONE 12, doi: 10.1371/journal.pone.0185468 l.pone.0127093.

Mugasha, W.A., Eid, T., Bollandsas, O.M., Malimbwi, R.E., Chamshama, S.A.O., Zahabu, E, Katani, J.Z., 2013. Allometric models for prediction of above- and belowground biomass of trees in the miombo woodlands of Tanzania. Forest Ecology and Management 310: 87–101.

Murty, D., Kirschbaum, M.U.F., Mcmurtrie, R., Mcgilvray, H., 2002. Does conversion of forest to agricultural land change soil carbon and nitrogen? A review of the literature. Global Change Biology 8: 105–123.

Mususa, P., 2010. 'Getting by': life on the Copperbelt after the privatisation of the Zambia Consolidated Copper Mines. Social Dynamics 36: 380–394.

Næsset, E., Ørka, H.O., Solberg, S., Bollandsås, O.M., Hansen, E.H., Mauya, E., Zahabu, E., Malimbwi, R., Chamuya, N., Olsson, H., Gobakken, T., 2016. Mapping and estimating forest area and aboveground biomass in miombo woodlands in Tanzania using data from airborne laser scanning, TanDEM-X, RapidEye, and global forest maps: A comparison of estimated precision. Remote Sensing of Environment 175: 282-300.

Negasi, S., Emiru, B., Tadesse, T., Treydte, A., Meles, K., 2017. Carbon stocks and sequestration potential of dry forests under community management in Tigray, Ethiopia. Ecological Processes 6, doi: 10.1186/s13717-017-0088-2

Nickless, A., Scholes, R.J., Archibald, S., 2011. A method for calculating the variance and confidence intervals for tree biomass estimates obtained from allometric equations. South African Journal of Science 107, doi:10.4102/ sajs.v107i5/6.356.

Nussbaum, M., Papritz, A., Baltensweiler, A., Walthert, L., 2014. Estimating soil organic carbon stocks of Swiss forest soils by robust external-drift kriging. Geoscientific Model Development 7: 1197–1210.

Oommen, T., Misra, D., Twarakavi, N.K.C., Prakash, A., Sahoo, B., Bandopadhyay, S., 2008. An objective analysis of Support Vector Machine based classification for remote sensing. Math Geoscience 40: 409–424.

Parker, C., Cranford, M., Roe, S., Manandhar, U., 2013. REDD+ Prospects in LDCs. LDC Paper Series. United Nations Reducing Emission from Deforestation and forest Degradation (UN-REDD+). Rome, Italy.

Peichl, M., Arain, M.A., 2006. Above- and belowground ecosystem biomass and carbon pools in an age-sequence of temperate pine plantation forests. Agricultural and Forestry Meteorology 140: 51–63.

Pelletier, J., Siampale, A., Legendre, P., Jantz, P., Laporte, N.T., Goetz, S.J., 2017. Human and natural controls of variation in aboveground tree biomass in African dry forests. Ecological Applications 27: 1578–1593.

Petropoulos, G.P., Kontoes, C., Keramitsoglou, I., 2011. Burnt area delineation from a unitemporal perspective based on Landsat TM imagery classification using Support Vector Machines. International Journal of Applied Earth Observation and Geoinformation 13: 70– 80.

Picard, N., Saint-André, L., Henry, M., 2012. Manual for Building Tree Volume and Biomass Allometric Equations: From Field Measurement to Prediction. Forestry Department Food and Agriculture Organization of the United Nations, Rome, Italy and Montpellier Cedex, France.

Pielke, R.A., Pitman, A., Niyogi, D., Mahmood, R., McAlpine, C., Hossain, F., Goldewijk, K.K., Nair, U., Betts, R., Fall, S., 2011. Land use/land cover changes and climate: modeling analysis and observational evidence. WIREs Clim. Change 2 (6): 828–850.

Pienaar, B., Thompson, D.I., Erasmus, B.F.N., Hill, T.R., Witkowski, E.T.F., 2014. Evidence for climate-induced range shift in *Brachystegia* (miombo) woodland. Southern African Journal of Science. 111, doi: 10.17159/ sajs.2015/20140280.

Poorter, L., Bongers, F., Aide, T.M., Zambrano, A.M.A., Balvanera, P., Becknell, J,M., Boukili, V., Brancalion, P.H.S., Broadbent, E.N., Chazdon, R.L., Craven, D., de Almeida-Cortez, J.S., Cabral, G.A.L., de Jong, B.H.L., Denslow, J.S., Dent, D.H., DeWalt, S.J., Dupuy, J.M., Durán, S.M., Espírito-Santo, M.M., Fandino, M.C., César, R.G., Hall, J.S., Hernandez-Stefanoni, J.L., Jakovac, C.C., Junqueira, A.B., Kennard, D., Letcher, S.G., Licona, J., Lohbeck, M., Marín-Spiotta, E., Martínez-Ramos, M., Massoca, P., Meave, J.A., Mesquita, R., Mora, F., Muñoz, R., Muscarella, R., Nunes, Y.R.F., Ochoa-Gaona, S., de Oliveira, A.A., Orihuela-Belmonte, E., Peña-Claros, M., Pérez-García, E.A., Piotto, D., Powers, J.S., Rodríguez-Velázquez, J., Romero-Pérez, I.E., Ruíz, J., Saldarriaga, J.G., Sanchez-Azofeifa, A., Schwartz, N.B., Steininger, M.K., Swenson, N.G., Toledo, M., Uriarte, M., van Breugel, M., van der Wal, H., Veloso, M.D.M., Vester, H.F.M., Vicentini, A., Vieira, I.C.G., Bentos, T.V., Williamson, G.B., Rozendaal, D.M.A., 2016. Biomass resilience of Neotropical secondary forests. Nature 530, 211-217.

Poulain, M., Peña, M., Schmidt, A., Schmidt, H., Schulte, A., 2010. Relationships between forest variables and remote sensing data in a *Nothofagus pumilio* forest. Geocarto International 25: 25–43.

Powell, S.L., Cohen, W.B., Healey, S.P., Kennedy, R.E., Moisen, G.G., Pierce, K.B., Ohmann, J.L., 2010. Quantification of live aboveground forest biomass dynamics with Landsat time-series and field inventory data: A comparison of empirical modeling approaches. Remote Sensing of Environment 114: 1053–1068.

Prins, E., Kikula, I.S., 1996. Deforestation and regrowth phenology in miombo woodland-assessed by Landsat Multispectral Scanner System data. Forest Ecology and Management 84: 263–266.

Puliti, S., Ene, L.T., Gobakken, T., Naesset, E., 2011. Use of partial-coverage UAV data in sampling for large scale forest inventories. Remote Sensing of Environment 194: 115–126.

Puliti, S., Solberg, S., Næsset, E., Gobakken, T., Zahabu, E., Mauya, E., Malimbwi, R.E., 2017. Modelling above Ground Biomass in Tanzanian Miombo Woodlands Using TanDEM-X WorldDEM and Field Data. Remote Sensing 9, doi: 10.3390/rs9100984.

Puyravaud, J., 2003. Standardizing the calculation of the annual rate of deforestation. Forest Ecology and Management 177: 593–596.

Raghubanshi, A.S., 1992. Effect of topography on selected soil properties and nitrogen mineralization in a dry tropical forest. Soil Biology and Biochemistry. 24: 145–150.

Ravindran, A., Yang, S., 2015. Effects of vegetation type on microbial biomass carbon and nitrogen in subalpine mountain forest soils. Journal of Microbiology Immunology and Infection 48: 362–369.

Ravindranath, N.H., Ostwald, M., 2008. Methods for Below-Ground Biomass. Springer, Netherlands.

Rawls, W.J., Pachepsky, Y.A., Ritchie, J.C., Sobecki, T.M., Bloodworth, H., 2003. Effect of soil organic carbon on soil water retention. Geoderma 116: 61–76.

RCMRD Geoportal, 2015. Zambia Land Cover 2010 Scheme II. Available from http://www.geoportal.rcmrd.org, accessed 11th April 2018.

Reddy, C.S., Rakesh, F., Jha, C.S., Athira, K., Singh, S., Alekhya, W.L.P., Rajashekar, G., Diwakar, P.G., Dadhwal, V.K., 2016. Geospatial assessment of long-term changes in carbon stocks and fluxes in forests of India (1930–2013). Global and Planetary Change 143: 50–65.

Robinson, E.J.Z., Ambers, H.J., Meshack, C., Lokina, R.B., 2013. Implementing REDD through community-based forest management: Lessons from Tanzania. Natural Resources Forum 37: 141–152.

Rodger, J.G., Twine, W.C., 2002. Tree canopies facilitate invasion of communal savanna rangelands by Lantana camara. African Journal of Range Forage Science 19: 131–135.

Rouse, J.W., Haas, R.H., Schell, J.A., Deering, D.W., 1974. Monitoring vegetation systems in the Great Plains with ERTS. Third ERTS Symposium, NASA.

Saito, M., Luyssaert, S., Poulter, B., Williams, M., Ciais, P., Bellassen, V., Ryan, C.M., Yue, C., Cadule, P., Peylin, P., 2014. Fire regimes and variability in aboveground woody biomass in Miombo woodland. J. of Geophysical Res. Biogeosci. 119 (5), 1014–1029.

Saiz, G., Bird, M., Domingues, T., Schrodt, F., Schwarz, M., Feldpausch, T.R., Veenendaal, E., Djagbletey, G., Hien, F., Compaore, H., Diallo, A., Lloyd, J., 2012. Variation in soil carbon stocks and their determinants across a precipitation gradient in West Africa. Global Change Biology 18: 1670–1683.

Schneibel, A., Stellmes, M., Rödger, A., Finckh, M., Revermann, R., Frantz, D., Hill, J., 2016. Evaluating the trade-off between food and timber resulting from the conversion of Miombo forests to agricultural land in Angola using multi-temporal Landsat data. Science of the Total Environment 548-549: 390–401.

Schneibel, A., Frantz, D., Röder, A., Stellmes, M., Fischer, K., Hill, J., 2017a. Using annual Landsat time series for the detection of dry forest degradation processes in south-central Angola. Remote Sensing 9, 905, doi: 10.3390/rs9090905.

Schneibel, A., Stellmes, M., Rödger, A., Frantz, D., Kowalski, B., HaB, E., Hill, J., 2017b. Assessment of spatio-temporal changes of smallholder cultivation patterns in the Angolan Miombo belt using segmentation of Landsat time series. Remote Sensing 195, 118-129.

Scholes, R.J., Archer, S.R., 1997. Tree-grass interactions in savannas. Annual Review of Ecological Systematics 28: 517–544.

Sebukeera, C., Muramira, E., Momokama, C., Elkholei, A., Elbagouri, I., Masumbuko, B., Rabesahala, V., 2006. Forests and Woodlands. United Nations Environment Programme, UNEP.

Seybold, C.A., Elrashidi, M.A., Engel, R.J., 2008. Linear regression models to estimate soil liquid limit and plasticity index from basic soil properties. Soil Science 173: 25–34.

Shalaby, A., Tateishi, R., 2007. Remote sensing and GIS for mapping and monitoring land cover and land-use changes in the Northwestern coastal zone of Egypt. Applied Geography 27: 28–41.

Shirima, D.D., Munishi, P.K.T., Lewis, S.L., Burgess, N.D., Marshall, A.R., Balmford, A., Swetnam, R.D., Zahabu, E.M., 2011. Carbon storage, structure and composition of miombo woodlands in Tanzania’s Eastern Arc Mountains. African Journal of Ecology 49: 332–342.

Shirima, D.D., Pfeifer, M., Platts, P.J., Totland, Ø., Moe, S.R., 2015a. Interactions between canopy structure and herbaceous biomass along environmental gradients in moist forest and dry Miombo woodlands of Tanzania. PLoS ONE 10, e0142784, doi: 10.1371/journal.pone.0142784.

Shirima, D.D., Totland, Ø., Munishi, P.K.T., Moe, S.R., 2015b. Relationship between tree species richness, evenness and aboveground carbon storage in Montane forests and Miombo woodlands of Tanzania. Basic and Applied Ecology 16: 239–249.

Shoko, C., Dube, T., Sibanda, M., Bangamwabo, V., 2016. Quantifying the spatial and temporal changes in forested landcover using landscape metrics derived from remotely sensed data in rural parts of Zimbabwe. Transactions of the Royal Society of South Africa 71: 105–113.

Sims, D.A., Gamon, J.A., 2002. Relationships between leaf pigment content and spectral reflectance across a wide range of species, leaf structures and developmental stages. Remote Sensing of Environment 81: 337–354.

Sonter, L.J., Johnson, J.A., Nicholson, C.C., Richardson, L.L., Watson, K.B., Ricketts, T.H., 2017. Multi-site interactions: Understanding the offsite impacts of land use change on the use and supply of ecosystem services. Ecosystem Services 81: 337–354.

Southern Africa Development Community (SADC), 2010. Adaptation and Mitigation Actions, Supported by Enabling Measures of Implementation (Southern Africa Sub-regional Framework of Climate Change Programmes). Southern Africa Development Community and United Nations Environment Programme.

Stahle, D.W., Mushove, P.T., Cleaveland, M.K., Roig, F., Haynes, G.A., 1999. Management implications of annual growth rings in *Pterocarpus angolensis* from Zimbabwe. Forest Ecology and Management 124: 217–229.

Stromgaard, P., 1985. Biomass estimation equations for miombo woodland, Zambia. Agroforestry Systems 3: 3–13.

Sun, H., Nelson, M., Chen, F., Husch, J., 2009. Soil mineral structural water loss during loss on ignition analyses. Canadian Journal of Soil Science 89: 603–610.

Syampungani, S., Chirwa, P.W., Akinnifesi, F.K., Sileshi, G., Ajayi, O.C., 2009. The miombo woodlands at the cross roads: Potential threats, sustainable livelihoods, policy gaps and challenges. Natural Resources Forum 33: 150–159.

Syampungani, S., Clendenning, J., Gumbo, D., Nasi, R., Moombe, K., Chirwa, P., Ribeiro, N., Grundy, I., Matakala, N., Martius, C., Kaliwile, M., Kabwe, G., Petrokofsky, G., 2014. The impact of land use and cover change on above and below-ground carbon stocks of the miombo woodlands since the 1950s: a systematic review protocol. Environmental Evidence 3, 25, doi: 10.1186/2047-2382-3-25.

Tamene, L., Mponela, P., Sileshi, G.W., Cheun, J.,Tondoh, J.E., 2016. Spatial variation in tree density and estimated aboveground carbon stocks in southern Africa. Forests 7, 57, doi: 10.3390 / f7030057.

Thomas, P., Pacham, J., 2007. Ecology of Woodlands and Forests: Description, dynamics and diversity. Cambridge University Press, Keele University and University of Woverhampton.

Thomas, S.C., Martin, A.R., 2012. Carbon Content of Tree Tissues: A Synthesis. Forests 3: 332–352.

Thompson, I., Mackey, B., McNulty, S., Mosseler, A., 2009. Forest Resilience, Biodiversity, and Climate Change. A Synthesis of Biodiversity/Resilience/Stability Relationship in Forest Ecosystems. Technical Series no. 43. Secretariat of the Convention on Biological Diversity, Montreal.

Trenberth, K., 2001. Stronger evidence of human influences on climate: The 2001 IPCC Assessment. Environment: Science and Policy for Sustainable Development 43: 8–19.

Trouet, V., Esper, J., Beeckman, H., 2010. Climate/growth relationships of *Brachystegia spiciformis* from the miombo woodland in south central Africa. Dendrochronologia 28: 161–171.

Trumbore, S.E., Czimczik, C.I., 2008. Geology: An uncertain future for soil carbon. Science 321: 1455–1456.

Tsui, C., Chen, Z., Hsieh, C., 2004. Relationships between soil properties and slope position in a lowland rain forest of southern Taiwan. Geoderma 123: 131–142.

Tucker, C.J., 1979. Red and photographic infrared linear combinations for monitoring vegetation. Remote Sensing of Environment 8: 127–150.

United Nations (UN), 2007. Bali Action Plan: Decision 1/CP.13. United Nations.

United Nations Framework Convention on Climate Change (UN), 2009. Reducing emissions from deforestation in developing countries: Approaches to stimulate action. Available from http:// unfcc.int/resource/docs, accessed 19 February 2018.

United States Department of Agriculture (USDA) and Natural Resources Conservation Services (NRCS), 1999. Soil Taxonomy A Basic System of Soil Classification for Making and Interpreting Soil Surveys, Second Ed. Agriculture Handbook. Washington DC, 1-886pp.

van Rooyen, M.W., van Rooyen, N., Stoffberg, G.H., 2013. Carbon sequestration potential of post-mining reforestation activities on the KwaZulu-Natal coast, South Africa. Forestry 86: 211–223.

Verburg, P.H., Van De Steeg, J., Veldkamp, A., Willemen, L., 2009. From land cover change to land function dynamics: a major challenge to improve land characterization. Journal of Environmental Management 90: 1327–1335.

Walczak, R., Rovdan, E., Witkowska-Walczak, B., 2002. Water retention characteristics of peat and sand mixtures. Int. Agrophysics 16: 161–166.

Walker, S.M., Desanker, P.V., 2004. The impact of land use on soil carbon in Miombo woodlands of Malawi. Forest Ecology and Management 203: 345–360.

Wang, J., Rich, P.M., Price, K.P., 2003. Temporal responses of NDVI to precipitation and temperature in the central Great Plains, USA. International Journal of Remote Sensing 24: 2345–2364.

Ward, D., 2005. Do we understand the causes of bush encroachment in African savannas? African Journal of Range & Forage Science 22: 101-105.

Weil, R.R., Brady, N.C., 2016. The Nature and Properties of soils (15th Ed). Pearson, London, UK.

Wigley, B.J., Bond, W.J., Hoffman, M.T., 2009. Bush encroachment under three contrasting land-use practices in a mesic South African savanna. African Journal of Ecology 47: 62–70.

Williams, C.A., Gu, H., MacLean, R., Masek, J.G., Collatz, G.J., 2016. Disturbance and the carbon balance of US forests: A quantitative review of impacts from harvests, fires, insects, and droughts. Global and Planetary Change 143: 66–80.

Williams, M., Ryan, C.M., Rees, R.M., Sambane, E., Fernando, J., Grace, J., 2008. Carbon sequestration and biodiversity of re-growing Miombo woodlands in Mozambique. Forest Ecology and Management 254: 145–155.

Xu, L., Saatch, S.S., Shapiro, A., Meyer, V., Ferraz, A., Yang, Y., Bastin, J., Banks, N., Boeckx, P., Verbeeck, H., Lewis, S.L., Muanza, E.T., Bongwele, E., Kayembe, F., Mbenza, D., Kalau, L., Mukendi, F., Ilunga, F., Ebuta, D., 2017. Spatial Distribution of Carbon Stored in Forests of the Democratic Republic of Congo. Scientific Reports 7, doi: 10.1038/s41598-017-15050-z.

Yang, F., Zhang, G., Yang, J., Li, D., Zhao, Y., Liu, F., Yang, R., Yang, F., 2014. Organic matter controls of soil water retention in an alpine grassland and its significance for hydrological processes. Journal of Hydrology 519: 3086–3093.

APPENDICES

Appendix A1: Maximum Likelihood: Classification error matrices for Luanshya

		Ground Truth ROI Pixels									
		Agricultural areas	**Bare land**	**Built-up areas**	**Dense woodlands**	**Grasslands**	**Paved areas**	**Riparian vegetation**	**Water bodies**	**Total**	**UA (%)**
LULC for 1986	**Agricultural areas**	-	-	-	-	-	-	-	-	-	-
	Bare land	-	112	3	0	0	0	0	0	**115**	**97**
	Built-up areas	-	0	18	0	0	0	0	0	**18**	**100**
	Dense woodlands	-	0	0	117	0	0	0	0	**117**	**100**
	Grasslands	-	0	0	0	187	0	0	0	**187**	**100**
	Paved areas	-	0	0	0	0	148	0	0	**148**	**100**
	Riparian vegetation	-	0	0	0	0	0	133	0	**133**	**100**
	Water bodies	-	0	0	0	0	0	0	107	**107**	**100**
	Total	-	112	21	117	187	148	133	107	**825**	
	PA (%)	-	**100**	**86**	**100**	**100**	**100**	**100**	**100**		
	Overall accuracy (%)		**99**								
	Kappa coefficient		**0.99**								
LULC for 1998	**Agricultural areas**	46	0	0	0	0	1	0	0	**47**	**98**
	Bare land	0	181	1	0	0	0	0	0	**182**	**100**
	Built-up areas	0	1	97	0	0	1	0	0	**99**	**98**
	Dense woodlands	0	0	0	122	0	0	0	0	**122**	**100**
	Less dense woodland	0	0	0	0	102	0	6	0	**108**	**94**
	Paved areas	0	0	0	0	0	115	0	0	**115**	**100**
	Riparian vegetation	0	0	0	2	0	0	105	0	**107**	**98**
	Water bodies	0	0	0	0	0	0	0	110	**110**	**100**
	Total	**46**	**182**	**98**	**124**	**102**	**117**	**111**	**110**	**890**	
	PA (%)	**100**	**100**	**99**	**98**	**100**	**98**	**95**	**100**		
	Overall accuracy (%)		**98**								
	Kappa coefficient		**0.98**								
LULC for 2001	**Agricultural areas**	76	0	0	0	3	0	0	0	**79**	**88**
	Bare land	0	152	0	0	0	0	0	0	**152**	**100**
	Built-up areas	0	4	58	0	0	2	0	0	**64**	**91**
	Dense woodlands	0	0	0	118	0	0	0	0	**118**	**99**
	Grasslands	0	0	0	0	97	0	0	1	**98**	**99**
	Paved areas	0	1	0	0	0	93	0	0	**94**	**98**
	Riparian vegetation	0	0	0	0	0	0	110	0	**110**	**97**
	Water bodies	0	0	0	0	0	0	0	109	**109**	**100**
	Total	**76**	**157**	**58**	**118**	**100**	**95**	**110**	**110**	**824**	
	PA (%)	**93**	**97**	**100**	**97**	**97**	**92**	**79**	**99**		
	Overall accuracy (%)		**94**								
	Kappa coefficient		**0.93**								
LULC for 2004	**Agricultural areas**	112	0	0	0	0	3	0	0	**115**	**94**
	Bare land	0	159	0	0	0	0	0	0	**159**	**100**
	Built-up areas	0	0	98	0	0	1	0	0	**99**	**99**
	Dense woodlands	0	0	0	122	0	0	3	0	**125**	**95**
	Grasslands	0	0	0	0	105	0	1	0	**106**	**93**
	Paved areas	3	0	0	0	0	157	0	0	**160**	**98**
	Riparian vegetation	0	0	0	2	1	0	67	0	**70**	**93**
	Water bodies	0	0	0	0	0	0	0	110	**110**	**100**
	Total	115	159	98	124	106	161	71	110	**944**	
	PA (%)	93	100	100	95	96	98	71	100		
	Overall accuracy (%)		**94**								
	Kappa coefficient		**0.93**								
LULC for 2011	**Agricultural areas**	112	0	0	3	0	0	0	0	**115**	**97**
	Bare land	0	113	4	0	0	1	0	0	**118**	**96**
	Built-up areas	0	1	72	0	0	3	0	0	**76**	**87**
	Dense woodlands	8	0	0	98	0	0	0	0	**106**	**93**
	Grasslands	0	0	0	0	105	0	0	0	**105**	**100**
	Paved areas	0	0	0	0	0	132	0	0	**132**	**100**
	Riparian vegetation	0	0	0	0	0	0	127	0	**127**	**100**
	Water bodies	0	0	0	0	0	0	0	110	**110**	**100**
	Total	120	114	76	101	105	136	127	110	**889**	
	PA (%)	93	99	57	97	100	96	100	100		
	Overall accuracy (%)		**91**								
	Kappa coefficient		**0.91**								
LULC for 2016	**Agricultural areas**	114	0	0	0	0	0	0	0	**114**	**98**
	Bare land	0	118	3	1	0	0	0	0	**122**	**98**
	Built-up areas	0	3	110	0	0	3	0	0	**116**	**94**
	Dense woodlands	0	0	0	111	0	0	0	0	**111**	**97**
	Grasslands	0	0	0	0	108	0	0	0	**108**	**98**
	Paved areas	0	0	10	0	0	112	0	0	**122**	**92**
	Riparian vegetation	0	0	0	0	0	0	135	0	**135**	**100**
	Water bodies	0	0	0	0	0	0	0	110	**110**	**100**
	Total	114	121	123	112	108	115	135	110	**1051**	
	PA (%)	100	98	89	97	98	97	100	100	**938**	
	Overall accuracy (%)		**97**								
	Kappa coefficient		**0.97**								

Appendix A2: Maximum Likelihood: Classification error matrices for Bushbuckridge

		Ground Truth ROI Pixels							
		Agricultural areas	Bare land	Dense woodlands	Grasslands	Paved areas	Water bodies	Total	UA (%)
LULC for 1992	**Agricultural areas**	-	-	-	-	-	-	-	-
	Bare land	-	64	0	0	20	0	**84**	**76**
	Dense woodlands	-	0	114	0	0	1	**115**	**99**
	Grasslands	-	0	0	182	0	0	**182**	**100**
	Paved areas	-	18	0	0	70	0	**88**	**80**
	Water bodies	-	0	0	0	0	95	**95**	**100**
	Total	**-**	**82**	**114**	**182**	**90**	**96**	**564**	
	PA (%)	**-**	**78**	**100**	**100**	**78**	**99**		
	Overall accuracy (%)		**93**						
	Kappa coefficient		**0.91**						
LULC for 1998	**Agricultural areas**	32	0	0	0	0	0	**32**	**100**
	Bare land	0	49	0	0	22	0	**71**	**69**
	Dense woodlands	0	0	53	1	0	3	**57**	**93**
	Grasslands	1	0	1	102	0	0	**104**	**98**
	Paved areas	0	17	0	0	84	0	**101**	**83**
	Water bodies	0	0	0	0	0	79	**79**	**100**
	Total	**33**	**66**	**54**	**103**	**106**	**82**	**444**	
	PA (%)	**97**	**74**	**98**	**99**	**79**	**96**		
	Overall accuracy (%)		**90**						
	Kappa coefficient		**0.88**						
LULC for 2001	**Agricultural areas**	107	0	1	0	0	0	**108**	**99**
	Bare land	0	20	0	0	12	0	**32**	**63**
	Dense woodlands	0	0	112	0	0	0	**112**	**100**
	Grasslands	0	0	0	129	0	0	**129**	**100**
	Paved areas	0	11	0	4	90	0	**105**	**86**
	Water bodies	0	0	0	0	0	144	**144**	**100**
	Total	**107**	**31**	**113**	**133**	**102**	**144**	**630**	
	PA (%)	**100**	**65**	**99**	**97**	**88**	**100**		
	Overall accuracy (%)		**96**						
	Kappa coefficient		**0.95**						
LULC for 2006	**Agricultural areas**	94	1	0	0	0	0	**95**	**99**
	Bare land	18	111	2	0	0	1	**132**	**84**
	Dense woodlands	0	0	103	0	0	0	**103**	**100**
	Grasslands	0	0	0	115	0	0	**115**	**100**
	Paved areas	2	2	0	0	107	0	**111**	**96**
	Water bodies	0	0	0	0	0	174	**174**	**100**
	Total	**114**	**114**	**105**	**115**	**107**	**175**	**730**	
	PA (%)	**83**	**97**	**98**	**100**	**100**	**99**		
	Overall accuracy (%)		**96**						
	Kappa coefficient		**0.96**						
LULC for 2010	**Agricultural areas**	79	0	0	0	0	0	**79**	**100**
	Bare land	23	106	6	0	11	10	**156**	**68**
	Dense woodlands	0	0	97	0	0	2	**99**	**98**
	Grasslands	0	0	0	110	0	0	**100**	**100**
	Paved areas	4	0	0	0	89	1	**94**	**95**
	Water bodies	0	1	0	0	0	95	**96**	**99**
	Total	**106**	**107**	**103**	**110**	**100**	**108**	**634**	
	PA (%)	**75**	**99**	**94**	**100**	**89**	**88**		
	Overall accuracy (%)		**91**						
	Kappa coefficient		**0.89**						
LULC for 2016	**Agricultural areas**	79	0	0	0	0	0	**79**	**100**
	Bare land	23	106	6	0	11	10	**156**	**68**
	Dense woodlands	0	0	97	0	0	2	**99**	**98**
	Grasslands	0	0	0	110	0	0	**100**	**100**
	Paved areas	4	0	0	0	89	1	**94**	**95**
	Water bodies	0	1	0	0	0	95	**96**	**99**
	Total	**106**	**107**	**103**	**110**	**100**	**108**	**634**	
	PA (%)	**75**	**99**	**94**	**100**	**89**	**88**		
	Overall accuracy (%)		**91**						
	Kappa coefficient		**0.89**						

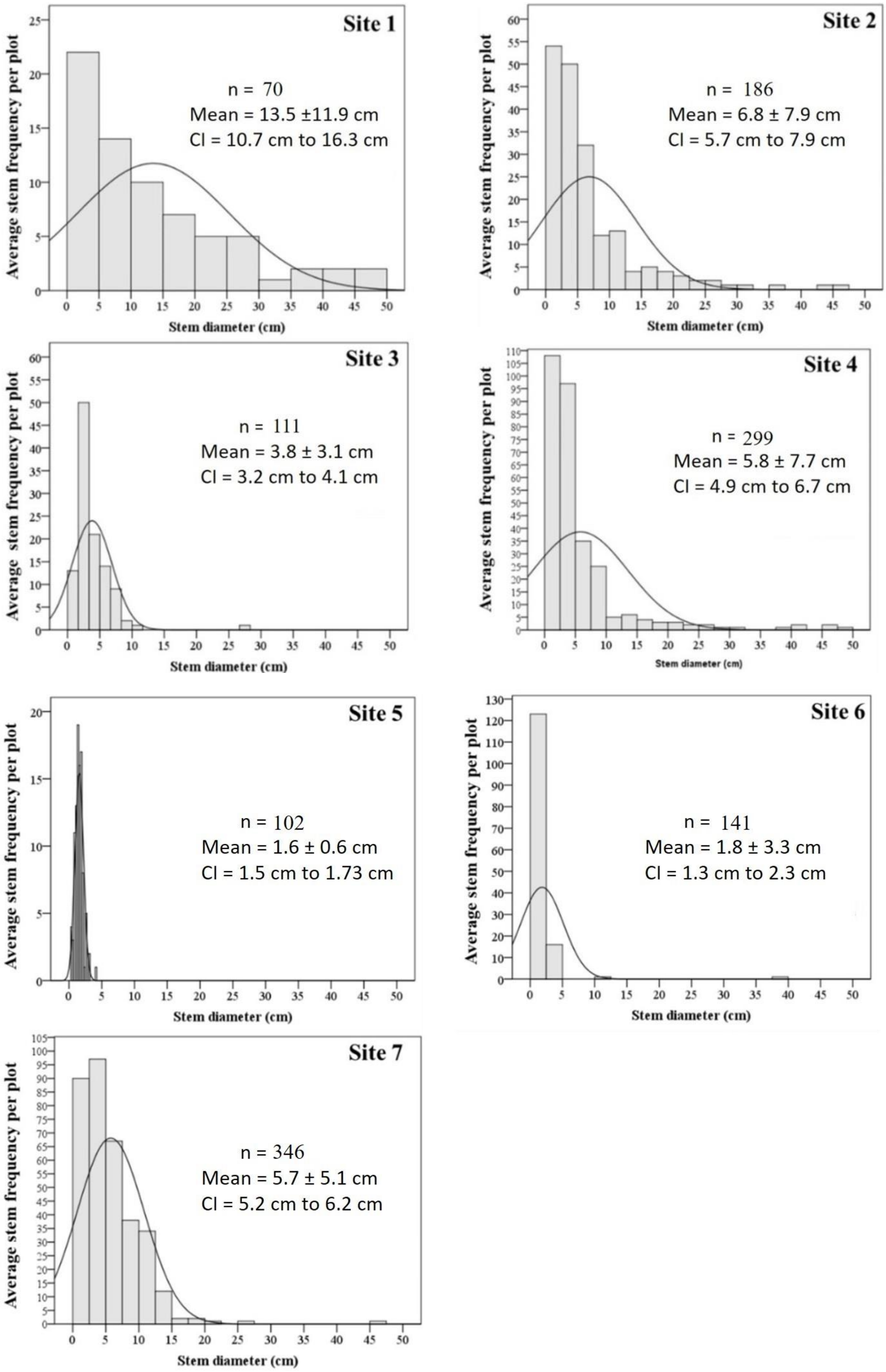

Appendix B1: Distribution of tree stem diameter in Luanshya, measured at 1.3 m above the ground. The legend shows the mean total number (n) of individual trees per sites (30 x 30 m), mean stem diameters and standard deviation and the confidence interval (CI) at 95% level of confidence.

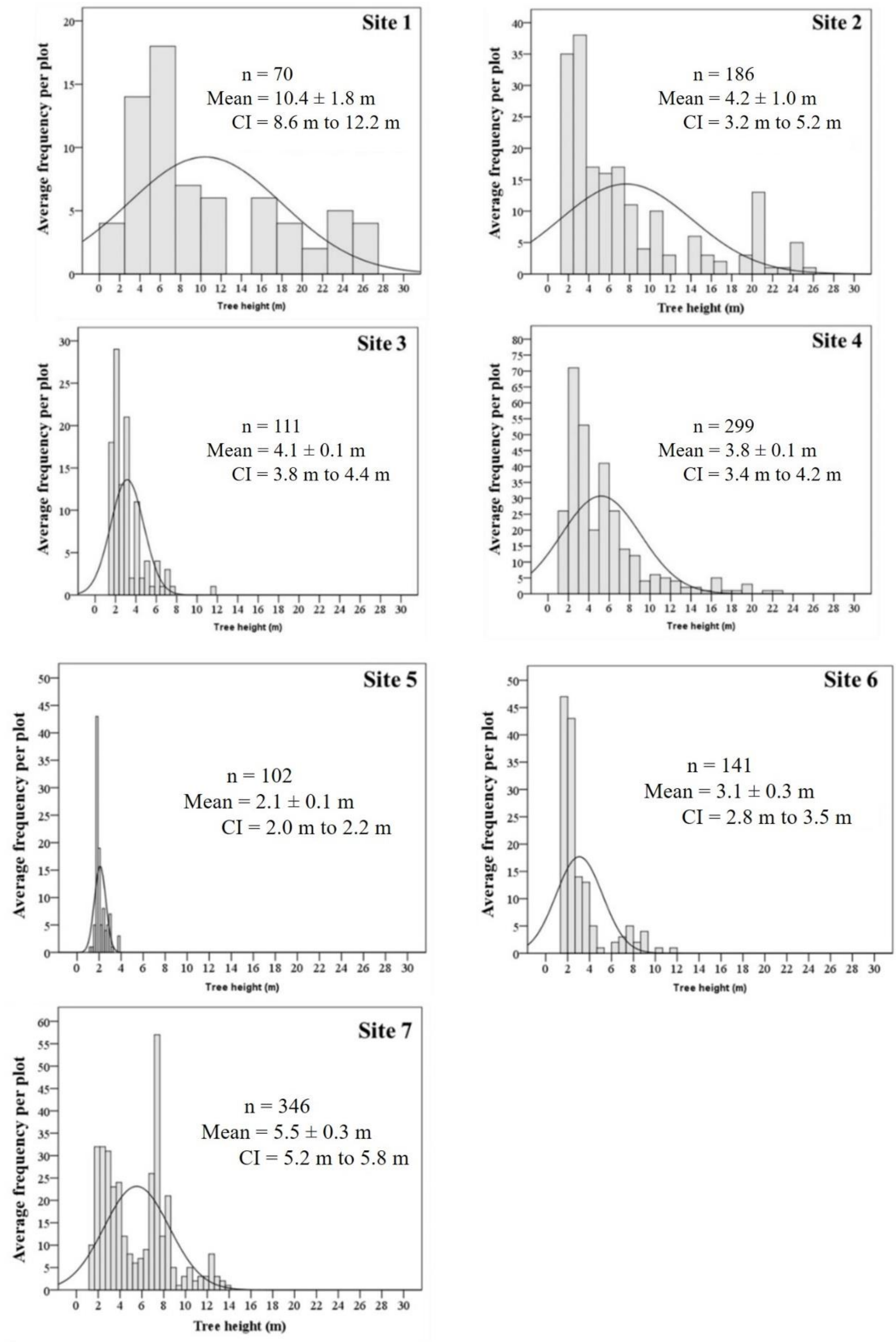

Appendix B2: Distribution of tree heights in Luanshya. Where n is the mean total number of individual trees per sites (30 x 30 m). The legend shows the total number (n) of individual trees per sites (90 x 90 m), mean tree heights and standard deviation and the CI at 95% level of confidence.

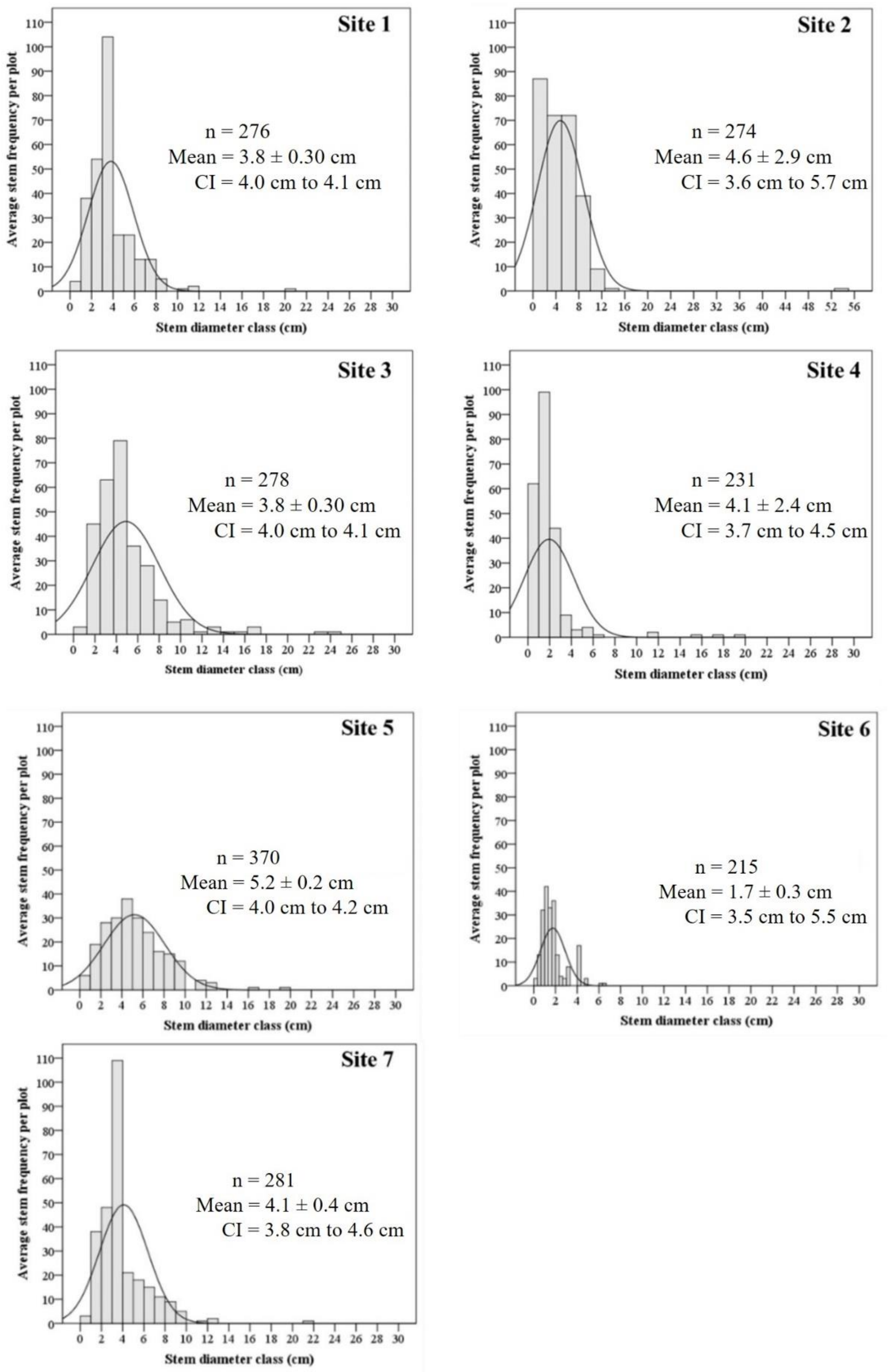

Appendix B3: Distribution of tree stem diameter in Bushbuckridge, measured at 1.3 m above the ground. The legend shows the mean total number (n) of individual trees per sites (30 x 30 m), mean stem diameters and standard deviation and the CI at 95% level of confidence.

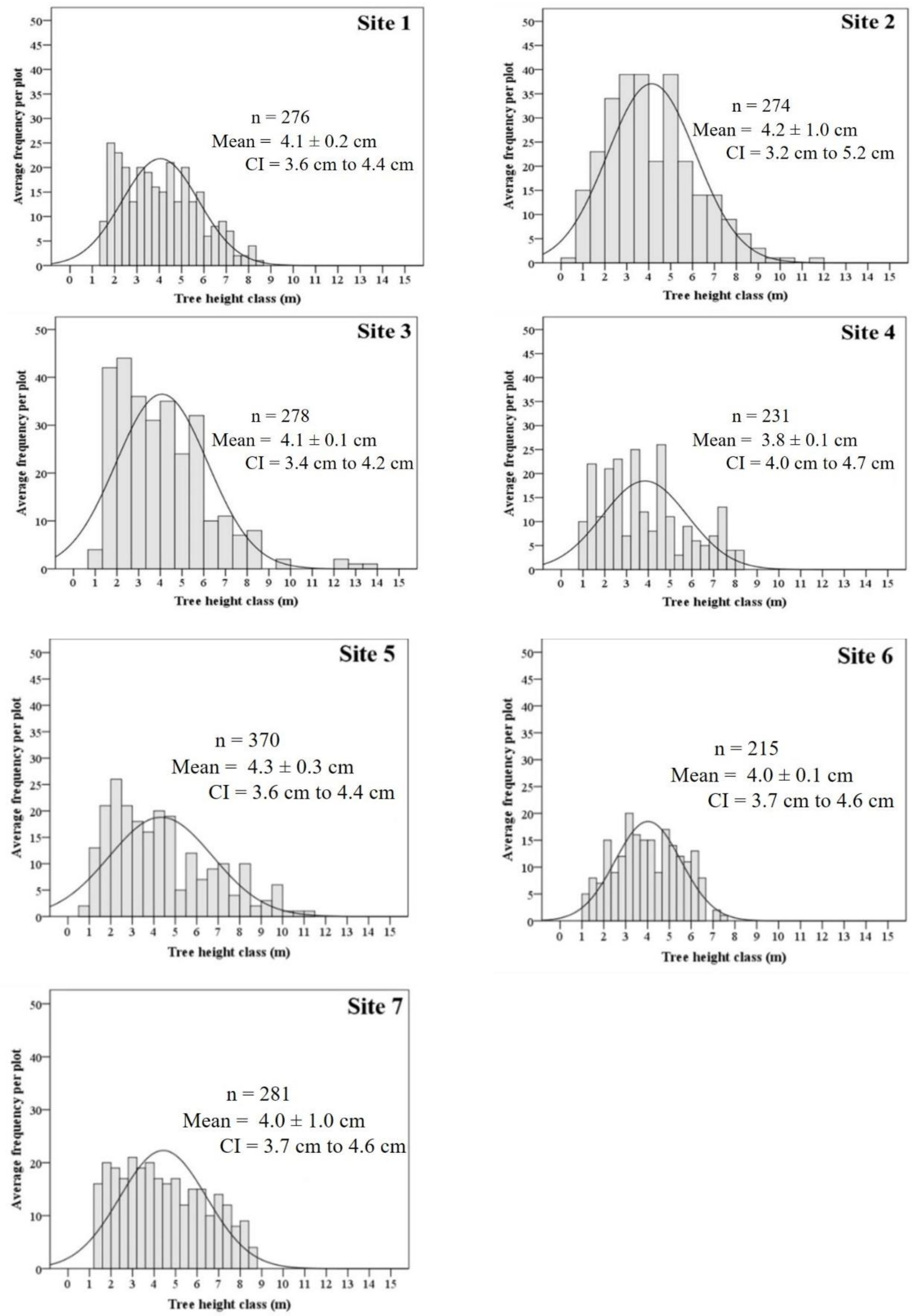

Appendix B4: Distribution of tree heights in Bushbuckridge. The legend shows the mean total number (n) of individual trees per sites (30 x 30 m), mean tree heights and standard deviation and the CI at 95% level of confidence.

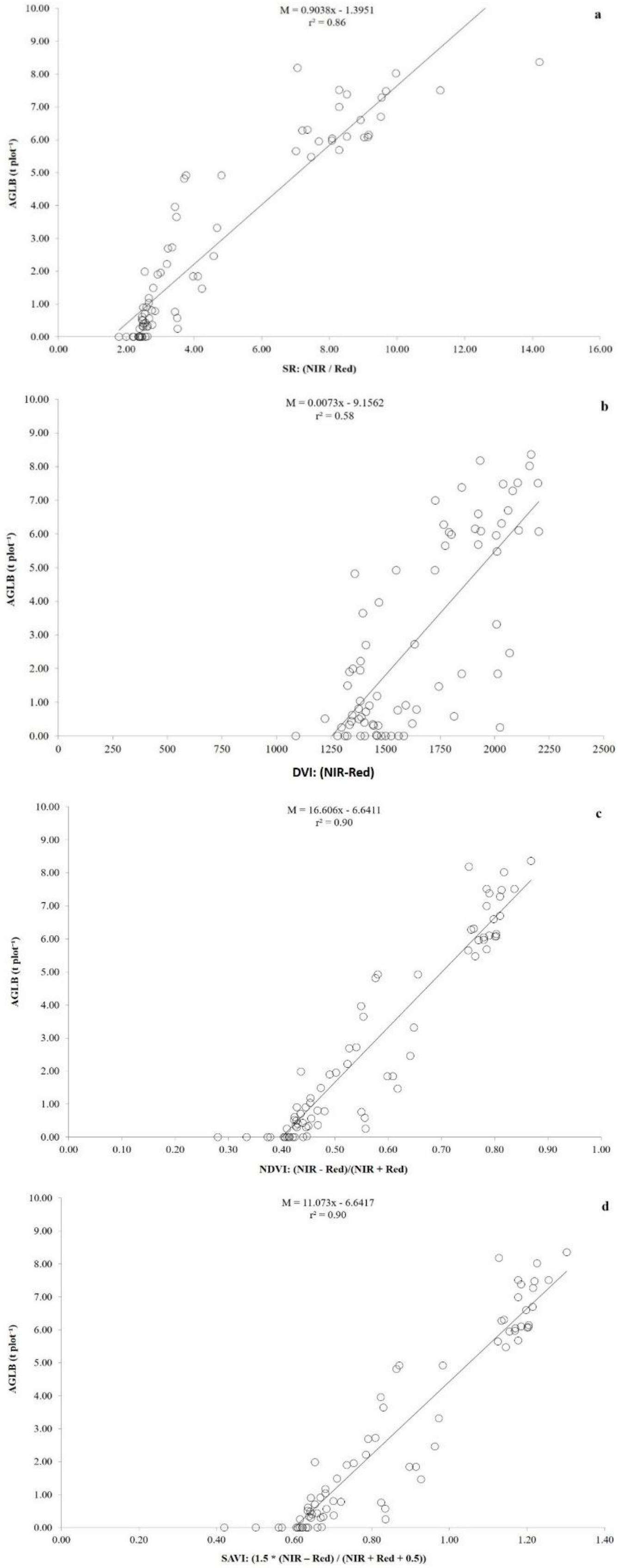

Appendix C: Linear regression models for estimating the average total AGLB per plot (30 x 30 m) from (a) SR index, (b) DVI, (c) NDVI and (d) SAVI.

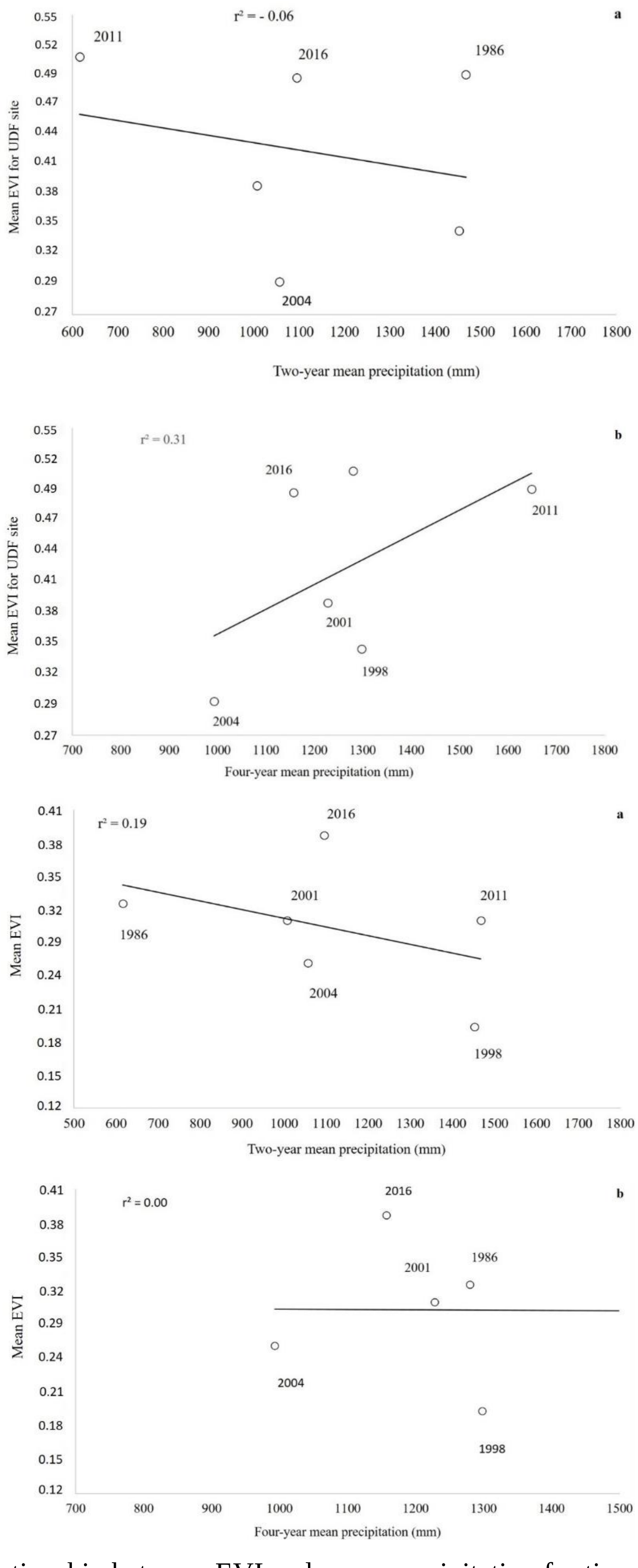

Appendix D1: Relationship between EVI and mean precipitation for time lags spanning two, and four years for the UDF site (a, c) and for the entire woodland cover in Luanshya.

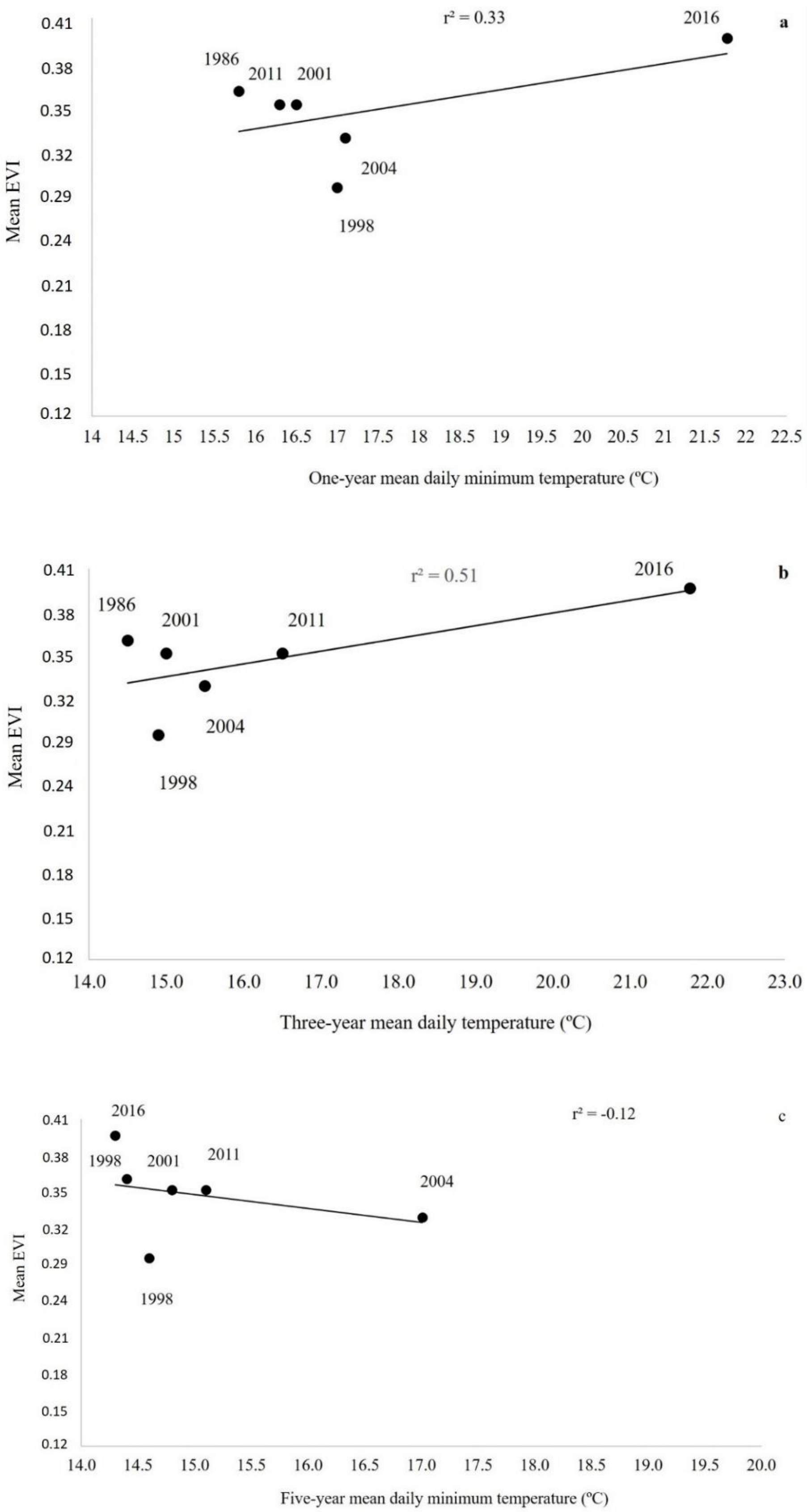

Appendix E1: Relationship between EVI and mean daily minimum temperature for time lags spanning (a) one year, (b) three years and (c) five years for the entire woodland cover in Luanshya.

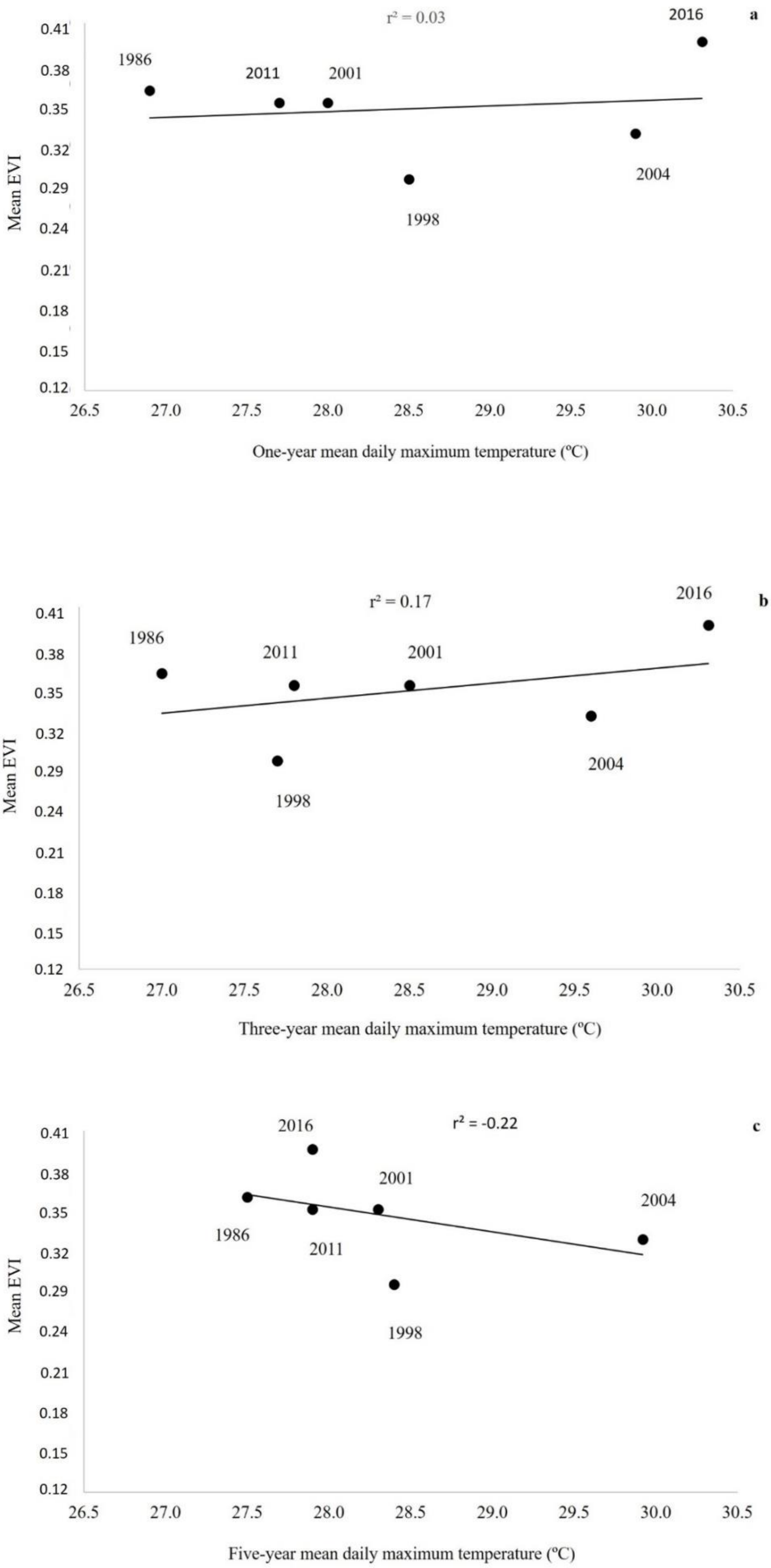

Appendix E2: Relationship between EVI and mean daily maximum temperature for time lags spanning (a) one year, (b) three years and (c) five years for the entire study area in Luanshya.

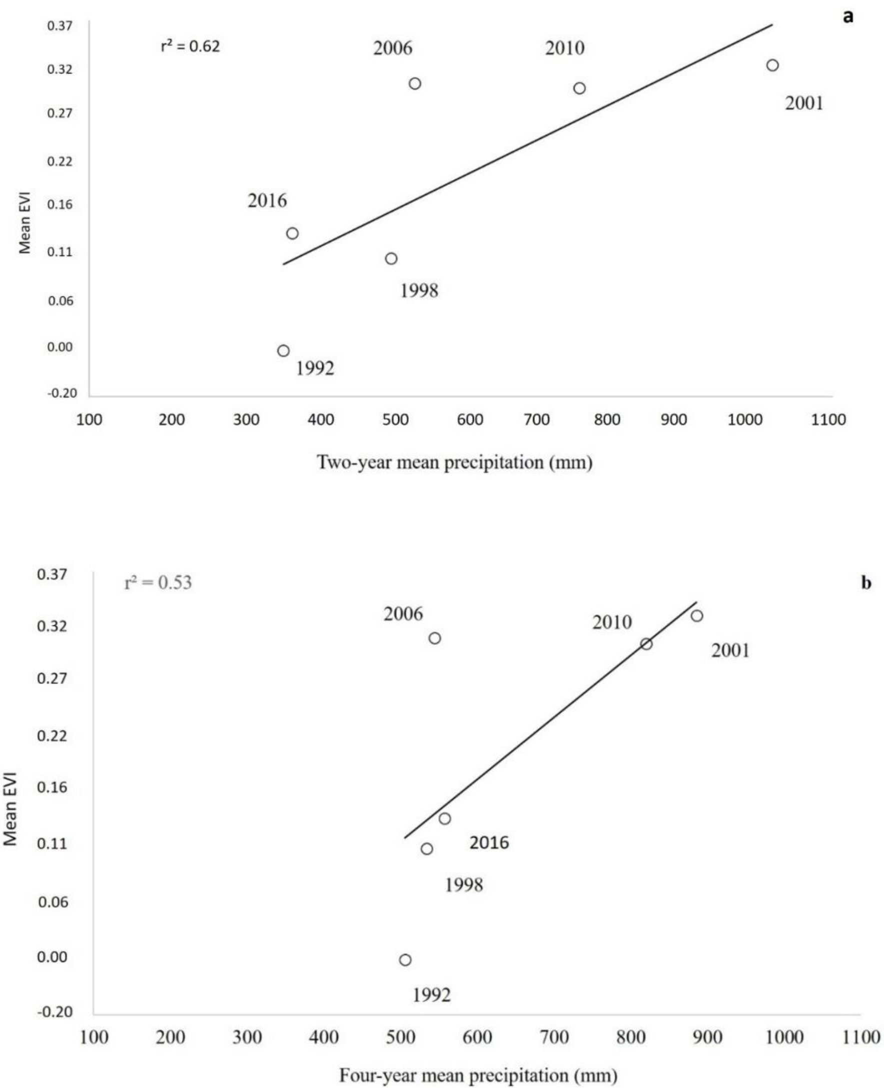

Appendix F: Relationships between mean EVI (for the entire study area in Bushbuckridge) and precipitation for time lags spanning (a) two years and (b) four years.

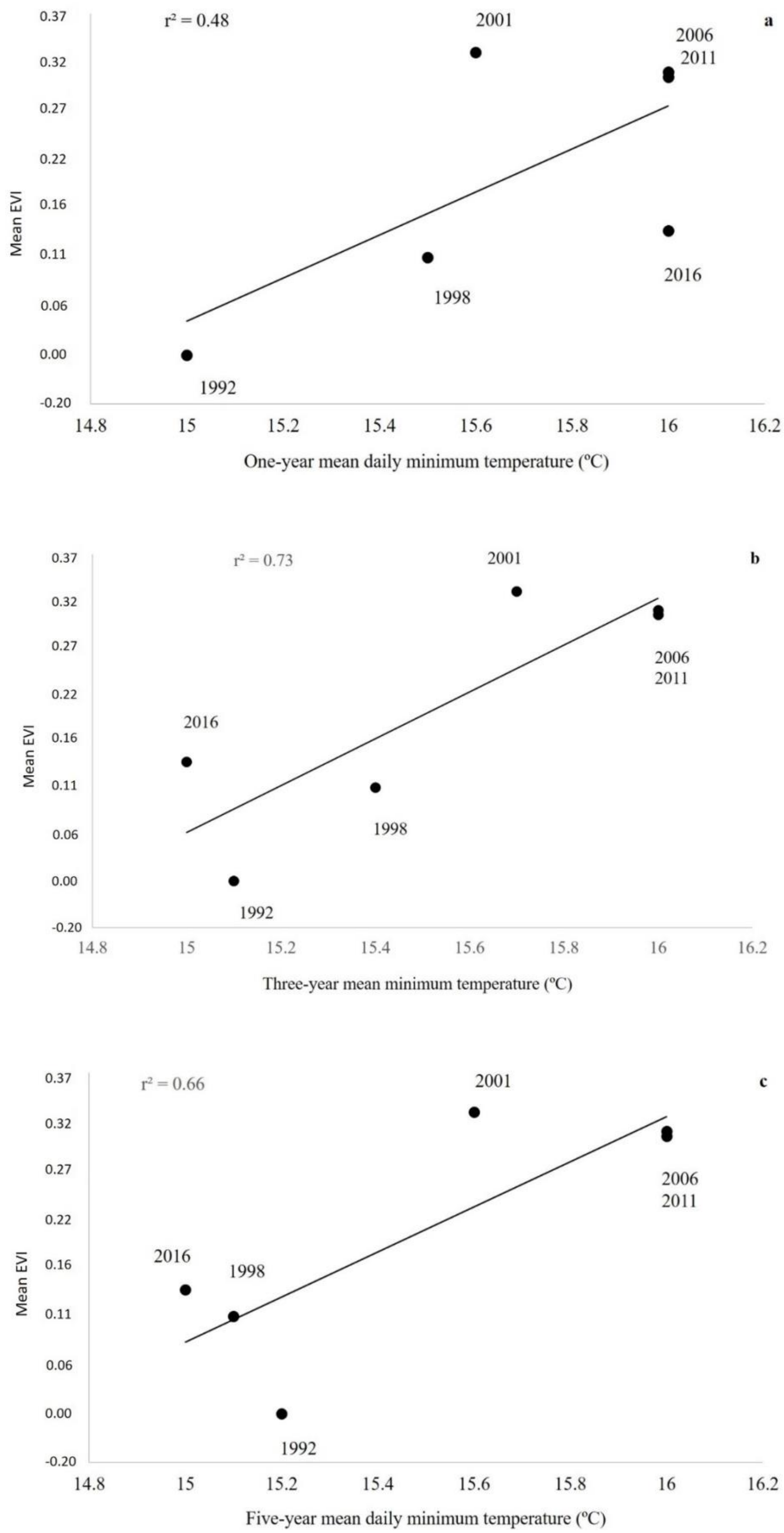

Appendix G1: Relationship between EVI and mean daily minimum temperature for time lags spanning (a) one year, (b) three years and (c) five years for the entire study area in Bushbuckridge.

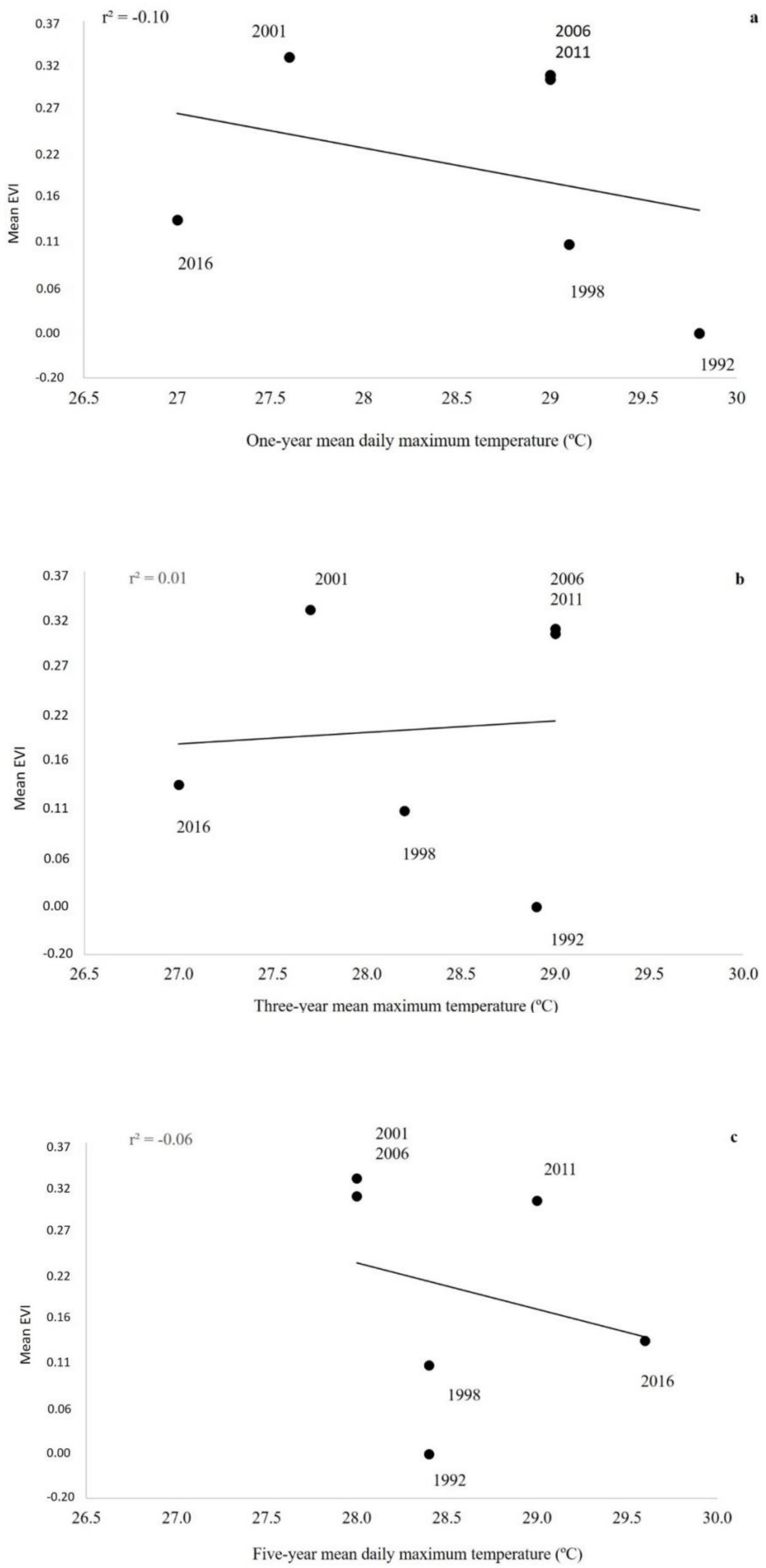

Appendix G2: Relationship between EVI and mean daily maximum temperature for time lags spanning one (a), three (b) and five (c) years for the entire woodland cover in Bushbuckridge.

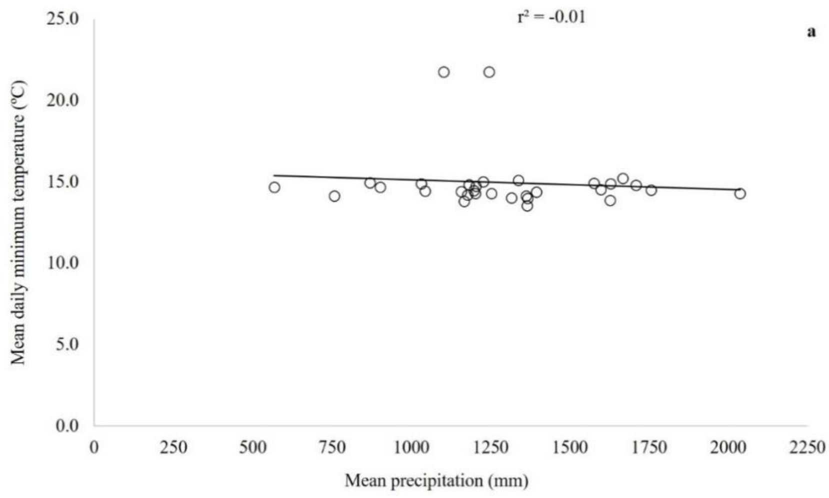

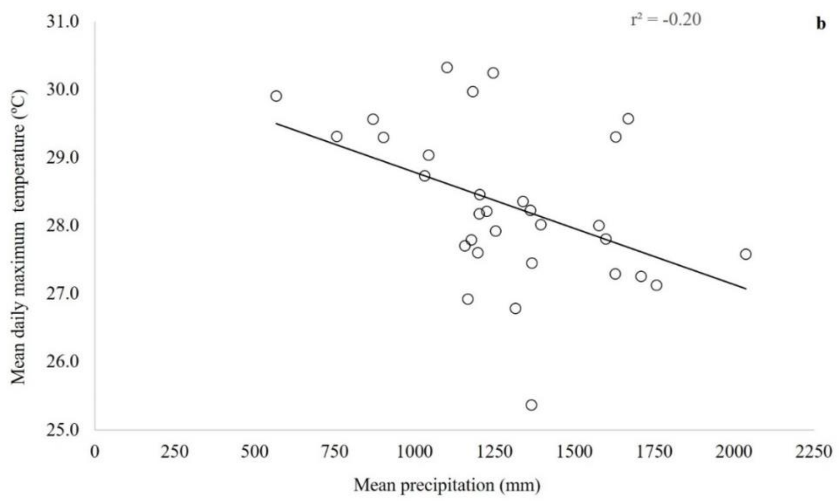

Appendix H1: Correlations between precipitation and mean daily minimum temperature (a), and mean daily maximum temperature (b) recorded from 1986 to 2016 in Luanshya.

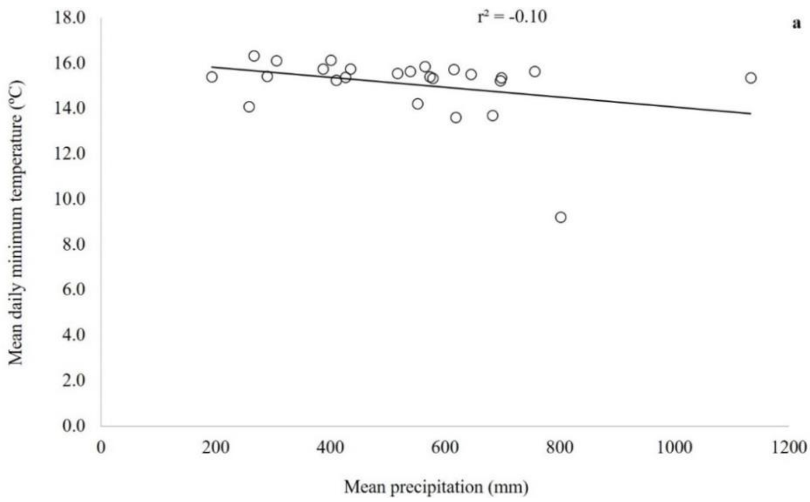

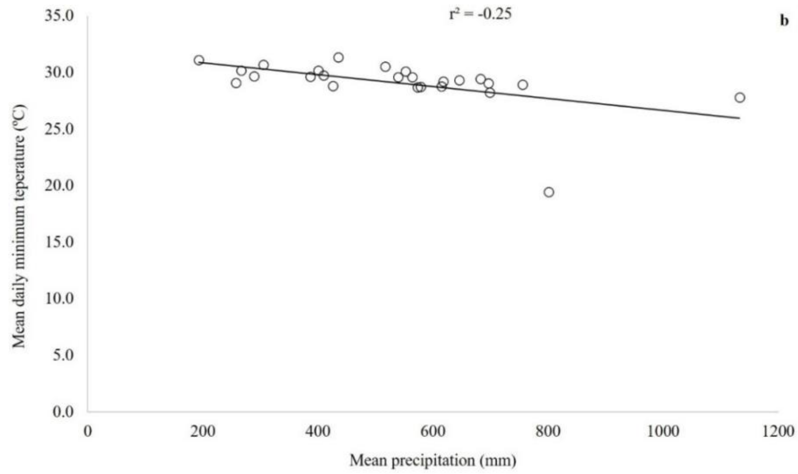

Appendix H2: Correlations between precipitation and mean daily minimum temperature (a), and mean daily maximum temperature (b) recorded from 1992 to 2016 in Bushbuckridge.